DEVELOPING A HIGH TEMPERATURE, OXIDATION RESISTANT MOLYBDENUM-SILICA COMPOSITE

A Dissertation
Presented to
The Academic Faculty

By

William L. Daloz

In Partial Fulfillment Of the Requirements for the Degree Doctor of Philosophy in Materials Science and Engineering

Georgia Institute of Technology
December, 2015

DEVELOPING A HIGH TEMPERATURE, OXIDATION RESISTANT MOLYBDENUM-SILICA COMPOSITE

Approved by:

Dr. Joe. K. Cochran, Advisor
School of Materials Science and Engineering
Georgia Institute of Technology

Dr. Thomas H. Sanders, Jr.
School of Materials Science and Engineering
Georgia Institute of Technology

Dr. Richard W. Neu
School of Materials Science and Engineering
Georgia Institute of Technology

Dr. Naresh N. Thadhani
School of Materials Science and Engineering
Georgia Institute of Technology

Dr. David L. McDowell
George W. Woodruff School of Mechanical Engineering
Georgia Institute of Technology

Approved: September 18, 2015

ACKNOWLEDGEMENTS

This work was sponsored by the Office of Naval Research through contracts N00014-12-C-0412 and N00014-13-P-1181, and I must first thank the project monitors, David Shifler, Steven Sullivan, and Robert Kowalik. I would also like to thank Dr. Joe Cohran, my advisor, for his support and continued interest in my success with this project, and also for keeping it funded and forwardly mobile. Without his support the innovations in this current project could not have been possible. Additional thanks must be given to my committee members who have devoted so much of their time to the review of this directly, but also for their assistance and guidance during my time here at Georgia Tech. I must also very sincerely thank Michael Middlemas who helped develop the basis for this project and helped familiarize me with the project and material system in general, as well as the equipment, the department, the school and the city of Atlanta as a whole. Most sincerely I must thank my colleague Peter Marshall, who has worked directly with me on almost every aspect of this project for the past several years. Both for the shared efforts and discussions which have moved this project forward and for the witty quips which have helped keep me focused. Finally I must thank my family, my mother Jan, my father Charles, my brother Joel and my wife Megan, who make all of this worthwhile.

TABLE OF CONTENTS

LIST OF TABLES

LIST OF FIGURES

NOMENCLATURE

The compositions studied in this work include a wide variety of phases at different volume fractions. Traditional alloys in MoSiB are listed as weight fractions of the Si and B, such as the most common 3:1 which refers to 3wt% Si, 1wt% B and 96wt% Mo. The system of naming used in this work is described in Chapter 5.2.1 and also given below for easy reference.

The names of the compositions are of the following general format:

XYaabb_cZ-d

Where *X*, and *Y* are the abbreviations for the phases present, as given in the table on the next page. The volume fractions are then given in *aa* and *bb* as 2 digit numbers, representing the final volume fractions of phases X and Y respectively in the final composition. These will not add up to 100, the remaining volume fraction is the Molybdenum solid solution matrix phase. In some cases multiple firings of the same composition were made, these are ordered chronologically and indicated by a dash then the consecutive number of the firing, *d*.

In some cases small fractions of elemental additives were included, and these are indicated after the underscore, where *c* is the atomic fraction of the molybdenum phase replaced by the added element, and *Z* is the element's symbol. The elemental additives incorporate generally into the molybdenum solid solution and thus cannot be listed as a volume of a unique phase, which is why they are instead listed as an atomic percent of the molybdenum phase.

Symbol	Phase
B	Mo_2B
T	T2, Mo_5SiB_2
A	A15, Mo3Si
S	Amorphous Pure Silica, SiO_2
Q	Quartz, Pure Crystalline SiO_2
C	Cristobalite, Pure Crystalline SiO_2
M	Mullite, $3Al_2O_3$-$2SiO_2$
SAS	Strontium Aluminosilicate, $SrAl_2Si_2O_8$
4Spod	Spodumene Lithium Silicate, $1Li_2O$-$1Al_2O_3$-$4SiO_2$
6Spod	Spodumene Lithium Silicate, $1Li_2O$-$1Al_2O_3$-$6SiO_2$
Nda	Neodymium Apatite, $Nd_{9.33}(SiO_4)_6O_2$

For example:

BS2128_1.5Mn-2

The above composition has 21 volume % of "B", the Mo_2B, and 28 volume % "S" SiO_2, and the remaining 51% of the volume is Molybdenum. The "_1.5Mn" indicates that Manganese, Mn, had been added at 1.5 atomic % of the total 51vol% Molybdenum phase. Finally the "-2" indicates that this is the second batch of that composition which was prepared and fired.

As a second example:

BSASNda202005

The BSASNda202005 would have 20vol% Mo_2B, 20 vol% Strontium aluminosilicate, and 05 vol% Neodymium apatite, with the remainder 55 vol% being Molybdenum. Since there is nothing at the end, there are no elemental additions and it is the first and only batch of that composition which was prepared.

SUMMARY

New materials are needed to increase the maximum use temperatures in jet turbine engines in order to increase efficiency. They must be able to withstand high stresses at temperatures of 1300°C and above, as well as resist environmental degradation. Alloys of Molybdenum have good high temperature strengths, and when alloyed with silicon and boron can achieve a self-healing borosilicate coating to prevent the otherwise rapid oxidation of Mo. The borosilicate intermetallics Mo_5SiB_2 and Mo_3Si must be finely and homogenously distributed throughout Mo matrix in order to achieve good mechanical and oxidation resistant properties. This microstructure is difficult through melt based processes, but powder processing results in excessive impurities which embrittle the molybdenum matrix. A powder approach was developed at GA Tech using reaction of BN and Si_3N_4 as Si and B sources, which decompose in firing to give good microstructure control, without the impurity oxygen that is otherwise picked up when using fine elemental Si and B starting powders. Unfortunately the Mo_3Si phase which is necessary to provide Si for oxidation protection results in high equilibrium Si contents in the Mo solid solution and leads to high ductile to brittle transition temperatures. Instead a new approach is used which replaces the Mo_3Si with SiO_2 directly as the source of silicon for the borosilicate coating and thus avoids the embrittlement of the Mo matrix. A first approach involving glass frits proved to be unusable because the frits are liquid internally during firing and at the end use temperatures. Instead when the borosilicide intermetallics Mo_2B or Mo_5SiB_2 are present they are solid internally, but upon oxidation act to flux the silica allowing it to flow only at the surface during oxidation. A number of issues including surface depletion and

crescents of silica in the microstructure were identified which are associated with unwanted reactions with residual oxygen before the reduction is complete during firing. Instead more stable silica sources including mullite, alkali- and alkaline-earth aluminosilicates were investigated. These also proved unusable due to undesirable reactions in the coating which form crystalline molybdates and disrupt oxidation resistance. Additional transition metal additives were also examined and show excellent improvements in the resistance of the coating to oxidation. Mechanisms of oxidation which define the success or failure of the coating are investigated and discussed in light of the experimental evidence. Finally a hot isostatic processing technique is presented which is able to achieve final products that have neither the Si embrittlement of the Mo_3Si alloys nor the detrimental microstructural issues previously seen in the Mo-Mo_5SiB_2-SiO_2 system.

CHAPTER 1.

INTRODUCTION

High temperature structural materials are needed to improve efficiency and power output in next generation jet turbines. By increasing the rotor inlet temperature, the efficiency is increased which means either greater power output for the same fuel use, or lower fuel needed to achieve the same power output. Current turbine temperatures are limited by the materials in the turbine blades and have come to rely on increasingly complex production methods and cooling systems. Current high output turbines use unidirectionally solidified single crystal Ni superalloys with elaborate networks of cooling channels and barrier coatings. While this does increase the temperatures possible, these complex systems lead to increasing deviation from ideal performance and are also very costly. If instead a new class of materials could replace the current alloys, this could not only increase use-temperatures but could do so without the elaborate cooling requirements. It would increase not only the use temperature but also reduce the inefficiency losses and bring it back towards the ideal performance. A new high temperature material could mean very significant increases in power output, and potentially do so at a reduction in total costs.

There are a number of materials which could be suitable higher temperature replacements for the current nickel superalloys; however they all have significant hurdles. A candidate material should be able to operate at substantially higher temperatures than the Ni, and meet or surpass oxidation and mechanical properties at both operating and room temperature. They must possess good high temperature strength and resistance to creep, high fracture toughness at low and high temperature, and also resistance to

oxidation, with additional considerations of density and cost. One possible group would be ceramics and intermetallics which have the necessary high temperature stability and high melting points, but are prohibitively brittle. In addition to lower strengths, the brittle nature of failure precludes opportunity for lifetime inspection or graceful failure. Impact might crack a blade, and the resulting debris could cause catastrophic destruction of the surrounding engine. The more attractive alternative would be refractory metals, however those are either prone to oxidation (Nb, Mo, W) or exorbitantly high priced (Pt, Pd, Rd).

Of the oxidation prone refractory metals, W is prohibitively dense for aerospace use however alloys of Nb or Mo could be usable if they are made to achieve oxidation protection. By alloying with other metals such as Si, they form an oxidation resistant oxide coating similar to $MoSi_2$, a refractory intermetallic commonly used in furnace heating elements.

Higher Mo intermetallics such as Mo_3Si do not form enough silica to completely coat the surface and prevent oxidation, however Akinc and Meyer [1] realized that addition of B acts as a flux and allow the silica to flow and form a complete coating. Berczik[2, 3] exploited these benefits by patenting a new class of MoSiB materials which consist of a high strength structural Mo matrix, combined with Mo_3Si (A15) and Mo_5SiB_2 (T2) intermetallics for oxidation resistance.

These materials have received a great deal of attention since the first Berczik patents, however they've been plagued by an inability to meet a suitable compromise between on one hand a high Mo content to benefit strength and fracture toughness, and on the other hand; high intermetallic contents to provide low initial oxidation losses and adequate long term oxidation protection. Ideally these alloys must contain pure and

continuous ductile molybdenum matrix with isolated but finely dispersed silicon and boron intermetallics to form the glass coating. This allows the Mo matrix to dominate fracture properties while permitting the intermetallics to act as ready sources of protective coating, as well as providing internal pins which inhibit high temperature creep.

The desired microstructure of isolated intermetallics within a Mo matrix is difficult to achieve by traditional melt-based processing because the solidification paths of high melting Mo results in the opposite microstructure; the Mo solidifies first and is thus isolated within a brittle intermetallic matrix. This is only avoidable when expensive and complicated rapid quenching techniques are used. Instead, powder processing techniques have proven able to produce a tailored microstructure in the green state, which upon firing in a reducing atmosphere results in the desired microstructure with a comparatively inexpensive and more easily scalable approach.

Most powder process techniques permit too much oxygen into the system adsorbed on the surface of the reactive silicon and boron powders, but a technique developed at GA Tech uses BN and Si_3N_4 starting powders which are reduced and reacted during firing to provide the desired final phases and arrangement. The use of nitride starting powders avoids excess oxygen which would severely embrittle the powder processed molybdenum.

The MoSiB system still has not managed to achieve a suitable balance of fracture toughness and oxidation resistance and recently this has been attributed to the embrittlement of the molybdenum matrix by silicon in solid solution. There is a finite solubility of Si in Mo solid solution when in equilibrium with the Mo_3Si phase, and it is unavoidable using most processing techniques. This work aims at the development of an

alternative Mo-Si-B type alloy which avoids the embrittlement issues by replacing the A15 (Mo_3Si) phase with alternate sources of SiO_2 and B_2O_3 for oxidation resistance.

The following chapter will discuss the history and advances leading towards the current project. Chapter 3 focuses on the unique experimental aspects of the process and analysis techniques used and some of the considerations and problems encountered. Chapter 4 covers initial attempts at replacing the A15 Mo_3Si phase with glass forming frits. Chapter 5 expands on the results of the Mo-SiO_2 concept and illustrates a bulk of the issues culminating in an alternate approach using other silicate sources besides SiO_2. Chapter 6 focuses on the selection process, results, and discussion of the alternate silicates examined. Chapter 7 involves a series of additional compositions and elemental additions aimed toward affecting oxidation and/or mechanical behavior. Chapter 8 discusses some of the concerns affecting the oxidation and proposed mechanisms of the formation of a glassy self-healing oxidation resistant coating and parameters affecting its success or failure. Finally, Chapter 9 focuses on the most recent changes in the research direction and suggestions for taking the next steps towards a functional material before concluding in Chapter 10.

CHAPTER 2.

LITERATURE REVIEW

This chapter reviews the motivation and history behind the development of MoSiB alloys. It also focuses on processing methods and limitations of the system which have been previously identified.

2.1. High Temperature Structural Materials

2.1.1. Improving Jet Engine Efficiency

Shown in Figure 2.1 is a measure of jet turbine efficiency expressed as a function of the horsepower produced for increasing inlet temperatures modified from Lemberg[4]. An obvious trend is shown; by simple increase of the rotor inlet temperatures, the power output can be greatly increased. There are always some losses and actual output will inherently deviate from ideal. In order to further increase inlet temperatures beyond the maximum use temperatures of the existing materials, increasingly complex technologies involving coatings and cooling channels have evolved (Figure 2.2). Shown on Figure 2.1 is the intended base use temperature of the MoSiB alloys (1300°C), compared to the base metal temperatures for current nickel alloys which have a maximum at around 1100°C. The actual output curve in red extends past the maximum use temperatures of Ni alone, with increased output achieved through cooling. The trend through the blue "cooling" section has a lower slope indicating increasing losses through cooling inefficiency, while the dotted blue line indicates the potential for improvement if cooling were unnecessary. A measurable increase can be seen then for the MoSiB case, if its base temperature is raised to 1300°C without cooling, it could be more efficient than Ni at 1600°C when considering the cooling losses. Of course MoSiB alloys could also use cooling and barrier

coatings, and the green triangle shows the area of further improvement expected by extending the slope of the cooling-enabled materials from the 1300°C base temperature.

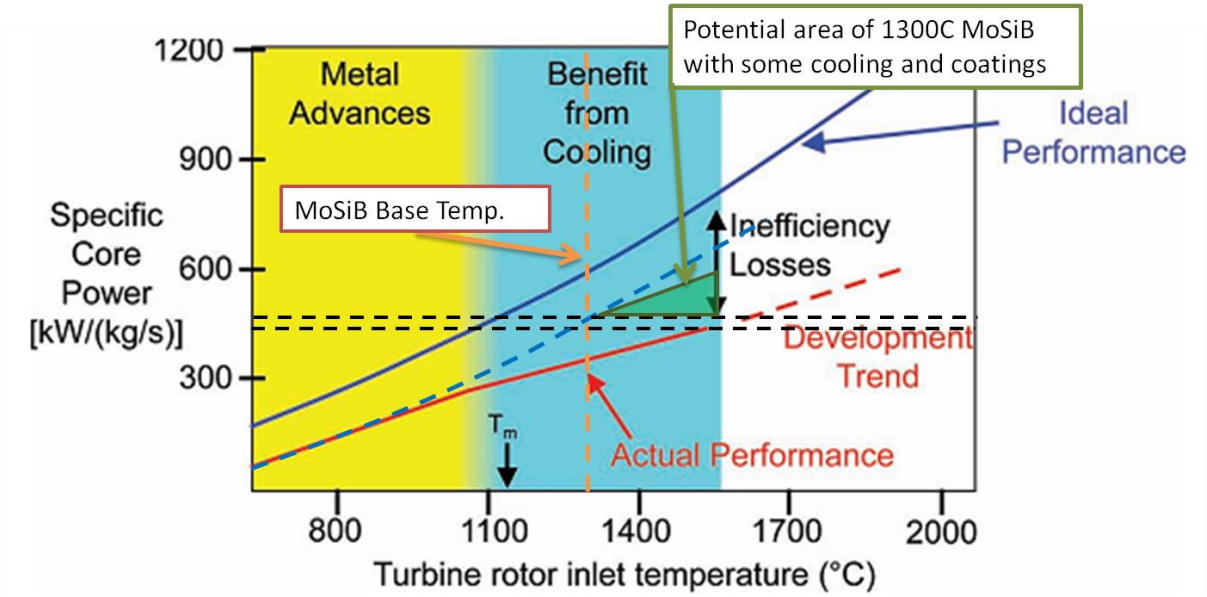

Figure 2.1: The actual and proposed increase in output power with increasing rotor inlet temperature of gas turbine engines.

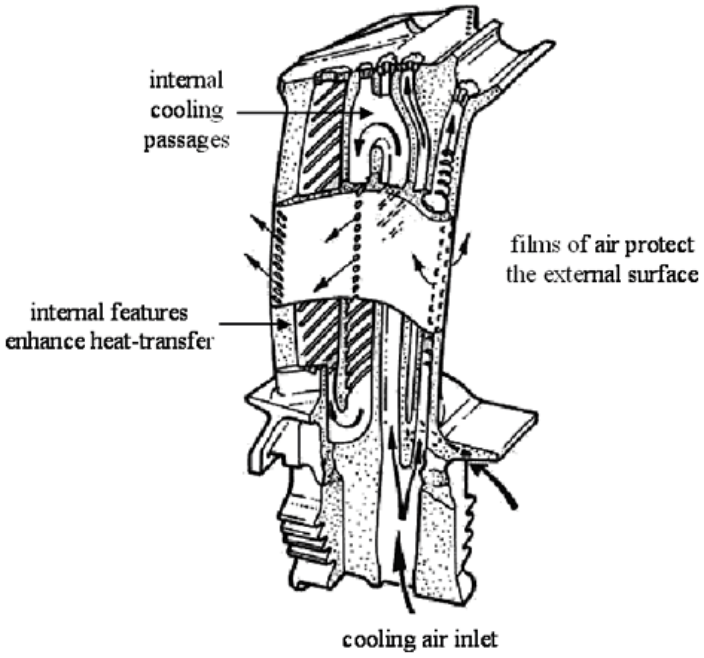

Figure 2.2: Example turbine blade cross section exposing cooling systems employed in jet turbine blades. [5]

2.1.2. Requirements of Jet Turbine Materials

The requirements for a new turbine material are not easily met. Jet turbine engines see not only high temperatures, but must endure many other challenges simultaneously. The rapid heating and cooling creates high thermal stresses. The rotational inertia on spinning blades coupled with vibration and rapidly moving combustion gases give constantly varying mechanical stresses on the components, and they must endure these for thousands of hours without deforming from stress, fatigue or creep. The phases must remain steady without microstructural changes from grain growth at the use temperatures, and they must be able to withstand environmental corrosive effects of combustion environments at very high temperatures.

2.1.3. Ni Superalloys

Current turbine blades are made using Ni superalloys. They're subjected to temperatures over 85% of their melting temperature and stresses approaching 150MPa with lifetimes in the thousands of hours, and must maintain close tolerances in order to achieve efficient engine operation. The Ni superalloys have dominated jet turbine technology for tens of years, with increasingly more complicated technologies to further increase their use temperatures. Advances in the past have focused on improving existing Ni superalloy technology through directional solidification, use of single crystals to prevent creep and grain boundary motion, thermal barrier coatings, and advanced internal cooling systems to achieve operating temperatures up to 1500°C. These improvements have become increasingly more expensive with fewer gains and are reaching their maximum feasible limits.

2.1.4. Refractory Metals

When examining alternative metals, the criterion of high melting point is important. Beyond just the obvious need to avoid melting near the use temperatures, high melting temperature also correlates to a high elastic modulus[6], a low thermal expansion and also governs the degree of creep at a given temperature. Typically a maximum usable creep rate occurs between ½ and $^{2}/_{3}$ of the melting point. To be used in flight, weight also becomes a concern.

Precious metals such as Pt, Pd and Re possess excellent oxidation resistance and have melting points above 1500°C; Rhenium doesn't melt until over 3000°C. However these metals are rare and prohibitively expensive, if it were possible to obtain enough quantity for engine production, the costs would be astronomical. Other refractory metals

such as tantalum and tungsten could provide adequate thermal resistance; both have low thermal expansion and high melting points also above 3000°C, but their high density (Ta = 16.4g/cc, W = 19.3g/cc) makes their use in aircraft highly unfavorable. [7]

Instead, alloys of Nb and Mo have taken the forefront.[8] They possess usably low cost and density, with high melting points and resistance to thermal shock. In the early part of this century, Nb based alloys received significant attention[9, 10] but they suffer from catastrophic oxidation and readily crumble. Mo alloys have better properties and have already found use in numerous high temperature applications, while alloys of Mo, Si and B have even been shown to form self-protective oxidation resistant coatings.

2.2. Molybdenum

2.2.1. Mechanical Properties of Molybdenum

The properties of Molybdenum make it an attractive high temperature structural material, and are listed in Table 2.1.[11] Molybdenum has the 6th highest melting point of any element at 2,623 °C. Creep resistance is strongly correlated to melting temperatures, typically materials are kept below ½ to $^{2}/_{3}$ of the melting point to avoid creep, and Molybdenum is thus quite creep resistant. It also has low thermal expansion (4.8 $\mu m \cdot m^{-1} \cdot K^{-1}$ at 25 °C) and high thermal conductivity (138 $W \cdot m^{-1} \cdot K^{-1}$) making it resistant to thermal shock.

Table 2.1 Selected Properties of pure Molybdenum.

Properties of Molybdenum	
Atomic wt. (g/mol)	95.96
Atom rad. (Ang)	1.54
Tm (C)	2623
Heat of fsn (kJ/mol)	37.48
Heat cap. RT (J/mol K)	24.06
Density (g/cm^3)	10.28
Structure	BCC
T cond (W/molK)	138
T exp (μm/mK)	4.8
E (GPa)	329
Poisson ν	0.31

Molybdenum is a body centered cubic metal. The yield strength in BCC metals is strongly dependent on temperature while the stress for crack propagation remains fairly constant. This leads to a crossover temperature whereby the dominant mode of failure shifts from ductile to brittle behavior known as the ductile to brittle transition temperature (DBTT). Below the DBTT, Mo becomes very brittle. DBTT of Mo has been reported to be between -60°C and 200°C, and is dependant strongly on impurities, with greater purity resulting in lower DBTT. [12, 13]

The strength of Mo typically follows Hall-Petch behavior and benefits from reduced grain size. Deformation proceeds by motion of dislocations, which cannot cross grain boundaries. According to the Hall-Petch assumption, the smaller grains lead to an increased number of grain boundaries and therefore higher resistance to dislocation motion and higher strength. For Mo with grains below 100μm, agreement with the Hall-Petch behavior has been observed by Orava [14]. In some cases however the opposite can

be true. If the grain boundaries are the weak point in the structure, failure may occur along the grain boundaries in which case smaller grains and more boundaries means lower strengths. Intergranular fracture has been observed for Mo, particularly with high impurity concentrations[15], and smaller grains could reduce strength in the case that intergranular fracture dominates.

Creep is a gradual deformation at high temperatures. It is a process of deformation by grain boundary motion and stress enhanced diffusion and rearrangement which occurs at high temperatures where self-diffusion is significant. As a result, creep also depends on grain size; smaller grains may increase creep by grain boundary sliding and also by enhanced diffusion along grain boundaries.

Impurities can have a significant effect on the mechanical properties of molybdenum. The most pronounced impurity effects are from carbon and oxygen.[16] The closely packed nature of Mo lattice results in most impurities locating substitutionally, but because of the large size of the Mo atom (139 pm) compared to impurities like O and C, large lattice stresses develop. These lattice stresses are partially relieved when the impurities are located at grain edges and so impurities segregate to dislocations and grain boundaries.[17] For BCC metals, impurities cause nonsymmetrical lattice distortion and interact with both edge and screw dislocations, as opposed to FCC, where symmetrical impurities only interact with the edge dislocations.[18] The impurities anchor dislocations preventing them from moving and thus deformability is reduced, yield strength is raised, and brittle failure predominates. Even very small amounts of oxygen in the ppm range can significantly reduce Mo deformability.

The DBTT is a transition where the stress for dislocation motion is eclipsed by the stress for crack propagation, and as such it varies directly with impurity concentration. DBTT in Mo is also sensitive to grain boundary strength, and above the brittle transition it fails by almost completely intergranular fracture. Grain boundary strength is in turn very sensitive to impurities due to the aforementioned solute segregation.

Most commercial Mo alloys include minor additions of Ti, Zr and very small amounts of carbon in order to prevent the serious issues of oxygen impurity. These additives all have higher oxygen affinity than Mo and act primarily to getter oxygen by forming oxides.

In addition to O, C and N, other impurities carry similar effects on the mechanical properties of Mo. R. Jaffee [19] looked at effects of various alloying additions and noted that Si has the greatest effect on strengthening Mo. Sturm and Heilmaier[20] have shown that increasing Si concentration in Mo also decreases toughness due to segregation of Si solute to the grain boundaries. Diffusion is also slow in the Mo lattice and high impurity concentrations which may be possible at higher temperatures are often "locked-in" after cooling and are difficult to anneal out. Because the solid solution concentration of Si in equilibrium with Mo increases with temperature, from less than 1% at 1300°C to about 3% at 1600°C (Figure 2.3), potential exists to reduce Si concentration in Mo by processing at lower temperatures.

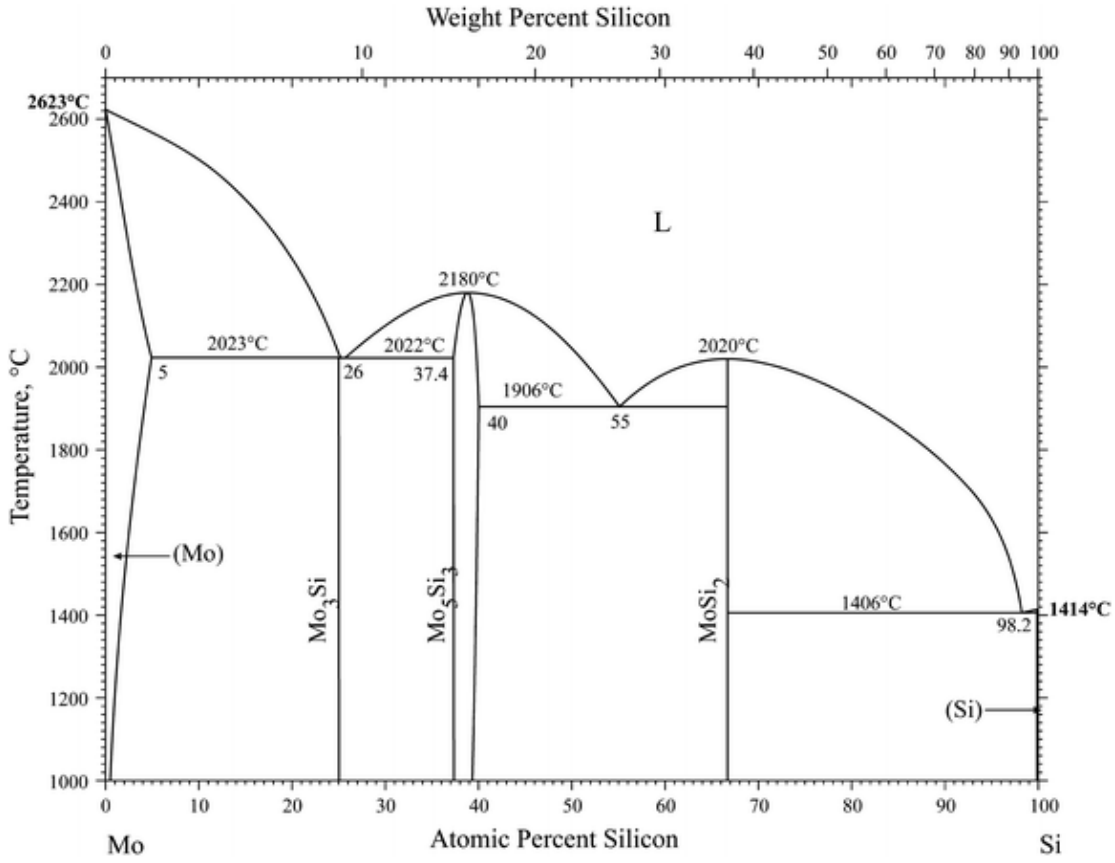

Figure 2.3: The molybdenum-silicon binary phase diagram.[21]

Again considering the effects of grain size, a decreasing grain size might benefit strength when impurities are present because it increases grain boundary area which in turn reduces impurities segregated on the grain boundaries. The same amount of impurity would be spread thinner over a greater total grain boundary area. To the contrary however if the segregation were still enough that intergranular fracture dominated, the high grain boundary area becomes a detriment.

Working of Mo alloys is also common practice and limits impurity embrittlement by creating dislocations which tie up the impurities off of the grain boundaries. [22] Repeated deformation creates dislocations and defects pile up making nucleation and mobility of new dislocations increasingly more difficult. The result is an increase in

strength and hardness, and is employed when making hardened Mo alloys for tools. Typically working reduces ductility, however investigations by Suzuki et al [23] showed that for arc melted molybdenum, ductility may be increased by hot working. Hot working can rearrange the grain structure and remove the segregated impurities from grain boundaries and instead tie them up internally on dislocations. The proposed effect is supported by the fact that when the Molybdenum is very high purity, the benefits of working disappear, confirming that the ductilizing effect is indeed due to rearrangement of impurities.

2.2.2. Oxidation of Mo

Oxidation is one of the biggest issues facing molybdenum based alloys for high temperature applications. Oxidation of molybdenum is catastrophic and rapid at high temperatures due to the formation of a gaseous oxide (MoO_3), and the rate of oxidation must be controlled and seriously limited if it is to have any high temperature usefulness in air. [24]

2.2.2.1. Low Temperature Oxidation of Mo

Molybdenum can pick up oxygen and water at room temperature but typically only a very thin layer on the surface and it does not easily corrode nor form any visible oxide at room temperature. In wet and humid environments Mo hydride can be formed. Even in very small amounts it gives the water a distinct “Molybdenum blue” hue. The formula is believed to be $HMoO_4$ and is stable with H_2O. A higher pH results in a dissolved MoO_4, while at lower pH Mo or MoO_2 are seen. In general however it’s not until higher temperatures that oxidation of Mo becomes a significant concern.

2.2.2.2. Derivation of Parabolic Kinetics

With a gaseous oxidant (O_2, air), the rate of oxidation of metals depends on the slowest of the simultaneous steps involved. For oxidation to occur, mass transport of the oxidant through the gaseous phase surrounding the metal, reaction between the oxidant and the metal at the surface, and gaseous diffusion of the products away from the surface must all occur. If the reaction product is a solid oxide scale, then another simultaneous set of steps must be considered, the mass transport of oxygen anions inward and/or the transport of metal cations outward through the scale, as well as reactions at the solid oxide/metal interface. In the case where the diffusion of oxygen through the scale is rate limiting, as the thickness grows, the rate of oxygen in or metal out decreases, which leads to the parabolic kinetics.

During oxidation an oxide forms at the surface leading to a basic relation as shown below:

Metal | Oxide | Gas (O_2)

and in order for reaction to proceed either one or both of the reactants must pass through the oxide scale. The transport of reactant ions depends on the nature of the scale. Ionic mobility depends on defects; Schottkey for substitutional ions and Frenkel for interstitial ions. Anion migration (O_2^-) leads to new oxide forming on the oxide/metal interface, cation migration (M^+) leads to oxide forming on the air/oxide interface. This is the basis of Wagner's theory of high-temperature diffusion-controlled oxidation.

Assuming ion transport controls the rate of oxidation rather than being reaction rate dependant, and that equilibrium is established at the interfaces; outward cation flux is equal and opposite the inward flux of cation defects (i.e. vacancies)

$$j_{M2+} = -j_{VM} = D_{VM} * ((\Delta C'_{VM})/X) \qquad (2.1)$$

j_{M2+} is cation flux, j_{VM} the metal vacancy flux, D_{VM} the diffusion coefficient, C is concentration at the interfaces and x the scale thickness. Since the interfaces are assumed in equilibrium, $\Delta C'_{VM}$ is constant, and the change in thickness with time (dx/dt) = $k't$ here k' = D_{VM} ($\Delta C'_{VM}$)/const. Integrating for x=0 at t=0, we get:

$$x^2 = 2\,k't \qquad (2.2)$$

This is the parabolic rate law, which shows that for diffusion controlled oxide growth, growth of the scale thickness is parabolic with time. Also, since the cation vacancy concentration is related to pO_2 by the reaction equation, we have C_{VM}= const. * $pO_2^{1/n}$ from which we can see the rate constant k' will be proportional to pO_2.

When the rate is limited by solid state diffusion through a growing scale, measuring oxidation either by change of scale thickness or by weight changes, the change will be proportional to the square root of time. This is referred to as parabolic oxidation.

$$x\,dx = k^2 dt \qquad (2.3)$$

where x is thickness and k' is the parabolic rate constant.

Rate of oxidation may instead follow a linear rate law when not restricted by solid state diffusion through a growing scale:

$$x = k_l t \qquad (2.4)$$

where x is the thickness and $\underline{k_l}$ is the linear rate constant. In this case the oxidation is not limited by diffusion. This may be the case if the diffusion is more rapid than the oxidation reaction rate. If the oxide is a vapor, and that vapor leaves quickly enough, the oxide does not build up enough to provide a diffusion barrier and the oxidation proceeds

linearly with time. Change in weight or thickness will be negative for a volatile oxide, and will be linear with time.

If for a volatile oxide product the oxide is not removed quickly but is still gaseous, rate kinetics will a combination of both linear and parabolic rates,

$$dx/dt = k'/x - k_l \quad (2.5)$$

During oxidation an oxide coating is formed which acts as a diffusion barrier, and parabolic oxidation progresses through the scale, however there is also a linear evaporation of the oxide scale. A steady-state oxide thickness (X) will be reached as the parabolic oxide growth defined by k' matches the linear evaporation rate of the oxide defined by k_l.

$$X = k'/k_l \quad (2.6)$$

At this steady state thickness, $dx/dt=0$, and measured thickness will be unchanging, while weight loss is linear.

2.2.2.3. High Temperature Oxidation of Mo

Molybdenum can exist in several oxidation states, most commonly +4 and +6. For Molybdenum below 500°C the reaction rate dominates and oxidation rates are very low and not a major concern. As temperatures approach 500°C, begins to form oxides MoO_2 and MoO_3.[25] The reaction rates increase and MoO_3 forms a yellow colored scale of needle-shaped crystals which does resist oxygen permeation, thus a scale limited parabolic rate is seen and rates of oxidation remain slow. Oxidation of molybdenum begins to become significant above 500°C when the molybdenum trioxide scale starts to evaporate. At higher temperatures the scale becomes less and less protective and oxygen transport to the metal is increasingly more rapid as temperatures rise. There is a

competition between the consumption of the Mo to form a MoO_3 scale and the evaporation of that scale similar to the paralinear oxidation scheme described above (Eq. 2.6). The competing gas diffusion and linear evaporation rates are both high and it reaches a steady state where formation and evaporation are equal and consumption of the metal is steady. Around 700°C the reaction rates are fast enough that they can be considered instantaneous, and the MoO_3 oxide becomes sufficiently volatile that there is no permanent scale to offer protection. The volatile MoO_3 has a limited range of possible liquid phase and is solid below 816°C but is still able to sublime to vapor at appreciable rates below the melting point; even below 800°C it volatilizes nearly as rapidly as it is formed.

Reaction products build up a gaseous barrier around the surface, and gaseous diffusion of the reaction products away becomes the rate limiting step. This is a fast process even in stagnant air, and metal consumption is rapid and linear (Eq. 2.4). Furthermore, the gaseous diffusion rates can be drastically increased by increasing gas flow rate[26], up to a maximum for a given temperature where the partial pressure of MoO_3 is minimized near the sample surface and the very quick reaction of

$$Mo + 3/2\ O_2 \rightarrow MoO_{3(g)}$$

is the only limiting step. In turbine blade applications very high flow leads to this sort of rapid catastrophic consumption of the molybdenum.

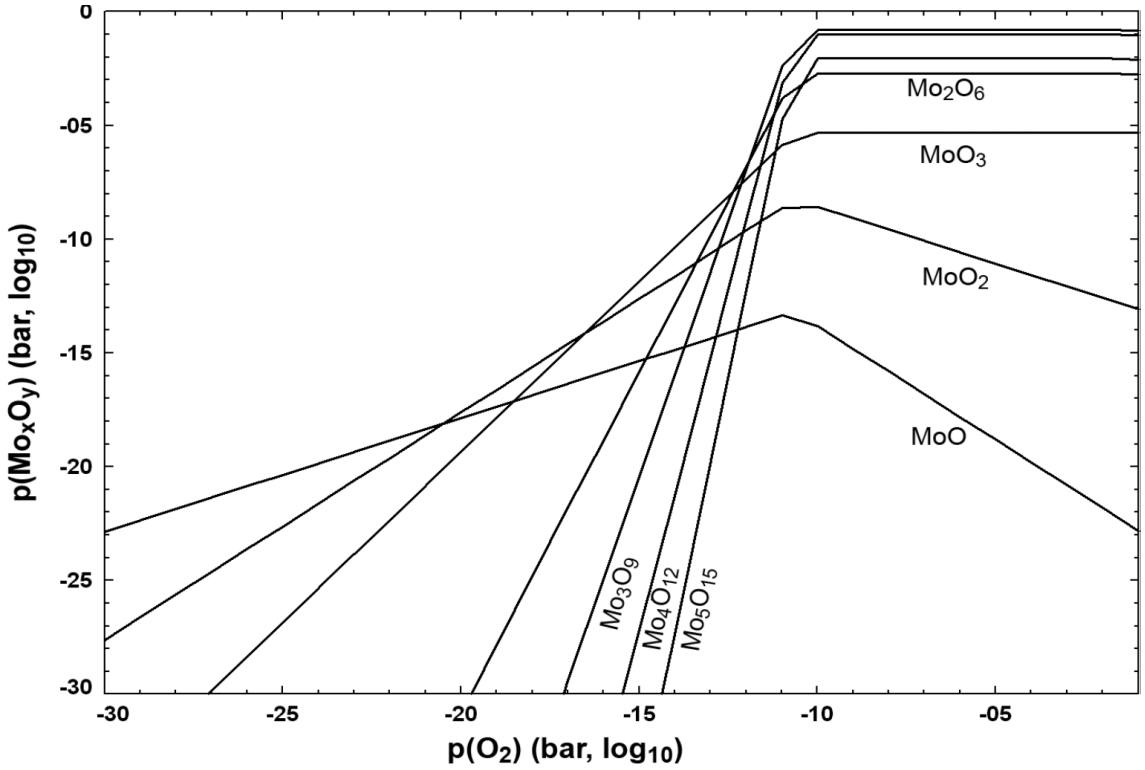

Figure 2.4: Partial pressures of Mo oxides versus partial pressure of Oxygen.[27]

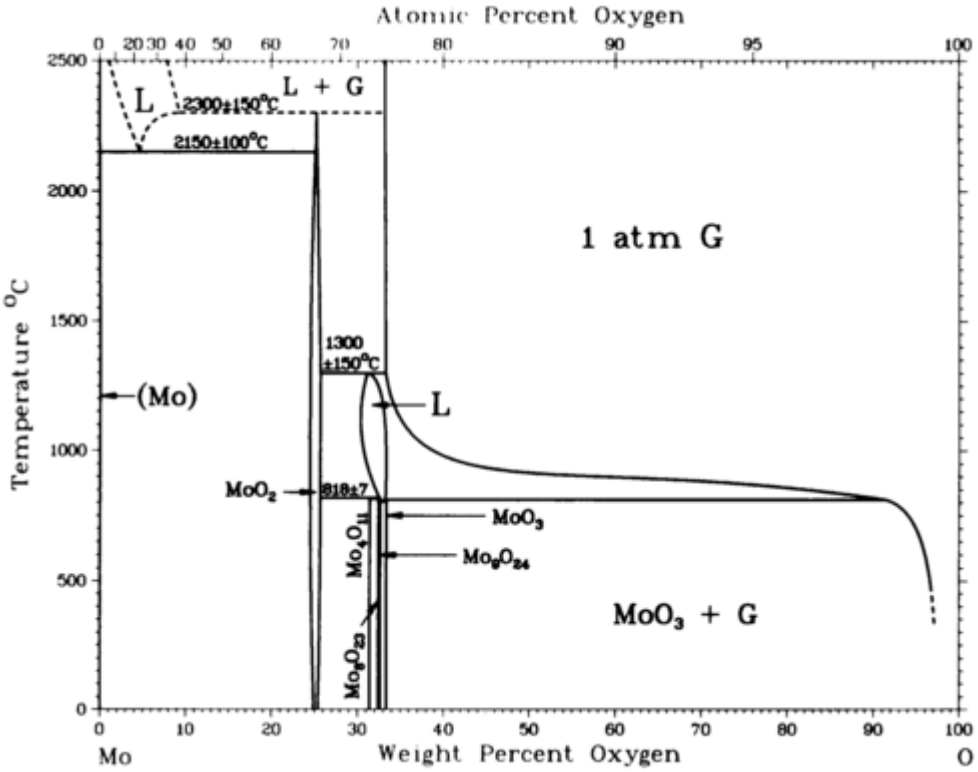

Figure 2.5: The Oxygen – Molybdenum binary phase diagram. [28]

The Mo-O phase diagram is shown in Figure 2.5. There are a number of intermediate oxides possible, but the +4 and +6 MoO_2 and MoO_3 dominate.[29] The solid MoO_3 can be easily reduced in hydrogen to MoO_2 even at temperatures near 450-470°C, but MoO_2 → Mo reduction is slow in hydrogen until 1100°C.[25]

Water vapor will also react with MoO_3(s) to form a volatile hydroxide, which can be significant in humid environments in the 400-600°C temperature range, as suggested by the vapor pressure diagrams of the $MoO_2(OH)_2$ species created by Speiser and St. Pierre[30]. This can increase the oxidation rates at temperatures slightly lower than is usually important for Mo, but above 600°C, the MoO_3 is increasingly more significant and humid environments have less effect at high temperature.

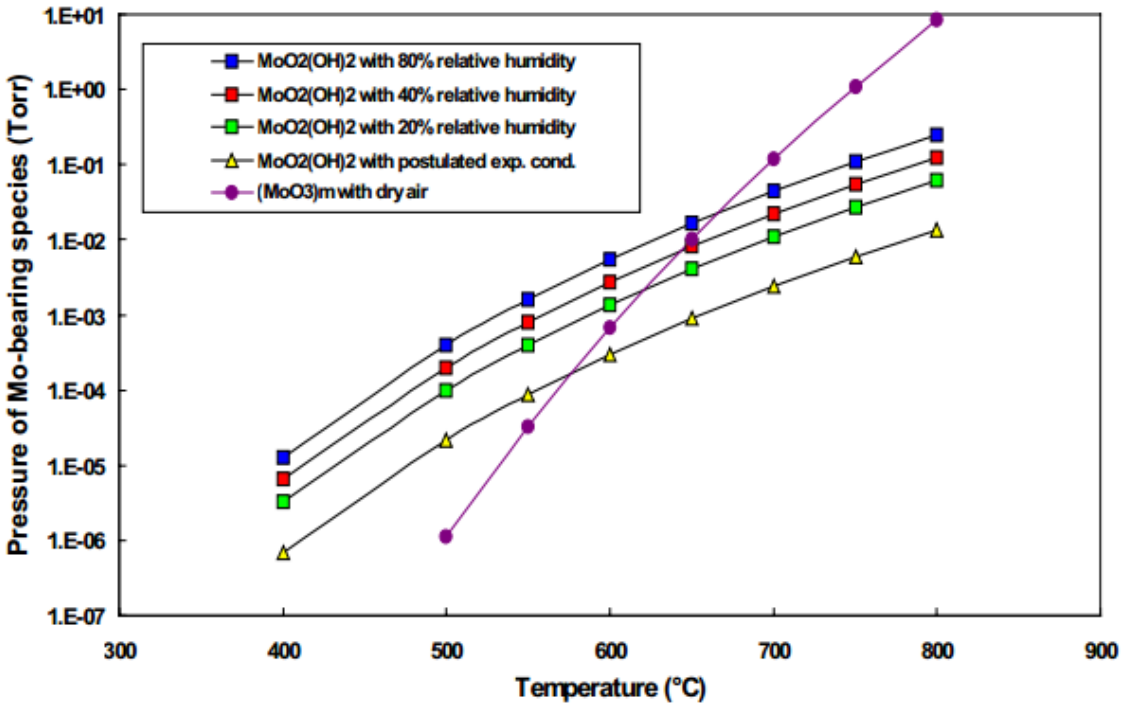

Figure 2.6: The Vapor pressures of Mo oxide and hydroxide species as a function of T and relative humidity.[32]

Figure 2.6 shows the variation in vapor pressure and importance of the MoO_3 volatility becoming dominant over the various hydroxide vapors above 600°C. As temperature increases, so does the vapor pressure of the MoO_3. The MoO_3 vapor has been shown to exist primarily in polymeric forms[33], with the $(MoO_3)_x$ where x=3, 4 and 5 being the dominant polymer species. The vapor pressure of MoO_3 exceeds atmospheric pressure and boils at 1150°C but the contribution of higher volatile polymers as well as volatile hydroxides add to the total vapor pressure and could reduce the boiling point below 1100°C.

Attempts have been made to prevent oxidation of molybdenum based on an applied coating to the molybdenum surface.[34] Undesirably, the coating could easily be compromised and minor damage to the coating could expose the underlying Molybdenum leading to rapid erosion and pesting.[35] Further, mismatch in the thermal expansions leads to spalling during the repeated thermal cycling and high heating and cooling rates associated with jet turbine use.

2.3. $MoSi_2$

Despite the rapid oxidation of Molybdenum at high temperatures, Molybdenum disilicide is a well known refractory used commonly to make heating elements.[36, 37] In the case of $MoSi_2$, the oxidation issues associated with Molybdenum are circumvented by formation of a protective silica scale. At high temperatures in oxidizing environments there is a simultaneous oxidation of Mo to molybdenum oxide:

$$2Mo + 3\,O_2 \rightarrow 2\,MoO_3$$

and Si to silica:

$$Si + O_2 \rightarrow SiO_2$$

The silica forms on the entire surface and quickly coalesces to a continuous scale. This then shifts from the rapid linear oxidation seen for pure Mo to a parabolic oxidation limited by the diffusion of oxygen through the silica scale. Because it is a pure silica scale, oxygen permeability is quite low and oxidation is effectively prevented. Unfortunately at lower temperatures around 700°C the oxidation of Mo is still significant, but the silica is unable to achieve continuity which results in a phenomenon known as pesting and can lead to eventual degradation of the entire piece. This can be prevented by initially heating the $MoSi_2$ to high temperatures in order to form the coating, but intermediate temperatures are generally avoided for $MoSi_2$.

While $MoSi_2$ has satisfactory oxidation resistance, it has very poor mechanical properties. At room temperature it has low strength and very low toughness, and the strength decreases rapidly with temperature. At high temperature it has nearly no rigidity and readily slumps making it useless for structural applications.

2.4. The MoSiB System

In the Early 90's Acink and Meyer[1] began investigating other Mo silicides such as Mo_3Si, and found that while it had poorer resistance to oxidation than $MoSi_2$, the oxidation rates could be significantly reduced by including Boron which reacts to form a flowing borosilicate scale. The Molybdenum-Silicon-Boron ternary phase diagram had been developed by Nowotny[38] in 1957 and was expanded by Perepezko and Nunes[39] in the early 90's. The isothermal section of the Mo-rich corner at 1600°C is shown in Figure 2.7, and the phases and relations are all effectively stable down to room temperature.

In 1997, Berczik[2, 3] first patented alloys in the phase triangle highlighted in green, which contains Mo_{ss} and the intermetallics A15 (Mo_3Si) and T2 (Mo_5SiB_2). These

three components have high melting temperatures and form stable equilibrium phases. The alloys were developed under the premise that they would have the high temperature mechanical properties of $Mo_{(ss)}$ phase while the equilibrium T2 and A15 intermetallics would react to form a molten borosilicate coating for oxidation protection similar to $MoSi_2$. The boron from the T2 phase allows for the fluxing of the molten silicate so that adequate surface coverage can be achieved quickly. The properties and structures of the phases are shown in Figure 2.8 and Table 2.3, and are discussed in the following sections. There is limited solubility between the various phases and the three phases are all stable from low to high temperature, without any phase transitions that might otherwise lead to mechanical stresses or unpredictable properties.

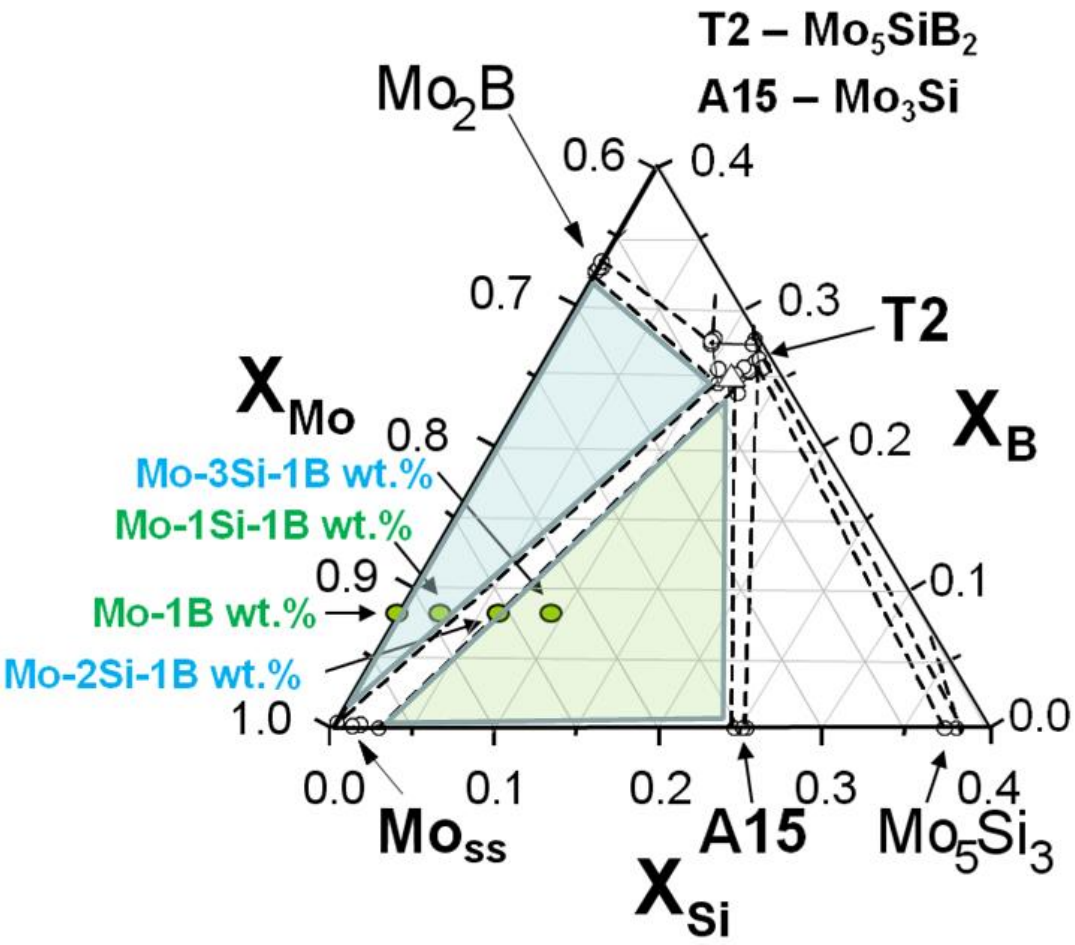

Figure 2.7: Isothermal section close-up of the Mo rich corner of the of the Mo-Si-B ternary phase diagram for 1600°C.[39]

2.4.1. Properties of the MoSiB phases

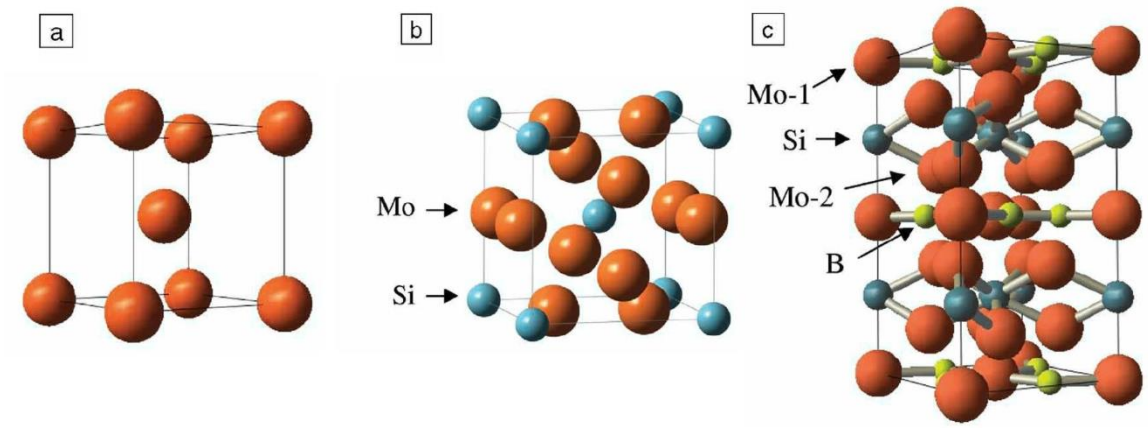

Figure 2.8: Unit cell structures of the relevant phases, a. α-Mo, b. Mo_3Si (A15) and c. Mo_5SiB_2 (T2). [39]

Table 2.2 Elemental properties of MoSiB constituents

	Elemental properties			
	Mo	**Si**	**B**	**O**
Density (g/cm3)	10.28	2.33	2.35	gas
at wt	96	28.1	10.8	16
Atom rad (Å)	1.54	1.17	0.85	0.73

Table 2.3: Selected properties of the relevant Mo-Si-B phases

	Properties of Relevant Phases					
	a-Mo	**$MoSi_2$**	**Mo_3Si**	**Mo_5SiB_2**	**Mo_2B**	**SiO_2**
Atomic wt. (g/mol)	95.96	152.13	564.3	529.71	202.7	60.08
T_m (C)	2623	2030	2025	2180	2273	1650
Heat cap. (J/mol K)	24.06	635.91	186.2	-	69	-
Density (g/cm3)	10.28	6.29	8.97	8.81	9.2	~2.4
Structure	BCC	Tetragonal I4/mmm	4mcm (A15)	Tetragonal D81 (T2)	4mcm (Al2Cu)	glass
T cond (W/molK)	138	53.9	-	-	-	-
CTE (E–6/°C) @25C	~5	-	~3	~6	-	~0.5
CTE @ 1300C	~6	-	~7	~8.5	-	-

2.4.2.1. Properties o' T2

From the initial works by Akinc and Meyer on Mo_3Si and Mo_5Si_3, addition of B leads to the Mo_5SiB_2 phase. The ternary intermetallic has a tetragonal unit cell (Figure 2.8) with an I4/mcm space group – commonly referred to as the T2 formation. Throughout this dissertation, "T2" will refer to the Mo_5SiB_2 phase. Numerous studies have identified that the actual composition typically sits at the B rich side of the T2 phase field with an effective composition of $Mo_5Si_{0.89}B_{2.11}$. The density varies from 8.8- 9 g/cc and melting point has been observed near 2180°C. It has a very low and nearly isotropic

thermal expansion of $7.9\pm0.1\times10^{-6}\ K^{-1}$ at room temperature which changes little with increasing temperatures, making it a good match with Mo. Ihara, Ito and Tanaka [40] isolated single crystalline Mo_5SiB_2 to study mechanical properties. Its mechanical properties at room temperature are poor; it has low fracture toughness around 2 MPa√m and is otherwise similar to $MoSi_2$. At higher temperature it has good creep resistance and maintains rigidity much better than $MoSi_2$ but fractures in a brittle manner and still has low fracture toughness. [41]

2.4.2.2.Properties o' A15

Along with the T2 phase, three-phase compositions near the Mo-rich corner of the Mo-Si-B ternary will also include the high Mo silicide Mo_3Si. This is too high of a Mo content to achieve silica passivation akin to $MoSi_2$, but it is capable of becoming protective when fluxed with B from the T2 phase. The Mo_3Si has the cubic Cr_3Si type structure known as A15, and "A15" will be used to refer to the Mo_3Si phase. The A15 phase has a lower density than Mo at 8.9g/cc. It melts at 2025°C and the Mo_3Si-Mo_5Si_3 eutectic occurs at 2020°C[42]. Low temperature mechanical properties are also poor with low fracture toughness <2 MPa√m, however A15 possesses a ductile to brittle temperature near 1100°C above which toughness increases to 3.5 MPa√m at 1300°C. It also exhibits good creep resistance at high temperatures. [40]

2.4.2.3. Properties o' α-Mo Solid Solution

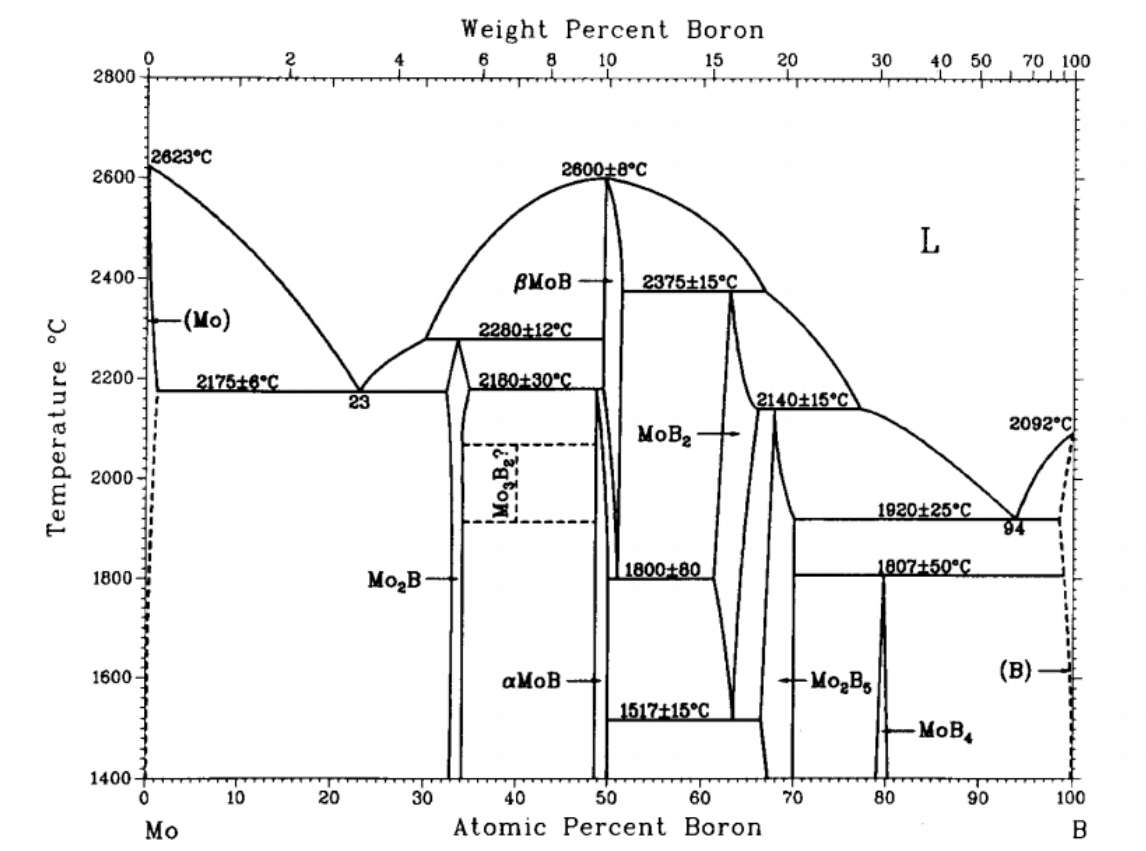

Figure 2.9: Mo-B binary phase diagram. [43]

Mo in MoSiB alloys differs from pure Mo. The α-Mo solid solution phase will be referred to as Mo_{ss} or generally as Mo. The BCC α-Mo lattice does not accommodate B easily and has almost no B solubility but permits increasing solubility of Si at higher temperatures (Figure 2.3 and Figure 2.7). Si in Mo_{ss} is low, <1at% until 1300°C but increases to nearly 3at% at 1600°C and above. Furthermore, the dissolution out is very slow, and even with long annealing times the amount of silicon in solid solution in Mo remains at the maximum levels dictated by the maximum temperature reached.[44]

Silicon in solution with Mo will reduce toughness and increase the DBTT. However it may also reduce creep and grain growth by solute drag. The influence of silicon on the strength and fracture toughness of molybdenum was studied by Sturm and Helimaier.[20] Mo_{ss} samples containing up to 1 wt % (3.3 at %) Si were fabricated by powder-metallurgical processing and HIP. Their lattice parameters, elastic constants, densities, grain sizes, strengths, ductility, and fracture toughness values were measured. Generally, Si additions caused pronounced solid solution strengthening with a corresponding reduction in toughness. Fracture toughness decreased from 24 MPa √m to only 4 MPa √m with addition of 1 wt% Si in Mo solid solution. For small Si concentrations (≤0.1 wt.%) solid solution softening was observed at room temperature and below. Above 0.1 wt% Si however, the room temperature ductility and fracture toughness dropped precipitously. This is attributed to the increase in strength and reduced yielding and is accompanied by a transition from transgranular to intergranular fracture. The Si atoms preferentially segregate to grain boundaries in Mo_{ss} to minimize stresses caused by substitution of the smaller size of the Si atom in the Mo BCC lattice. Because the Si locates preferentially on the grain boundaries it enables brittle failure along grain boundaries. While smaller grains means more grain boundary area to spread out the silicon, even with high grain boundary area only a small fraction of Si is needed to embrittle grain boundaries thus negating or reversing the Hall-Petch behavior. In Sturm & Heilmaier's study, the yield strength was insensitive to the grain size, i.e., a Hall–Petch relationship was not observed.

In another study, Heilmaier[45] again saw no effects on linear elastic strength with varying grain sizes and notes that as little as 0.3 at% Si in Mo_{ss} can lead to brittle failure

at room temperature. Burk et. al. [46]investigated addition of Zr to improve ductility in Si containing compositions. Zr is a larger atom than Mo and creates compressive stresses when substituting on Mo sites. The compressive stresses can link and negate the tensile stresses of the Si substitution and reduce the driving force for Si segregation. Compositions were prepared by mechanical alloying with 0.7v% Y_2O_3, a 0.7v% La_2O_3 and a 1at% Zr to affect mechanical behavior. For a-Mo with 1.5 at% Si, addition of Zr was shown by Auger analysis of boundaries to indeed reduce the Si levels at the boundary, which lead to an increase in ductility. The increased ductility was accompanied by an 8% increase in transgranular failure supporting the proposed mechanism of toughening, however some gettering of O by Zr may also be contributing to the improved mechanical behavior much similar to the TZM alloys. Unfortunately Zr proves to be catastrophic to oxidation protection above 1150 °C.

The finite solubility of Si in Mo_{ss} allows diffusion of Si through the Mo lattice, however the self-diffusion of Mo in pure BCC Mo has been measured as $1.5x10^{-17}$ m^2/s at 1600°C and so diffusion is quite slow[47]. In the A15, Mo_3Si has a body centered cubic Si frame with two Mo atoms at each of the face centers. The Mo atoms produce saddle points between nearest Si-Si neighbors and limit diffusion in that system, which causes slow Si and Mo diffusion in A15 as well. Diffusion is also slow for the body centered tetragonal T2 where the layered structure makes Si self-diffusion difficult along any direction except along the Si planes parallel to the c-axis. B may have some mobility by substitution and interdiffusion with Si but interdiffusion coefficients of Si and B have been measured for T2 at 1600°C and are on the order of 10^{-14} to 10^{-15} m^2/s, with corresponding activation energies of approximately 355kJ/mol for Si and 338 kJ/mol for

B.[48] The slow diffusion of the atoms in each of the phases in this system is beneficial for high temperature stability and is effective in limiting creep and grain growth but can make annealing to rearrange the microstructure or equilibrate solid solution excess ineffective and prohibitively slow.

2.5. Multiphase Alloys

Some work has investigated the 2 phase field which consists of Mo and T2 only. The phase field however is inherently limited to a specific B:Si ratio dictated by the T2 stoichiometry. Sakidja et al. [49] managed to increase the range of T2 around stoichiometry by alloying with Nb and Cr. Ideally this could both simplify the system and reduce driving force for solute segregation by replacing the Mo. Unfortunately the limitations on oxidation resistance are too great, due to both the limited B:Si composition ratio of the glass, and the lower content allowable in order to maintain continuous Mo for mechanical properties. Other issues were encountered because of the slow diffusion which results in nonequilibrium A15 and Mo_2B based on local inhomogeneties.

The three-phase compositions have focused on two main categories, those optimized for oxidation resistance which is of interest in scientific consideration, and those optimized for structural commercial use. The first are those alloys investigated in what is often referred to as the Akinc & Meyer phase triangle, which consist of Mo_5Si_3, Mo_3Si and Mo_5SiB_2. These provide excellent oxidation protection and have advantages in terms of toughness over the related $MoSi_2$ system, and were essential in identifying the possibility for higher Mo-content silicides to become oxidation resistant with the addition of boron. However, these brittle Mo intermetallic alloys still have low toughness and are unusable in demanding structural applications.

The other group of compositions, sometimes called the Berczik triangle, is highlighted in green in Figure 2.7. It encompasses the range patented by Berczik containing Mo_3Si, and Mo_5SiB_2 as well as the pure α-Mo solid solution phase. This covers Mo-Si-B system from 1.6–15.2 at% Si and 0.0-39.4 at% B. The Mo, even at low fractions provides great toughening. At low fractions the Mo act to arrest cracks, but when the Mo phase is continuous, large benefits to toughness can be realized while the boron and silicon in the intermetallics is still able to create oxidation protection. Primary focus of the Berczik studies as well as our research has focused on 3-phase alloys in this field with 3 wt% Si and 1 wt% B, so-called 3:1; indicated by a green dot in Figure 2.7.

2.6. Oxidation in MoSiB Alloys

2.6.1. Oxidation Below 1000°C

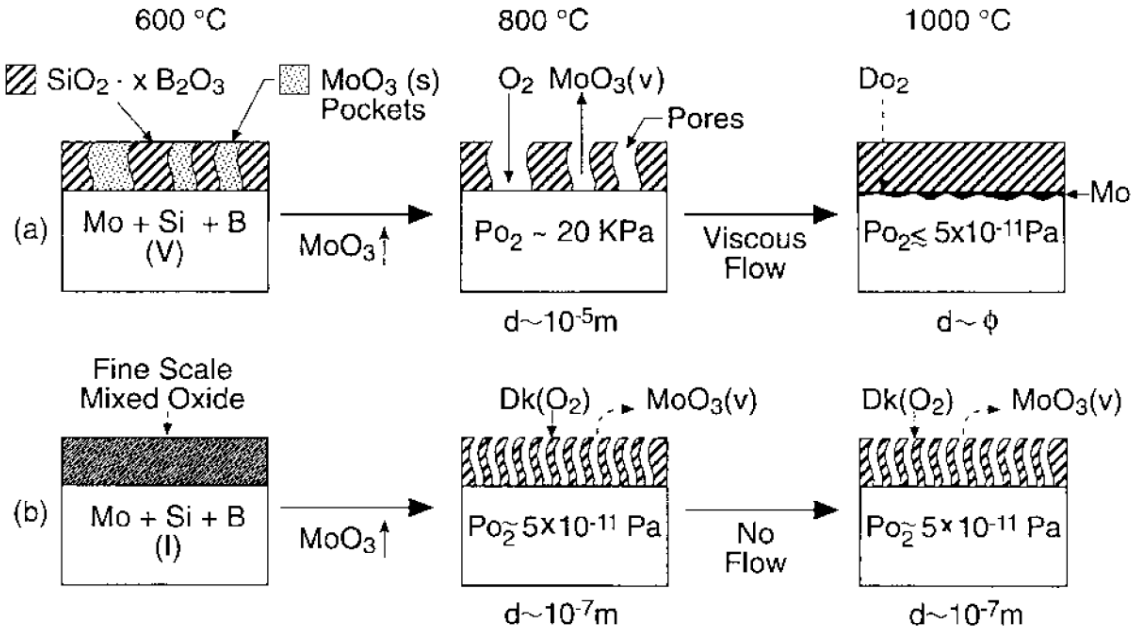

Figure 2.10: Schematic of oxidation protection on MoSiB Alloys. Top when B is present, bottom Mo3Si without B. [1, 50]

The oxidation of MoSiB alloys at lower temperatures is very similar to that of pure Mo and below 600°C the oxidation rates are inconsequential. As with pure Mo, oxidation begins to become increasingly more significant above 600°C when the molybdenum trioxide scale evaporation is noticeable, but like the pesting case for $MoSi_2$, at these temperatures silica and boron cannot form a protective coating. No protection exists until around 750°C the boron and silica react forming a boron-fluxed silica glass[1] which spreads to coat the surface. Along with the reaction of the intermetallics to form MoO_3 and glass there is a simultaneous rapid reaction of any still-exposed Mo. This is the

first oxidation regime of concern, the time where the coating is forming but is not yet fully formed and there is a transient weight loss of molybdenum.

2.6.2. Oxidation Above 1100°C

The expected use temperatures are above 1100°C, and should demonstrate oxidation resistance at least to 1300°C, and perhaps up to 1400°C or higher. At these temperatures MoSiB alloys exhibit a 2 part oxidation resistance which can be broken down into two main regimes; the transient and the parabolic. The transient regime (*i* in Figure 2.11) represents the linear losses when subjected to temperatures of 800°C and above while there is evaporation of exposed molybdenum and the weight loss is rapid and linear. It behaves similarly to the oxidation of pure molybdenum where the rate is limited only by the inward and outward diffusion of the gaseous reactants and products, except that in the MoSiB case it's also limited by the amount of exposed molybdenum at the surface.

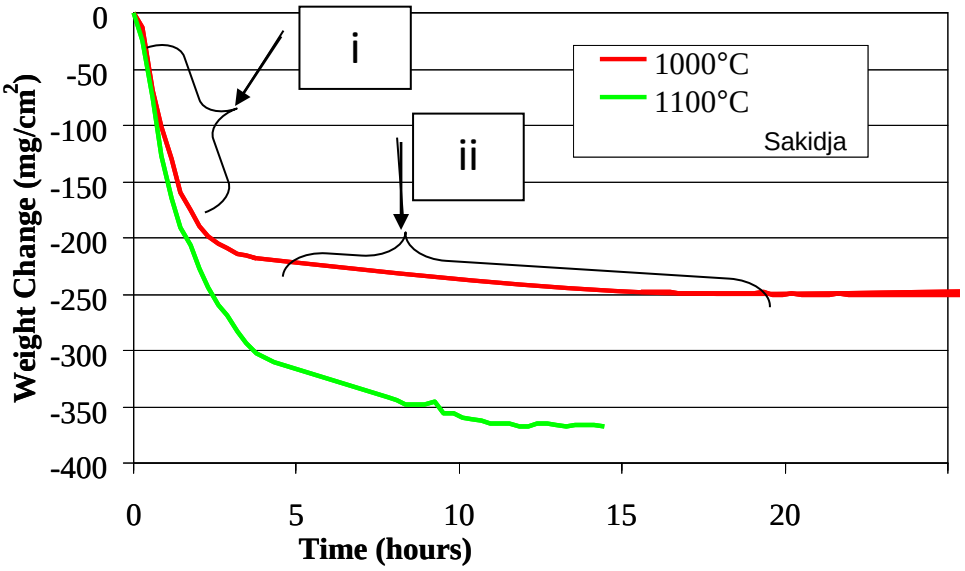

Figure 2.11: Example of the 2 stage oxidation protection shown as weight loss vs time for 3:1 MoSiB alloys in air. "i" indicates the initial period in the first few minutes to hours of rapid transient loss, and "ii" is the second period of parabolic loss once a coating has formed.

During the initial transient period while MoO_3 is evaporating away there is also a simultaneous reaction of the T2 and A15 which oxidize to form B_2O_3 and SiO_2:

$$Mo_3Si + O_2 \rightarrow MoO_{3(g)} + SiO_{2(l)}$$

and

$$Mo_5SiB_2 + O_2 \rightarrow MoO_{3(g)} + B_2O_{3\,(l)} + SiO_{2(l)}$$

When temperatures exceed 800°C the silica and boria are able to coalesce and the boria acts to actively flux regions of high silica forming a borosilicate glass. With increasing temperature the glass viscosity lowers, aiding the spreading of the glass over the boron and silicon deficient regions of pure Mo_{ss} (Figure 2.10).

Some finite solubility of MoO_3 remains in the newly forming glass while most continues to evaporate away. Two atomic percent of Molybdenum is known in glazes to give yellowing color, but little or no additional solubility is possible[51]. Mo also leads to

some opacification of glazes because it devitrifies on cooling when present at higher fractions. It's also been shown to reduce surface tension in sealing glasses and it may enhance the sealing of the borosilicate coating.

The transient weight loss regime concludes once sufficient borosilicate has formed and can completely coat over the surface, preventing gaseous oxygen from reaching the reactive Mo and intermetallics beneath. Once a complete coating is formed some time is required for homogenization of the glass but generally once it is sealed, the transient regime is considered over and the second parabolic regime begins. Further oxidation rate is greatly slowed and becomes dependent on the rate of oxygen diffusion inward through the glass layer and MoO_3 gas out. It's not fully determined whether it's the MoO_3 outward or O_2 inward which is rate limiting, but based on the $MoSi_2$ system and considerations of activation energy, it appears Oxygen diffusion dominates.

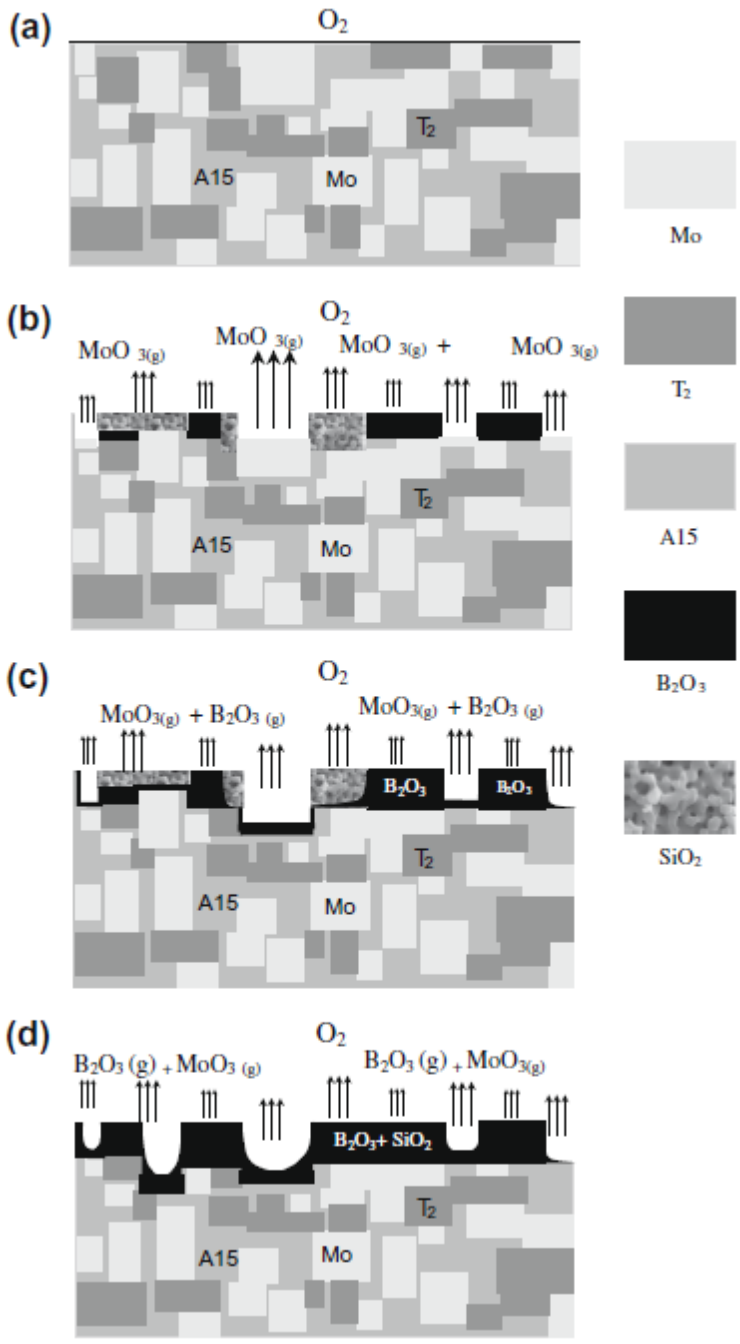

Figure 2.12: Example schematic of oxidation mechanisms for MoSiB. [52]

The schematic Figure 2.12is taken from Rioult [52] and illustrates the mechanisms which occur during the formation of the borosilicate scale, whereby the MoO_3 evaporates from each phase upon initial exposure to oxygen (a); the Mo continues to evaporate from pure Mo grains, while pure silica forms over A15 and borosilicate forms over T2 (b); then the borosilicate fluxes the pure silica regions and coats the surface (c) resulting in a final uneven but complete coating through which a slow evaporation of B_2O_3 and MoO_3 proceeds (d).

Once the borosilicate coating is complete, the weight loss with time is no longer linear but parabolically proportional to the square root of time, similar to Eq. 2.6, and the parabolic rate constant is controlled by diffusion rate through the film. The film thickness increases with time but at a decreasing rate due to limiting oxygen transport. An example of the glassy coating for MoSiB alloy at 1100°C is shown in Figure 2.13.

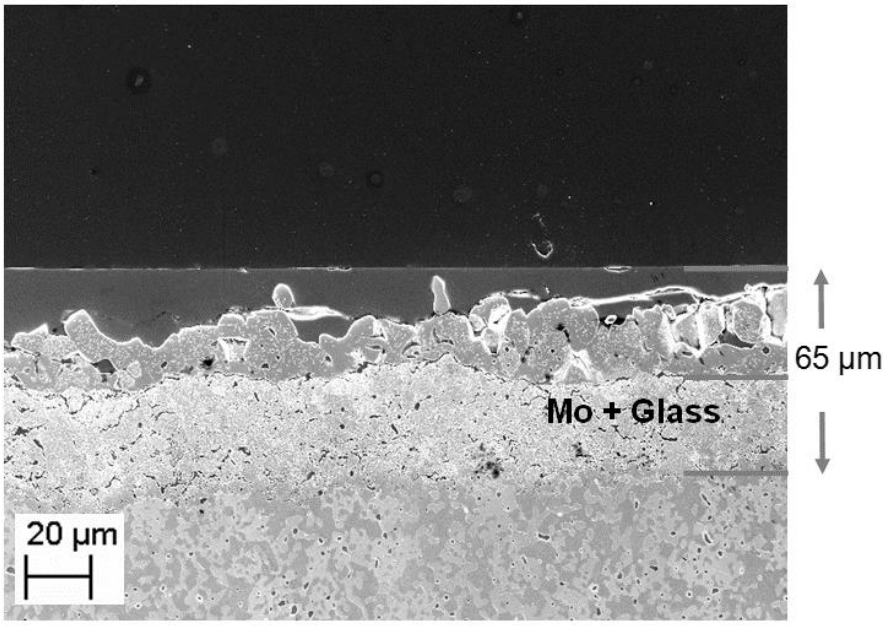

Figure 2.13: Glass coating of a 3:1 MoSiB alloy oxidized for 100 hr. at 1100°C.

2.6.3. Composition Effects on Oxidation

The time, temperature and severity of the losses depend significantly on glass viscosity which in turn is most easily defined by the glass composition.[7] Figure 2.14 shows the effect of boron on silica. Boron is one of the most effective modifiers of silicate glasses; the addition of 30 mol% B_2O_3 will reduce the viscosity of a silica glass by eight orders of magnitude.

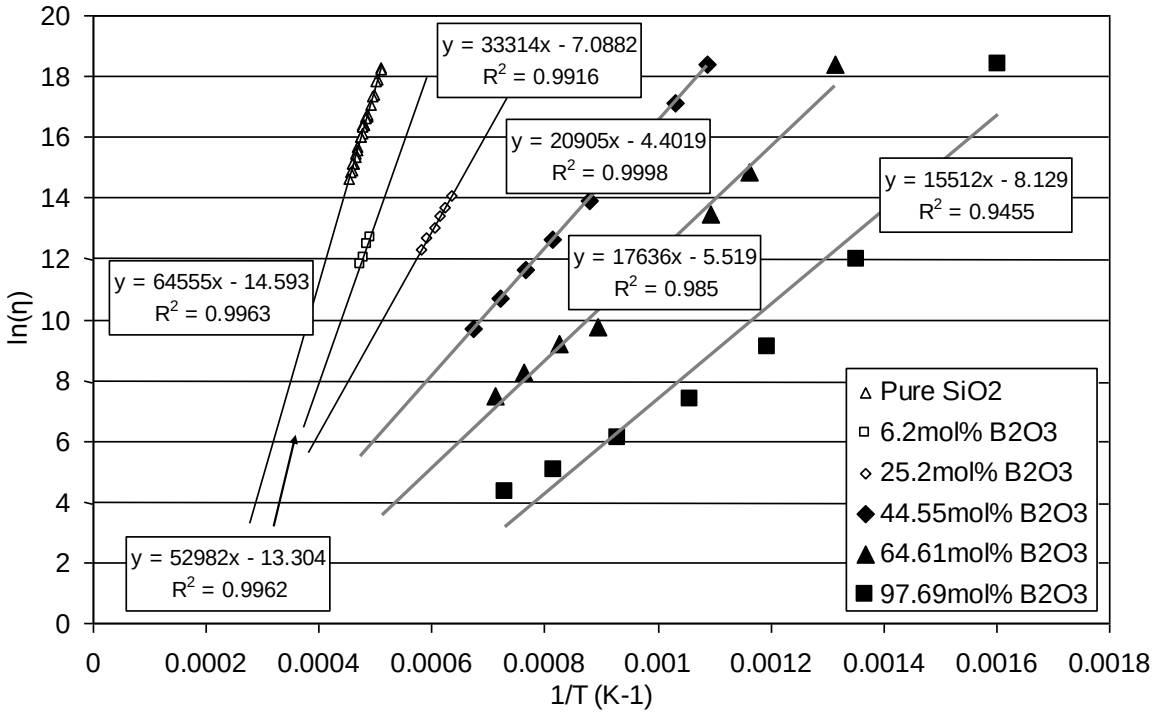

Figure 2.14: The viscosity (Pa·s) as a function of temperature for various borosilicate compositions, fit to data obtained from Brückner [53] and Priven [54]

During the transient stage when the glass is beginning to form, boron acts to lower the melting point of the glass as well as reduce the viscosity for a faster and more effective coating of the surface.[55] Acink and Meyer[1] (Figure 2.11), and Helmick also[56], observed that pores were located above the Mo regions and gaseous diffusion of

oxygen through the pores in the glass extends the transient regime. In order to suppress transient losses through such pores it is very important for the glass scale to be able to flow together into a coherent continuous layer over the Mo regions. High boron content promotes flow for sealing of the pores and is important in limiting transient losses.

Once the coating is formed however, the oxidation rate is dominated instead by diffusion through the glass, and the diffusivity of oxygen in glasses is known to be a function of the viscosity which decreases with increasing boron content (Figure 2.14). Thus long term protection favors lower B:Si ratios. Too low of a viscosity can be problematic in the transient regime also. At 700°C, Parthasarathy[57, 58] observed loss by bubbling through the glassy layer. The glass had a reported viscosity of $5*10^6$ Pa-s, which is lower than the viscosity of 10^9 Pa-s needed to suppress bubble formation in the silicate melt. At higher temperatures above ~1150°C the partial pressures of the vapor species which include the polymeric and hydrated MoO_3 oxides as well as B_2O_3 can exceed ambient pressure and lead to bubble formation.

The B:Si ratio must be carefully tailored for the intended application, and must have high enough B:Si to seal pores and limit weight losses during the transient stage but low enough to prohibit formation of bubbles and to slow diffusion of reactants and products once a good coating is formed.

Mendiratta[57] attempted to optimize the B: Si ratio of the borosilicate coating and found a 1:1 B:Si atomic ratio ideal, at 11at% each, but did not investigate higher Si contents than 1:1. In his work he tested six different Mo–Si–B alloy compositions in a cyclic oxidation environment that cycled from 1200°C to room temperature to determine behavior as a function of B:Si. The Mo–11Si–11B (at.%) alloy performed best in this

type of test, showing a very small mass change over 100 h of testing. Alloys that did not perform well tended to have high levels of boron and lower levels of silicon. The worst performing alloy was Mo–4Si–10B, with Mo–7Si–11B improving slightly, then Mo–7Si–13B further improving, and Mo–7Si–14B showing the best performance of the silicon deficient alloys. This indicates that in the absence of silicon, the addition of boron may improve oxidation resistance slightly, but not significantly enough to be considered protective. It was also found that none of the alloys were passivated at lower temperatures, and all suffered from catastrophic oxidation between 700 and 800°C. Bubbles were observed in the Mo–11Si–11B alloy scale at 800°C, indicating that oxidation of molybdenum was occurring and that the MoO_3 bubbles were moving through the scale. This behavior illustrates the ease with which material may be transported across the protective scale if the alloy chemistry is not optimized.

Middlemas[59] developed a model for the oxidation of MoSiB alloys which considers the effects of glass composition on mass loss during both the transient and the diffusion controlled oxidation regimes. Based on composition effects on the porosity, viscosity, surface tension and diffusivity of the glass, an optimal Si:B ratio was determined which minimized the overall metal recession for a given temperature. For an alloy with 50% Mo by volume at 1100°C in air, the atomic Si:B ratio for minimal material loss was determined to be nearly 1:1, corresponding to approximately a 3:1 weight ratio which was pursued in the Mo-3Si-1B alloys. This composition is indicated in the green Berczik phase triangle highlighted in Figure 2.7.

2.6.2.1. B_2O_3 volatility

Also important is the volatility of B_2O_3 at higher temperatures. As discussed, high boron content is beneficial at the initial stages of oxidation and low boron content preferred for long term protection. Serendipitously, B_2O_3 is increasingly more volatile above 800°C which results in lower B contents at longer times - essentially raising the viscosity of the glass with time and temperature.

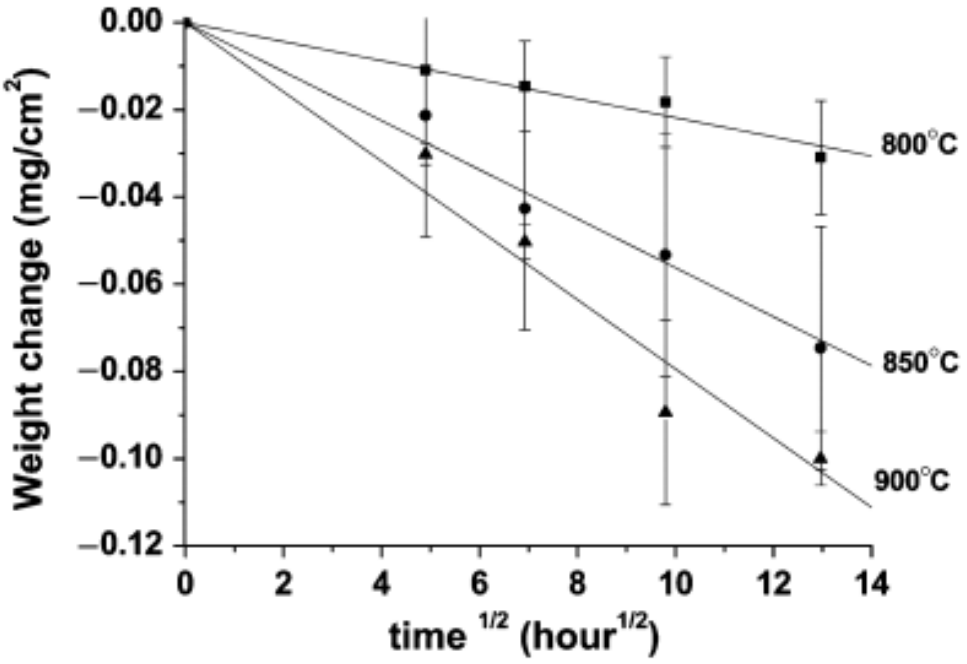

Figure 2.15: The measured weight change of a borosilicate glass with 2mol% B_2O_3 due to B_2O_3 volatilization.[60]

Figure 2.15 shows weight change of a borosilicate glass as a function of temperature. This was studied by Zhang et al. [60] in the 800-900°C range, for Sr/Ba sealing glasses which contain around 40 mol% Alkaline earth, 20% B_2O_3 and 40%SiO_2.

This hasn't been explicitly studied in the MoSiB system, and may be affected by presence of the Mo or other glass modifiers that may stabilize or destabilize the B_2O_3 in the borosilicate. The B_2O_3 volatilization is also affected by the flow rate surrounding the surface of the glass such that higher flow rates will enhance the B_2O_3 loss. Rate of boria loss also depends on the composition, and Zhang noted the total weight loss of 20mol% B_2O_3 glass was greater than order of magnitude higher than for a 2mol% B_2O_3 glass under the same conditions. The nonlinear increase in loss with higher boron contents may indicate that higher B_2O_3 fractions raise the volatility. Also phase separation is possible between the silica tetrahedra and borate groups which can make locally separated regions of high boron even more volatile.

The dominant gas species in dry air is BO_2, however in humid or post-combustion environments, the volatilization of boron is dramatically increased with increasing partial pressure of water vapor in the surrounding atmosphere. The formation of hydrated boric acids in wet atmospheres, most significantly as $B_3H_3O_6$, becomes a more and more important contributor to the overall vapor pressure with increasing water vapor partial pressure and at higher temperature.[61]

2.6.4. Effect of Microstructural Size Scale

In addition to the phases and composition present, the size scale and distribution of the phases in the microstructure is important to oxidation. In order for the oxidation protection to be effective the intermetallics should be closely spaced and evenly distributed – any large regions of pure Mo, or isolated A15 would be unable to protect themselves unless there is a flowing B-fluxed glass from nearby T2. Oxidation resistance benefits obviously by increased fraction of intermetallics, but at the cost of mechanical

properties which are dominated by the Mo_{ss}. For a given fraction of intermetallics however, Rioult et. al. [52] observed that a refined microstructure scale also benefits oxidation resistance. The transient stage shortened and the degree of material consumed is less when the size scale is small and the intermetallics evenly distributed.

In the studies by Rioult he examined MoSiB alloys which do not have continuous Mo matrix. He suggests that the T2 grains are essential in the formation of the coating, and that oxidation necessarily extends to at least a depth from the surface where from every given point a T2 grain is encountered. Statistically then, a finer and more homogenously distributed microstructure should require a lesser depth to encounter a T2 grain, and therefore a finer microstructure is able to seal faster and at lower depths of penetration. If instead the material contains a continuous matrix of Mo, it would make oxidation of the pure Mo more difficult to close off, however the basic premise remains of a finer microstructure requiring a lesser depth to form and coalesce a complete borosilicate coating.

2.6.5. Effect of Flow Rate

Flow rate is known to increase the oxidation of pure Mo. When the oxidation is limited only by gaseous diffusion of reactants in and products out, the increased availability of oxygen and removal of oxide directly increases the flow rate, however in the MoSiB system other factors must be considered. Helmick [56] investigated the effects of flow rate on the oxidation protection of MoSiB alloys. In one case he observed for a single sample oxidized in flowing air at 1cm/sec and 816°C that the leading edge of the sample behaved differently than the trailing edge. The downstream section of the sample had many bubbles while the upstream portion did not. The trailing edge was exposed to

an atmosphere which was enriched in MoO_3 vapor that had evaporated from the leading edge, and as a result the evaporation of MoO_3 from the trailing edge was reduced. This was also seen as MoO_3 spheres that were seen within the glass and illustrates the importance of removing MoO_3 vapor in order to form a continuous glass.

Further flow rate studies in Helmick's work investigated the oxidation of Mo-3Si-1B under static, 1cm/sec and 10cm/sec flow rates at temperatures of 816°C, 1000°C and 1100°C. At 816°C, static air is able to form a coating but flow rate increases oxidation and prevents a complete scale. The cause is attributed to an increased volatilization of B_2O_3 from the borosilicate in the flowing atmosphere, and that at the low temperature and reduced boria content, the glass is unable to flow enough to form a complete coating. At 1000°C however, the increased temperature permits lower viscosity of the glass and for all flow rates a coating is able to be formed. Again at 1100°C the flow rate becomes a concern. At the higher temperature the vapor pressure of the MoO_3 is greater, and for 1cm/sec the improved removal of MoO_3 vapor allows sealing of the borosilicate, however the vapor pressure of B_2O_3 is also higher and at 10cm/sec the volatility of boria again becomes a significant concern and results in too high of a glass viscosity to seal completely.

2.6.6. Internal Oxidation

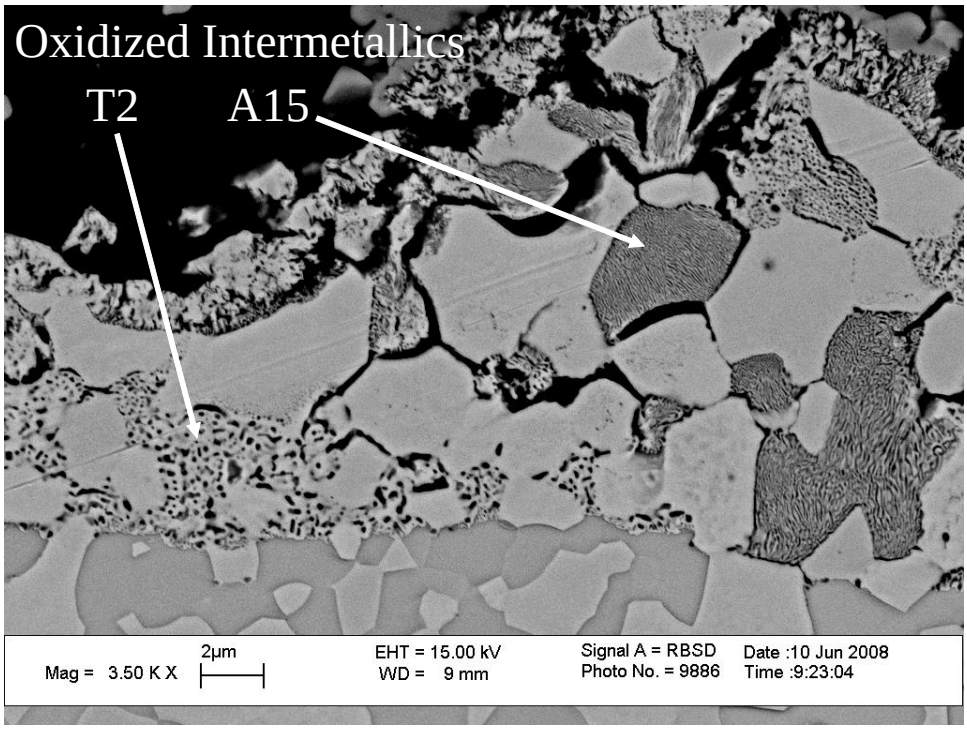

Figure 2.16: The Oxide-Alloy interface in a 3:1 MoSiB alloy oxidized in air at 1100°C.[59]

After the coating forms, when oxygen diffusion through the scale is limiting, oxidation still proceeds but at a much slower rate. When oxygen diffusion into the bulk is greater than the cations out, internal oxidation of the bulk occurs. Figure 2.16 shows the interface between the borosilicate and the bulk MoSiB from Middlemas after oxidation at 1100°C for 20h. It can be seen beneath the glass that there is a significant amount of internal oxidation present. The dark region at the top left of the micrograph is the formed glass. As the layer thickens the pO_2 decreases across the layer. When the pO_2 is low enough, MoO_3 is no longer the preferred oxidation product and MoO_2 is stable. Further into the alloy, the pO_2 at the oxide/alloy interface is low enough such that the Mo is

stable and Oxygen reacts preferentially with the Silicon and Boron in the intermetallics. This forms an internally oxidized zone below the glassy coating which consists of separated oxide and pure Mo within the intermetallic grains alongside unoxidized Mo grains. The indicated zones in Figure 2.16 are the regions of T2 and A15 which have been partially oxidized, while the light gray Mo regions have not. There is a volume expansion associated with the glass formed which causes the glass to be pushed out, thus separating the grains in this region and also contributing to growth of the glass layer. The same order of glass, MoO_2 and internal oxidation can also be seen in Figure 2.13.

2.6.7. Effect of Pre-oxidation and Low pO_2

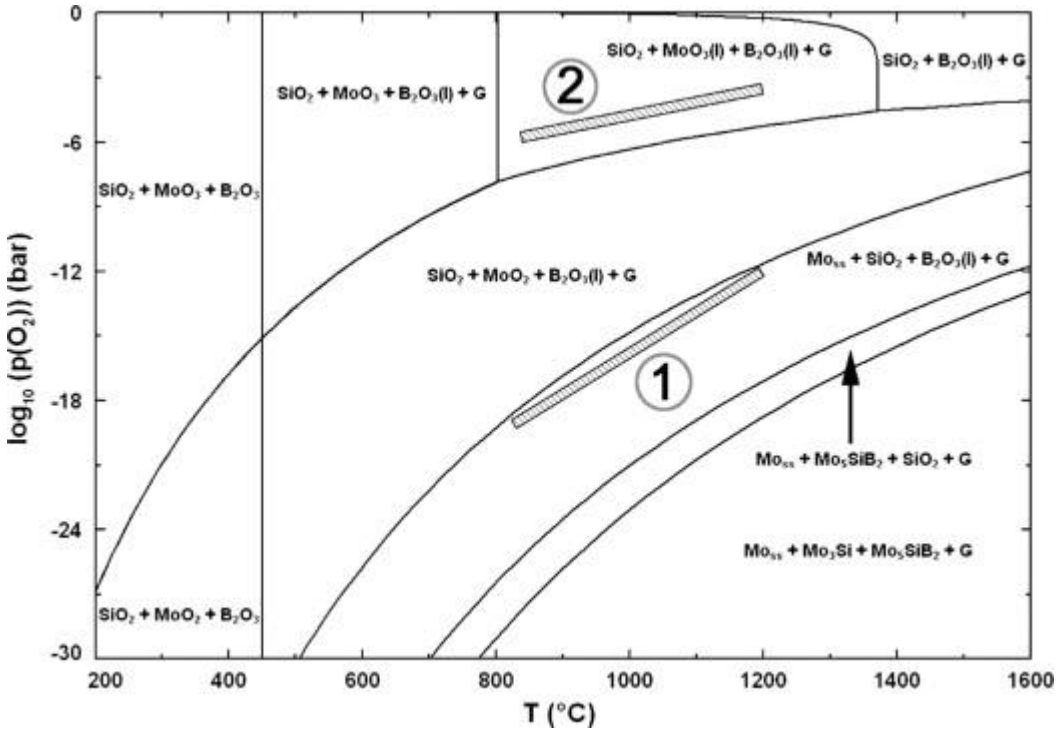

Figure 2.17: The oxide phase stability regions as a function of temperature and pO_2. [62]

The internal oxidation of B and Si is possible because B and Si have higher oxygen affinity than Mo, and at low pO_2 where the Mo is stable, B and Si still oxidize. The oxide phase stabilities are shown in Figure 2.17. Burk & Crist [62] examined the effect of low partial pressures of oxygen in order to form the borosilicate coating without any MoO_3 loss. Mo-MoO_2 equilibrium at 1200°C exists at partial pressures of oxygen of nearly 10 E^{-12} pO_2 and MoO_3 is near 10 E^{-6}. These partials are much lower than ambient air but at low pO_2 the Mo is stable without oxidizing. At pO_2 between 10 E^{-18} and 10 E^{-12}, Si and B both oxidize but Mo does not. The goal of the Burk & Crist study was to form the borosilicate in this low pO_2 range by oxidizing the B and Si without oxidizing Mo. What they found was that at low pO_2 it is possible to oxidize only the internal B and Si, but the SiO_2 at low pO_2 can form volatile SiO. So called "active oxidation"[63, 64] can occur and deplete the formed Silicate scale. B_2O_3 evaporation is also significant for pO_2 between 10 E^{-19} and 10 E-^{12} bar and prevents it from being available to flux the silica and form a wetted flowing coating. Above pO_2 = 10 E^{-16}, volatility of MoO_3 can be suppressed, but the simultaneous formation of MoO_3 and borosilicate disrupts the forming scale resulting in local silica droplets which do not coat the surface evenly. This indicates the importance of removing the MoO_3 for a protective scale to form.

Advantages can still be seen by pre-oxidizing in low pO_2 or at high temperature. In the $MoSi_2$ system, $MoSi_2$ elements must be primed before use by first bringing them up to high temperatures in order to form the silica scale before they can be used for limited times in the pesting temperature range, and to limit degradation during heat up and cool down. Similarly the MoSiB alloys may benefit from pre-oxidation at high temperatures to form the coatings, which would then remain protective at other

temperature ranges. A coating composition could be tailored to form quickly and effectively at 1300°C for example. Holding at those temperatures could permit B_2O_3 loss to decrease oxygen diffusivity, and the resulting high viscosity complete coating could be heat cycled repeatedly without repeating the high transient losses.

2.6.8. Coatings

Environmental barrier coatings made of ceramics and similar inherently resistant materials are commonplace in current Ni-superalloy jet engine blades. The use of such coatings is limited in its applicability to the Mo based alloys, because any spallation or cracks in a coating lead to an open pathway for oxidation and volatilization of the underlying Mo. In this type of scenario a crack could lead to catastrophic destruction of the blade in a short time.

If instead a coating could be applied to a MoSiB alloy with inherent oxidation resistance however, it could be possible to make a very resistant and more damage tolerant piece. Alumina forming coatings are attractive because they form a very stable oxide which is not only an effective barrier against oxygen but also resistant to moisture and other environmental factors. Work by Perepezko et. al. focused on numerous such coatings which remain the most promising for use in conjunction with inherently resistant MoSiB alloys. [65, 66] Aluminum pack cementation results in a Mo_3Al A15 analog and a Mo_3Al_8 phase at the outer surface. This has good adherence to the base MoSiB, while under oxidizing conditions quickly reacts to form a protective alumina coating even at low temperatures where the MoSiB would suffer from pesting. Issues were identified of gradual diffusion of Al into the bulk however usable lifetimes in the thousands of hours are reasonable to expect at 1300°C. Unfortunately the coating was demonstrated to

exhibit difficulties with cracking upon thermal cycling because of thermal mismatch, but that it was capable of self healing by formation of new protective oxide in the cracks. This type of coating could be used along with the type of oxidation resistant alloys described in this dissertation to bolster its usefulness.

2.7. Mechanical Behavior of MoSiB Alloys

MoSiB alloys have been shown to possess the necessary strengths and oxidation resistance, but not both at the same time. A balance must be met between a high intermetallic content to benefit oxidation resistance as well as creep strength, and a low intermetallic content needed to improve toughness below 1000°C.

2.6.9. High Temperature Mechanical Behavior

This system gained attention initially because of the excellent high temperature properties of molybdenum itself. Due to its high melting point it can perform well above the limits of lower melting materials. In the MoSiB system, the Mo is benefitted further by the presence of the refractory intermetallics. The structure of the high temperature intermetallics makes their deformation by creep slow, and the intermetallic phases along with Mo_{ss} can provide additional toughening and creep resistance by a Zener pinning type effect. The refractory intermetallics act as grain boundary pins and promote high temperature stability. Creep proceeds by rearrangement and diffusion in order to accommodate applied stresses, however presence of other phases on grain boundaries requires the formation of new interfaces for the grain boundary to move around or past. This creates a thermodynamic barrier and is effective in limiting grain boundary mobility, and as a result reduces the creep rate significantly.

Grain growth is also limited by the diffusion of atoms from shrinking to growing grains. Grain growth of the molybdenum should also be restricted by Zener pinning by the intermetallics because the grains would need to grow around the intermetallics which creates additional interfaces and is thermodynamically unfavorable. A fine homogenous distribution of isolated the intermetallics would be most effective to reduce the ability for the Mo grains to rearrange by creep or growth. The more isolated intermetallics would also be less prone to grain growth themselves because they would need to transport atoms through the Mo to reach the other intermetallics. Due to the low diffusivity rates it can be expected that grain growth will not occur appreciably for isolated intermetallics. Though the isolated intermetallics would primarily exist at molybdenum grain boundaries, the grain boundary diffusion in this system is still slow.

There is possibility for some rearrangement of the structure to reduce interfacial energy by promoting lower energy interfaces. As was confirmed by Sakidja[67], a semicoherent Mo(ss)-T2 interface can exist with a lattice mismatch between the (110)Mo planes and (220)T2 planes of only 4.43%. As the grain grows, energy is minimized by maximizing the low energy interface which them promotes the growth of a plate parallel to that interface. Due to the intermetallic being generally located at grain boundaries, it is unlikely that the same orientation will be preferred by both boundaries. Some driving force would still exist for the rearrangement of the particle to maximize coherence. The diffusion of atoms along the grain boundary for particle rearrangement is feasible but the preferred growth planes are most significant in melt-based processing.

In general the high temperature stability benefits from larger fractions and finer distribution of the intermetallic phases. The work by Schneibel and Lin[68] showed high

creep resistance for MoSiB alloys, and also that the creep rate is dependent on the A15 Mo_3Si deformation. As noted previously the structure of A15 makes rearrangement and diffusion difficult and gives it high creep strength. They also showed a nearly linear decrease in creep resistance for incremental increase in α-Mo volume fraction. Reducing the volume fraction of the less creep resistant α-Mo in favor of the more rigid intermetallics directly correlates to the creep resistance. However a pure Mo at 1200°C still compares well versus Nickel, and the alloys tested by Jain and Kumar [69] also out-performed Ni-based alloys over the temperature and stress regime investigated.

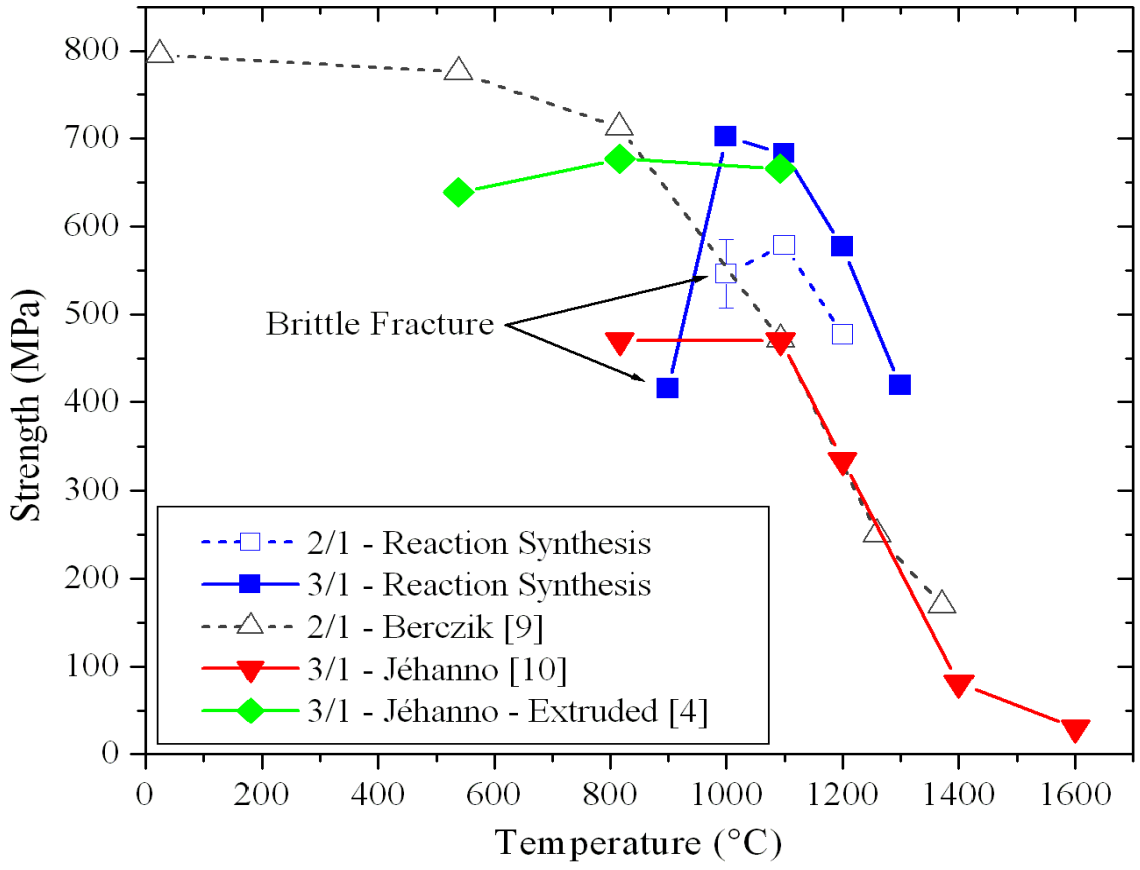

Figure 2.18: Tensile strengths of various MoSiB alloys at elevated temperatures.

The high temperature strengths of some MoSiB alloys are shown in Figure 2.18. The alloys all show obvious decrease in strength at higher temperatures but remain above the 150MPa limits of Ni superalloy up to temperatures of 1300°C and greater. The reaction synthesis compositions perform better above 1100°C than similar alloys from Jehanno and from the Berczik patent, however at lower temperatures the alloys all fail in a brittle manner. This is more evident in Figure 2.19 which shows tensile data of GTRS dogbone specimens as a function of temperature. While significant deformation and high strain to failure (>8% elongation) is present at 1300°C, much less ductility is seen at 1200°C and none at 1000°C and below. This is related to the ductile to brittle transition temperature and is a primary difficulty in achieving alloys in this system with usable low temperature toughness.

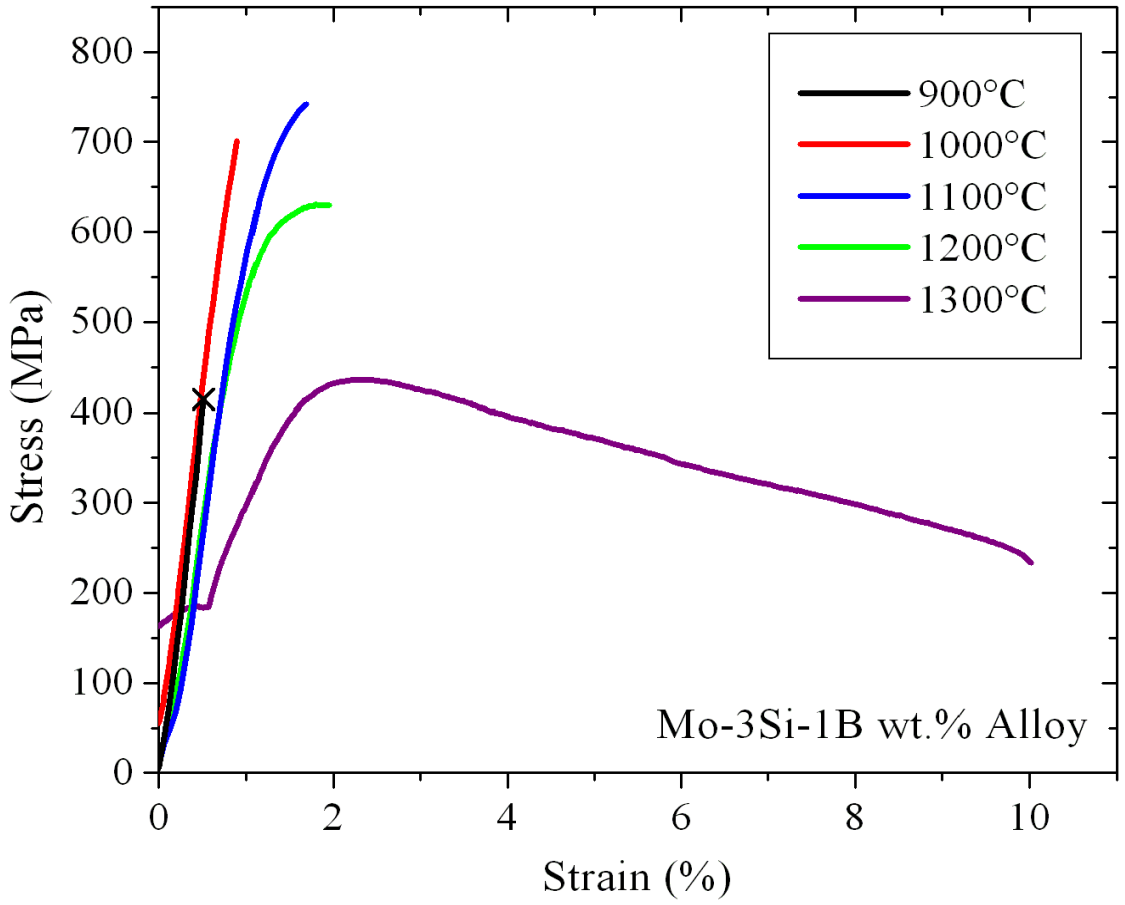

Figure 2.19: Stress-Strain behaviour of a 3:1 MoSiB alloy at elevated temperature.

2.7.2. Low Temperature Mechanical Behavior

As demonstrated, the MoSiB alloys have usable high temperature strength and creep resistance but suffer from a high DBTT which results in poor toughness and damage tolerance at any temperatures below 1000°C. The DBTT of Mo alloys needs to be low for usable fracture toughness at low temperature. While it is possible to get this transition below room temperature for pure molybdenum, MoSiB alloys have not reported a DBTT below 800°C[70]. Increasing the fraction of α-Mo would increase toughness, but inherently reduces both the creep resistance and ability to form an

oxidation resistant coating. Instead improving ductility of the Mo phase itself would increase the toughness of the system without increasing fraction of Mo phase and thus without compromising oxidation properties.

The failure properties of brittle phase/ductile matrix composites are known to be dominated by the matrix phase. Work by Kumar, Ritchie and others exposed that the mechanical properties at low and high temperature are dominated by the matrix phase.[17, 69, 72-77] For good strength, the Mo_{ss} must be present as a continuous matrix and the brittle intermetallics must be isolated. Conversely, oxidation resistance and creep resistance are improved by minimizing Mo volume fraction and minimizing its connectivity. [78] A minimum of 50% Mo by volume is assumed necessary for toughness, however many MoSiB alloys focusing on oxidation resistance only have Mo fractions on the order of 20-40%.[4, 79] Essentially the creep resistance is improved markedly by lower a-Mo fraction and high intermetallic connectivity, while the low temperature toughness benefits from the reverse. Further the small grain sizes which may benefit toughness allow increased diffusivity and lower the creep resistance.

The importance of the matrix phase on the mechanical response of Mo-Si-B alloys was confirmed by Jéhanno et al[45]. They examined the tensile response of two MoSiB alloy with 3wt% Si and 1 wt%B, one with an interconnected intermetallic matrix, the other with a matrix of a-Mo made by rapid solidification and extrusion. The DBTT measured for the intermetallic matrix was ~1150°C and 200 °C higher than for the Mo matrix (~950 °C).

Jehanno produced alloys with 50vol% brittle phase in Mo matrix. At 1400°C and a strain rate of $10^{-4/s}$ a maximum stress of 45 MPa and a plastic strain to failure of

~400% were reported indicating that a MoSiB material containing 50% Mo can have continuous Mo phase while maintaining good high temperature mechanical properties.

Most pure Mo alloys also generally follow a Hall-Petch relationship and strength benefits also from reduced grain size. Jehanno[80] also showed addition of Y_2O_3 and La_2O_3 in MoSiB can reduce grain size. They note a reduction in DBTT compared to another composition, however the comparison alloy did not have continuous Mo phase and the DBTT effect cannot be separated from effects of matrix phase.

The DBTT of the Mo matrix, as mentioned previously is very sensitive to impurities, most significantly oxygen; a few hundred ppm of which can raise the DBTT well above ambient.[16] Nitrogen and carbon were also shown to be detrimental to the cold ductility of molybdenum, but not nearly so much as oxygen.[15] As discussed in section 2.2.1 it has been shown by Sturm et al.[20] that increasing Si concentration in Mo decreases toughness due to solute segregation of Si to the grain boundaries. In Mo/Mo_3Si alloys, the solid solution concentration of Si in equilibrium in the Mo increases with temperature, from less than 1% at 1200°C to about 3% at 1600°C. Due to slow diffusion in the system the values remain high in solution after processing, even when brought back down to low temperatures or over long anneals. Sturm showed that Si caused pronounced solid solution strengthening and contributes to lower toughness of the Mo and thus the entire alloy. It is then important for toughness that impurities be minimized especially carbon and oxygen, and in MoSiB systems; silicon.

2.7.2.1. Estimating Toughness by Vickers Indentation

Hardness tests may be used to estimate fracture toughness of brittle materials by the Vickers indentation fracture toughness method. While the values obtained from this

type of test are questionable[81], a range of values may be found and compared to other similar materials. This could provide a simple useful evaluation metric for comparing different compositions.

Kim[44] studied consolidation and hardness relationships for powder metallurgical processed Mo. It is generally known that hardness is closely dependent upon the porosity and grain size of the sample. Kim found that the dominant effect on the hardness value of molybdenum samples is changed from the porosity dominated to grain size dominated above a sintered density of 90%. Below 90% theoretical density, hardness is proportional to the density, or more exactly the fraction of porosity, but above 90% hardness decreases with increasing grain size following the Hall-Petch relationship.

Vickers may also be used to estimate fracture toughness by measuring the crack lengths formed as a function of load from the corners of indents in brittle materials. Typically these can be fairly inaccurate however and most rely on empirically fit equations for a specific material. A number of methods can be used to estimate toughness from Vickers indentation cracks, but Miyoshi's equation developed for Si_3N_4[82] is one most commonly used and is used in Japanese Industrial Standard (JIS) R 1607.30T.[83] The general equation for fracture resistance is:

$$K = \zeta(E/H)^n P c^{-3/2}$$

where *E* is the Young's modulus, *H* is hardness, P is the load and c is the the half-length of the measured crack. ζ and *n* are material independent parameters given by the models and for Miyoshi's equation ζ=0.018 and n= ½.

The intermetallic materials are generally known to be brittle and the MoSiB alloys have no room temperature ductility. Chu et al. used crack length measurements from

Vickers hardness indents to calculate the room temperature fracture toughness of the T2 intermetallic to be 3.2 MPa√m, but the samples examined had nonequilibrium phases present. Looking instead at pure single crystals, Ihara et al. performed Vickers indentation harness tests on T2 averaging at 18GPa but dependent on orientation. They also managed to observe cracking and calculate a Vickers "fracture toughness" of 1.5 to 2 MPa √m, which is smaller than people have seen for T2 in 3 phase alloys, perhaps due to the flawed nature of the test in general. Comparing the fracture toughness measured by notched 3-point bend for polycrystalline A15, 3.0 MPa√m, Rosales and Schneibel determined that fracture toughness measurement by Vickers indentation cracks gives lower values of only 2.45 MPa√m.

2.8. Microstructure Engineering

The proposed ideal microstructure for MoSiB consists of isolated but finely dispersed intermetallics within a fine grained Mo matrix. Attempts at achieving the desired microstructure have followed two main paths, melt processing and powder metallurgy.

2.8.1. Melt-based Processing

Nunes[39] plotted the liquidus projection of the Mo-Rich corner of the Mo-Si-B system shown in Figure 2.20. From a melt within the Mo-A15-T2 phase triangle, the Mo liquidus extends over the entire phase triangle and Molybdenum solidifies first from the melt. The subsequent solidification of the other phases results in a final microstructure of isolated Mo dendrites within a matrix of intermetallics.

Alloys cooled from melts may also form nonequilibrium phases which remain even after long anneals due to slow diffusion rates. Very fast cooling rates are necessary

for melts to produce a supersaturated Mo from which the intermetallics may be precipitated by subsequent heat treatment[8], but the necessary cooling rates have been difficult to achieve.[4]

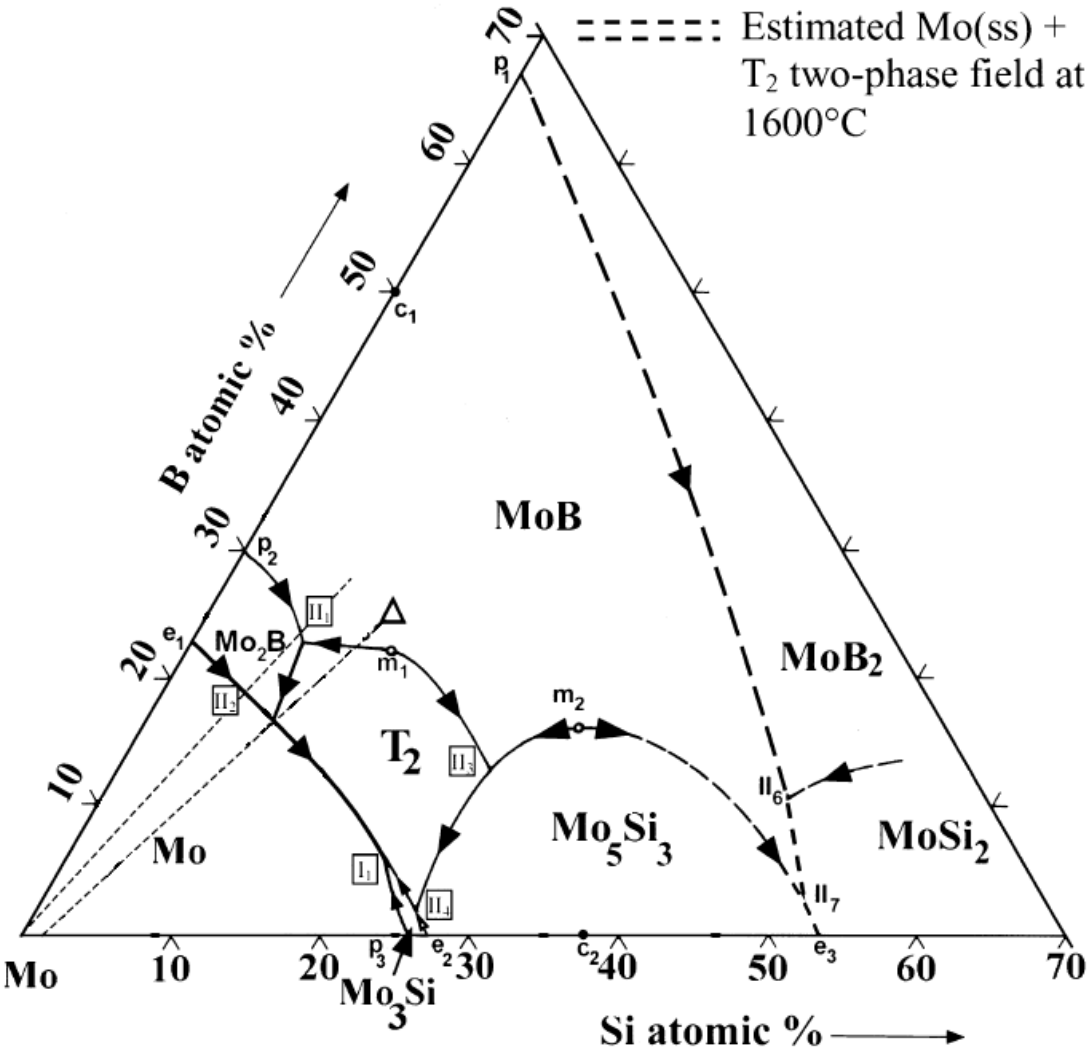

Figure 2.20: The liquidus projection plotted by Nunes et al. for the Mo-rich portion of the Mo-Si-B phase diagram. The different regions of primary solidification are indicated with the invariant eutectic for Mo_{ss}-A15-T2 is marked at point I_1.[39]

Despite the difficulties, arc melting has been used in a number of studies both for primary processing of pieces or to be ground and reconsolidated as in the work of Behrani, Thom, Kramer and Akinc. [1] Most use high amperage DC arc melting for the primary melting because of the difficulties in exceeding the melting point of these materials otherwise. The microstructure has some ability for rearrangement but the cooling rates are difficult to control from the arc melted liquid and changes in microstructural arrangement are mostly limited to changing the phases present.

One approach is to rapidly solidify from the melt. MoSiB melts from a plasma rotating electrode process (PREP)[69] and Argon plasma sprayed and splat quenched powders [84] can be used and subsequently consolidated to form desirable final microstructures. The output of such processes however is limited in scale and can be prohibitively expensive while suffering additionally from increased impurities as well as difficulties with loss of Si and B during processing.

2.8.2.1. Cold/Hot Working

Some success has been had by Pratt & Whitney using arc melting and plasma spray atomization[3]. By rapidly quenching the melt through atomization a roughly homogenous set of granules is created. The non-ideal melt microstructure is retained of Mo isolated within an intermetallic matrix, however subsequent hot and cold working is able to redistribute the phases to a usable microstructure.

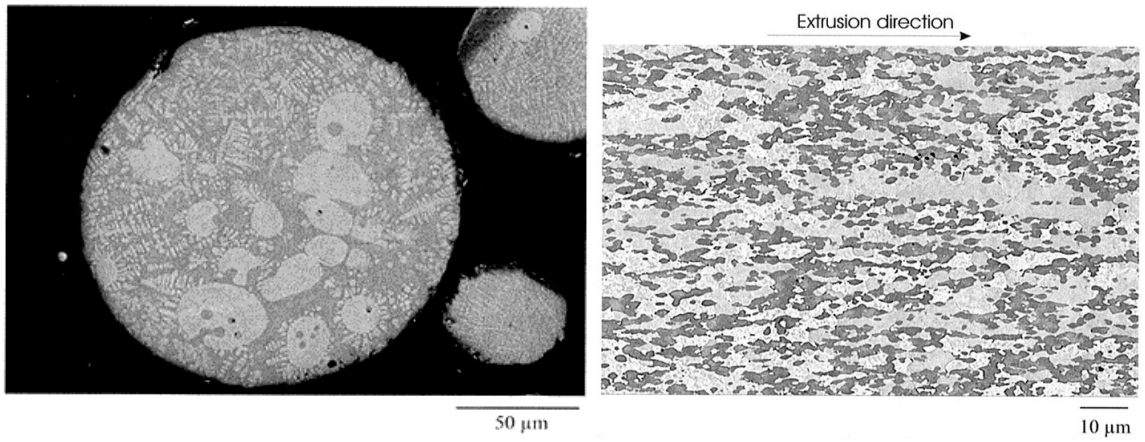

Figure 2.21: Right: Micrograph of as prepared arc melted, atomized Mo-3Si-1B granules, with isolated Mo (light) in intermetallic matrix (dark) Left: Mo-3Si-1B microstructure after HIP consolidation and extrusion.

Once arc melted and atomized, the resulting powders are cold isostatically pressed (CIP) into bars, and packed into Mo cans which are then extruded. The cans are heated to 1510°C in a controlled Ar-5%H_2 atmosphere then extruded to a 5:1 reduction ratio by a high strain rate method. To develop fully continuous Mo, high temperature swaging was needed and the 2:1 wt% Si:B provided the best results after swaging.

Another approach uses hot isostatic pressing (HIP) of the powders to achieve homogenous and pore free consolidation of a piece. After HIP the arc melted and atomized microstructure remains and the HIPed bar must be then extruded at high temperatures and low strain. The more malleable Mo can then deform and join into the desired continuous Mo matrix with dispersed intermetallics.

These methods are unfortunately difficult for large scale production; the process of arc melting and atomization itself is time consuming and expensive, and has low yields. The need for subsequent highly intensive post-processing further increases the difficulty. In order to hot forge the MoSiB alloys, temperatures in excess of 1500°C may

be required which is very difficult to achieve on a production scale; and even once extruded, final shapes must be separately machined.

2.8.2. Powder Processing and Mechanical Alloying

Powder metallurgy methods provide opportunity to control the microstructure prior to consolidation and may be able to circumvent the difficulties in reforming the microstructure through heat treatment.[44] PM methods include both pre-alloyed powder such as those splat quenched powders prepared by plasma arc rotating-electrode process[85] or mixing and sintering of elemental powders[86]. Traditionally powder processing routes have been discounted due to oxidation of the Mo, Si and B powders during processing which leads to unacceptably high oxygen impurity levels in the final alloy.

Mechanical alloying is a powder based approach which aims to create Mo-matrix MoSiB alloys *in situ*. [11] The process uses high impact, high energy milling to force nonequilibrium solid solution of Si and B within the Mo. The repeated deformation and folding can permit supersaturation of over 10at% Si in Mo, well beyond the limits expressed in the phase diagram. After the mechanical deformation and super saturation, anneals at high temperatures and long times permit the precipitation of the intermetallics within the Mo matrix. This also maintains very fine grain sizes.

Unfortunately mechanical alloying suffers from limitations on the extent of solid solution which can be forced into the a-Mo phase. It also results in excess of the Si and B remaining in the final Mo with as much as 6at%, and high Si contents in Mo have been shown to have severe negative effects on its ductility. Furthermore, the high energy milling media and container are potential sources of contamination as well, and can alter

the behavior of the alloy unpredictably. There has also been difficulty in reproducing the process.[87] Despite these setbacks it remains one of the most promising methods to produce usable MoSiB alloys on a large scale.

2.8.3. Georgia Tech Reaction Synthesis (GTRS) Process

In 2007 Cochran, Middlemas and Rockett at GA Tech demonstrated a powder metallurgical approach based on reaction of Mo, Si_3N_4 and BN starting powders.[88] This is not a reaction sintering process; it is termed "reaction synthesis" because the final phases are reacted in-situ during the firing from nitride precursors. Because of the low temperature stability of the nitride starting powders, the problem of impurities from powder oxidation is avoided. Upon firing in a reducing atmosphere, the nitrides break down and react with the Mo to form the desired intermetallic phases.

$$3\ Mo + 1/3\ Si_3N_4 \leftrightarrow Mo_3Si + 2/3\ N_2$$

$$5\ Mo + 1/3\ Si_3N_4 + 2\ BN \leftrightarrow Mo_5SiB_2 + 5/3\ N_2$$

The ability to produce a ductile pure molybdenum specimen using this method has been demonstrated, and a ductile alloy should also be achievable using this method through adjustments to the microstructure, compositions, and phase contents. The approach allows for a wide range of microstructural control through changes in powders and processing following simple and inexpensive procedures already in use in ceramics manufacture. Furthermore it allows for adjustments to the composition and phases present by simple adjustments of starting powders.

2.9. Elemental Additions

Sakidja's thesis work [89] was on quaternary transition metal additions. His goal was mainly to investigate their effects on the stability of the phases, T2 and BCC structures, and to alter solidification pathways and tailor the microstructures from melts. Regarding additions; Hume-Rothery rules predict extended solid solution when (1) atomic size diff is less than 15%, (2) the additive has the same structure, (3) there is a small difference in electronegativity, and (4) the alloying element has lower density.

Group VIB metals (Mo, Cr & W) arrange in body centered cubic structures. The BCC metals are quite stable and have high Tm, and the stability of additives within the BCC is related to atomic size differences and *e/a* (charge/size) due to strong hybridization of *d* and *s* shell valence e-. Sakidja's work showed that Group V B (V, Nb & Ta) can be added into the BCC metals easily, and that Group IV B (Ti, Zr, Hf) can also; however they transition to HCP at lower temperatures. In general however, most transition metals are quite soluble in Mo BCC solid solution.

Ochiai[90] attempted to improve oxidation resistance of the Mo_3Si intermetallics alone at lower temperatures (900°C) through alloying with Cr and Al. He noted that they can improve low temperature oxidation by forming passivating Al_2O_3 or Cr_2O_3 layers, but the improvement is insignificant without high levels of additions (>30mol% Cr to Mo_3Si) which eliminates the usefulness of this approach.

Table 2.4: List of elemental additions investigated by Mendiratta et al.

Element	Composition/Composition Range (Atomic Percent)
W	Mo-7.5 to 30W - 15 to 19.5Si - 5 to 10B
Nb	Mo-30Nb-30Si-10B
V	Mo-20 to 30V - 12 to 30Si - 6 to 10B
Cr	Mo-20Cr-12Si-10B
Re	Mo-7.5 to 23Re - 7.5 to 20 Si-10B
Ge	Mo-5Ge-11Si-8B
Al	Mo-5Al-11Si-11B
Hf	Mo-0.3 to 10Hf - 9 to 12Si - 9 to 12B
Ti+Cr	Mo-18Ti-11Cr-9Si-9B

Mendiratta and Dimiduk[91] examined quaternary additions to Mo-11Si-11B (at %) of the following compositions listed in Table 2.4. The goal for these additions was to improve oxidation also in the lower T transient regime, and to possibly alter the microstructure to promote more continuous Mo. Vanadium oxidation is similar to Mo, and was added with the hope that it's earlier volatilization (from A15 and T2 analogs w/ V) could liberate B & Si earlier and allow lower sooner formation of a borosilicate layer during heat up. Re additions are investigated because it is a known ductilizer for Mo, but its oxidation was unknown. Ge was added to modify the glass. Al additions should affect the microstructure and strength by gettering O, and improve oxidation resistance by formation of Al_2O_3 at lower T and by reducing O permeability in the oxide glass scale at higher T. Hf and Ti+Cr were investigated alongside work by Pratt & Whitney, also hoping to improve oxidation resistance. While all of the additions could be theoretically justifiable, all of the examined composition additives showed significantly decreased oxidation performance. Only very small (<0.5at%) Hf additions indicated some minor improvements, but were generally not worthwhile.

Alternate approaches to modify the glass properties by elemental additions have focused on affecting the properties of the borosilicate glass itself, rather than relying on formation of other oxides. Glass additives can be defined by their behavior in a glass, which depends on the electronegativity and is given by the β parameter:

$$\beta = \frac{io}{co}$$

where $i_o = 1 - \exp(-0.18(\Delta X))$; $c_o = 1\text{-}i_o$ and $\Delta X =$ the difference in electronegativity of the cation and the anion (oxygen). For $0 < \beta < 1$ the cation is a glass network former, for $\beta = 1$ it is a glass dweller, and for $\beta > 1$ it is a network modifier.

Transition metals have $\beta > 1$ and are network modifiers. Pratt & Whitney patented Fe-containing MoSiB for oxidation improvement[92]. The patent covers up to 2% Fe, Cu, Co and Ni. Oxidation results are given at 1370°C, and transient losses were ~150 mg/cm^2 and levels off to ~0.6mg/cm^2*h for allowing additions of 0.3 at% Fe and 0.2 at% Ni. The patent further claims the additions "result in the formation of an oxide scale which is protective for hundreds of hours (700hrs+) at 2500°F (1370°C)". Minor additions of these elements improve the high temperature oxidation resistance of the alloy without any significant effect on the lower and intermediate temperature oxidation resistance of the alloys. Another patent[3] suggests improving oxidation with Ti, Zr, Hf, and/or Al to the alloy to: (1) promote wetting of the borosilicate layer once it has formed, (2) raise the melting point of the borosilicate, and (3) form a more refractory oxide layer below the initial borosilicate layer further impeding oxygen transport to the molybdenum matrix.

The mechanisms behind the observed improvement with small additions of Fe, Ni, Co and Cu were investigated by Sossaman et. al.[93] It was confirmed that the oxidation rates are significantly decreased by even small 0.05wt% additions of Fe. The

time required for surface coverage by the glass was decreased, and the continuity of the protective later was improved. Without Fe, a porous borosilicate existed with open pore channels which allow continued oxygen availability for continued rapid oxidation into the substrate, whereas the Fe-containing samples showed a thin protective borosilicate layer atop a thick MoO_2 layer.

Fe in multi-component silicate glasses acts as a network modifier and effectively as a flux.[94] It occupies interstitials within the glass matrix and creates NBOs (Non Bridging Oxygen) which disrupts connectivity and results in lower glass viscosity and increased ability to flow. It was assumed by Sossaman et al. that the Fe substitutes on Si sites in the A15 phase and during oxidation the Fe allows the otherwise pure SiO_2 formed from the A15 to flow even before it has been fluxed by boron. Iron is also a more stable modifier in the glass, unlike B_2O_3 and Fe doesn't volatilize appreciably from the glass at 1300°C.

The Pratt patents also mention benefits from adding Co, Cr, Cu and Ni. Co, Cr and Cu all should have roughly similar reactions with Mo. According to Perepezko and Sakidja's work they have good mutual solubility in the Mo and T2 phases and substitute on the Mo sites. Fe is different in that it substitutes for the Si in A15.

2.9.1. Manganese

Manganese could be another possible additive for improving oxidation resistance. It is a commonly available transition metal which has a density of 7.2 g/cc. It melts at 1246 °C and boils at 2061°C. Mn and Mo are both common alloying elements in steels, but rarely are alloyed alone together. Mn solubility in Mo is low until high temperatures, but at room temperature BCC Mo can still incorporate just over 2at% Mn

substitutionally. Rapid cooling from a melt can sustain as much as 30 at% Mn in Mo. Mn produces difficulties in most melt-based systems however, due to its high vapor pressure. This is exacerbated when alloying with Mo by the combination of high temperatures needed to melt Molybdenum as well as vacuum atmospheres used to prevent Mo oxidation. This is likely why Mn was omitted from most of the previous MoSiB studies – it cannot be easily added by any melt-based processes.

Mn in glass is very similar glass modifier to Fe, also to Co and Ni. By increasing NBO's and decreasing glass polymerization, it reduces viscosity. The effect on viscosity is much less pronounced than boria, but should be more permanent than boria which volatilizes away. While Mn itself is volatile, the oxide is much more stable and should remain within the glass as a modifier. Mn additions can reduce viscosity for a longer time and should help the glass be able to heal itself of channels bubbles or voids.

Mechanically, Mn embrittles Mo similarly to most other elemental additions and causes solid solution strengthening which raises the ductile to brittle transition. Work by Bruckart, LaChance, Craighead and Jaffee[95] showed increase in Mo tensile strength up to 0.8% Mn with corresponding decrease in ductility. Hardness also increases. However Rendall, Johnstone and Carrington[96] showed that at least 0.5 at% Mn can be added to Mo and can still be rolled and forged without cracking, and that only when passing 1at% Mn does cracking occur during working. Provided Mn contents are kept low, there should be no issues with it affecting Mo ductility or forming unwanted additional phases.

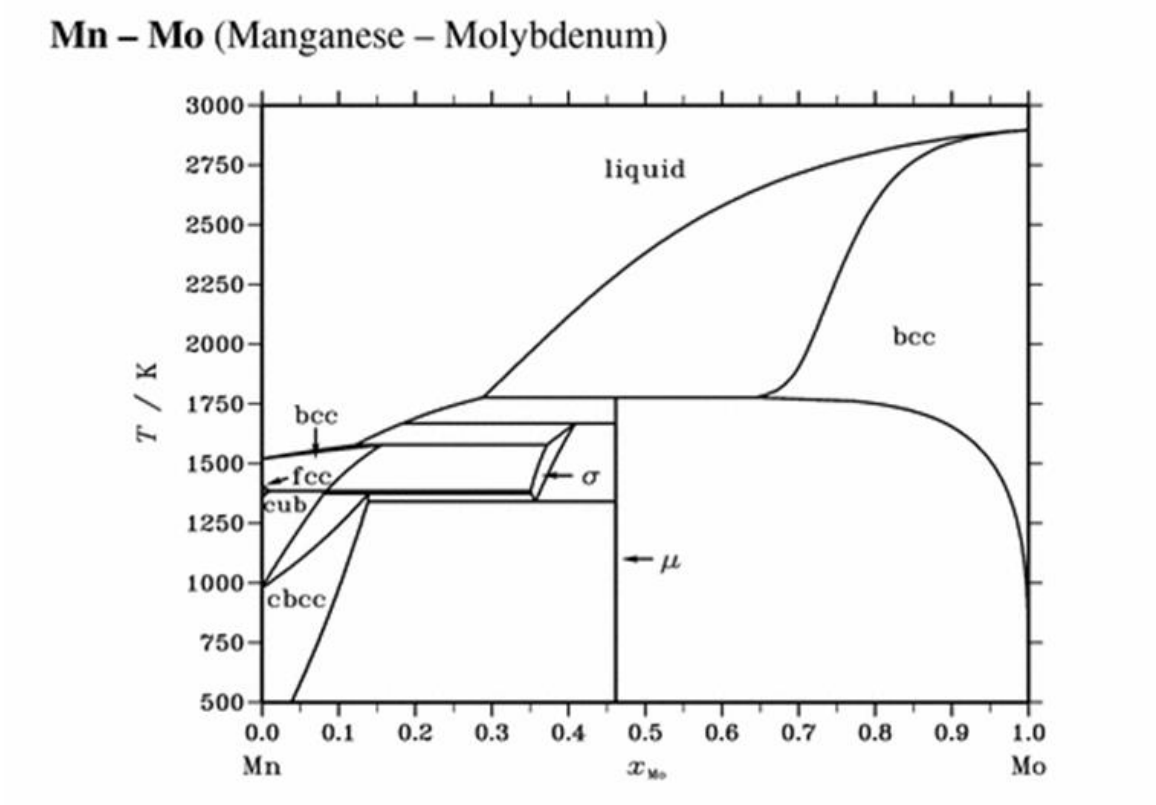

Figure 2.22: Calculated phase diagram for Mn and Mo.[97]

Alloys including Mn and Mo with BaO_2 and SrO_2 were studied by Drennan and Brown[98] for pyrotechnics, who had concluded Mn and Mo were capable reducers for sustaining combustion of the dioxides, but have little other impact on our work. Schniebel, Ritchie & Kruzic[79] were the only ones to add Mn to MoSiB. They were attempting to lower the thermal expansion in hopes of better matching applied low-expansion barrier coatings. However they offer no information on the levels added, effects on oxidation, strength, microstructure or otherwise, and give no quantitative values of the effects. They do mention, as I've previously expressed, that addition of Mn is very difficult in arc melting due to rapid Mn evaporation at the high melting point of Mo.

Based on the above information, Mn, Co, Cr Ni, Fe and Y may show promise as glass modifiers. At low additions they should not upset the Mo ductility or the desired phases, but may be capable of providing a more protective glass coating. Mn is of particular interest because not only do its properties appear promising, it falls outside of existing patents and by the volatility issues with melt processing it is uniquely limited only to a powder-based process like ours.

2.10. Current Work - Silica Addition

The current work is based on the successes of the GTRS Process to create MoSiB pieces with oxidation resistance, but the failure of any MoSiB process to achieve usably low DBTT. The embrittlement of Mo by silicon from A15 is the primary explanation for the poor ductility of MoSiB alloys below 1000°C; however the A15 is traditionally necessary as the source of Si to form protective SiO_2. Since it is SiO_2 which is ultimately desired for oxidation protection; in order to avoid Si in solid solution in the Mo the compositions investigated here will include SiO_2 directly instead of using A15.

Use of low melting glass may be able to provide a coating, and using the GTRS process glass frit powders should be able to be added to Mo and distribute evenly without contributing Si to embrittle the Mo, while being able to flow and create a self healing barrier coating similar to MoSiB.

As an additional benefit, replacing the A15 with glass particles embedded in the matrix requires a lower volume fraction of brittle glass formers in order to provide the same amount of protective coating. This is because the Mo silicide intermetallics must decompose to form the oxides and only produce a fraction of their volume in glass. Using SiO_2 directly, a higher Mo fraction may be feasible, also benefitting toughness.

Rather than lower melting glass frits, pure SiO_2 alone can have melting points as high as 1600°C, and is stable with Mo without contributing Si into the Mo_{ss}. Unlike the frits which are fluid by themselves by 1000°C, when using pure SiO_2 some boron must also be present to flux the glass and promote flow and rapid coating. The boron containing intermetallics Mo_3SiB_2 (T2) and Mo_2B exist as solid stable phases in equilibrium with Mo over a wide range of temperatures and do not contribute to Si embrittlement. Mo_2B in an oxidizing environment would react to form a boria glass by the following reaction:

$$Mo_2B + O_{2(air)} \rightarrow MoO_3 + B_2O_{3(glass)}$$

This reaction is thermodynamically favorable at all temperatures and becomes kinetically relevant above 600°C. The B_2O_3 will act to flux the SiO_2 glass in the same manner as in the MoSiB alloys. In this manner the glass formers remain solid in the material during processing and use, and only when exposed to oxygen at the surface does it become flowing to provide protection. The properties of the glass, namely viscosity and O diffusivity, can be optimized for different temperature ranges and environments by changing the composition, specifically the Si to B ratio, which in turn may be altered by changing the ratio of starting powders.

Including Mo_2B could also limit potential problems due to internal oxidation in the Mo – SiO_2 system. Internal oxidation requires that the formation of the internal oxide, in this case MoO_3, be: 1) energetically favorable; more specifically the most favorable oxide (i.e. most negative free energy of all possible oxides) and 2) oxygen must diffuse in faster than the reactant metal diffusing out. The second criterion is met when a glassy coating exists; and oxygen diffuses inward through the protective glassy layer and reacts

at the metal/oxide interface. In the case of traditional MoSiB alloys with the A15 and T2 intermetallics, the silica and boria oxides are more favorable than MoO_3, and low pO_2, such as beneath the coating, results in the reactions:

$$Mo_3Si + O_2 \rightarrow 3\,Mo + SiO_2$$

and

$$Mo_5SiB_2 + 5/2\,O_2 \rightarrow 5\,Mo + SiO_2 + B_2O_3$$

with Mo and SiO_2*B_2O_3 glass as products. Because the oxygen that diffuses into the metal preferentially reacts with the more active borosilicides, it leaves a region below the outermost oxide coating which contains Mo metal and borosilicate glass as shown previously in Figure 2.16.

If instead we have a case where the boron and silicon are present already as oxides (SiO_2 and B_2O_3), below the oxide layer the Mo is the most reactive species and forms $MoO_{3(gas)}$ at the oxide/metal interface. This could create significant bubbling and disrupt the protective coating allowing for much more rapid oxygen transport through the outer layer. The inclusion of the boride phase should allow for the boron to getter and react first with the inward diffusing oxygen to form a zone below the primary coating with B_2O_3 glass in a Mo rich matrix and thus limiting internal formation of MoO_3 that could potentially disrupt the protective layer.

Perepezko shows that there is no Si solubility in the Mo-T_2-Mo_2B triangle at 1600°C and below, Figure 2.23. This indicates that with no Si in Mo, compositions in the Mo-T_2-Mo_2B triangle will be ductile if the Mo phase is sufficient in volume and connected. Thus, compositions such as Mo-T_2-Mo_2B plus SiO_2 should be ductile.

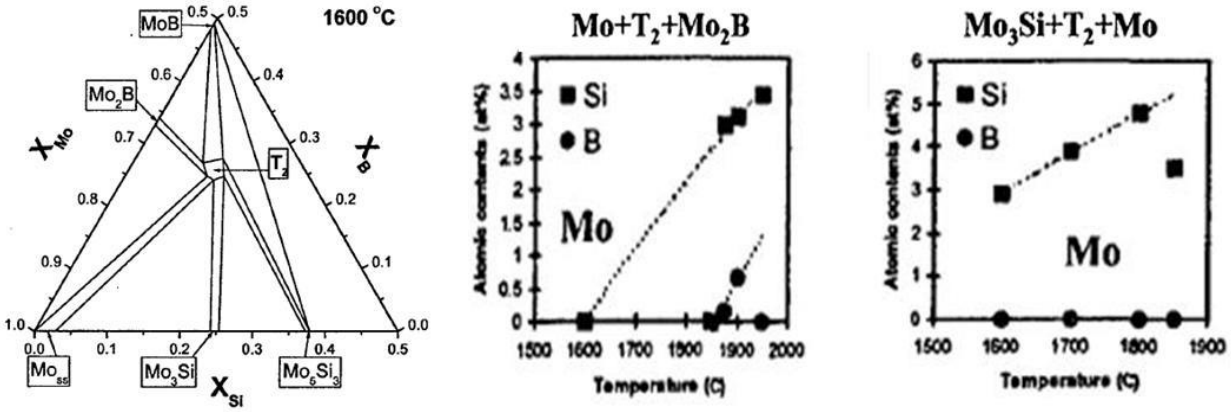

Figure 2.23: Isothermal section in Mo-Si-B system at 1600°C and Si solubility in Mo in the Mo-T_2-Mo_2B and Mo_{SS}-T_2-Mo_3Si triangles as a function of temperature.[8, 20]

The compositions studied here will be shifted from the traditional MoSiB system in the T2-A15-$Mo_{(ss)}$ phase triangle highlighted in green in Figure 2.7 to the $Mo_{(ss)}$-T2-Mo_2B ternary and $Mo_{(ss)}$-Mo_2B binary highlighted in blue. The silica for glass forming which would have been provided by the A15 phase will in this case be replaced directly with amorphous SiO_2 mixed in as a powder in the green state. The Mo, T2, and Mo_2B are still reacted during firing from BN, Si_3N_4 and Mo precursors. The desired result will be a composite consisting of a ductile Si-free Molybdenum matrix phase with finely and evenly dispersed Mo_2B, T2 and SiO_2 for self-healing oxidation resistance similar to that of MoSiB alloys.

Use of Silica instead of glass forming intermetallics for oxidation resistance may seem obvious but it hasn't been approached at all in the literature. Adding silica cannot be done while maintaining a desirable microstructure except through powder processing, which typically does not meet the requirements of low impurity content. Only the techniques developed previously at GA Tech by Cochran and Middlemas avoid the

traditional issues associated with a powder based approach. This work aims to adapt and further develop the unique ability of the GT powder processing techniques and chemistries to produce high toughness and oxidation resistant alloys of Mo with SiO_2, Mo_2B, and T2.

Mullite addition was also evaluated as a refractory phase to pin grain boundaries and restrict creep. This phase needs to be inert and not modify the glass or Mo negatively and also should match the thermal expansion of the molybdenum closely. Mullite serves all of these needs. Mullite has a thermal expansion of 5.4 μm/mK which closely matches Mo (4.8 μm/mK) and forms strong, clean interfaces with Mo as in the work by Bartolome et al.[99] and Sivakumar et al.[100].

There have been a number of studies regarding Mo-mullite composites [99, 100]; however these all focus on using Mo as a secondary phase in a mullite matrix to add toughness to mullite refractories. Our approach is radically different but is based on some similar principles, mostly the closely matched thermal expansions. It may also contribute beneficial Al to the glass which could reduce oxygen diffusivity and improve oxidation resistance in the long term.

It is not fully understood if there is any Si contribution to Mo from T2 equilibrium; and one goal of this study is to determine if T2 embrittles the Mo_{ss} the same way as A15, and if so further investigation would only consider Mo_2B composites.

Investigation of bend tests at varying temperature are simple and effective measurements of strength and will be pursued in order to separate the contributions of chemistry, microstructural size scale, molybdenum volume fraction, and microstructural contiguity on the DBTT, yield strength, and strain to fracture estimated from three point

bending. There is good probability that with a more complete understanding of the processing effects on microstructure and final properties that appropriate adjustments could be made to drastically improve mechanical properties.

Firing in reduced atmosphere is required to produce the desired final phases and phase distribution but may cause problems resulting from volatilization of Si and B oxides formed from residual oxygen in the starting Mo powders. The possibility of a B depleted surface layer, SiO volatilization and redeposition and other related reactions cannot be ignored and may cause both poor toughness and high initial weight losses during oxidation.

Many oxidation resistant samples are unable to achieve good oxidation protection, either by too drastically high initial transient losses, insufficiently low rates of long term oxidation, or failure due to the inability to completely seal off the surface and move from transient to parabolic oxidation kinetics. Understanding effects of composition and contents will enable development of a coating which will eliminate transient weight loss.

Elemental additions to affect mechanical or oxidation properties may also prove to be beneficial, by gettering detrimental impurities, affecting the behavior of the glass coatings, altering the phase stability ranges or a combination of all of those things. The effect of individual elements, their dependence on phase fraction, and possible reactions and interactions are also investigated further.

CHAPTER 3.

TECHNICAL PROCEDURE

Batches were prepared by the Georgia Tech Reaction Sintering (GTRS) method developed by Michael Middlemas et al[59]. The process uses a modified powder processing route which utilizes the reaction of molybdenum, silicon nitride (Si_3N_4) and boron nitride (BN) powders to synthesize a fine dispersion of the intermetallic phases T2 and A15 in a Mo_{ss} matrix. Si_3N_4 and BN decompose to Si, B and N_2 gas during firing, and thus avoid the high oxygen contents seen when using fine elemental Si and B powders in traditional powder processing routes.

3.1. Raw Materials

The powders used are listed in Table 3.1 and shown in Figure 3.1. Powders must be fine in order to develop desirable microstructures and to aid in reaction and sintering, they must be commercially available on a scale which could support the final intended use, and they must be of suitably high purity, specifically with low oxygen content. All of the initial powders should be stable at room temperature and not oxidize appreciably.

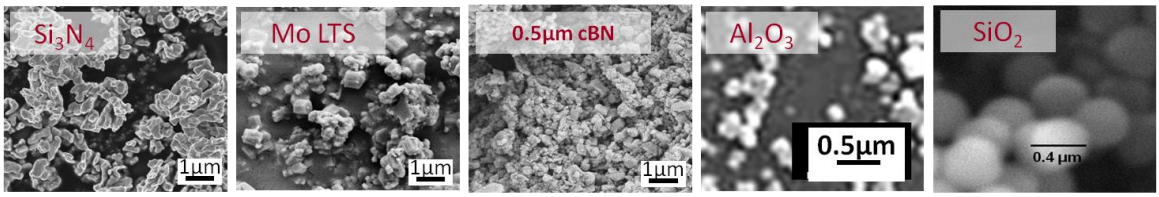

Figure 3.1: SEM micrographs of raw material powders used.

Table 3.1: Raw materials properties.

Raw Material	Supplier	Grade	Purity	Particle Size (μm)
Mo	Climax	LTS	99.95%	~1
Si3N4	UBE	SN-EO3	99%	0.5
BN	Advanced Abrasives	cubic 0.5	99.50%	0.5
Al2O3				
PMMA binder	Elvacite	2008	-	-
Amorphous SiO2	Alfa Aesar	L16985	99.90%	0.5 or 1
SiO2 Quartz	US Silica	Sil-Co-Sil 40	99.80%	~20
SiO2 Cristobalite	Kremer	58689	-	8

Fine chemically-pure powders are commercially available and listed in Table 3.1. Mo with small average particle size is beneficial for finer grain size, better dispersion and isolation of glass formers. Fine grained (1 μm) and chemically pure Mo was obtained from Climax Molybdenum (Climax, CO; LTS grade). The boron is provided by reaction from 0.5 μm cubic boron nitride from Advanced Abrasives (Township, NJ). The cubic BN polymorph has been shown to develop better isotropy in the final microstructures. Reaction of Si_3N_4 provides Si for the formation of the silicide intermetallics, and SN-E03 grade silicon nitride was purchased from UBE Industries (NYC). Commercially available high-fire glazing glass frits were chosen to investigate replacing A15 directly with glass. Glaze frit 3195 from FerroFrit, and frits 1780 and 1491 from AGC (Alpharetta, GA) were purchased. The as-received particle sizes are large and the frits

were sieved to -635 mesh. Additional screening can be done by settling and decanting to remove large particles or vice versa for removal of fines.

In the case of SiO_2 containing samples, the Si_3N_4 which would have formed A15 was replaced with SiO_2. Si_3N_4 is only added when necessary in enough quantity to form the T2 phase, BN will be included which will react during sintering by the same mechanisms as for the MoSiB case, but here forming Mo_2B and/or T2. Monosize spherical SiO_2 grown by the Stöber process has excellent purity and very precise narrow size distributions and was obtained with particle diameters of 0.5 and 1μm (Alfa Aesar).

Additionally, mullite powder was pre-reacted from fine high purity alumina (Sumitomo AKP-10), or purchased as pre-made mullite (AEE). The monoclinic Sr-Celsian ($SrAl_2Si_2O_8$) was produced by a reaction of the SiO_2, Al_2O_3 and $SrCO_3$ (Alfa Aesar) which are milled and spray dried in the same manner, calcined at 925°C and reacted at 1200°C for 12 hours.[14] "Sil-co-Sil 40" brand fine ground silica was used as a quartz source. It was verified by XRD to be beta (low) quartz and has a nominal size range of less than 30 micron with average size around 10 μm, and sieving at 635 mesh was used to remove the coarsest particles. Cristobalite powder was obtained from Kremer Pigments (NYC).

3.2. Processing

3.2.1. Batching & Mixing

The starting powders were mixed and homogenously distributed before forming and reaction firing. Spray drying has been shown to create a stable homogenous distribution of the starting powders in the green state which remains after firing. Mo, SiO_2, Si_3N_4 and BN with binders, lubricants and dispersants are mixed by ball milling for

12-24h with alumina media. Milling was done in acetone; the milling medium must be non-aqueous to avoid oxidation or formation of hydrides. Polymethyl Methacrylate PMMA (Elvacite 2008) was added as a dispersant and binder at 3wt% of the powder. The low molecular weight PMMA breaks down into the monomers around 400°C and evaporates out. This leaves behind no residual carbon and was able to be removed without requiring oxygen for burnout. Additionally 0.5wt% stearic acid may be added as a lubricant to prevent lamination cracking when dry-pressing.

3.2.2. Dispersion

Good dispersion is important during spray drying because settling in the hoses or retaining jar prior to spray drying can lead to inhomogeneties in the final product, disrupt the desired final microstructure, or offset the intended composition. Dispersion of the slurries provides some unique difficulties for SiO_2-containing compositions compared to the MoSiB case. Ideally the binder and dispersant would be one in the same to allow good mixing and for ease of processing, as is the case with the Elvacite PMMA.

Most effective dispersants are of the electrosteric or electrostatic type, and bond to the charge on at the particle surface which depends on its isoelectric point. The isoelectric point (IEP) is the pH at which the surface has no net charge; at pH above the IEP negative surface charges dominate or vice versa. Compared to Mo and the nitride powders, SiO_2 has a low isoelectric point and requires different dispersants than the Mo and nitride powders. Because of the oppositely charged surfaces at neutral pH, different electrostatic dispersants could cause agglomeration in one or the other. Dropping the pH below the IEP of SiO_2 (pH ~3) could allow a like-charge on the various particle surfaces, but would require a very acidic suspension. Another possibility would be the use of

stearic dispersants like polystyrene (PS) which are mostly unaffected by surface charge, but these are also less effective dispersants. Dispersant and binder election faces additional difficulties to fit the needs of this unique system; namely the need to be soluble in non-polar solvents because aqueous solutions readily form hydroxides with Mo, and the need for a clean evaporation to avoid carbon residues and since no oxygen can be present for burnout.

A variety of amines and other grades of PMMA which are soluble in acetone were tested by mixing the powders in glass vials and observing the settling. All cases settled within hours but were stable long enough to permit spray-drying, as long as the slurries are agitated prior to loading the syringes. The amines were discarded due to toxicity concerns. In the end, the Elvacite grade 2008 PMMA resin was selected because it is known to burn out cleanly in a variety of conditions, including under vacuum and in reducing and inert atmospheres, and provides adequate dispersion as well as acting as a binder for the pressed green samples.

3.2.3. Spray Drying

The resulting slurry of solids, dispersant and acetone was then spray-dried with an ultrasonic atomizer to create small uniform spray-dried granules with a well dispersed elemental ordering in the green state. Ultrasonic atomization creates a narrow size distribution and better shape of spray-dried particles and is preferred to blown two-fluid type nozzles. The ultrasonic atomization nozzle was obtained through Sono-Tek (Milton, NY). The frequency was optimized for a slurry flow rate of 20cc/min.

The atomized slurry was sprayed into a lab-sized 50 gallon oven. Figure 3.2 shows the spray-dry processing setup. The low boiling point of acetone allows relatively

low spray-dry temperatures which are kept near 60°C, and a blanket atmosphere of blowing N_2 prevents the acetone vapor from being combustible and sweeps away the acetone-saturated atmosphere.

Figure 3.2: Ultrasonic spraydry setup includes blown N_2 gas with a preheater, ultrasonic nozzle and control, heated chamber and a steady-rate syringe pump.

The size of the spray dried granule depends on the slurry viscosity, density and ultrasonic frequency of the atomization nozzle. Solids loading of 10-15% was deemed best for producing a narrow even size distribution in a timely fashion. After spray-drying the powders were then screened to 100 mesh for optimal flow and fill of the granulated powder. The process has been replicated off site and was demonstrated to be capable of

scale-up to industrial production levels. Figure 3.3 shows the spray-dried granules with size around 100 μm in diameter.[13] Pellets and bars were pressed from the spray dried powders to 500MPa in a floating die under vacuum.

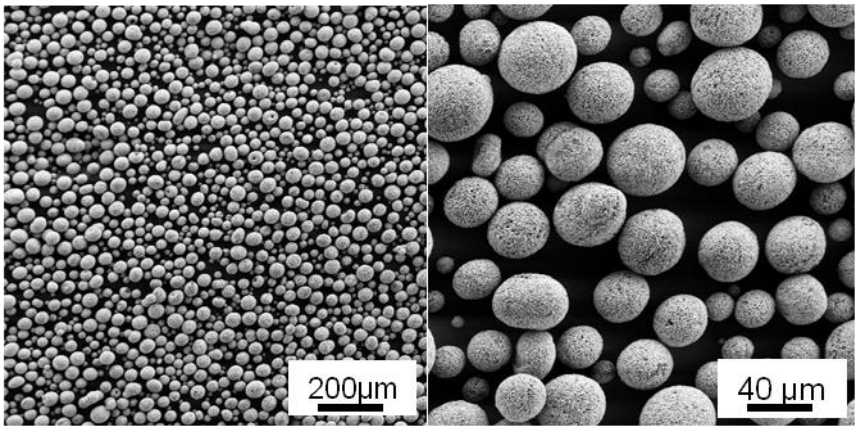

Figure 3.3: Mixed and spray dried granules of Mo, Si_3N_4, and BN powders

3.3. Firing

Once mixed, spray-dried and pressed, the compacts were sintered and reacted in a controlled reducing atmosphere of Ar/10% H_2 to achieve final density greater than 90% of theoretical. Inlet gas was gettered by Ti to remove any residual oxygen and water vapor. A hold of 4 hours at 400°C was used to remove the binder, and final temperatures of 1400-1600°C are required for sintering and reaction of the nitrides.

The nitrides react with Molybdenum during firing in reducing environment which depending on composition results in formation of T2, A15 and/or molybdenum boride and nitrogen gas.

$$3\ Mo + 1/3\ Si_3N_4 \rightarrow Mo_3Si + 2/3\ N_2$$

$$5\ Mo + 1/3\ Si_3N_4 + 2\ BN \rightarrow Mo_5SiB_2 + 5/3\ N_2.$$

$$2Mo + BN \rightarrow Mo_2B + ½\ N_2$$

The reactions become thermodynamically favorable and have been shown by thermo-gravimetric analysis to begin at ~1200°C and will go to completion in 6 hours at 1300°C. The fraction of boride is determined by the initial ratios of starting materials. Due to slow diffusion, the final distribution of intermetallics does not vary significantly with firing schedule but instead is governed by initial dispersion of the nitrides, necessitating small starting powder sizes and good mixing.

Additional studies investigated the merits of cold-isostatic pressing on initial forming and also addition of a hot-isostatic pressing step to achieve higher density. Cold isostatic pressing (CIP) involves using a vinyl bag and pressing uniformly in an oil or hydraulic bath. It can achieve better packing and higher green densities without directional remnants or lamination that could be seen in uni-axial pressing and by altering the bag shape CIPing could be used to produce near-net shapes in the green state. Hot isostatic pressing (HIP) uses similar applied pressure from inert gas during firing at higher temperatures. The increased pressure aids the driving force for sintering and ensures removal of any remnant porosity, and the increased pressure can enable complete sintering at lower temperatures, and thus with reduced grain growth among other benefits. In the HIP, the material must have no open porosity or be encapsulated in a hermetic can that can be deformed by the HIP environment. Samples were prepared and dry pressed either by CIP (1” diameter x 5” length bars) or by the uni-axial die pressing described before, and wrapped in Mo foil as a barrier to contamination from the cans

before they were encapsulated in steel cans. The steel cans were evacuated and welded hermetically prior to HIP. The encapsulated bars and/or pellets were subjected to hot isostatic pressing at 1500°C at 50 Ksi pressure in inert Ar gas. The HIPed bars produced have higher density and thus more mechanically sound and can be hot swaged. Swaging and hot extrusion permits structural rearrangement and has been identified in the Berczik patents and others to improve the continuity of the Mo matrix in order to increase ductility and possibly reduce the DBTT.

3.4. Analysis

3.4.1. Density

The Archimedes density method was used to determine the final bulk density, and degree of open porosity to compare to the expected theoretical density. The method is based on Archimedes principle of buoyancy and requires measurement of a dry weight (W_{dry}), a saturated weight (i.e. with water saturating open pores but not beading on the surface – W_{sat}) and a suspended weight (weight while suspended in water – W_{susp}). After measuring a dry weight the samples are held underwater in an evacuated chamber for 15 minutes so that the water replaces air in any open pores before measuring a suspended weight under water. The sample is patted dry with a moist towel and weighed again to get the saturated weight. The bulk density of a sample is given as:

$$\rho_{Bulk} = \frac{W_{Dry}}{W_{Sat} - W_{Susp}} \qquad \text{(Eq. 3.1)}$$

The percentage of open porosity of the sample is calculated as:

$$\%O.P. = \frac{W_{Sat} - W_{Dry}}{W_{Sat} - W_{Susp}} * 100 \qquad \text{(Eq. 3.2)}$$

which corresponds to the volume of surface connected porosity. The volumes and weights before and after firing are measured and correlated to degree of Mo, oxide and adsorbed water driven off, and reaction of the nitrides. Volume change and linear shrinkage during firing are also recorded.

3.4.2. XRD

The resulting fired composites were characterized by qualitative and quantitative refinement of X-ray diffraction patterns. XRD can be used to identify the crystalline phases present and their relative weight fractions. The X-ray diffraction data was used for identifying final phases present to verify the proposed reactions are occurring, to verify completion of reactions during the pre-reaction of intermetallics and other added compounds, and to check that no unwanted compounds are forming.

XRD analysis was performed using a Panalytical X'Pert PRO Alpha-1 Xray diffractometer. The instrument was operated using Cu Kα radiation with 0.15418 nm wavelength (8048eV) and an X'celerator wide range 1D Silicon strip detector in a Bragg-Brentano parafocusing geometry on polished flat solid samples or pressed flat powders. The resulting XRD patterns were analyzed using Jade 8 (MDI) and X'Pert HiScore Plus software and the ICDD powder diffraction file (PDF) database. The software permits Reitveld refinement for matching the observed peak profiles in order to obtain quantitative phase fraction and unit cell dimension results.

Mo-Si phase diagrams indicate a Si solubility as high as 3% or more at 1600°C, and results by Perepezko[8] indicate that the system is very slow to approach equilibrium when cooled; the high Si content is "frozen" in at the level of the maximum process temperature unless very long anneals in the hundreds of hours are considered. Due to the

smaller Si atoms locating substitutionally in the Mo BCC lattice, Sturm[20] showed that the Si content can be roughly observed by the steady decrease in the BCC molybdenum unit cell dimensions with increasing Si solid solution. XRD refinement of the measured Mo unit cell dimensions should provide a reference to the degree of Si present in solid solution.

XRD was also used after oxidation testing to identify any crystalline phases present. It cannot identify amorphous phases beyond presence of an "amorphous hump" but can identify crystalline oxides, molybdates, and other potential oxidation products both on the surface and within or beneath the glass coating. Pyrex glass which is a similar borosilicate composition to the glass formed on these materials has mass attenuation of $\mu/\rho = 33 cm^2/g$. With an estimated density of ~3g/cc, the depth penetration through glass is significantly high such that for 10-200 μm thick glasses we can expect to see peaks from the underlying crystalline phases.

3.4.3. SEM/Imaging/Microstructure

While XRD can determine the phases present and their relative fractions, microscopy allows examination of their size scale and distribution, as well as being able to observe non-crystalline phases, porosity and more. In order to determine the nature of the microstructure and understand the effects of various processing changes, the microstructure must be examined. Samples were cross sectioned and polished to 1200 grit and examined in an Amray 1810 SEM in secondary and backscatter imaging. Fracture surfaces of mechanical test samples were also examined under SEM. Oxidation samples which form a glassy nonconductive coating must be gold coated prior to electron microscopy. Oxidation samples were epoxy mounted under vacuum to impregnate the

structure and prevent damage when cross sectioned. The cross sectioned pieces are mounted in a thermoplastic resin and gold coated before SEM examination, while other oxidation samples were gold coated and the oxidized surface was imaged directly.

The prior works by Middlemas used a combination of backscatter electron (BSE) imaging and electron backscatter diffraction (EBSD) to determine the content and arrangement of the various phases, Figure 3.4. EBSD uses crystal diffraction to identify phases and create a phase map image. It can differentiate between otherwise similar phases based on their crystal structure and can also identify grain boundaries and individual orientations. EBSD was employed because it provides a clear and effective distinction between the A15 and T2 intermetallics which can be difficult to differentiate otherwise. The low phase contrast by atomic number between Mo_2B and molybdenum makes distinguishing them by BSE also difficult. In the current study EBSD was used when available to differentiate the Mo and Mo_2B. Also a combination of both high gain backscattered electron imaging and slow atmospheric oxidation of Mo-Mo_2B alloys allow the phases to be roughly distinguished. Mean grain sizes, volume fractions and qualititative assessment of the arrangements are taken from micrograph images.

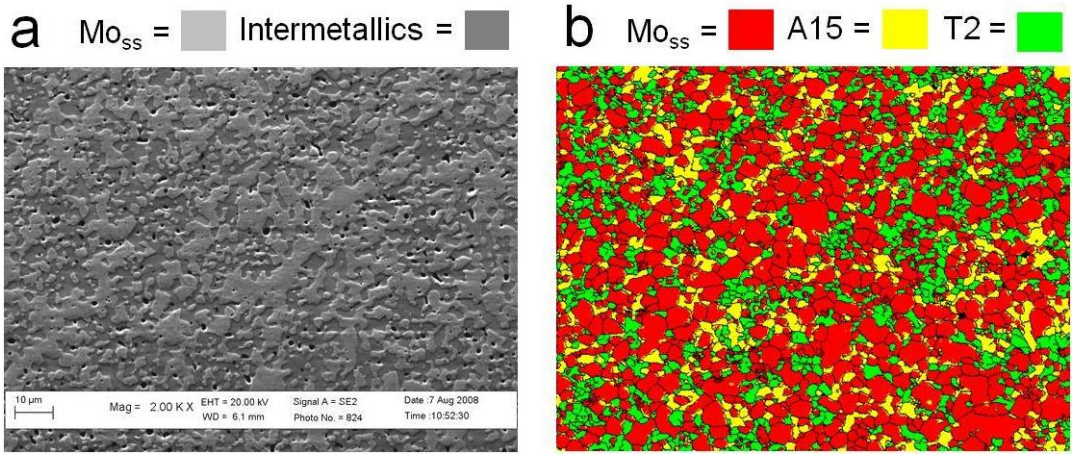

Figure 3.4: Microstructure of Mo-3Si-1B shown in (a) backscatter SEM imaging and (b) EBSD to show phase regions and grain size of all three phases

3.5. Oxidation Testing

Oxidation tests were carried out for the various samples at temperatures of 1000°C, 1100°C and 1300°C on 12.5mm diameter x 5mm thick pellets. The rate of oxidation was measured in terms of weight lost per area (mg/cm^2) on a lab scale with 0.1 mg resolution. Surfaces and cross-sections were analyzed by XRD and metallography/microscopy as described in the prior sections.

Oxidation studies were performed at specific temperatures in oxidizing atmospheres. It is expected that the oxidation will proceed in much the same way as the Mo3SiB alloys wherein, as time increases, the film thickness will increase but at a decreasing rate. Oxidation tests mimicked those done for the Mo-3Si-1B samples and compared directly. Oxidation studies were performed in air in the expected transient temperature regime from 500-700°C in order to evaluate the removal of Mo as MoO_3, the reaction of Mo_2B to form B_2O_3, and the interaction between the B_2O_3 and SiO_2 to form a glass. Samples were also studied in the temperature regime from 800 to 1000°C to

evaluate the homogenization of the glass, effectiveness of the B_2O_3 on fluxing the SiO_2, and ability of the system to form a protective coating. Further studies at 1100°C, the temperature for which a 3:1 Si:B ratio (by weight) is optimized, were conducted to evaluate the time required for a protective coating to be formed and the effectiveness of the coating at limiting oxidation over longer periods into the tens of hours. Studies will further be performed at 1200 and 1300°C with considerations of the effectiveness of the coating at higher temperatures and effects of the changing glass composition to optimize for various temperatures and to evaluate effects of to boria evaporation, increased $MoO_{3(g)}$ partial pressures, etc.

The rate of oxidation was measured in terms of weight lost per area (mg/cm^2) for the 12.5mm diameter x 5mm thick pellets. The initial losses attributed to the transient regime and calculated parabolic rate constants in the parabolic regime were used to judge compositions. Oxidized pellets were sectioned and examined by optical and electron microscopy to observe the mechanisms by which the oxidation proceeds in each specific system. The method of forming the coating, rate of the coating's growth during isothermal holds and recession of the metal were studied for the compositions with varying phases and B:Si ratios.

As a given volume of material is removed, the volume of each phase exposed is directly related to their volume fractions. O_2 exists in excess in the ambient atmosphere. All Mo_2B can be assumed to react by:

$$Mo_2B + 3\ O_2 \rightarrow MoO_3 + B_2O_3$$

and Mo can be expected to react by:

$$Mo + {}^3\!/_2\ O_2 \rightarrow MoO_3$$

while the SiO_2 remains as SiO_2 glass. It is further assumed that all of the B_2O_3 mixes with the SiO_2 to form a borosilicate glass.

For example, composition BS2128 with 21% Mo_2B and 28% SiO_2 by volume, a loss of material from the surface would expose 5.4 moles of Mo for every mole of SiO_2 and Mo_2B. Per mole of SiO_2, this corresponds to a loss of weight of 705g of Mo as MoO_3 vapor from reaction of Mo and Mo_2B, while forming 33g of B_2O_3 and 61g of SiO_2. In terms of volume, the ratio of material lost to glass coating formed comes out to approximately 3.05:1. This means that based on this simplified model, it would require a loss of 3mm of material from the surface to form a coating 1mm thick. Weight lost and coating thickness values can then be interchanged for the parabolic model and compared to actual values.

Oxidation was compared to the parabolic rate in Equation 2.2. Based on the assumptions in the model, the weight loss should be directly proportional to the thickness of the glass layer formed. Oxidation behavior was evaluated as a function of the microstructural parameters of particle size and spacing, and of glass properties based on composition. Deviations and consistencies with the model were considered.

In the works by Helmick, large transient losses were attributed to MoO_3 evaporation through pores in the forming glass[56]. Based on this realization, the opportunity to limit initial losses exists by preoxidizing the samples to form coatings before exposure to the harsh real-world environments. This type of pretreatment is common practice for $MoSi_2$ furnace elements to limit pesting. Samples for pre-oxidaton may be heated in inert atmosphere to 1100°C and then subjected to limited oxygen partials to oxidize the Si and B while retaining Mo. In the controlled high T low pO_2

environment, the glass should be formed rapidly and with low enough viscosity for effective coating without oxidizing Mo and its associated weight losses. Preoxidized samples were further oxidized in air and compared to the samples that were not preoxidized.

After oxidation testing, as-oxidized surfaces and polished cross sections of the pellets were examined using optical and scanning electron microscopy to gauge the effectiveness of the borosilicate coating and understand the mechanisms behind its success or failure.

3.6. Mechanical Testing

Mechanical testing of 3 or 4-point bend bars was performed at room temperature to compare different compositions to look qualitatively for ductility and give an indication of fracture toughness. Bend bars with dimensions 20x2x2mm were floating die pressed to 2500psi and fired with the same procedure as above and were tested on an MTS Insight machine in 4 point bending with outer span of 17.65mm and 6mm inner span, at a nominal strain rate of 0.3mm/min. The resulting fracture surfaces were analyzed by SEM.

Hardness tests using a Vickers diamond indenter were used to compare compositions and possibly indicate solid solution strengthening effects. Indents were also made to possibly estimate fracture toughness by the Vickers indentation fracture toughness method. While the values obtained from this type of test are questionable, a range of values may be found and compared to other similar materials. This could provide a simple evaluation metric for comparing different compositions. Samples were

loaded at 500g and 1kg for 30s with a standard diamond Vickers hardness indenter. Fracture toughness was calculated from Miyoshi's equation:

$$K = \zeta(E/H)^{n} P c^{-3/2}$$

where E is the Young's modulus, H is hardness, P is the load and c is the the half-length of the measured crack. ζ and n are material independent parameters given by the models and for Miyoshi's equation ζ=0.018 and n= ½.

CHAPTER 4. MOLYBDENUM + GLASS FRIT

4.1. Introduction

Mo-Si-B intermetallic alloys have the potential to possess the oxidation resistance and mechanical properties required for the next generation of jet turbine engine blades. Three-phase alloys in the α-Mo, Mo_3Si (A15), and Mo_5SiB_2 (T2) compatibility triangle have been shown to possess the high strengths necessary at high temperatures as well as environmental resistance against oxidation of the Mo metal by formation of a borosilicate glass upon reaction of the intermetallics. A major hurdle preventing their implementation is that they suffer from poor ductility and low toughness at lower temperatures.

These alloys must contain pure and continuous ductile molybdenum with isolated but finely dispersed silicon and boron to form the glass coating. However, Si has been identified as a cause of poor fracture toughness in Mo alloys. To avoid embrittlement by Si in solid solution in the Mo, the compositions here are shifted away from the T2-A15-$Mo_{(ss)}$ phase triangle to avoid A15 and thus have limited or no Si solubility in the Mo. The silica to form the glass coating which would have been provided by the A15 phase will in this case be replaced directly with commercially available glass frits mixed in as a powder in the green state. The desired result is a composite consisting of a ductile Si-free Molybdenum matrix phase with finely and evenly dispersed glassy regions for self-healing oxidation resistance similar to that of MoSiB alloys.

Another additional benefit of this system over MoSiB is the potential for a reduction in density. The density of Mo is 10.28 g/cm^3, and the frit glass is roughly 2.5 g/cm^3 depending on composition. As shown in Table 4.2, the proposed composites could have a density as low as 7.8 g/cc. This is significantly lower than for MoSiB alloys

(~9.55 g/cm^3) and Ni-based superalloys (~8.95 g/cm^3) and is another advantage over both competing material systems.

Use of glasses instead of glass forming hasn't been approached previously because adding glass cannot be done while maintaining a desirable microstructure except through powder processing, which typically does not meet the requirements of low impurity content. The GA Tech reaction sintering (GTRS) process developed by Cochran and Middlemas avoids these issues and has been specifically designed for high surface area Mo and for creating a tailored composite microstructure. This chapter discuses the work done to adapt and further develop the GTRS powder processing techniques and chemistries to produce oxidation resistant alloys of Mo with ability to form self-healing in-situ oxidation protective coatings from added glass frits.

4.2. Mo+Frit Experimental Considerations

The Mo and frit batches were prepared with either 20 or 40 volume % of the frits listed in Table 4.1 and were processed following the route described previously in Chapter 3. The process has been proven to produce alloys of nearly full density and having the desired fine grain size and microstructural homogeneity. In this case the Si and B nitrides used to form the molybdenum borosilicate intermetallics were replaced with the commercial glass frits. A Mo-3Si-1B at% alloy produces ~20% of its volume in glass upon oxidation, so an equivalent 20vol% frit was added to pure Mo. The starting powders of Mo and sieved glass frit, along with binders, lubricants and dispersants were mixed by ball milling in acetone to avoid oxidation or formation of hydrides with Mo. The resulting slurry was then spray-dried to create a well dispersed elemental ordering in the green state consisting of evenly distributed frit and Mo particles and entrapped in

flow-able spray dried granules. Pellets and bars were pressed to 60ksi from the spray dried powder in a floating die under vacuum.

Table 4.1: Properties of the glass frits tested

Manufacturer	ID	Density	Soft T (°C)	Expansion (E-6)	Mean P Size (μm)	Chemistry
Ferro	3195				8.2	$CaO, Na_2O, Al_2O_3, B_2O_3, SiO_2$
AGC	1780	2.5	780	5.2	5	$SiO_2, B_2O_3, BaO, Al_2O_3$
AGC	1491	3.7	673	9.0	1.2	$SiO_2, B_2O_3, BaO, Al_2O_3$

The pressed compacts were sintered and reacted in the previously described manner in a controlled reducing atmosphere of Ar/10% H_2, with a 4 hour hold at 400°C remove residual binder, and final holds of 4 hours at 1600°C for sintering.

4.3. Mo + Frit Results

4.3.1. Microstructure and Density

The compositions and fired densities are listed in Table 4.2. The batches were fired with 20 or 40 volume% of the frit listed in the first column, with the remainder being pure Mo. Of the compositions all pellets were able to be fired to at least 89% theoretical density. The glass containing samples had effectively zero open porosity making further hot isostatic pressing possible without encapsulation, though that was not pursued.

Table 4.2: Mo-Frit compositions tested and measured fired densities

Batch	Green Dens. (g/cc)	Fired Dens. (g/cc)	Theo. Dens.	% Theoretical	Open Porosity
20% 3195	4.70	7.82	8.77	89%	0.3%
20% 1790	5.03	8.29	8.77	95%	0.1%
20% 1491	5.43	8.75	8.77	100%	0.0%
40% 1491	4.42	7.67	7.8	98%	0.5%
40% 1780	5.20	8.42	8.77	96%	0.1%

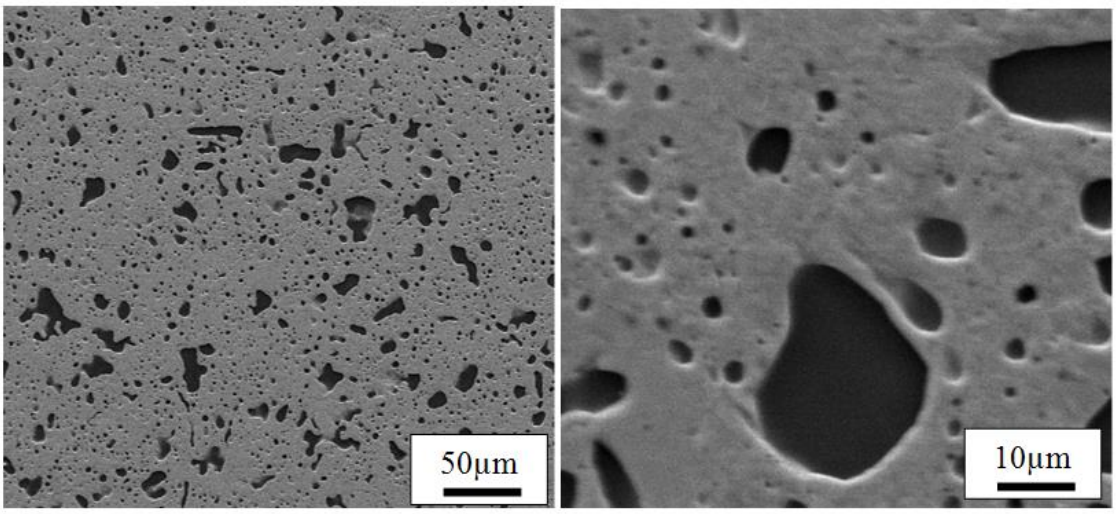

Figure 4.1: Micrographs of the polished Mo – 20vol% 3195 frit sample showing the as-fired microstructure.

Figure 4.1 shows the polished as-fired microstructure of the Mo sample containing 20 vol% 3195 Frit. EDS of the light area shows pure Mo, while the dark regions show mostly Si. Observation in a light microscope showed refraction and reflection from the larger dark regions seen in the SEM which reveals that these are glass and not pores or grain pullout. The glass is arranging with rounded edges which would indicate it's not wetting and coating Mo grain boundaries. Electrical conductivity measurements confirmed an effectively zero resistivity indicating a continuous Mo matrix. This is advantageous because if the glass wet and coated the Mo grains it would severely embrittle the alloy. Area counting of the glassy regions in the micrographs shows approximately 20% of the volume is glass which closely matches the expected glass volume fraction and indicates very low porosity.

The sizes of the SiO_2 regions range from submicron to over 50 microns. The larger regions may be due to large frit particles or frit agglomeration. Large initial chunks of frit which had only been sieved to <635 mesh can only be guaranteed to have at least two minimum dimensions of <20um. Milling the frits was pursued in an attempt to reduce the size of the glass regions.

Milling took place with a slurry of 10vol% solids in water and Darvan 821 as dispersant at 1wt% of the solids. The slurry was ball milled for 24 hours with mixed-size 99% alumina milling media added to 45% of the slurry volume. The final particle size was measured by Beckman-Coulter laser particle size analyzer and by BET surface area. As screened (<635 mesh) average particle size was measured to be 8.22 um diameter, with 90% below 15.7 um and only the finest 10% below 2.7μm. BET results of the stock powders screened <635 mesh showed for SH732A Frit a mean surface area of 0.6887

m^2/g and the 3195 frit, 0.5584 m^2/g. After 24h milling time, mean particle size was reduced to 2.59 µm, with the fines fraction nearly unchanged; 10% d < 2.25 µm but the larger fraction d90 (90% d <) reduced to 5.13 µm. Milling for 48 hours reduced the average sizes further, but mostly by increasing the fine end of the particle spread with a mean of 1.6 µm, 90% < 3.4 and 10% < 0.3 µm.

This shows that milling is a viable means for obtaining smaller frit sizes. Again however dispersants become an issue, especially since the Darvan 821 dispersant used during milling is difficult to wash from the milled particles and may cause detrimental interactions with the Elvacite and acetone used during the spray drying process. Samples fired with milled frit still had large silica regions suggesting they're caused by agglomeration in the slurry and/or flow during firing.

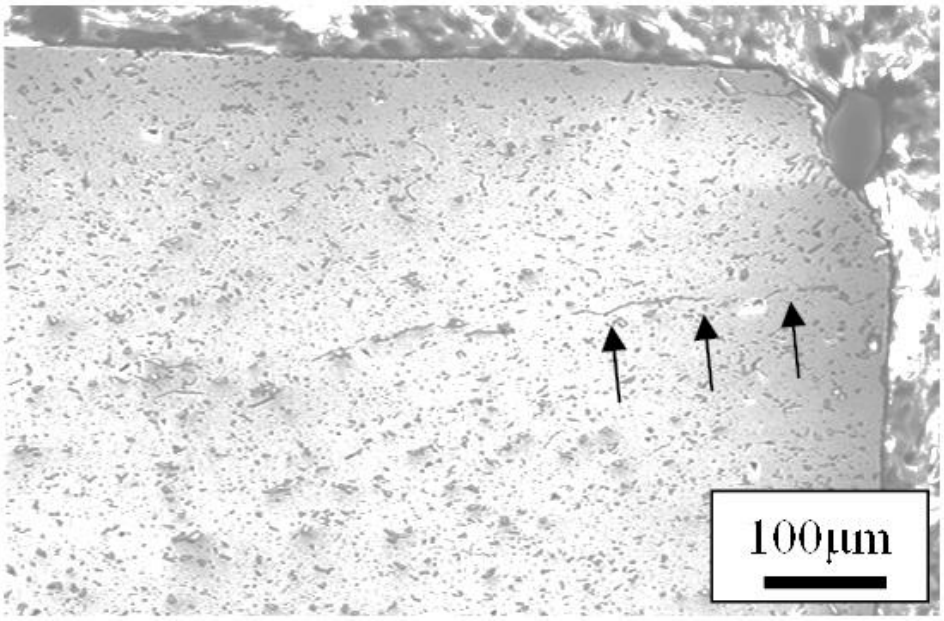

Figure 4.2: Polished cross section of as-fired Mo with 20vol% 3195 frit. A remnant crack which filled with glass during firing is indicated with arrows

A remnant of a crack or lamination crack from pressing is evident in Figure 4.2. The crack after firing is filled with glass. This indicates that the glass is flowing and filling pores and voids and may account for the larger than expected regions of glass. This low internal porosity combined with the 0% open porosity measured by Archimedes method further corroborate the assumption that glass is filling pores.

4.3.1.1.Glass Beads

Glass beads were observed on the surface, not completely covering it. The beads are likely due to some of the glass being pushed out during shrinkage and densification. During sintering, the glass becomes fluid near 1000°C. The liquid/solid interfaces between the glass and metals are less stable than the solid/solid interfaces, yet more stable than the solid/vapor. As a result, when the glass is fluid during firing it flows to replace the solid/vapor interfaces with solid/liquid interfaces which pushes out most of the air during the initial stages of sintering. Then as sintering proceeds driven by the reduction in free energy of replacing the solid/liquid interfaces with solid/solid interfaces, shrinkage of the part occurs which expels a portion of the fluid glass. This is consistent with the observation of more glassy beads toward the center of the pellet than at the edges.

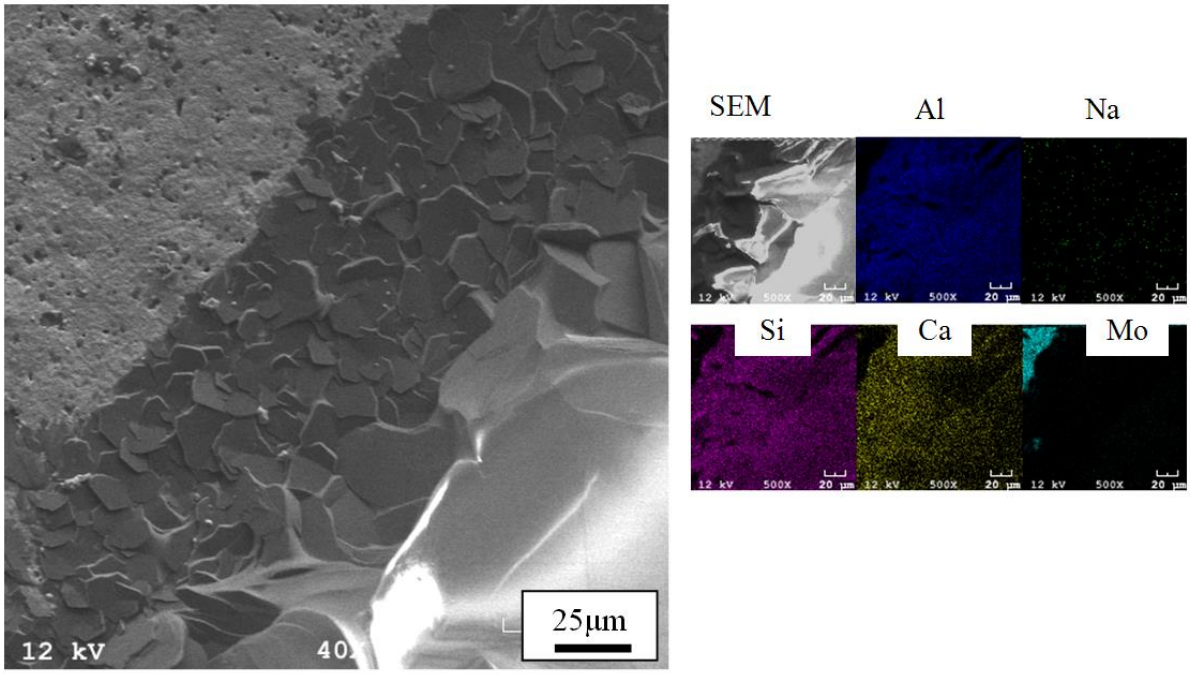

Figure 4.3: SEM and EDS micrographs of the corner of a glassy expelled blob on the as-fired surface. EDS element maps of the same location are shown to the right.

These beads on the surface of the 3195 containing sample were examined in SEM. Figure 4.3 shows the edge of a glass protrusion observed on the as-fired Mo + 20% 3195 Frit sample's surface. The top left of the image is the expected surface of Mo interspersed with Silicate particles. The tallest part of the protrusion of expelled glass (bottom right) appears to be glassy with rough edges from spallation caused by thermal shock during cooling. The glass is surrounded by a region of mostly hexagonal flakes seen as the band diagonally across the image.

EDS phase maps of the glassy bead and surrounding flake and Mo are also shown in Figure 4.3. The crystalline flake and glassy bead appear to be the same composition, mostly Ca, Al, and Si which matches the 3195 frit. This would imply that the flakes are most likely crystalline plagioclase feldspar. Si, Al and Ca – the main components of the

frit, are evenly dispersed in the glass and crystalline phase, while the Mo remains exclusively outside the beads.

A second frit composition was also examined (AGC 1780) which is composed nearly exclusively of silicon, aluminum and barium. After firing this also exhibited glass beads on the surface but without crystallization.

The samples were oxidized at 1000°C and 1300°C and the surfaces visually examined. A glass coating did form but was too fluid to coat well, with numerous bubbles and pores. Within the first half hour the glassy coating had begun to devitrify; evident as opaque regions in the glass coating.

4.3.2. Mechanical Results

4-point bend tests were conducted to look qualitatively for ductility using a 4-point bend apparatus with an outer diameter of 17.65mm and 6mm inner diameter and a rate of 0.3mm/min. The results are plotted in Figure 4.4.

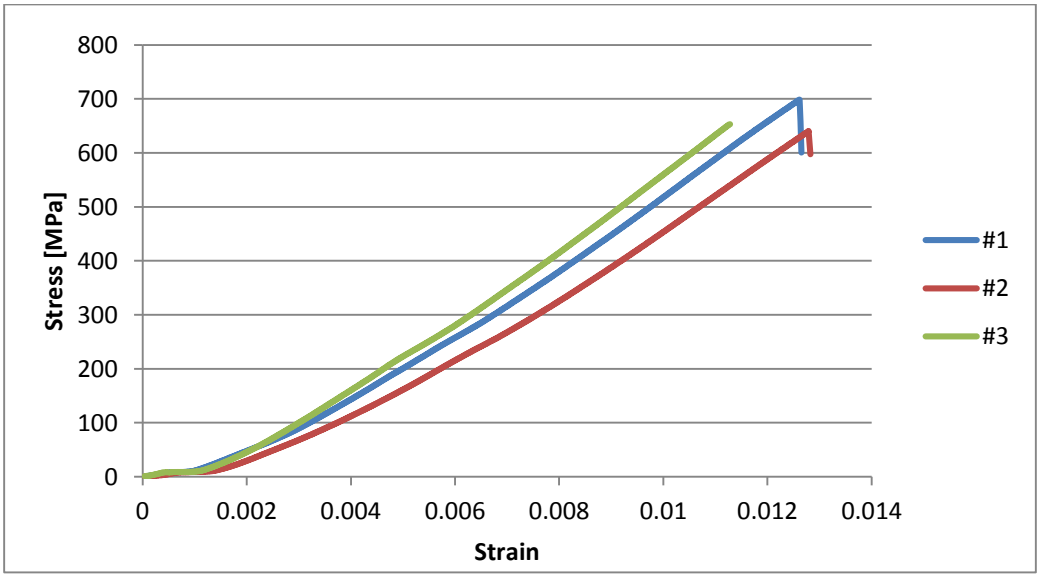

Figure 4.4: Stress strain curves from 4 point bend tests of three samples of Mo with 20vol% 3195 frit.

In order to verify that the powder and sintering process can produce ductile bars, test bars were made by the same procedure with Mo alone and Mo with Stearic Acid. Bend tests of pure Mo made with the same process were conducted to look qualitatively for ductility. The results are plotted below in Figure 4.5. Significant ductility in the Mo samples can be seen (Figure 4.6) and shows that there is no inherent embrittlement of the Mo using our powder processing technique. Calculated fracture strains are 15% and 11.5% for the Mo + stearic and Mo-alone respectively. Other tests were concluded without fracture as they approached the mechanical limits of the test instrument.

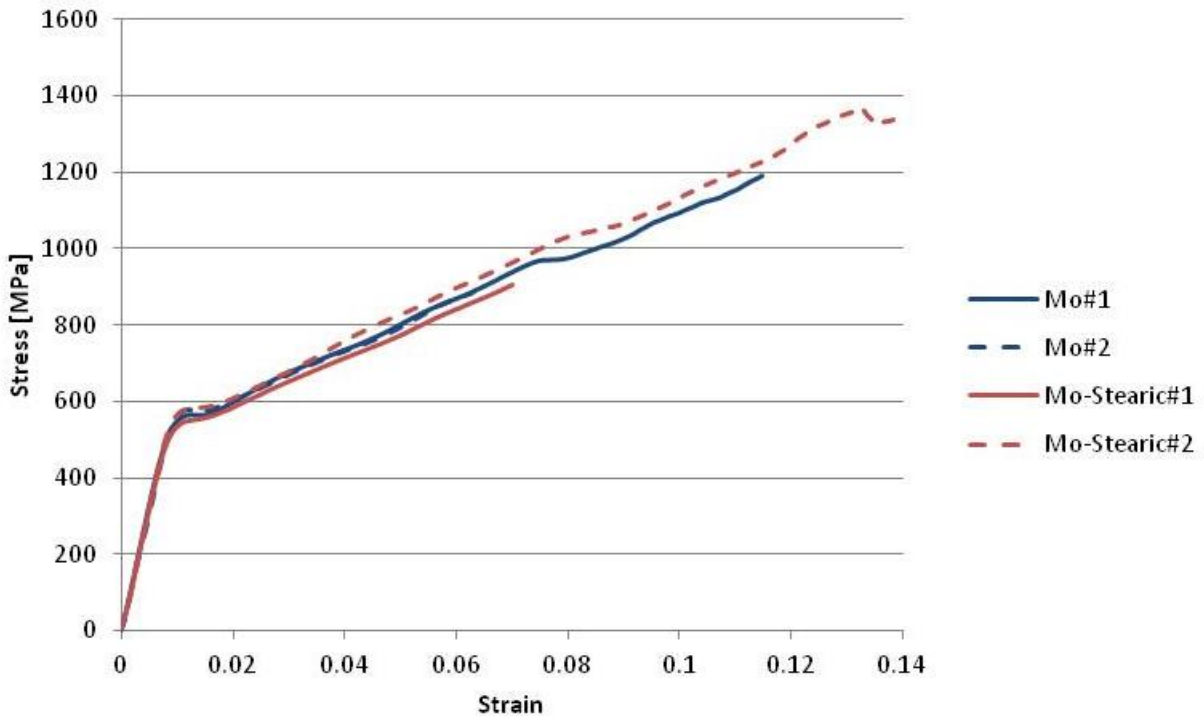

Figure 4.5: Stress strain curves from 4 point bend tests of samples of pure Mo and Mo pressed with stearic acid.

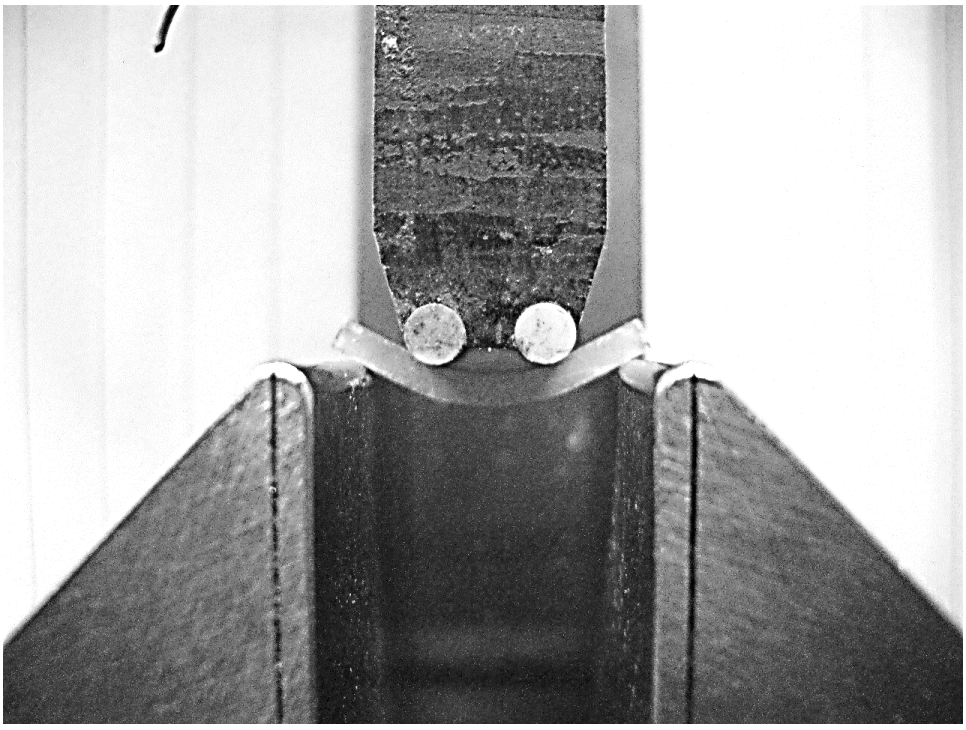

Figure 4.6: Photograph of ductile 4 point bend bar Mo-Stearic #2.

Vickers indentation was used also to look for indications of toughness. Mo with 20v% 3195 frit was loaded at 500g and 1kg for 30s with a standard Vickers hardness indenter. None of the indentations showed cracks, which inhibits toughness measurements. The average measured hardness value was 225 which is close to the hardness for pure Mo. No cracking was observed which precludes the opportunity for measuring fracture toughness. The lack of cracks based on the general Vickers toughness equation suggests that the toughness is at least greater than 3.0 MPa$\sqrt{m}$.

4.4. Mo + Frit Conclusions

A Mo based alloy using SiO_2 instead of A15 creates an opportunity to provide oxidation resistance with much less detriment to the strength of Mo. These alloys can be produced by powder processing and reaction sintering with relative ease and cost

effectiveness. Alloys based on this system will have lower Si contents in solution with Mo and the possibility for lower fractions of glass formers to create same coating, both of which can lead to greater strengths and fracture toughness.

The opportunity to produce a desirable microstructure of fine particles within a continuous Mo matrix is an important goal within this field of study and has been demonstrated for this system. To date, only this specific powder processing method has shown the ability to create a dispersed microstructure which includes glass powders or lower melting phases, and without detrimental impurity contents in the Mo. Unfortunately the low melting point of the frits means they would be liquid during initial processing and internally liquid at the end-use temperatures, thus creating non-ideal fired microstructures as well as drastically reducing creep resistance. It would not have sufficient strength in engines at 1300°C. Instead a pure Silica source such as pure amorphous SiO_2, cristobalite or quartz, all of which have melting points above 1500°C, must be used, and will be the topic of the next chapter.

The results of the early oxidation results show promise in meeting the needs of oxidation resistance and are able to create a self-healing coating in a similar manner to current leading MoSiB systems. The composition of the glass however is not optimized, and opportunity for significant improvement exists with only simple changes to composition and processing. Since composition can be tailored by initial powders using this powder based approach, compositions with oxidation properties which exceed those of the MoSiB alloys are not unreasonable to expect.

CHAPTER 5.

Mo + T2 + SiO_2 ALLOYS

5.1. Introduction and Justification for SiO_2 Addition

Initial attempts recounted in the previous chapter verified that commercially available glaze frits could be added to Mo using the GTRS powder processing technique and were able to create acceptable microstructures with usable oxidation resistance. However the low melting point of the frits means they would be liquid during initial processing and internally liquid at the end-use temperatures, thus creating non-ideal fired microstructures as well as drastically reducing creep resistance. The flowable glass during processing also appears to limit the low temperature mechanical properties resulting in brittle room temperature behavior. Instead a pure Silica source such as pure amorphous SiO_2, cristobalite or quartz, all of which have melting points above 1500°C, must be used.

Some boron must also be present to flux the glass and promote flow and rapid coating. The boron containing intermetallics Mo_3SiB_2 (T2) and Mo_2B exist as solid stable phases in equilibrium with Mo over a wide range of temperatures and do not contribute to Si embrittlement. While they are stable refractory phases within the bulk, when they are exposed to oxygen they from a low viscosity boria glass only at the surface and only during oxidation.

5.2. Experimental

5.2.1. Batches

Two classes of systems have been investigated, one with silica in an amorphous form and the other crystalline, but all with a chemically pure Mo phase of greater than 50 volume percent. Additional phases include; dimolybdenum boride (Mo_2B), T2, and mullite. The compositions are given in Table 5.1. For the systems with silica, compositions were chosen which are within the Mo-Mo_2B-T2 ternary and Mo-Mo_2B binary and avoid Si solid solution by avoiding the A15 phase. These compositions are batched corresponding to Mo-1Si-1B wt% and Mo-0Si-1B but with silica added to a 3:1 Si:B ratio in terms of final glass composition.

Table 5.1: Mo composite compositions examined in this study.

Batch	Final Volume Fraction					Theoretical Density	Si:B Wt. Ratio
	Mo	Mo2B	Mullite	Silica	T2		
B10	90	10	-	-	-	10.12	0:1
B20	80	20	-	-	-	10.02	0:1
S10	90	-	-	10	-	9.46	1:0
BM0505	90	5	5	-	-	9.82	1:1.4
BM1010	80	10	10	-	-	9.42	1:1.4
BT0521	74	5	-	-	21	9.87	1:0.4
BS2128	51	21	-	28	-	7.76	3:1
TQ3113	56	-	-	13	31	8.79	2.1:1
TS3115	54	-	-	15	31	8.65	2.1:1
TQ2713	60	-	-	13	27	8.85	2.3:1
BST052021	54	5	-	20	21	8.35	2.6:1
TS2322	55	-	-	22	23	8.23	3.5:1

The naming convention uses the initials of the phases present, and their respective volume fractions (excluding the a-Mo phase). For example the composition as shown in Table 5.1 labeled BS2128 which has "B" (the boride phase Mo_2B) with a final volume fraction of 21% and "S" the silica SiO_2, at a final volume fraction of 28%, and the remainder 51% the interconnected a-Mo matrix. Likewise B20 has the final phase composition of approximately 20 vol% Mo_2B with the remainder being Mo. This corresponds to 99 wt% Mo with 1 wt% B which is indicated as Mo-0Si-1B shown in Figure 2.7.

The B20 composition was prepared to validate that the Mo_2B is being formed in the right proportions and maintaining desirable arrangement. Then silicon nitride was added to form T2. This results in a final phase distribution in the Mo-Mo_2B-T2 phase triangle with 5vol% Mo_2B and 21% T2 (BT0521), for a final composition of Mo, 1 wt% Si and 1 wt% B (Mo-1Si-1B) which should still avoid the contribution of Si from A15. In the third and fourth compositions, SiO_2 was added to the first and second compositions to alter the glass composition to the optimized 3:1 Si:B weight ratio. This results in Mo with 21v%Mo_2B and 28v% SiO_2 (BS2128) and 5v%Mo_2B, 20v% SiO_2 and 21v%T2 (BST052021). These batches maintain greater than the proposed 50 vol% minimum of Mo required for strength while providing adequate glass formers in the optimized ratio for oxidation protection. The final volume fractions are given in Table 5.1.

A series of additional Mo-silica-borosilicate type compositions were examined in which the Mo_2B boron source is entirely replaced with T2. The T2 could have benefits over Mo_2B by retaining boron in the system. The ratio of Si:B was varied also as this is well known to affect the glass composition and thus oxidation behavior, but should have

little to no effect on either the mechanical properties of the Mo phase or the distribution in the final microstructure.

Additionally it's been noted that boria is volatile at the oxidation temperatures. This is a potentially useful feature of MoSiB alloys because it allows for a low viscosity (i.e. high boria) glass initially with short transient losses, but which thickens over time due to loss of volatile boria and develops a higher viscosity and thus lower oxygen diffusivity to benefit long term protection. In the Mo_2B samples, unlike MoSiB, the boria is present alone upon initially forming, as opposed to being formed simultaneously with silica by oxidation of T2. The consequences of this are twofold. The lone boria may be more volatile than it is in the borosilicate formed from T2, and the difference in boria volatility could affect the composition in unpredictable ways and result in higher than expected boria losses and a higher viscosity than planned for. Secondly, the flow of the pure boria may not be as effective or react as uniformly when contacting the silica.

Mo in equilibrium with T2 does not have any Si in solid solution, and should maintain the same benefits of the Mo-Mo_2B-SiO_2 system. Further, T2 instead of Mo_2B negates the issue of pure isolated boria forming during initial stages of oxidation from Mo_2B. Using T2 may also possibly reduce detrimental reactions of boria that could occur during firing.

5.2.2. Pre-Reacting Starting Phases

Reacting the T2 and Mo_2B prior to the final firing was done to evaluate any differences or possible advantages. Pure T2 has a range of possible compositions shown in the ternary phase triangle, and batches were prepared to form pure T2 of either perfect stoichiometry or at the B-rich corner of the T2 phase field. The reactions for BN to react

with Mo and lose N_2 become favorable at just less than 1150°C. For pre-reacting the intermetallics, it's important to assure complete reaction but with minimal densification so it can be broken up and evenly dispersed when mixing to prepare the final alloy. Middlemas has reported on densification of the pure intermetallic phases at 1600°C for 2h and there was negligible densification of either T2 or Mo_2B at 1600°C. He also noted using TGA that the reaction to T2 was 93% complete after reaching 1400°C when heated at a rate of 3°C /min in Ar/5%H_2 and that the TGA losses were rapid and linear above ~1200°C. Based on that knowledge, a 1300°C hold for 2h should be more than enough to drive the reaction to completion and do so without sintering the T2 powder.

A first set of tests were run to verify the proposed order of reactions and temperatures to prepare pre-reacted intermetallic powders. T2 and also A15 were pre-reacted and the reactions verified through XRD. Compositions included an A15-Silica, Mo_2B fired 6h at 1300°C, Off stoichiometric T2 (0.85) fired 2h to 1500, and 2 batches of stoichiometric T2, one fired 6h at 1300 and another 2h at 1500°C.

Table 5.2: Table of for pre-reaction firing schedules and crystalline phases identified

Composition	Firing	Crystalline Phases
50:50 A15 + Amorphous SiO_2	3h @ 1300	Mo, Mo_3Si
Mo_2B	6h @ 1300	Mo_2B, MoB
T2 Off-Stoichiometric $Mo_5 Si_{0.85} B_{2.15}$	6h @ 1300	$Mo_5Si_{0.89}B_{2.11}$
T2 Off-Stoichiometric $Mo_5 Si_{0.85} B_{2.15}$	2h @ 1500	$Mo_5Si_{0.89}B_{2.11}$
T2 Stoichiometric	6h @ 1300	Mo_5SiB_2, MoB, Mo_3Si_5
T2 Stoichiometric	2h @ 1500	Mo_5SiB_2

For the A15-silica sample, peaks for A15, as well as Mo were observed with no other unresolved peaks. Analysis indicates 26.4% A15 and 73.6% Mo by weight percent of the crystalline phases. No amorphous hump was identifiable, but the range and resolution of the scan may not be great enough for the relatively low weight fraction of glass expected.

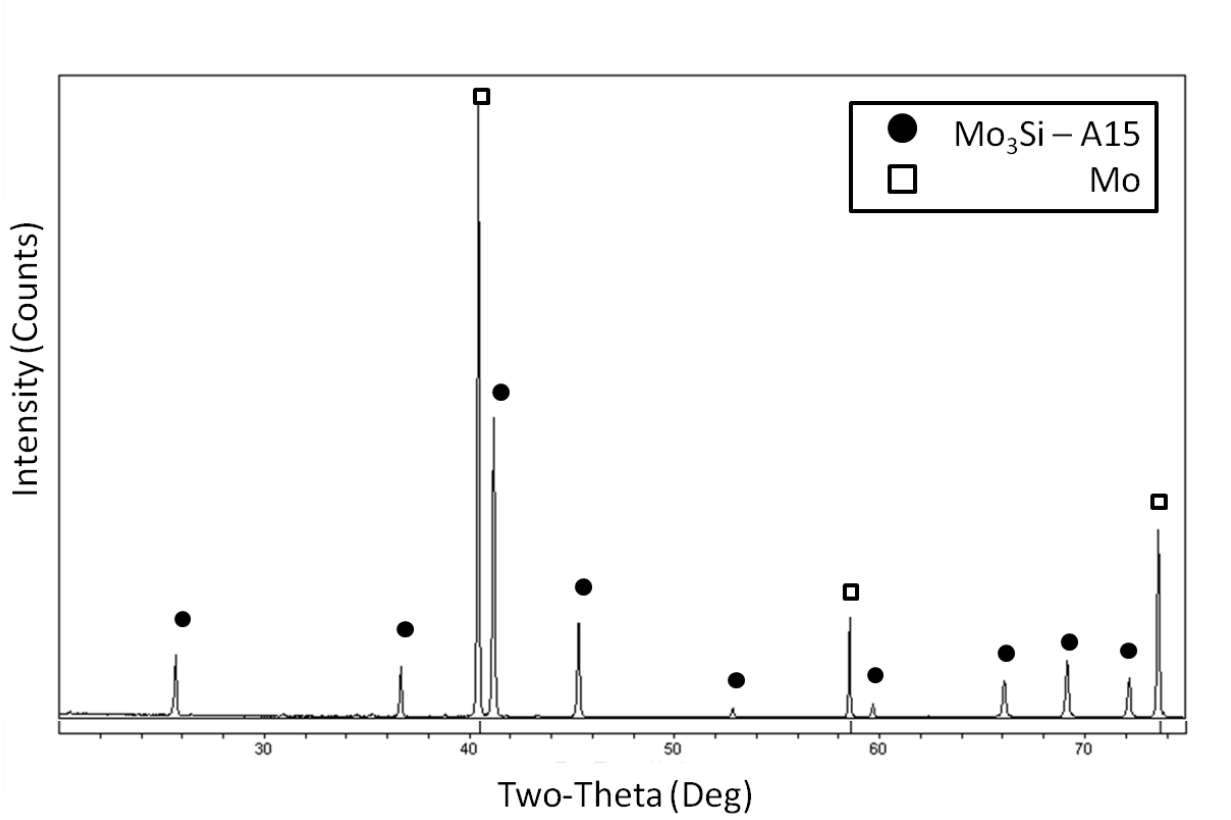

Figure 5.1: XRD Pattern of A15 and SiO_2 after reaction for 3h at 1300°C.

The off stoichiometric T2 ($Mo_5 Si_{0.9} B_{2.1}$) fired 2h at 1500°C and at 1300°C both showed T2 peaks which most nearly matched the off stoichiometric pattern for $Mo_5Si_{0.89}B_{2.11}$, which is the nearest indexed pattern to the expected stoichiometry and corresponds to the Si-deficient B-rich edge of the T2 phase region. Some Mo and trace

Mo_2B is also detectable, each under 2wt%. Presence of these phases is reasonable if the composition has crossed over the T2 corner into the Mo-Mo_2B-T2 triangle.

Diffraction of the stoichiometric T2 has some nonequilibrium phases containing just Mo+B (MoB) and just Mo+Si (Mo_5Si_3) when held at 1300°C. The slow diffusion is forming higher B or higher Si phases where the starting powders weren't well mixed, but when held at 1500°C they reach equilibrium and the MoB and Mo_5Si_3 peaks disappear. Some excess of Si is present and compositions had drifted slightly into A15 triangle - a range which needs to be strictly avoided to prevent Si in Mo_{ss}.

The Mo_2B fully reacted at 1300°C within 6h and at 1500°C in 2h. Some MoB was present there indicating its composition is slightly toward the B end of the Mo_2B stoichiometry, and further shows that little to no B loss occurred. The compositions all end slightly toward Mo deficiency, which is not surprising when you consider the 3 or so wt% Mo typically lost as MoO_3 which was not figured into the original batch calculations.

From those results, it was verified that the T2 could be prereacted, and the T2 was prepared at the off-stoichiometric 0.9 Si composition with a 2h at 1500°C firing. The 0.9 Si T2 should be safely within the T2 region without borides and without risk of contributing Si to Mo_{ss}.

5.2.3. Amorphous versus Crystalline Silica

Alongside pre-reaction of the intermetallics, we've investigated using coarser quartz and fine crystalline cristobalite as opposed to the fine amorphous silica. The hope is that the quartz will resist melting (amorphous SiO_2 can begin to soften at 1250°C).

Based on the need to accommodate increased atomic vibration at higher temperatures, SiO_2 undergoes the following transitions:

α-Quartz (573°C) → β-quartz (870 °C)→ β-tridymite (1470 °C)→ β (low) cristobalite

and the cristobalite melts at 1705°C (Figure 5.2). The tridymite transition is often skipped in the absence of certain specific trace compound additions, leading instead to a transition from β -Quartz to β-cristobalite at 1050°C. A rapid increase in temperature can skip the cristobalite transition altogether leading to a melt forming directly from β-Quartz at 1550°C.

Cooling rapidly can also maintain the high-temperature polymorphs even to room temperature, though they will be metastable or unstable and convert to the lower polymorphs over time.

In our system, alpha quartz should undergo transition to cristobalite which raises the melting point to 1700°C. The first alpha-beta quartz transition occurs at 573°C which may cause problems because of its instantaneous displacive transition which has a significant volume change (2.65 to 2.53 g/cc). This is a known problem for quartz-containing ceramics.

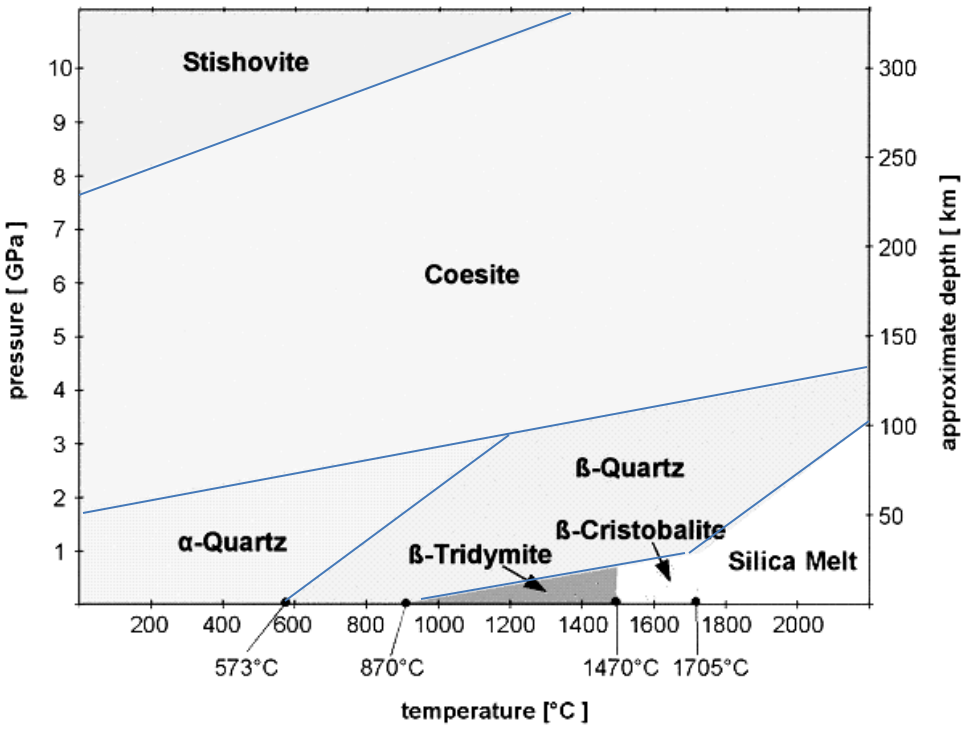

Figure 5.2: Crystalline phases of SiO_2 as a function of pressure and temperature.[101]

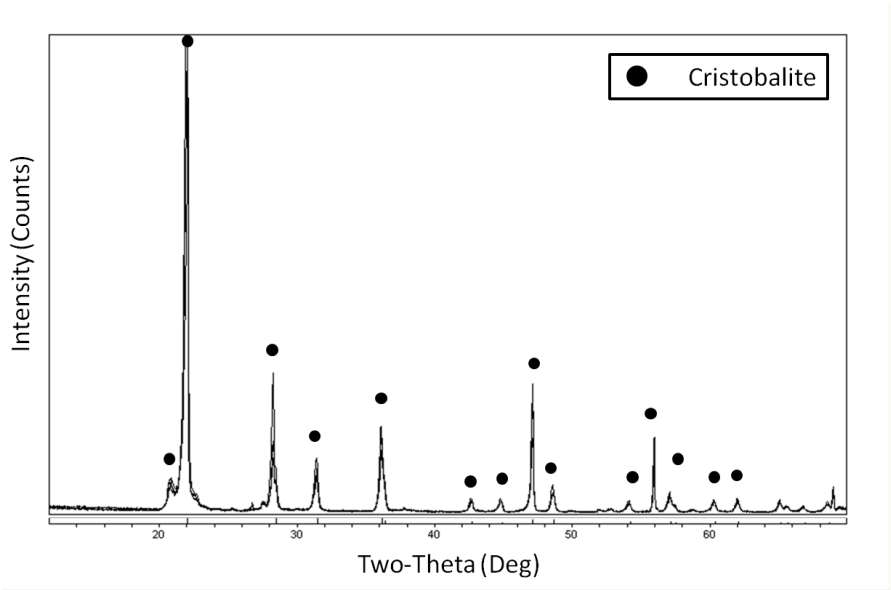

Figure 5.3: Overlaid XRD patterns of coarse and fine cristobalite powder after heat treatment at 1400°C or 1600°C

In order to verify stability of the starting cristobalite powders, some was fired alone. Figure 5.3 shows the patterns overlaid from both fine & coarse Kremer cristobalite powders heat treated at 1400°C and at 1600°C. All four patterns clearly line up and all peaks indicate low Cristobalite.

5.2.4. Testing and Analysis

After firing, analysis was executed as described in Chapter 3. Oxidation tests were carried out for the various samples at temperatures of 1000°C, 1100°C and 1300°C on 12.5mm diameter x 5mm thick pellets.

It is expected that the oxidation would proceed in much the same way as the Mo3Si1B alloys where, as time increases, the film thickness increases but at a decreasing rate. As a given volume of material is removed, the volume of each phase exposed is directly related to their volume fractions. O_2 exists in excess in the ambient atmosphere. All Mo_2B can be assumed to react by:

$$Mo_2B + 3\ O_2 \rightarrow MoO_3 + B_2O_3$$

and Mo can be expected to react by:

$$Mo + {}^3\!/_2\ O_2 \rightarrow MoO_3$$

while the SiO_2 remains as SiO_2 glass. It is further assumed that all of the B_2O_3 mixes with the SiO_2 to form a borosilicate glass.

Mechanical tests of 4-point bend bars in these compositions were also performed at room temperature to compare these different compositions and give an indication of fracture toughness and the resulting fracture surfaces were analyzed by SEM.

5.3. Results

5.3.1. Boride Batches

5.3.1.1.Density/Firing

Pellets of the first three compositions from Table 5.1were prepared. The fired densities as well as % open porosity are given in Table 5.3. “BS2128 Vac” refers to pellets which were pressed under vacuum, and “BS2128 1500” was fired with a 4 hr hold at 1300°C to react the BN and then at 1500°C to sinter for 6hr.

Table 5.3: Results of Archimedes density measurements for the initial compositions.

Batch	Green Density (g/cm^3)	% Theoretical	Fired Density (g/cm^3)	% Theoretical	% Open porosity
B20	4.55	45%	9.41	94%	2.41%
BT0521	4.42	45%	9.18	93%	3.36%
BS2128	3.97	51%	8.20	105.7%	0.86%
BS2128 Vac	3.90	50%	8.17	105.2%	1.25%
BS2128 1500	3.88	50%	8.11	104.5%	1.31%

The final densities shown in Table 5.3 indicate successful sintering to densities above 90% theoretical. The samples pressed under vacuum and those fired with a longer hold at 1500°C instead of 1600°C showed the same degree of densification with no change in phase distribution. The glass containing samples had effectively zero open porosity making further hot isostatic pressing possible without encapsulation.

Densities for the BS2128 samples are actually higher than theoretical values and are higher than for traditional MoSiB by the same reaction process, suggesting that

sintering may be enhanced by unwanted liquid phase during firing. Even with improved sintering, the higher than theoretical density is impossible unless there is a change in the ratios of the phases present. This is likely the result of a Mo rich zone at the surface that can be seen later in Figure 5.10. The zone is depleted of boride, perhaps due to reaction with residual oxygen and boria volatilization during firing and is discussed in greater detail in section 5.3.1.3.4.

The poorest densities are those which contain the boride phases. Of the compositions from the Mo-Mo_2B binary, and Mo_2B-Mo-T2 ternary (B20 and BT0521), after sintering for 4h at 1600°C, they both exhibited high porosity and reduced sintering – only reaching 90% theoretical density. Room for improvement may exist with longer sintering; however longer sintering will also lead to grain growth and possible restructuring as the borides migrate and phases grow. Fortunately while the small atomic size of B should be fairly mobile, it's large enough to locate substitutionally rather than interstitially. As a result the B solubility in Mo and off-stoichiometric capacity of B in the intermetallics is very low. Another issue is the boron loss which may be exacerbated by longer holds at high T.

5.3.1.2.XRD Phase Verification and Analysis

To demonstrate that the formation of Mo_2B is feasible from BN and Mo precursors, presence of Mo_2B, and T2 and the content thereof were verified using quantitative refinement of X-ray diffraction data.

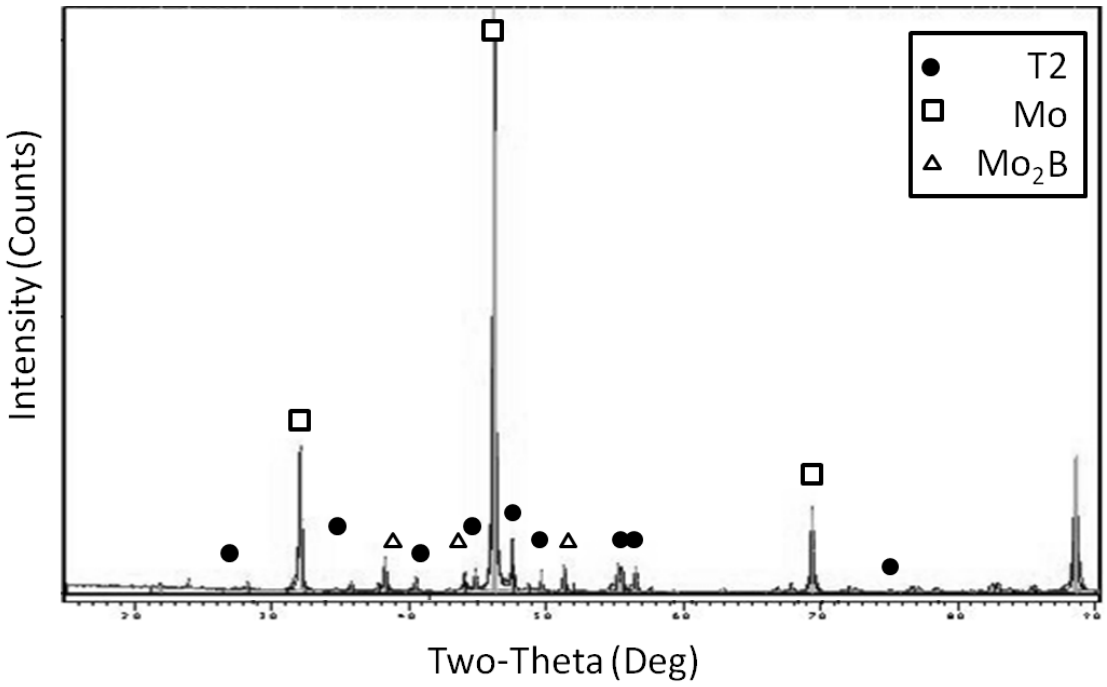

Figure 5.4: XRD phase identification of BST052021 containing Mo_2B, SiO_2, Mo and T2.

Secondly, Reitveld refinement was used to investigate changes in the Mo unit cell dimensions, of which a decrease can be correlated to substitution of smaller Si atoms in the Mo lattice. Semi-quantitative analyses of the X-ray data were used to obtain estimates of the unit cell sizes of the various phases and results are shown in

Table 5.4. The "ideal" phase fractions listed in the first row are the values for Mo-3Si-1B, and ideal unit cell dimensions are those expected for the pure phase. TQ, TS, BT and BS samples have ideal phase fractions defined by the naming convention.

Table 5.4: Measured phase fractions and unit cell dimensions from Rietveld refinement of XRD scans.

	Phase Fraction (vol %)				Cell Dim (A)				Goodness
	Mo	T2	A15	Mo2B	Mo (a, b, c)	T2 (a)	T2 (c)	A15	of fit
IDEAL	56.8	27.2	16.0	-	3.147	6.01	11.049	4.89	<4
Mo powder	100	-	-	-	3.14698	-	-	-	3.5
MoSiB 3:1 Extruded	59.9	27.1	13.0	-	3.14581	6.03363	11.08197	4.90069	5.5
DST MoSiB 3:1	62.6	24.2	13.1	-	3.14544	6.02861	11.07625	4.89205	1.8
TQ2713	71.3	28.7	-	-	3.1473	6.02514	11.0693	-	5.7
TS2322	65.1	24.9	-	-	3.1498	6.03066	11.08407	-	3.4
BT3535	34.3	40.7	-	25.0	3.14588	6.01361	11.05	-	4.5
BS2128	82.7	-	-	17.3	3.14696	-	-	-	1.8

The Rietveld refinement includes a goodness of fit which ideally should be below 4, which in most cases it is near or below. Pure Mo tested alone indicates exceptional fit with the expected values at a goodness of fit = 3.5. Comparing the 3:1 MoSiB compositions which contain A15 to the T2, Mo_2B and SiO_2 containing samples we see consistently Mo in 3:1 has lattice constants which are smaller than theoretical values. The smaller Silicon atoms locate substitutionally in Molybdenum solid solution and will decrease the Mo lattice parameter as evidenced in the work by Sturm[20]. In the case of TQ, TS and BS where the A15 has been replaced with SiO_2 directly we expect a no change in lattice parameter from pure Mo since there should be little or no Si substitution for Mo to reduce its unit cell size. Indeed this is seen. The plot in Figure 5.5 indicates the reduction in Mo unit cell size expected for increasing Si solid solution as measured by Kruger[45]. Plotting the measured lattice parameters versus that line suggests values

near 3at% Si in the MoSiB 3:1 cases, but no Si in the Mo for the TS, TQ or BS samples. In fact, some of the measured values are larger than for pure Mo, however the deviations are minor and within experimental error. Neither B nor Si will fit interstitially in the Mo lattice and thus cannot be causing the observed increased lattice parameter.

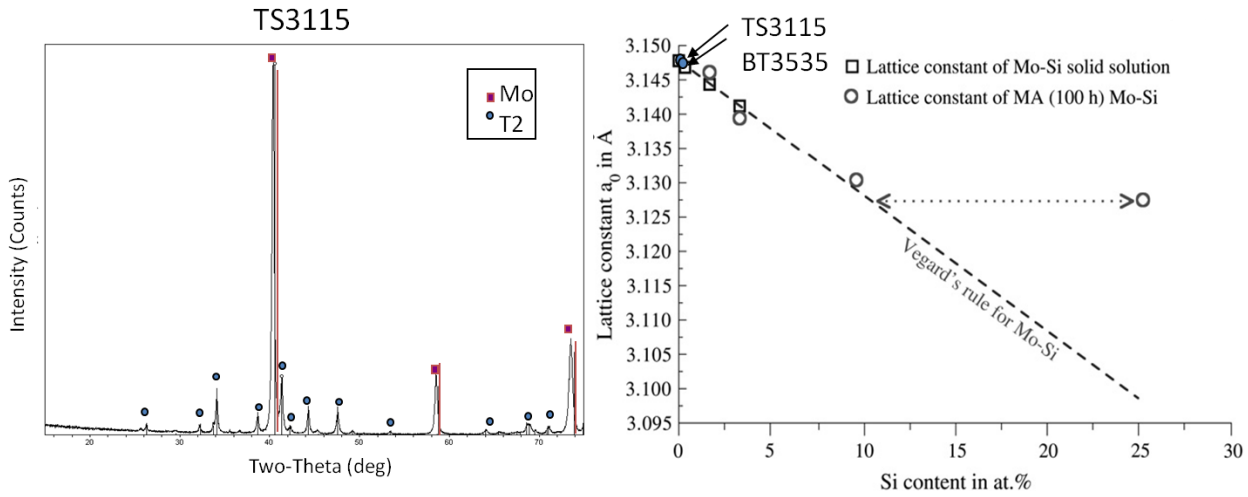

Figure 5.5: XRD Refinement of Mo-T2-SiO_2 compositions marked versus measured Mo lattice constants as a function of Si content.[45]

When comparing the T2 peak locations of the XRD scans to others in the literature, we see that our T2 as-formed is closest to the boron-rich end of the T2 phase, and the XRD patterns fit best with indexed patterns for B-rich T2 ($Mo_5Si_{0.89}B_{2.11}$). This is expected since the desired composition is as near as possible to the Mo_2B-T2-Mo phase field in order to minimize any possible Si in Mo_{ss}. Other researchers have also reported the same B-rich composition.

The T2 has the I4/mcm tetragonal unit cell shown in Figure 2.7c. The XRD refinement results show some slight expansion, most notably in the c-axis. The unit cell is

not close packed and B has lower bond strength than Si so despite smaller atomic size of B, its substitution for Si results in the observed expansion of the unit cell dimensions.

The measured at% boron was higher than was expected from the batch and might be attributed to an increase in B vacancies. We see in the BT sample a lack of Mo_2B which suggests we're not fully in the Mo-Mo_2B-T2 three-phase zone. Also in the BT there was a greater than expected ratio of T2 to Mo_2B, which may be due to B vacancies in the T2 allowing a greater fraction of T2 from the same atom% Si and Mo. This reduces bond strength and could cause an overall expansion of the T2 primarily in the *a* and *b* directions which is observed.

5.3.1.3.Fired Results

5.3.1.3.1. Microstructure

Phase fractions are also measured and compared to expected values in Table 5.3, and show good match to the expected values once you consider that the XRD is unable to measure the amorphous SiO_2; the measured values consider crystalline phases only. It's worth noting however that the SiO_2 added as quartz does not show quartz in the fired XRD scans, whether at 1500°C or 1600°C firing. A micrograph of the B10 sample containing 10%Mo_2B in Mo is shown in Figure 5.6 and shows isolated and roughly equiaxed grains of Mo_2B in the Mo matrix. This morphology is believed to occur in the other composites, adjusted for phase fraction. Some large Mo-only regions can be vaguely distinguished and may indicate need for better dispersion.

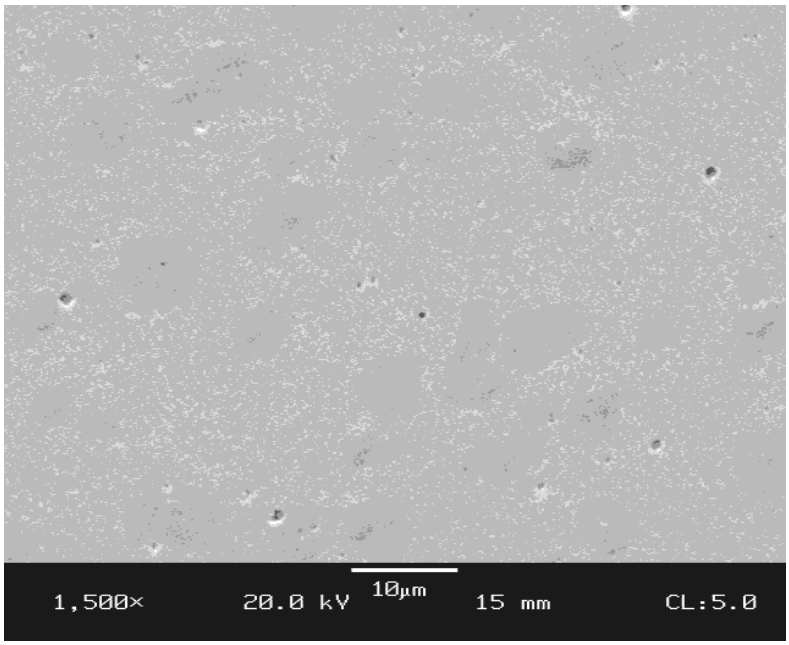

Figure 5.6: SEM image of B10 (Mo-10v% Mo_2B) showing Mo_2B grains (dark) within a Mo matrix.

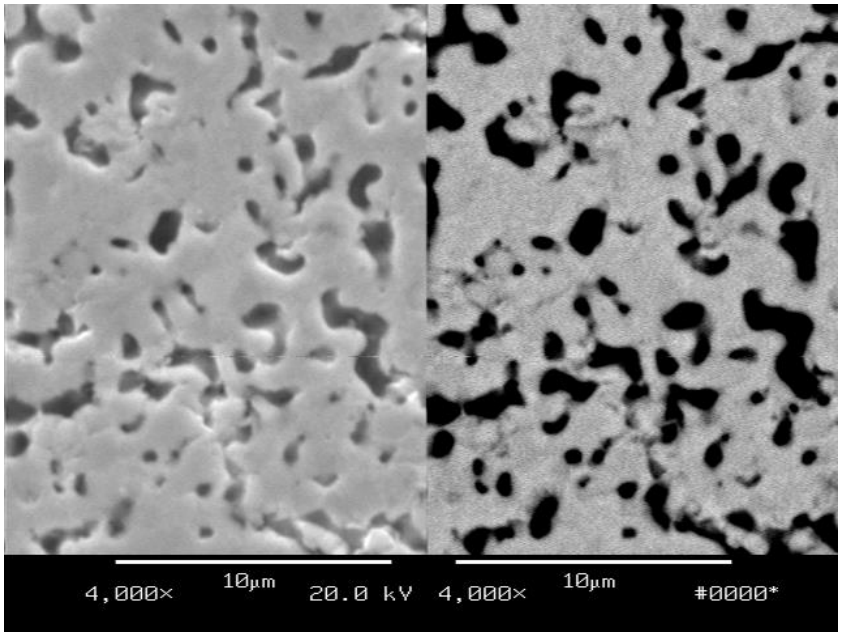

Figure 5.7: SEM image of the microstructure of BS2128 fired to 1600°C for 6hr. Image right is backscattered electrons showing contrast between phases. SiO_2 is dark, Mo light.

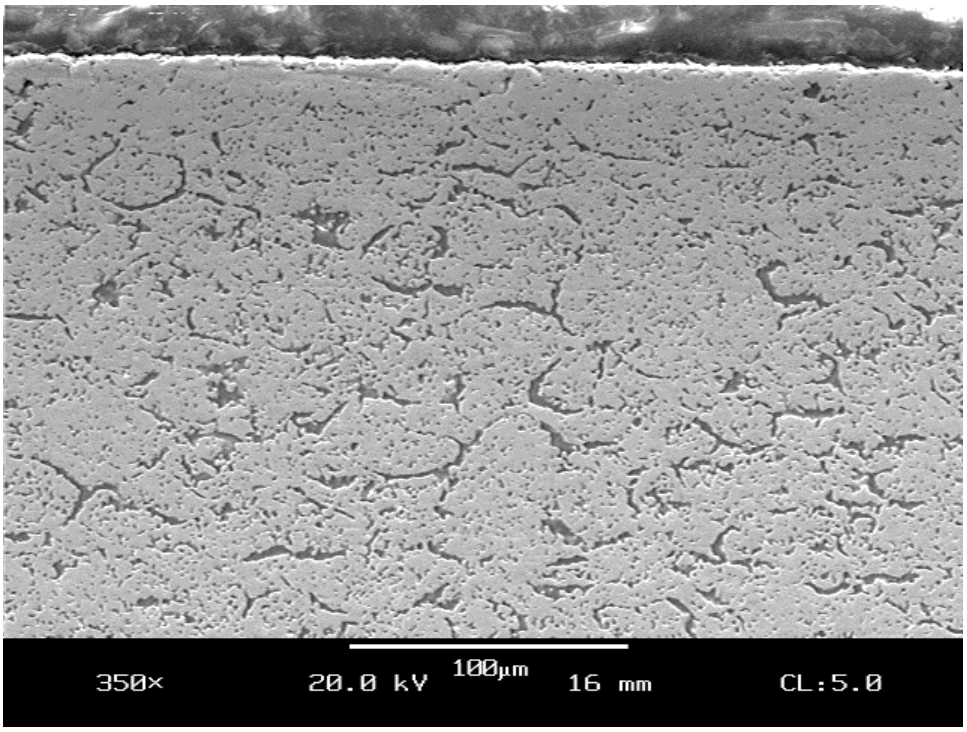

Figure 5.8: SEM image of edge of BS2128 pellet fired to 1600°C for 6hr.

The micrographs which are shown in Figure 5.7 and Figure 5.8 show the fired microstructure of the BS2128 which contains both Mo_2B and SiO_2. The low phase contrast makes Mo_2B indistinguishable from the Mo and both appear as the lighter phase in the images while the SiO_2 is the dark phase. The Mo and Mo_2B are believed to exist in a similarly homogenous distribution to the B10 case (Figure 5.6), and a good dispersion of the SiO_2 in the BS samples has been achieved.

5.3.1.3.2. Ballooning

After firing, two main issues were immediately observable; some of the pellets were expanded in the center, like a balloon, while others had glass beads dotting the surface. The BS2128 pellets were the first to exhibit ballooning (Figure 5.9), and many

other BS2128 pellets also exhibited problems with lamination cracks forming during firing.

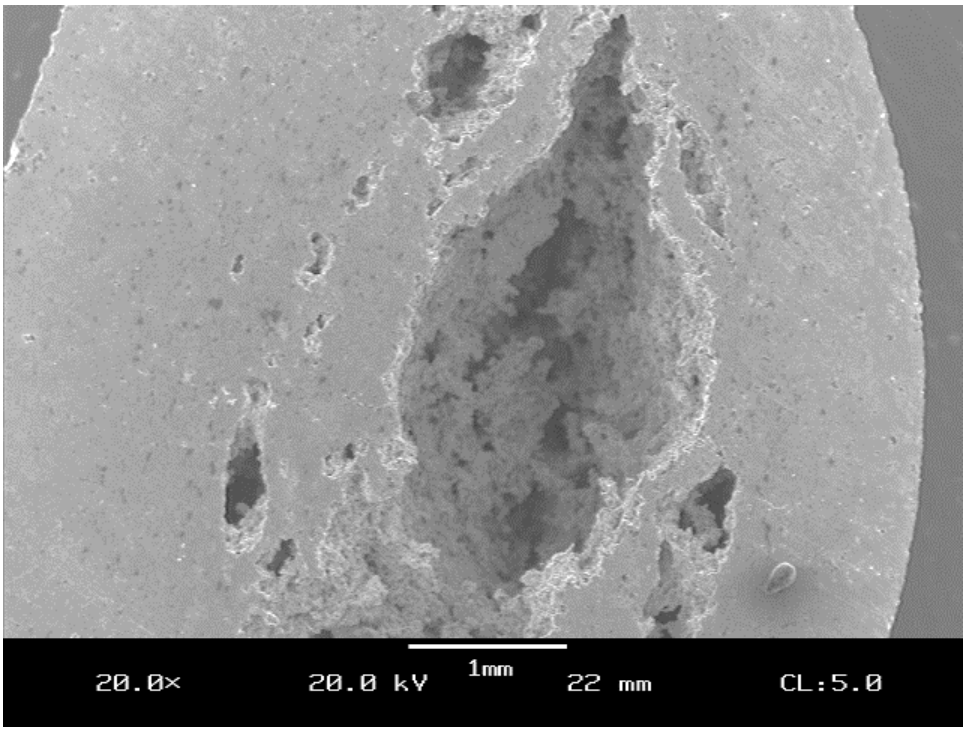

Figure 5.9: SEM Image of BS2128 sample cross section exhibiting the "ballooning" phenomena creating a large internal void from gas pressure during firing.

A later batch of TS2322 with low-O Mo exhibited ballooning as well, and upon re-examination only those batches which used fresh Mo powders exhibit the ballooning issue. Later batches (once oxygen had been picked up by Mo powder) of BS2128 saw the phenomenon go away and not until the later set when a new bag of Mo powder was used did it return. The assumption is that the assisted sintering seen in the SiO_2 systems (TS & BS) coupled with high reactivity and sinterability of the fine low-O Mo leads to closed porosity before reactions are complete internally. The closed structure cannot release the nitrogen evolved from reaction of the nitrides internally and the samples either expand or

crack. A hold at 800°C did not reduce ballooning; however a hold at 1250°C did, indicating that it's indeed the nitride reactions above 1200°C responsible for the gas generation which is causing internal expansion or in other cases cracking.

5.3.1.3.3. Internally Fluid Glass

The second instantly observable phenomenon was expelled glass beads on the surfaces of some samples post-firing or crescent lenses of glass from flow internally. Expelled glass was previously observed at the surface in the Mo + Frit samples for which the added glass is inherently fluid during firing. We believe in the BS samples that the residual O on the Mo powders is reacting preferentially with B and the resulting B_2O_3 is fluxing the glass to a lower viscosity liquid to allow flow during firing.

In both cases there is a liquid during firing, either inherently liquid above 1000°C for the frits or fluid silica from unintentional reaction of boria. We can assume that the liquid/solid interfaces are more stable than the solid/vapor and during initial sintering the voids between solid particles are closed off and replaced with the liquid. This is corroborated by the lack of any open porosity. As sintering proceeds further the solid-solid interfaces are preferred over the liquid-solid interface so the liquid phase in the pore structure is forced out. The liquid is then expelled as the final stages of shrinkage occur, which results in the observed glass beads at the surface.

For most BS2128 we saw no beading, but instead see the potentially problematic crescent shaped lenses of glass inside the structure. The micrograph in Figure 5.8 shows crescent shaped glass regions. The radius of the regions matches the radius of the spray dried spheres and they are elongated perpendicular to the direction of pressing which indicates that these regions exist between the pressed spray dried granules and are being

filled with glass during firing. The lenticular crescent shaped sections of silica glass are larger than would be caused by agglomerates of silica powder, and much larger than the particle size of the raw silica. The liquid glass is not being forced out as the previously mentioned beading case, but rather occupying the larger empty regions between the spray dried particles. The glass remaining internally could be due in part to a closer matched surface energy between liquid and solid which would decrease the driving force for sintering that expels the glass for the previous samples, or just a more viscous liquid. This is further supported by the presence of samples with lamination crack that had also filled with glass, such as the one shown in Figure 4.2.

The crescents are problematic because they reduce connectivity of the toughening Mo matrix and increase connectivity of the brittle glass phase and would significantly reduce overall toughness in the system. The pure silica should be solid well above the 1500°C processing temperatures, unless it's affected by a flux such as boria, which may react from the boron nitride and any residual oxygen in the powders, specifically on Mo.

5.3.1.3.4. Depletion

Microscopic evaluation of the cross sections also exposes a third matter, the depletion of SiO_2 and B from the pellet surfaces, Figure 5.10. The depletion of boron and silica from the surfaces during firing becomes a significant issue. It leads to a high weight loss before protection is achieved due to limited glass-formers available at the early stages of oxidation. A depleted layer of 100 μm on an average 12mm pellet of 4mm thickness leads to a total depleted zone volume of ~0.0375 cm^3. Assuming a density of 10 g/cc, that's 0.375 grams lost before any glass is available to provide protection. That would correspond to just over a 100mg/cm^2 weight loss that could be avoided simply by

removing the depleted layer. As a side note: for our size pellet it neatly works out to around 1mg/cm^2 of weight loss for every 1µm of depleted layer depth.

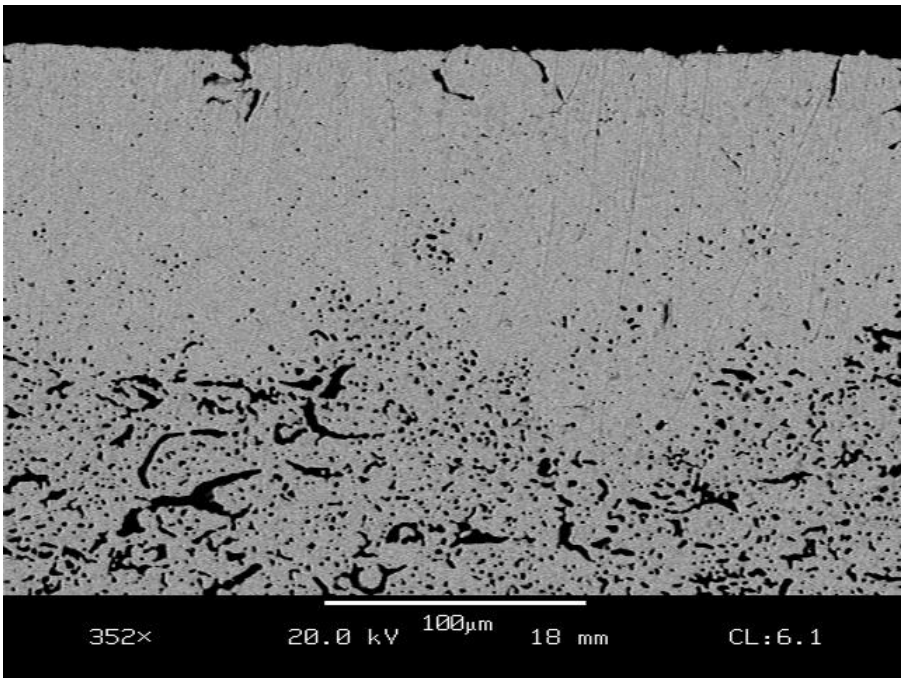

Figure 5.10: BS2128 as-fired with ~100µm depleted of Si and B from the surface (top).

5.3.1.4.Residual Oxygen Effects

It's very important for the initial oxidation performance that the depletion from the surface be avoided. It appears to be caused by reaction and evaporation of the boron and/or boride during firing. The starting Mo powder contains some residual O. This may preferentially react with the BN to form volatile B_2O_3. The B_2O_3 may also be responsible for fluxing of the SiO_2 which then flows into the interparticle areas creating the crescent shaped SiO_2 pockets.

5.3.1.4.1. Boride Depletion

A series of different firing conditions with varying temperatures and holds were examined to evaluate the effects of time and temperature affecting depletion. The goal was to understand the cause of and the reactions associated with B depletion and possible boria flux formed during firing. Further, the weight losses during firing may also shed light on other possible reactions occurring. For example if a sample had a 100um depleted zone on a typical pellet of BS2128, that corresponds to 0.02g of Mo_2B lost. That equates to 10E-5 moles Mo_2B or 5E-5 moles B_2O_3 produced. Assuming the Oxygen is provided by MoO_3, the same number moles MoO_3 must be initially present and involved in the reaction. TGA of the pure as-received Mo powders indicates a 2% total mass loss during reduction due to evolution of MoO_3 from residual oxygen. If 2wt% of the Mo is MoO_3 and volatilizes from BS2128, which is 51v/o Mo, it would lose 1.3% of its total weight during firing.

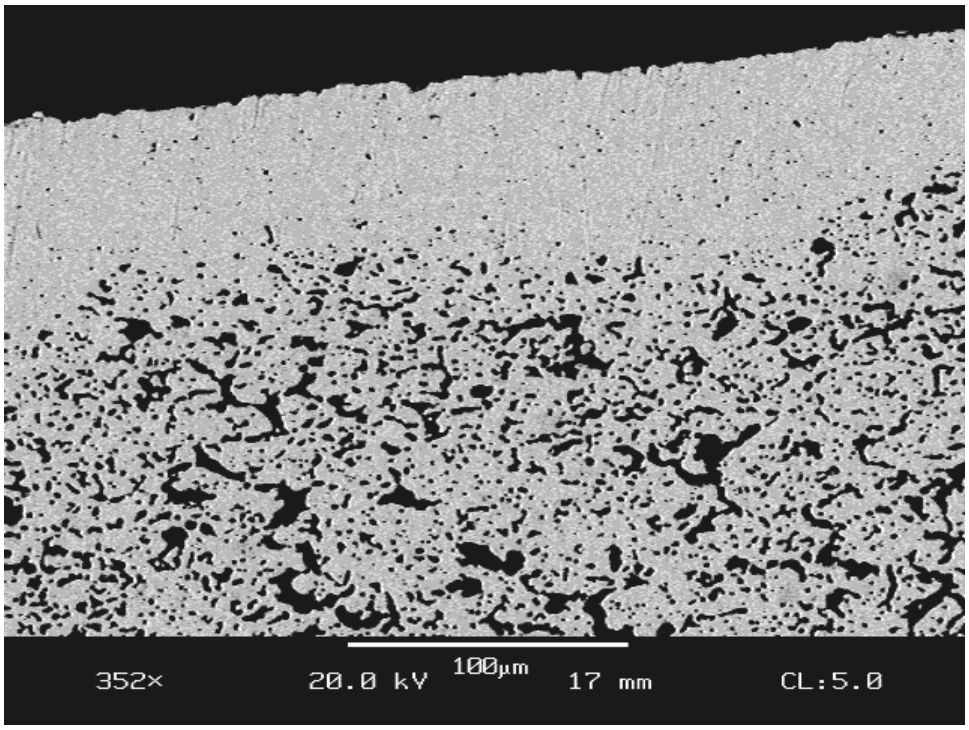

Figure 5.11: BS2128-2 #1 fired in Ar/10%H_2 with 3°C/min heating rate and 6h hold 1600°C.

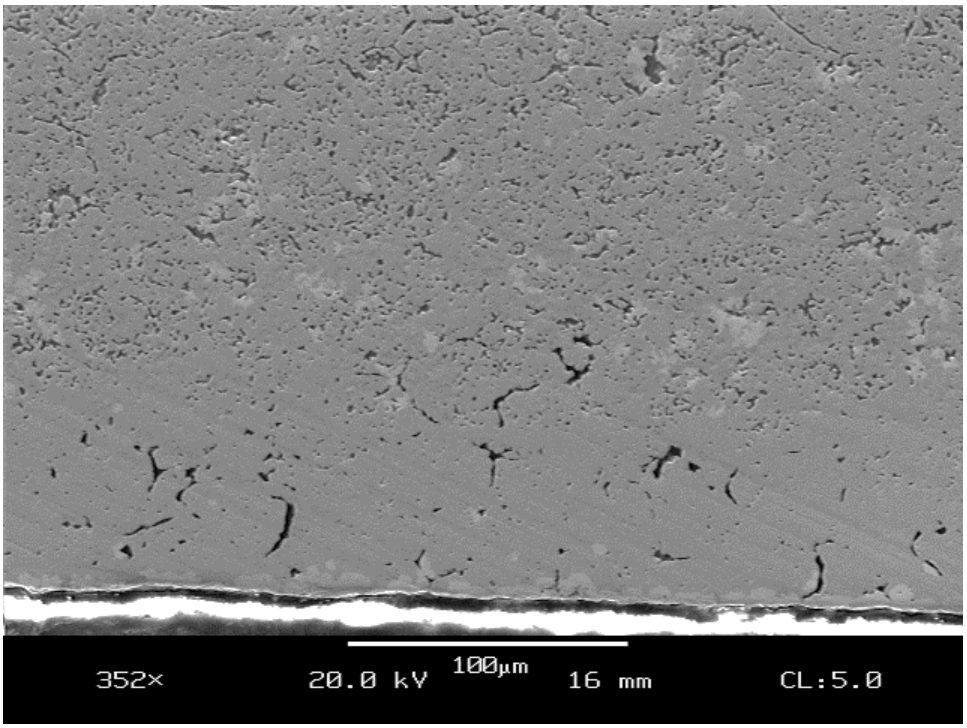

Figure 5.12: BS2128-1 #4 fired in Ar/10%H_2 with 3°C /min heating rate and 4h hold at 1300°C and a 4 hr hold at 1600°C.

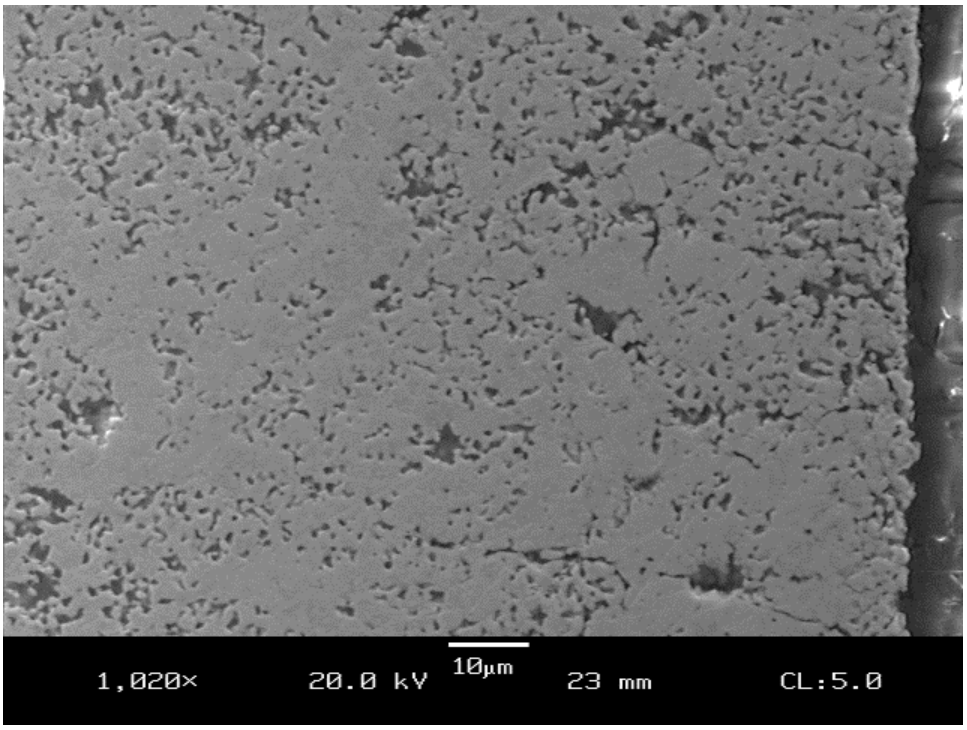

Figure 5.13: BS2128-1 #5 fired in Ar/10%H_2 with 3C/min heating rate and held at 1300°C for 10h.

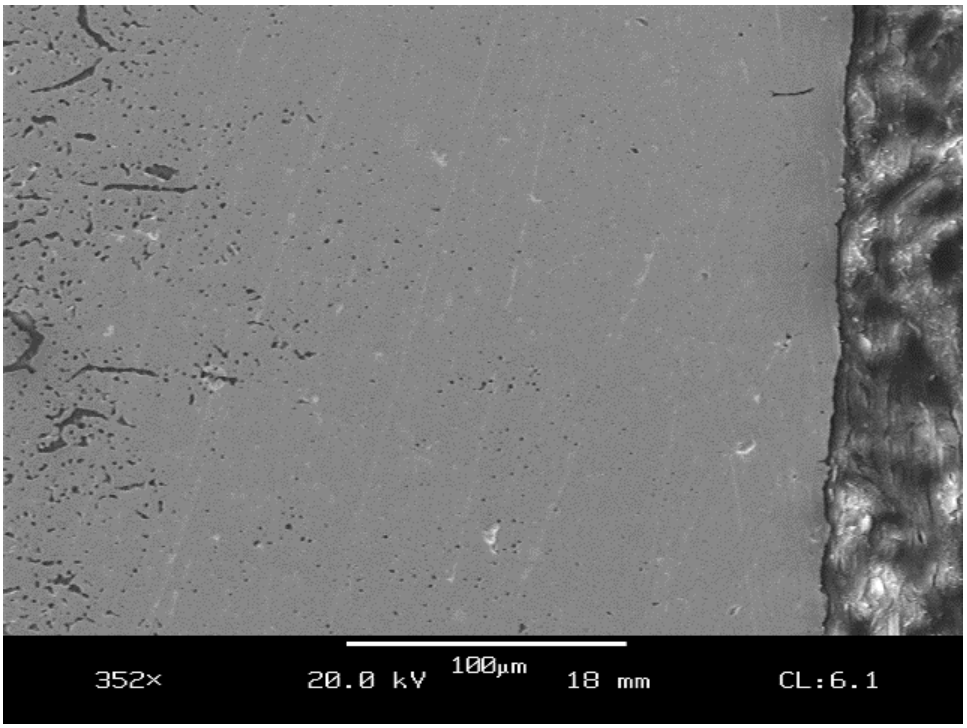

Figure 5.14: BS2128-1 #6 fired in Ar/10%H_2 with 3°C/min heating rate and 6h hold at 1000°C and a 4 hr hold at 1600°C.

Table 5.5: Resulting surface depletion of BS2128 for varying firing conditions.

Sample	Firing	Depletion	
BS2128-2 #1	6h @1600C	Moderate ~100um	
BS2128-1 #4	4h@1300 4h@1600	Moderate ~100um	
BS2128-1 #5	10h @ 1300	None	
BS2128-1 #6	6h @ 1000 C 4h @ 1600 C	Severe ~200 um	

Figure 5.11shows a sample of BS2128 (-2 #1) fired with the typical 3°C/min 6h hold at 1600°C schedule, and depletion is noticeable with a depth of 50 to 100 µm. The sample #4 shown in Figure 5.12 was a pellet of BS2128 fired with an intermediate 4h hold at 1300°C and 4h at 1600 C. It achieved full density but the presence of ~ 100 µm depletion can be seen and the larger SiO_2 lenticular regions remain even in the depleted zone. The sample exposed only to 10h at 1300°C is shown in Figure 5.13. There is no depleted layer in this instance. It reached only 88% theoretical density and showed 12-17% open porosity. Finally, when fired with an intermediate hold of 6h at 1000°C prior to final firing for 4h at 1600°C, (Figure 5.14) again full density was achieved but an even greater depletion depth is present.

The first sample held for 1300°C for 10h didn't exhibit a depleted zone, but the one with a 6h hold at 1000°C followed by 4h at 1600°C showed an increased depleted zone versus 1600°C firings without the 1000°C hold. This would suggest that the

depletion is occurring above 1300°C, but is affected by the reactions occurring at 1000°C. Possibly the formation of B_2O_3 is occurring around 1000°C by reactions such as:

$$BN + MoO_3 \rightarrow Mo + N_2 + B_2O_3$$

instead of the ideal hydrogen reduction of Mo oxides and reaction to Mo_2B:

$$BN + MoO_3 + H_2 \rightarrow Mo_2B + N_2 + H_2O$$

The 1300°C fired sample was the only one which didn't exhibit the depleted zone which could indicate that while the reaction to form B_2O_3 probably occurs below 1300°C, it is not until over 1300°C that any appreciable volatilization and depletion occurs.

The depletion of silica near the edges may possibly be caused by SiO_2 being fluxed by boria and moving to the center via capillary action. However the SiO_2 contents are not greater than the expected volume fraction in the center region, they are only less than expected near the surfaces. The depleted layer is also observed in the case of samples containing only Mo and SiO_2, even when there is no B present to form a flux. Additionally, the arrangement of the depleted layer would be different if the SiO_2 were leaving as opposed to moving the pellet center.

From the previous arguments it appears more likely that the SiO_2 is volatilizing. Silica decomposes to volatile SiO in reducing Hydrogen environments at temperatures as low as 1000°C. In hydrogen reducing environments above 1050°C SiO_2 reduces to form SiO and H_2O gas[102]. SiO_2 can also be affected by water vapor. The reduction of residual Mo oxides by hydrogen evolves H_2O, and could create a significant H_2O vapor pressure. H_2O can not only corrode SiO_2, but may also react with Boron to form volatile boric acid. (H_3BO_3) and could contribute to depletion of both.

5.3.1.4.2. TGA to understand Oxygen contents

TGA was used next to examine the reactions occurring and the associated temperatures as well as roughly the speed and degree of the reactions. Another goal of the TGA test series was to determine if and how much the pressing a pellet affects its weight loss and reactions during firing compared to a loose powder bed. Finally TGA can help to learn more about the processes accounting for the weight loss by running powder samples in an inert atmosphere and comparing it to the weight loss curves for the same powder in reducing atmosphere.

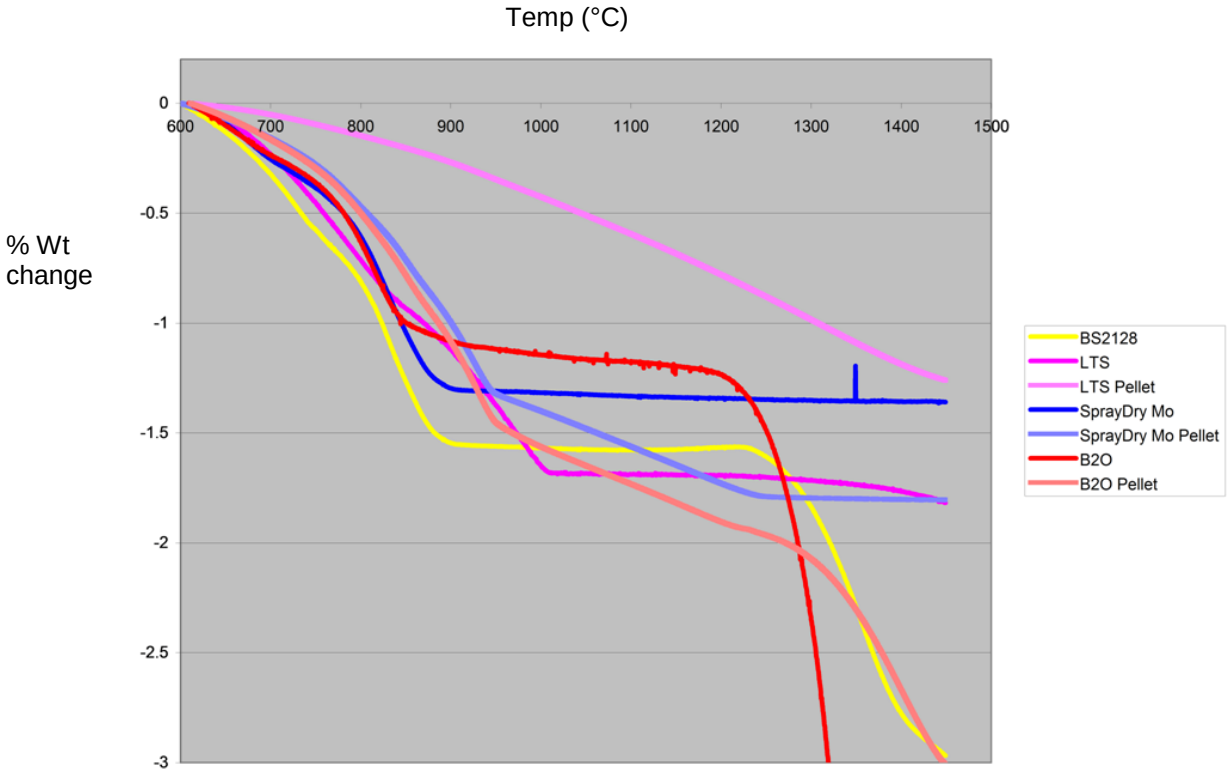

Figure 5.15: TGA traces of Mo and MoSiB samples heated in Argon as pressed pellets versus loose powders, normalized at 600°C.

In The TGA traces shown in Figure 5.15, the lighter colored lines of each color correspond to the pressed pellet data, for comparison with the solid color lines for the equivalent loose powder. LTS is the Low Temperature Sintering (LTS) Mo powder as-received from Climax. The "MoStr" is the same LTS Mo, but spray dried with binder and stearic acid at ~3wt%. "Boride" is the same but with addition of BN, and BS2128 is the powder batched to form the BS2128 composition.

The initial 0.2 -0.5 % weight loss under 200°C is associated with removal of any low weight hydrocarbons and adsorbed water vapor, and can be ignored. From 200-600°C, the differences depend on evaporation and burnout of the binders and lubricants if present. In the figure, all of the TGA curves have been normalized at 600°C to avoid the differences in binder burnout, adsorbed water and other unimportant low temperature processes.

In the above TGA traces, one thing is clear; that the weight losses in the pressed pellets are slower. For the Mo, both LTS and spray dried LTS weight losses are similar in both the pressed and loose powders until 800°C, where the loss is more rapid for the loose powder. After 950°C, the loose powders are leveling off indicating completion of the de-oxidation reaction, whereas from 950-1200°C there is a slow and matched-slope loss for both pellets. It appears that there are two reactions occurring, one which is mostly complete by 950°C, the other is significantly slower in the pressed case. Most likely the first reaction is the existing MoO_3 being removed as vapor. The second is slower reactions associated with reduction of the Mo oxides which depends on diffusion of the H_2 into the pressed pellet.

5.3.1.4.3. Effect of Compaction

Following the TGA results which indicate that the rate of Mo oxide reduction is related to the compaction of the samples, a set of pellets were prepared with varying degrees of compaction to see differences in depletion or silica crescents. The Mo_2B samples have been the most susceptible to deep depletion layers. BS1025 pellets were fired to 1550˚C, and an 8 hr hold at 800˚C was added to allow early reduction of any residual O which might contribute to formation and loss of volatile B_2O_3 later in the firing.

Table 5.6: Pressing & firing results for BS1025 pressed in a 6mm die; #1 pressed to 1000lbs, #2 to 1500, and #3 to 2500lbs.

Pellet	Press kpsi	Green D	Fired D	Linear Shrink	Wt Loss
#1	23	50%	106%	24%	8.1%
#2	34	52%	104%	22%	7.8%
#3	57	54%	103%	20%	7.6%

The green densities showed that, as expected, green density increases with increased pressure during compaction and asymptotically approaches a maximum around 55%. Comparing green and fired properties for varying die pressures given if Table 5.6, the lowest pressed pellet had the highest shrinkage, which is consistent with it having the lowest green and highest fired density. The higher than 100% densities imply a loss of the lower density components, namely B and/or SiO_2. The fact that pellet #1 has the highest density suggests it has the highest loss of B and SiO_2. It is probable that the lower initial

density allows for a more open structure and easier removal of SiO_2 as volatile SiO and/or B as volatile B_2O_3 or H_2BO_3.

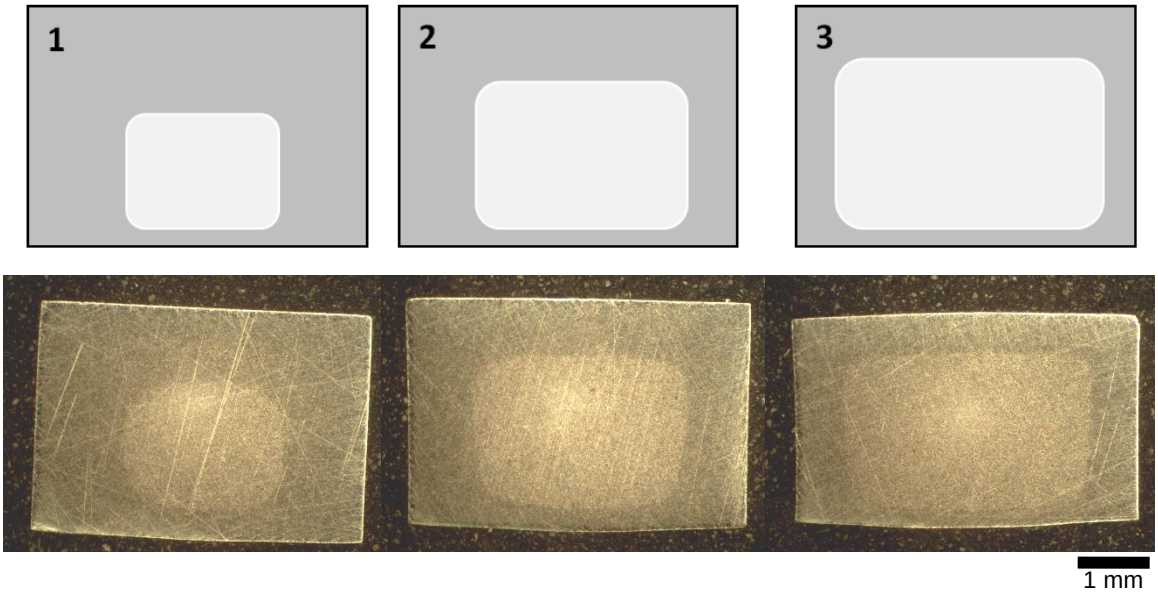

Figure 5.16: Depletion layers as affected by green density, shown schematically (top) and optically (bottom) with increasing pressed density from left to right.

Cross sections of the pellets are shown microscopically and illustrated above (Figure 5.16), where the center regions are regions of high SiO_2 content and connectivity. The bottoms of the images were the bottoms of the pellets during firing.

There is a direct correlation between the sizes of the regions of high SiO_2 in the pellets' centers. Smaller SiO_2 regions correspond to higher total density, implying SiO_2 loss is responsible for the variations in density and giving rise to measured density higher than the calculated theoretical density. The loss occurs to the greatest depth for the lowest initial density, implying that the more open structure allows greater loss, by increasing mobility of either reactants moving in or products moving out. This further suggests that

the material is lost as a vapor, and also that the loss occurs either before or concurrent with the necking stages of sintering while the initial open structure still remains. There is also a smaller depth of loss from the bottoms, which sit on a plate during firing. This further supports that a vapor reaction is occurring.

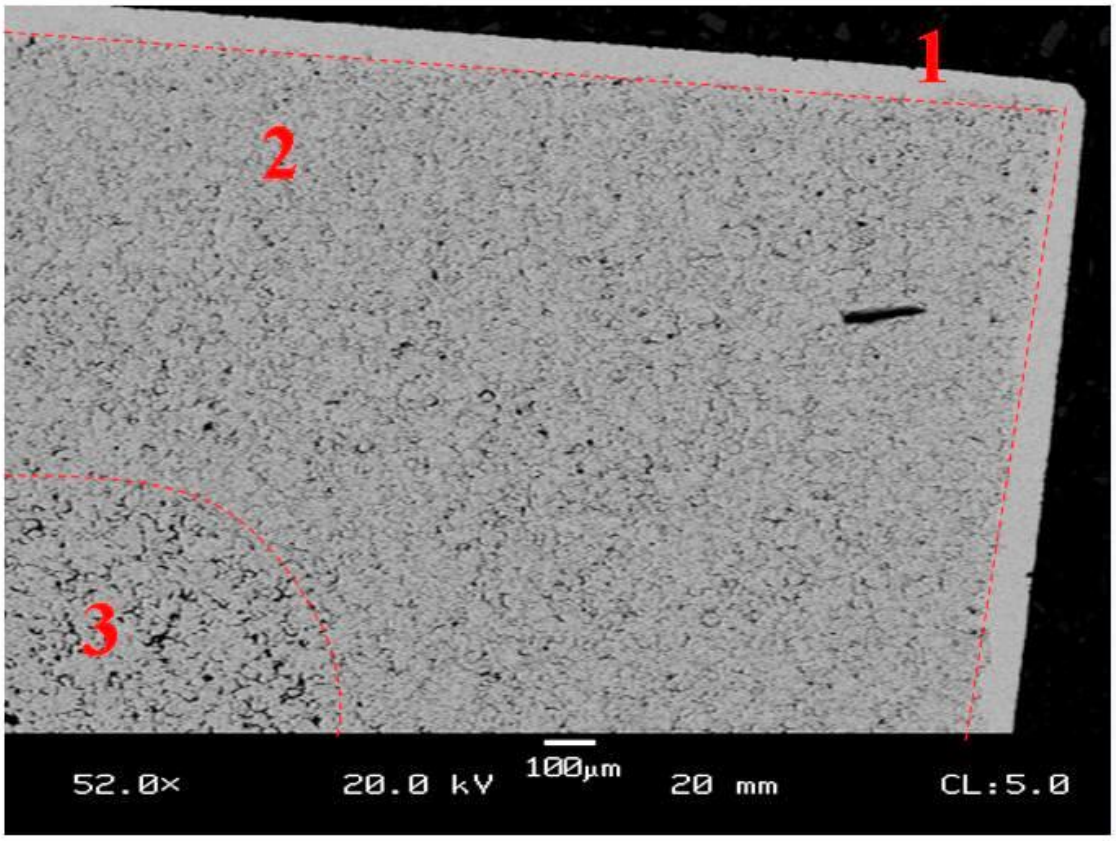

Figure 5.17: SEM of BS1025 cross section as-fired showing 3 distinct regions of depletion

In Figure 5.17 you can see there are actually three distinct regions associated with depletion. From the outside in, the first is just a short depth from the surface which is almost completely void of both SiO_2 and T2, indicated with the number "1". The second, marked "2" is that which has a reduced volume fraction of SiO_2 and the SiO_2 is also less connected, and the final (no. 3) being the high SiO_2 region with large connected zones of SiO_2.

The size of the innermost depleted region (3) is very dependent on initial pressed density, while the fully-depleted outer zone (1) is much less so. This fact implies that loss is occurring by two separate processes. The green piece consists of spray-dried particles with closely packed SiO_2, BN and Mo, which are pressed together to a certain green density dependent on pressing conditions. Void spaces exist between the crushed spray-dried particles. The proposed scenario is as follows: as the piece is firing, the SiO_2 becomes able to flow, perhaps by fluxing from formation of B_2O_3, and behaves similarly to the fluid glass in the frit samples at high temperatures during firing. From surface energy considerations the liquid B-fluxed SiO_2 replaces the air within the porous unsintered granules during the first stages of sintering. Sintering proceeds next in favor of the more stable solid/solid interfaces. This occurs first within the well connected spray-dried granules and creates a microstructure of homogenous isolated SiO_2 within the granules, but also expels some SiO_2 to the granule surfaces, and thus the intergranule regions. This leads to the large, connected crescent-shaped zones. A highly connected SiO_2 matrix is formed in the interparticle voids, while within the spray dried particles some SiO_2 also exists but is much less connected.

Then the reducing atmosphere in our firing conditions reduces some of the SiO_2 to volatile SiO in a process similar to "active oxidation" of Si by the reaction:

$$SiO_2 + H_2 \rightarrow H_2O + SiO_{(vapor)}$$

The connectivity of the SiO_2 in the interparticle regions allows for a more rapid volatilization of SiO in the reducing atmosphere, which continues steadily and concurrently with the sintering and densification processes. Meanwhile the isolated SiO_2 within the granules remains. This creates the consistent second zone where SiO_2 internal to the spray dried particles is not depleted, but interparticle (crescent) SiO_2 has been depleted to a specific depth (region 2). The depth, as shown by the compaction study, is dependent on ease of gas transport of vaporized SiO, and so can only proceed as long as open porosity exists to the surface. This type of depletion occurs to a lesser depth towards the bottom of the pellet where gas diffusion is restricted by the bottom plate.

Next, after a certain period dependent on initial green density, the sintering completes its second stage and becomes closed, which cuts off the gaseous internal volatilization of SiO_2. This leads to the central zone (3) where the interconnected intergranular lenses of SiO_2 are no longer depleted, and they - as well as the isolated internal SiO_2 – both remain. The stable internal (3) and external (2) zones are formed and this likely all occurs before the completion of the final hold during the firing schedule.

Finally, during the final hold, the piece is held at the maximum firing temperature (1500-1600°C) and additional SiO_2 and Boria continue to volatilize. At this point, because of the closed nature of the sintered piece, the SiO_2 and B_2O_3 must diffuse through the solid to the surface rather than diffusing as a gas through the open porosity during sintering. The SiO_2 and boride are evaporated completely and roughly equally, but

at a much slower rate and only from the near surface. This leads to the final outermost zone (1) which is almost completely depleted of both B and SiO_2.

This scenario fits well with the observed results and further confirms that boron and residual oxygen are causing the issues. Boron nitride should react directly to molybdenum boride, and both should be stable in reducing atmospheres, even in the presence of SiO_2. Further, the SiO_2 should be solid at 1500˚C if it is pure, and could only flow into the interparticle regions if it were fluxed, such as by interaction with B_2O_3 in the system. Test runs of pure SiO_2 powder fired to 1300˚C remained friable with no sintering, further supporting that a flux such as B_2O_3 must be present for the observed flow in firing.

5.3.1.4.4. BN – MoO_3 Reaction/Reduction Test

Ideally any residual oxygen on the Mo is reduced by the H2 atmosphere without interacting with the nitrides.

$$MoO_3 + H_2 + BN + Si_3N_4 \rightarrow Mo_5SiB_2 + N_2 + H_2O$$

However, a nonideal reaction between Boron Nitride and the residual O on Mo to form boria:

$$MoO_3 + BN \rightarrow Mo + B_2O_3 + N_2$$

is presumed responsible for the boride depletion and other negative effects associated with fluxing the silica. Boron may also form volatile boric acid with the water generated by reduction of the oxides:

$$B + H_2O \rightarrow H_3BO_{4(vapor)}$$

The reaction between Mo oxide and BN was studied in greater depth. MoO_3 powder was fired together with BN to determine at which temperatures the B loss might be occurring,

and to investigate possible reactions of MoO_3, O, H_2 and BN to form free volatile B_2O_3 or H_3BO_3 in processing.

We developed a series of experiments to investigate the plausibility of this theorized reaction series. A MoO_3 pellet and BN pellet were pressed and placed in a tube for firing. The MoO_3 is upstream and near but not touching the BN pellet. These were subjected to Ti gettered Ar-10%H_2 flowing at the standard 150cc/min for 6 hrs at 850˚C. From the proposed reactions it could be expected that the MoO_3 would react and the resulting H_2O vapor be taken downstream where it reacts with the BN.

We assume all of the weight loss of the MoO_3 is from O leaving and from this can calculate an H_2O volume created. This can be compared to the H_2 volume passed over during the firing time to get an estimate of the vapor content (pH_2/H_2O). Also, XRD analysis of the resultant weight fractions of the various Mo and Mo oxides remaining in the MoO_3 pellet should also allow a check of the expected H_2O volume formed compared to weight lost. The remaining discrepancy would be explained by MoO_3 evaporation taking Mo with it (evaporation of MoO_3 instead of reduction to H_2O.)

Next, the H_2O vapor formed is expected to continue downstream to react with BN. Verification of reaction between BN and water should be visible macroscopically as vitrification if indeed B_2O_3 is forming. Also there should be no weight change in the BN unless it reacts, in which case there would be a weight loss from N_2 gas liberated by oxidation of BN, and possible weight gain from H and O if the B reacts to form solid or liquid B_2O_3 and H_3BO_3. Weight loss from volatilization of B_2O_3 and H_3BO_3 should be negligible in this test because of their low vapor pressures at 850˚C.

From both of the firings, weight loss and XRD of the fired MoO_3 pellet indicates with no uncertainty a complete reduction of the MoO_3 to Mo. The pellet was XRD scanned on the surface and also crushed and scanned as a loose powder, and in both tests the only peaks visible were identified as pure Mo. The expected weight loss for full reduction would be approximately 33.8% and measured weight loss was 33.6%, less than 0.5% error. Downstream, no change in weight or appearance was seen in either the BN or the BN/SiO_2.

The volume of H_2 gas is known from 10v%H_2 gas flowing at 150cc/min for 6h at 850°C (1123K). That gives a volume of 0.54l of H_2 or 0.024mol. Since pure Mo remained, the weight lost is only from O removed from MoO_3 during complete reduction to Mo, which gives 0.09874g = 0.00617 mol O. If the Mo oxide present is partially MoO_2, the same relation exists; that all weight lost from the Mo oxides is as oxygen.[98] The liberation of O must all be attributed to reduction by the reaction:

$$MoO_3 + 3H_2 \rightarrow Mo + 3H_2O$$

Assuming all O was lost as H_2O that's 0.00617 mol H_2O and 0.0179 mol excess H_2 which gives pH_2/H_2O = 2.906. nH_2O/nH_2 = 25.6% and pH_2 of the total gas is 10% so ppH_2O of the total gas = 2.56% . Relative humidity is given by vapor pressure H_2O over its saturated vapor pressure e^*_w and is low according to the Buck equation for humidity:

$$e_w^* = (1.0007 + 3.46E^{-6}P) * (6.1121)e^{\left(\frac{17.502\,T}{240.97+T}\right)}$$

which all fails to explain exactly what's going on between the boron, boria, and residual oxygen.

5.3.1.4.5. Gettering O for Depletion Control

The problems associated with residual oxygen must be caused by reaction of the H_2O and O reacting with the boron in the system. These problems may be limited by using elemental additions to getter the O and keep it from reacting with the Boron. It's necessary however that these gettering additions have oxides which are less stable than SiO_2 so as not to reduce SiO_2 and thereby liberate Si which would then embrittle the Mo.

Ti and Zr are possible gettering agents and are used industrially to getter oxygen impurities in the production TZM alloys. These are both compatible and available. Cr & V may also reduce Mo-oxides. Ti is slightly and Zr significantly more stable an oxide former than SiO_2 and should reduce it, but proper quantity they should be able to getter oxygen from the Mo first to prevent SiO_2 liquid but without enough present to reduce any of the SiO_2.

Al, Ta and Ti were added to BS2322. These were unable to form usable samples however because the Al and Ta melt during processing. Unless they oxidize, the metals are liquid during firing which creates serious issues. The Ti doesn't melt but was notably ineffective at reducing the SiO_2 and crescents, and depletion remained.

5.3.1.4.6. Residual Oxygen Sources

Another route to limit the problems of residual oxygen could be to use powders with lower initial oxygen. Even a pure Mo will develop an adsorbed oxygen layer quickly in air, and with the small size of our powders drastically increases exposed surface area and reactivity. Results from Taebel and Lawthers[103] showed a significant weight gain with time for Mo powders exposed in air. From discussions with Climax (our Mo supplier) oxygen analysis, BET surface area, trace analysis, and density measurements

were all taken for their LTS material. They also examined the shelf life of the powders.[104]

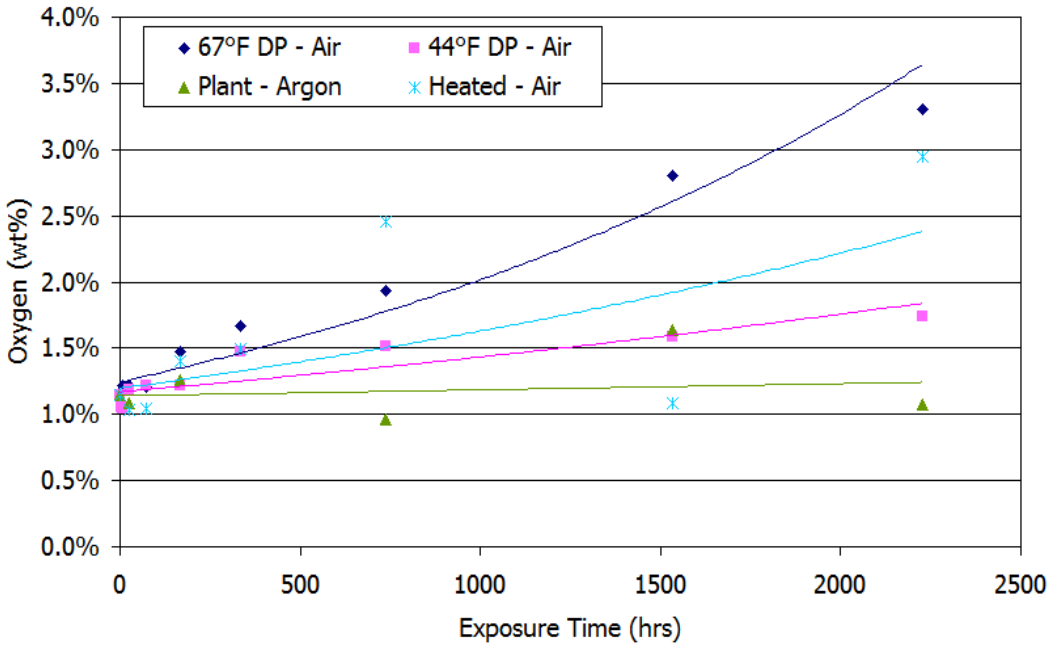

Figure 5.18: Measured Oxygen uptake with time on LTS Mo powders. (From Climax)

The conclusion of the shelf-life study (Figure 5.18) was that oxygen uptake is appreciable, especially in humid environments and higher temperatures. Packaging in Argon and assuring a good seal was sufficient to keep high purity and low oxygen contents for long periods of time, and that its containment is independent of temperature. By using salt jars to simulate various dewpoints, it was found that moisture plays the most significant part in the re-oxidation of the powder. Even in the absence of Argon, a lower storage temperature was beneficial due to lower moisture contents in the air. Redundant protection can be achieved by storing in a chilled environment after sealing in Argon.

Because moisture is so effective at promoting oxygen pickup, exposure to air, especially humid air and direct exposure to water should be strictly avoided. Acetone is known to pick up and retain water and so we must take care to use only fresh dehydrated acetone in our processing.

The lowest Oxygen content of Mo powders that we've received contained 0.5 wt% O, in which enough O is still present to oxidize a significant portion of the boron. Most of our Mo powders contain anywhere from 1-3 wt% Oxygen. Even in the case of 0.5wt% O, if all the oxygen were to react with the boride it's sufficient to convert almost half of the boron in our typical composition ranges to boria.

The next step was to determine whether the detrimental oxygen was dependant on the initial levels in the Mo powder and reaction with air, or if the majority of detrimental oxygen is picked up during the processing. With powders containing lower initial O impurity, there should be less O present to form B_2O_3. This should result in both a more consistent microstructure with few or no crescent regions and also reduced or eliminated depleted layers. Oxygen uptake during processing should also have an effect, and may completely eclipse the importance of initial O content. It may be that a pickup of O is unavoidable from mixing in acetone which may be partially hydrated, from the heated spray-dry atmosphere, or elsewhere during processing.

The severity of the processing effects as opposed to the initial purity's effects needs to be known, and if it proves to be the much greater contributor we'll know that we don't necessarily need a high initial purity Mo.

To test this, two samples were prepared using two different Mo powders with a known difference in initial oxygen contents, keeping all other variables the same

(including acetone) and with all the processing done identically after spray drying. A different final microstructure (specifically depleted zone) with a lower initial-oxygen Mo would indicate that the initial O content is a key factor.

As a secondary test, an additional sample was prepared. This used low O powder, but with fresh acetone, evacuated bottle during milling, shorter milling times, and dry box storage for absolute minimization of contact with air throughout process. A difference there in the fired microstructure with regards to connectivity and depletion would show the degree of importance of not only low initial oxygen but also maintaining low O throughout the processing stage.

As a few side notes, we can also examine the water content of the acetone by adding salts such as potassium fluoride which takes up the water and separates from the acetone. While not particularly useful for dehydrating the acetone it gives an option to visually assess the acetone purity with regard to water if this proves to be important. We also see bluing of the suspension while spray drying in almost every case; a fact which could indicate formation of Mo hydrides – possibly from water in the acetone – and could be something that needs to be dealt with or worked around.

In either case, regardless of the source of oxygen, it may be possible to reduce the oxygen during firing before it can cause problems. High H_2 contents at lower temperatures (~800°C) during firing should reduce any O on Mo before it's able to react with the boron, and before the reducing atmosphere causes significant SiO volatilization. Then at the higher temperatures, we can lower the H_2 to lessen the reduction potential of the atmosphere and prevent it reducing and depleting the SiO_2 through the remainder of the firing schedule.

Our attempts at holding in higher pH_2 around 800°C made little change on the final microstructure however, and must not have appreciably reduced the Mo oxides before the BN was active enough to react with the resulting water vapor or the form oxides itself. We had been assuming a system whereby excess initial Oxygen present on Mo as surface oxides is reacting with BN to form boria which causes B depletion as it evaporates away and also causes large glassy silicate regions by internally fluxing the silica during firing. Also, we assume the reduction of Mo oxides to take place by reduction with H_2 gas to form H_2O vapor. It must also be considered that H_2O may also react with BN to form boric acid vapor which may also contribute to depletion. The reaction of the Mo oxides with H_2 to form water vapor must be reacting with BN to form boric acid. The boric acid then vaporizes away, and may also be picked up by the SiO_2 where it acts as a flux. At this point no conclusive means to fully prevent depletion or SiO_2 crescents had been found.

5.3.1.5.Oxidation Results

Apart from the difficulties in processing and the effects on the final microstructure, samples were subjected to high temperature oxidation testing to verify that they are indeed effective in preventing oxidation. The first batch subjected to oxidation studies was that titled BS2128, consisting of Mo with 21 vol% Mo_2B and 28 vol% SiO_2 which corresponds to a B:Si wt. ratio of 3:1 and matches that of the 3:1 MoSiB alloys. According to Middlemas' optimization model the 3:1 Si:B weight ratio should be the ideal ratio for oxidation resistance around 1100°C.[59]

First a series of one pellet each was subjected to 1000°C in air for periods of 10m, 20m, 30m, 45m and 1hr. then weighed and examined. The pellets suffered varying

degrees of lamination cracking which was discussed earlier; these laminations make calculating valid weight loss/area values difficult as the cracks introduced much more surface area than calculations based on pellet area expect. Also since the pellets had varying degrees of lamination, and different pellets were used at each time step, comparison of weight losses for the different times is also difficult. The advantage however is that the formation of the glassy layer on the outside can be examined for each step.

In the 1000°C oxidized samples at 1min a fairly large degree of loss had occurred leaving behind a sponge-like matrix of glass with a large volume of interconnected porosity. There was a distinct yellow coloration indicating presence of MoO_3, possibly deposited while cooling down. A section was scratched away revealing the surface to be lumpy with Mo regions exposed. At 20m the layer is thinner but denser due to melting and coalescence of the glass. The region of yellow is lessened with an overall darkening of the coating due to joining of the glass; however a high degree of connected porosity remains and the surface is not protected. At 30 and 45m the trend continues until 1hr where a solid coating is finally formed. It is expected that at the lower 1000°C temperatures the glass viscosity is too high to allow rapid coalescence and fast coating of the glassy region. There is enough glass present to coat the surface however it takes too long to join into a continuous coating, instead holding the positions it had prior to removal of the Mo (necked individual glass particles with porous channels).

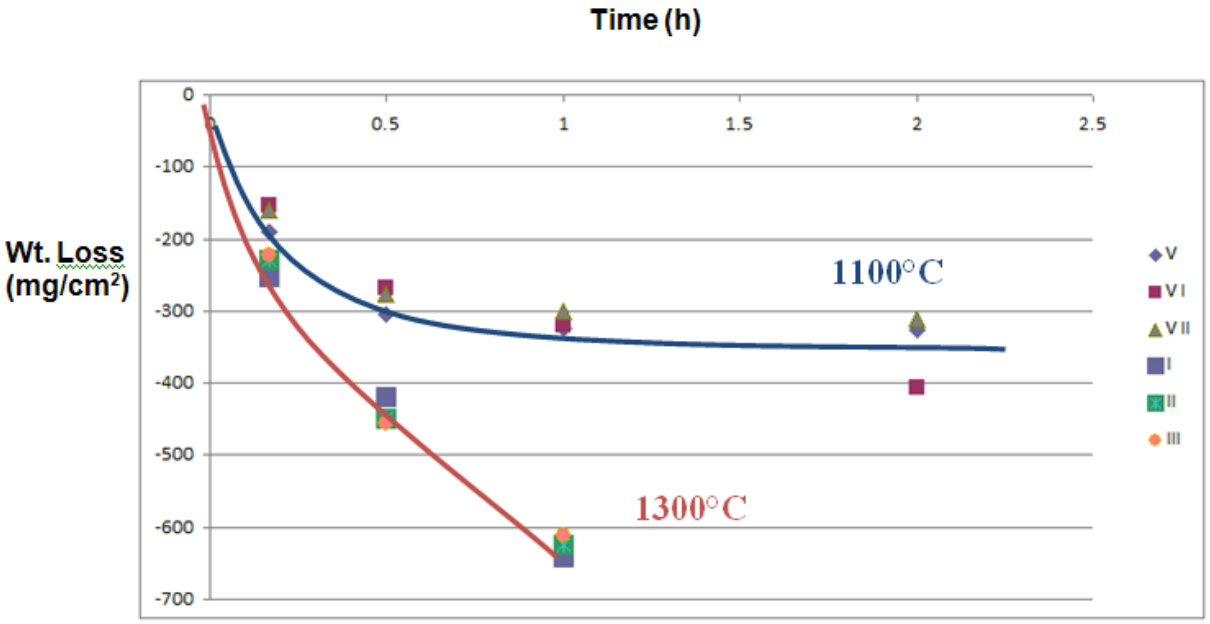

Figure 5.19: Weight loss/area (mg/cm^2) vs. time for BS2128 pellets in oxidation. The samples I, II and III were oxidized in air at 1300°C, and V, VI and VII were oxidized in air at 1100°C.

Samples were then subjected to oxidation tests in air at 1100°C, the results of which are shown in Figure 5.19. These were done in interrupted oxidation, with each pellet being oxidized in air (Keith) then removed from heat, examined, and reintroduced to the oxidizing furnace. This was done for times of 10min, ½ hr, 1hr and 2hrs. Interrupted oxidation allows more accurate estimates of weight loss / area since the loss on each sample is tracked, and also considers the effect of thermal cycling. Thermal cycling likely increases weight losses due to potential for thermal stress cracking and also repeatedly being subjected to the possible pesting and transient losses at intermediate temperatures and it closer mimics the end use goals for turbine blades.

At 1100°C the oxidation proceeds by eroding the Mo and leaving interconnected foam of glass behind. After the coating formed, oxidation appeared to reduce significantly following the expected parabolic rate law. Only sample VI did not show a

leveling off of weight loss, but this sample had significant lamination cracking and the large excess surface area was unable to completely coat. Results for 3:1 MoSiB oxidized in air at 1100°C are shown previously in (Figure 2.11). The losses shown in the figure for the Mo-Mo_2B-SiO_2 alloy compare well with those for MoSiB. It is also notable that there is nearly no change from 2 hours to 24 hours indicating that the coating offers good protection once it is formed.

As a side note, replacing the A15 with silica can increase measured weight loss values. In the silicate containing samples, the coating evolves from SiO_2 and the oxygen is already present in the composite; there is no weight gain from atmospheric Oxygen reacting with Si as there would be when forming SiO_2 from oxidation of A15 (Mo_3Si).

Further oxidation testing in air at 1300°C is also shown if Figure 5.19. The results showed that oxidation resistance was compromised at the higher temperature, and oxidation proceeded in a nearly linear fashion. This is perhaps due to the rapid volatilization of the Mo below the forming glass layer and the lower viscosity of the glass at higher temperature being unable to trap the rapidly forming bubbles. The surface appeared to be irregular with large open pore channels above the Mo regions. It is also important remember that the 3:1 Si:B ratio is optimized for resistance at 1100°C.

5.3.2. T2 – SiO_2 Results

While some oxidation protection is present and potentially usable in the BS samples at 1100°C, the higher temperature oxidation resistance of the BS2128 was poor. Coupled with the high initial losses, issues of crescent-shaped silica regions within the microstructure, and depletion from the surfaces, the second series of samples containing pre-fired T2 and silica were prepared. The compositions include T2 with quartz referred

to as TQ, T2 with amorphous SiO_2 (TS) and T2 with cristobalite (TC), as well as compositions with Mo_2B, amorphous silica and T2 (BST)

5.3.2.1.Firing

The next batches prepared are listed in Table 5.1, and the fired densities are given below in Table 5.7. In these T2 containing samples the T2 was pre-reacted, ground and then added to slurries with Mo and SiO_2 to be spray-dried and otherwise produced according to the GTRS method. Pre-reacting the T2 should alleviate some of the boria issues previously encountered since the nitride reactions are complete before firing even begins. For one, it would prevent ballooning. Another advantage of this is that reactions between silicon nitride and silica have been identified which could lead to silica loss. Silicon nitride and silicon dioxide can react at temperatures near 1500°C to form oxynitrides, which subsequently decompose into volatile N_2 and SiO. This reaction has been shown to occur even in pure N_2 atmospheres (which reduces its driving force) and to result in as much as 30% wt loss as SiO.[105] By pre-reacting the T2 we avoid the possibility for Si_3N_4 and SiO_2 interaction.

Table 5.7: Mo-T2-Silica compositions and fired densities

Batch	Green D (g/cc)	% TD	Fired D (g/cc)	% TD	% Open Porosity
TQ3113	4.61	52.3%	8.53	97.0%	3.7%
TS3115	4.55	53.0%	8.68	101.0%	2.8%
TQ2713	4.64	52.4%	8.07	91.1%	5.0%
TQ2713 - 1600	4.62	52.2%	8.77	99.1%	0.0%
BST052021	4.29	51.9%	8.39	101.5%	1.2%
TS2322	4.27	52.6%	8.27	101.7%	1.7%

In order to investigate the advantages, if any, of starting with crystalline or amorphous silica; samples were prepared of Mo, T2 and silica, with 31v% T2 and either 13v% quartz (TQ3113) or 15v% amorphous SiO_2 (TS3115). The compositions were adjusted for the lower density of the amorphous silica to give same final weight of SiO_2. The samples were fired for 12h at 1500°C, which should be low enough to prevent vitrification of the crystalline silica. Crescent regions were still observed however, alongside severe depletion.

XRD did not show visible peaks for cristobalite or quartz, but neither did it show a significant amorphous hump and it may be that the large density difference and greater transmission through silica is making it difficult to distinguish. The lack of cristobalite in any samples with B, but stable presence of it otherwise suggests that the B is responsible for vitrification of the crystalline silica.

5.3.2.2.Oxidation Results

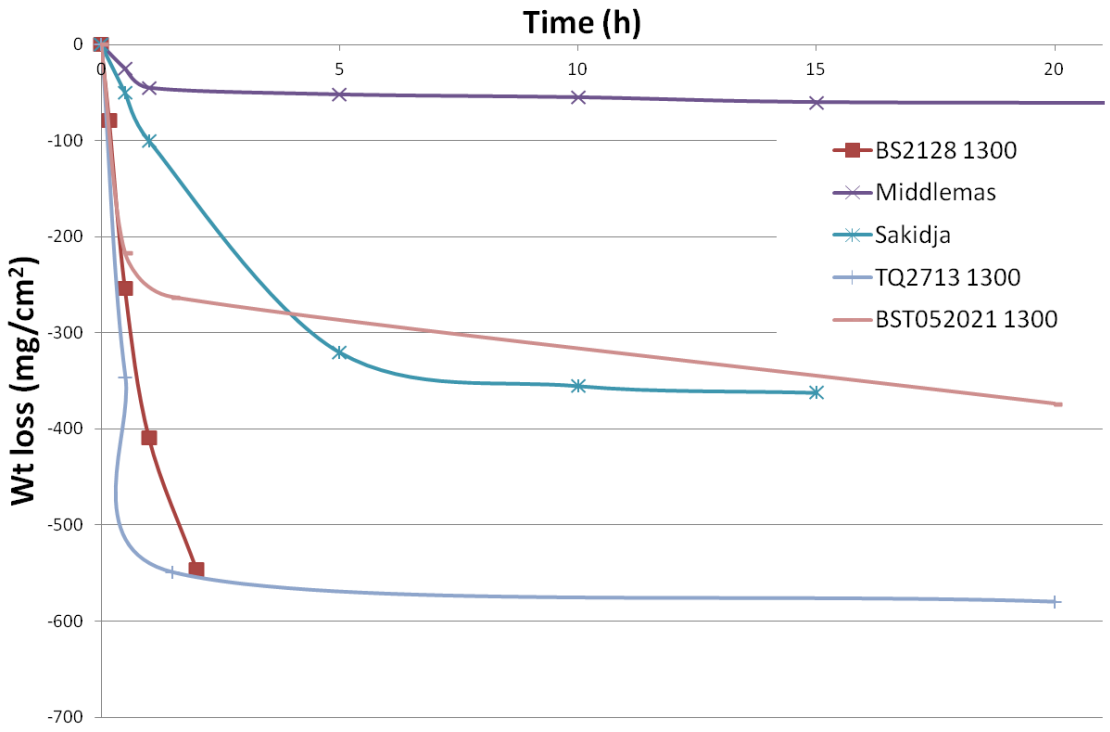

Figure 5.20: Oxidation of TQ2713 and BST052021 compared to BS and MoSiB 3:1 samples.

Oxidation of the first T2-Quartz samples is shown above in Figure 5.20. While the initial losses are severe, after 500mg/cm^2 loss the TQ2713 does begin to level off to parabolic oxidation. BST052021 which is lower viscosity has shorter initial high-loss transient period with only half the weight loss, which is expected of a lower viscosity coating. The parabolic rates achieved however are much too high for usable lifetimes – also expected of lower viscosity coatings.

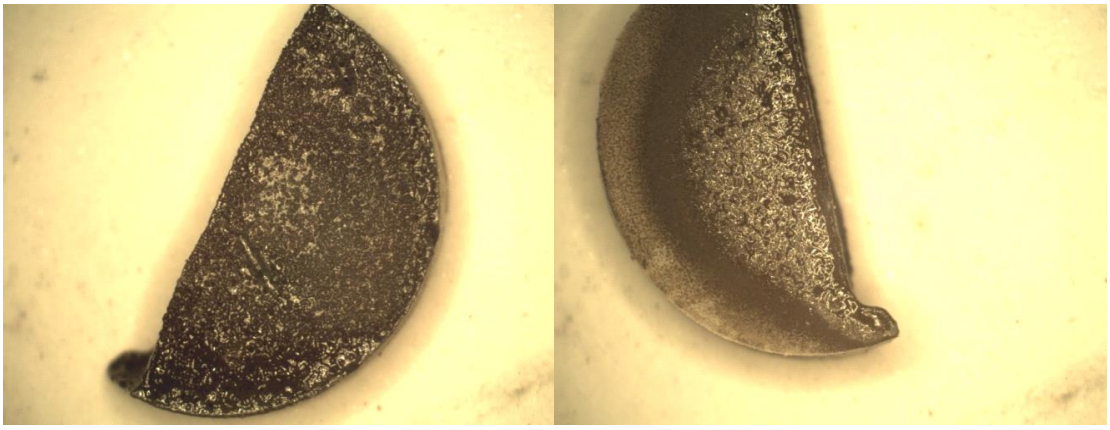

Figure 5.21: TQ2713 pellet surface after 45m at 1200°C, bottom of pellet (right) and top of pellet (left)

Figure 5.21above shows the TQ2713 sample halved and oxidized at 1200°C for 45m. The surfaces are generally smooth without spallation, some pock marks are visible from either different localized penetration or bubbles forming and bursting. The coating seems to have filled in these channels and is no longer oxidizing through them. Around the edge of the top (right image) there's a friable glass layer that's not melted, suggesting too high viscosity. This is likely a B depletion effect, and possibly also from faster B evaporation from that side of the pellet resulting in higher silica content in that region of glass. With that in mind, the adequate protection which was observed is likely formed from a B-depleted surface layer, which has higher Si:B ratio than the expected batch would otherwise dictate. In other words, in order for the actual bulk material to create a similar glass to the depleted outer composition we would need a lower overall B content.

Figure 5.22: TQ2713 pellet surface after oxidation at 1300°C, for 90m (right) and 20h (left)

Figure 5.22 shows the surface as oxidized at 1300°C. It appears to have a clean smooth glassy coating after 90m, but again pock marked possibly due to bursting bubbles at the surface. At 20 hours there was a fair bit of overall shrinkage and thickening of the glassy layer but it remains glassy and smooth. Some thin spots exist where bubbles or channels persisted for longer times and may still be actively oxidizing.

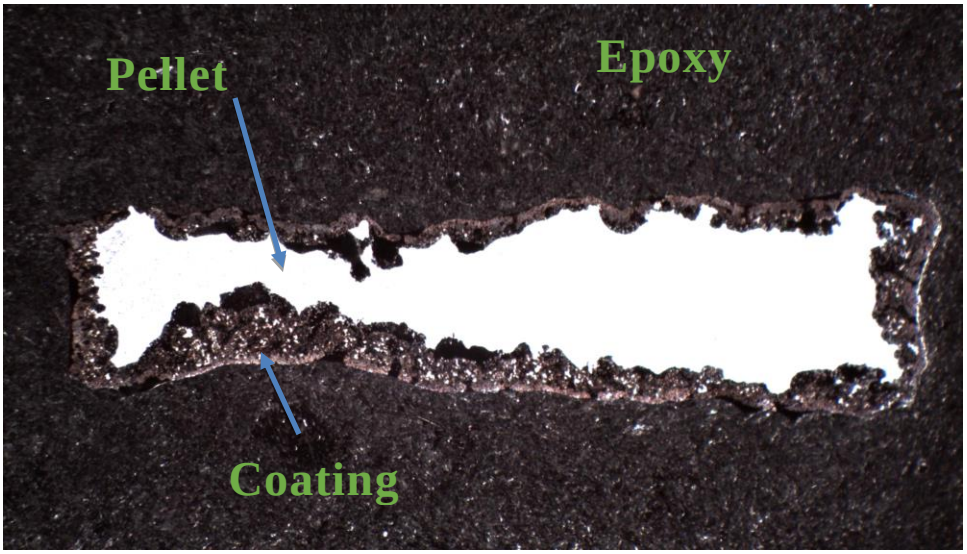

Figure 5.23: Oxidized coating on pellet cross section of TQ2713 after in 20h in air at 1300°C, mounted in epoxy resin

The cross section (Figure 5.23) shows the continued penetration and degradation of the sample. The protective layer appears to be less glassy than it looks from the surface, though the actual composition is unknown. Small islands of metal remain encapsulated within. Dark highly glassy regions remain and seem to be sealing in between the oxidized material. The MoO_2 is not present as a layer under the glass but dispersed throughout it and towards the surface, and it appears the oxidation is proceeding relatively quickly through the glass and undercutting the material. This may indicate high oxygen diffusivity (D_{O2}) from too low a glass viscosity. While a glass is forming, it is not effectively limiting oxygen transport and allows the oxidation front to continue inward. It is also possibly that the low viscosity has allowed some fluid motion transfer by convection or stirring, perhaps enhanced by bubbles, to effectively increase oxygen transport kinetics beyond a linear diffusion rate. This could explain why the islands of metal and Mo-oxides exist in the glass. XRD shows significant amorphous fraction as well as crystalline MoO_2.

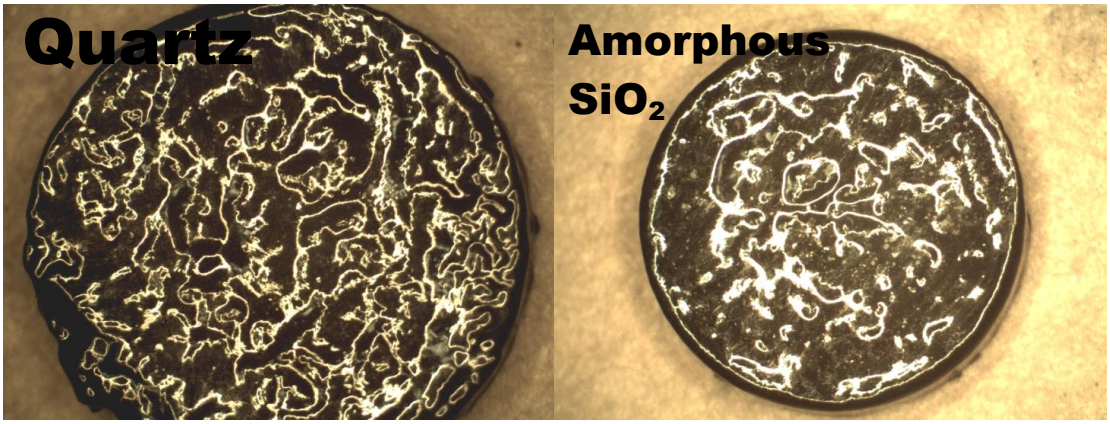

Figure 5.24: Optical comparison of crystalline vs. amorphous oxidized 90m at 1300°C in air. TQ with quartz (right) and, TS with amorphous SiO2 (left).

The next samples oxidized investigated whether there is a difference in oxidation performance between different SiO_2 sources, namely quartz (TQ) and amorphous silica (TS). The optical images after 90 minutes at 1300°C are shown in Figure 5.24. They behaved generally very similarly, but TS looks smoother, has lower weight loss and better edge retention. They both are formulated to form the same volume of glass per unit volume, but due to lower density of quartz the TQ has a slightly more Mo.

A similar composition TQ2713 was also oxidized at 1200°C in air. At 1200°C the TQ was consumed fairly rapidly and was wholly consumed within 20h. It formed a glossy black coat after 30m which had visible porosity/holes in the scale. The cross section of the oxidized sample showed a large degree of MoO_2 surrounded by glass and small islands of Mo within. Also there was a large degree of open internal porosity.

Composition BST052021 had the best oxidation resistance compared to the TQ2713 and TS2614 samples. It seems that were it extended to longer times it would not continue to oxidize much further.

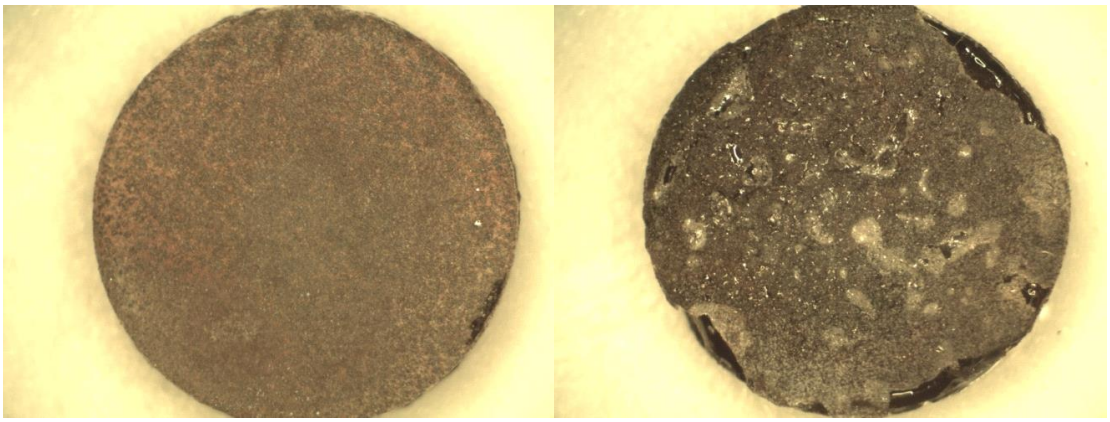

Figure 5.25: BST052021 oxidized in air at 1300°C; 90m (right) and 20h (left).

Figure 5.25 shows the BST052021 surface after oxidation at 1300°C. There's obviously a different mechanism here, with a thicker more solid glass layer forming first on the outer surface – presumably due to the B depletion leading to higher viscosity surface glass. As time proceeds a protective internal glass of the bulk composition is forming below and throughout the earlier high viscosity depletion-based layer. The oxidation rates have leveled off to less than 10 mg/cm^2*h, which up to this point is one of the best long term rates we'd seen at 1300°C.

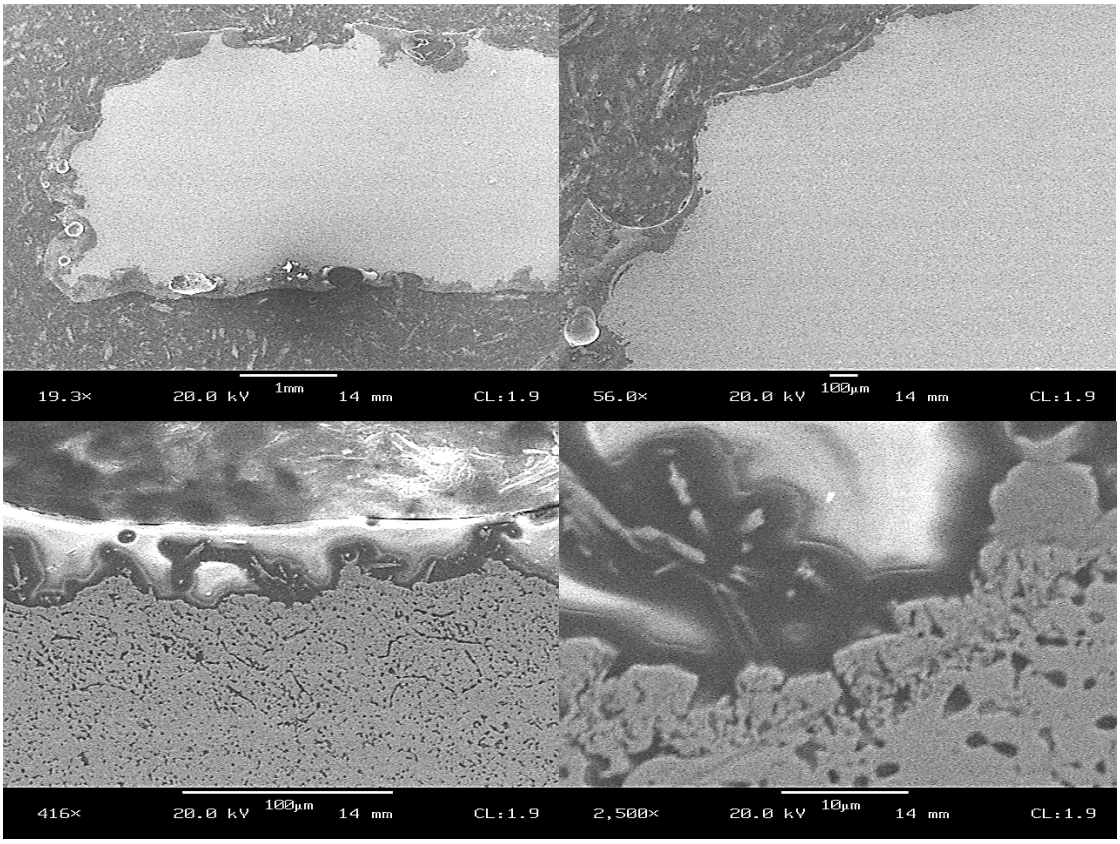

Figure 5.26: SEM images of the BST052021cross section after oxidation 20h at 1300°C in air.

Close up examination the oxidized cross section (Figure 5.26) reveals that there a few large bubbles, but the glass has a good fully wetting coat over the underlying material. Bubbles may be differentiated from open channels by the fact that none of the mounting epoxy has filled into them. The large empty circles may be due to bursting of a large bubble or sealed bubbles in the glass which cracked during mounting. Definite internal oxidation is visible, and crystalline needles of MoO_2 exist within the glass rather than as an internal layer under the glass. XRD indicates the needles are indeed MoO_2, and the glass has high glassy content.

The needles look conspicuously like those observed by Rioult and Perepezko[52] for Mo + T2 only. It's possible the lower viscosity caused by higher B content increases

both Mo and O diffusion allowing Mo to react within the glassy layer rather than at the glass/bulk interface. Also the lack of an A15 phase should change the equilibrium pO_2 at the glass/bulk interface such that Mo can oxidize within the glass.

Samples were halved and oxidized again. After oxidation there can be seen a different mechanism on the surface compared to the cut face, even though the composition should theoretically be the same. Figure 5.27 shows the BST052021 after 20h oxidation at 1300°C with the cut face on the right side. The surface at the top has a good coating, but through the center inward from the cut face is continued bubbling and oxidation. The outer region of the pellet at the top edge in the figure may have higher viscosity glass due to the more pronounced T2 depletion layer vs. the SiO_2 depletion, leading to lower B content in the glass. Meanwhile along the cut face no depletion had occurred and more boride and T2 is present, but the resultant lower viscosity does not provide good oxidation resistance.

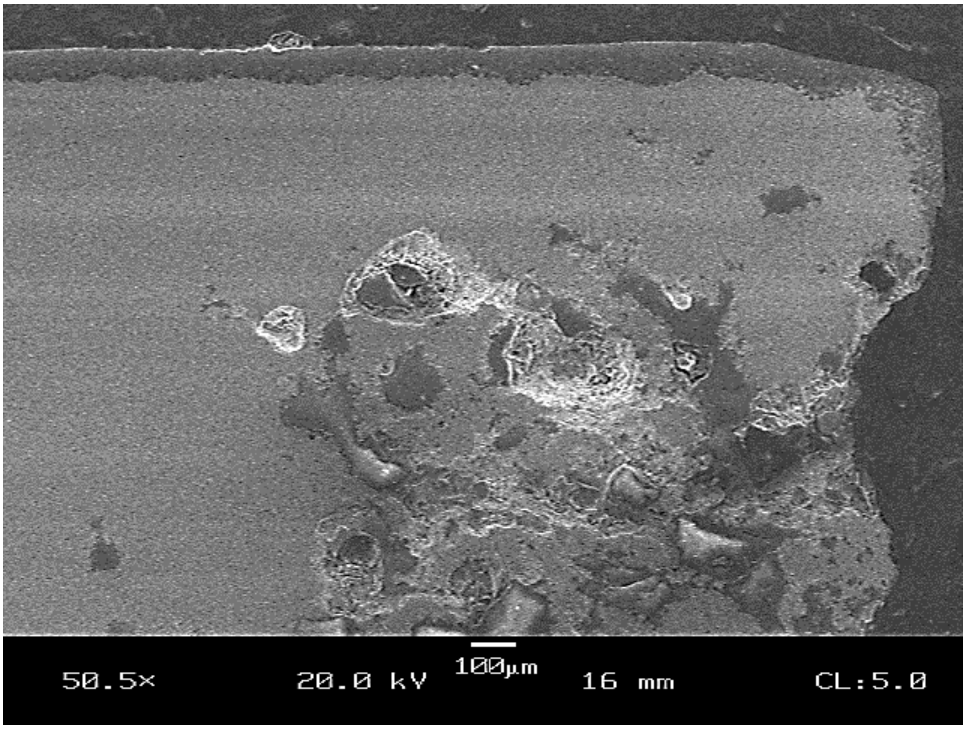

Figure 5.27: Cross section of halved BST052021 pellet after 20h at 1300°C with the cut face on the right side.

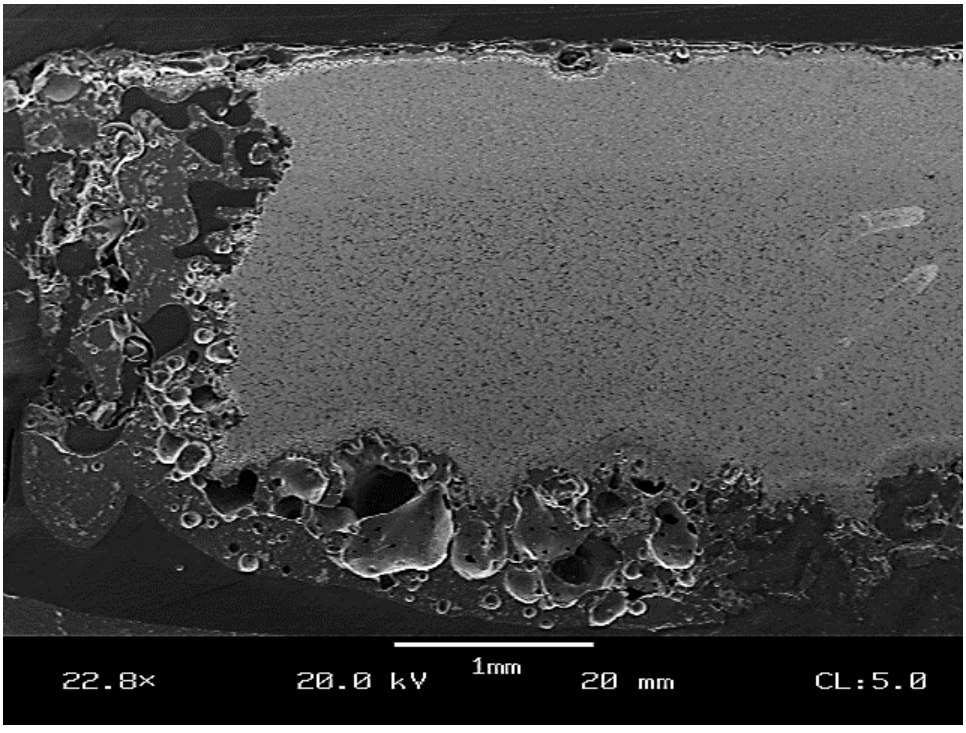

Figure 5.28: Cross section of BS1025 after 90m at 1200°C

If we look back at oxidation tests done on a BS1025, which should've been a lower viscosity glass than 3:1 Si:B, its performance is great at 1000°C and awful at 1300°C. At 1200°C (Figure 5.28) there's a very distinctly different layer at the top which contains less connected silica and is probably depleted in silicon and boron, yet that's by far the better oxidation resistant edge. The resistance is most successful where the higher boride loss occurred and on the poorest performing edge which was more depleted in SiO_2, the material is consumed rapidly. This also points to the fact that inadequate oxidation resistance is caused by too low viscosity as a result of an already low-viscosity composition exacerbated by uneven depletion.

5.3.2.2.1. Oxidation on Ground Surfaces

It is apparent that depletion of glass formers as discussed previously is affecting the oxidation performance, and contributing to the high initial losses seen in this system compared to other MoSiB compositions. Additional samples were prepared and the surfaces were ground with a 220 grit paper for roughly 2 minutes per side, removing somewhere near 0.01 mm from the surfaces and edges. This should remove some or the entire depleted zone, which previously was measured typically 50-75μm deep. They were then polished to 400 then 600 grit before oxidation. The results of the ground vs. unground cases are presented in Figure 5.29. Indeed a reduction in initial losses is observed but the mechanism remains the same and complete failure is only slightly delayed. If however the compositions were protective, removing the high Mo depleted layer could reduce the initial losses by nearly 100mg/cm^2.

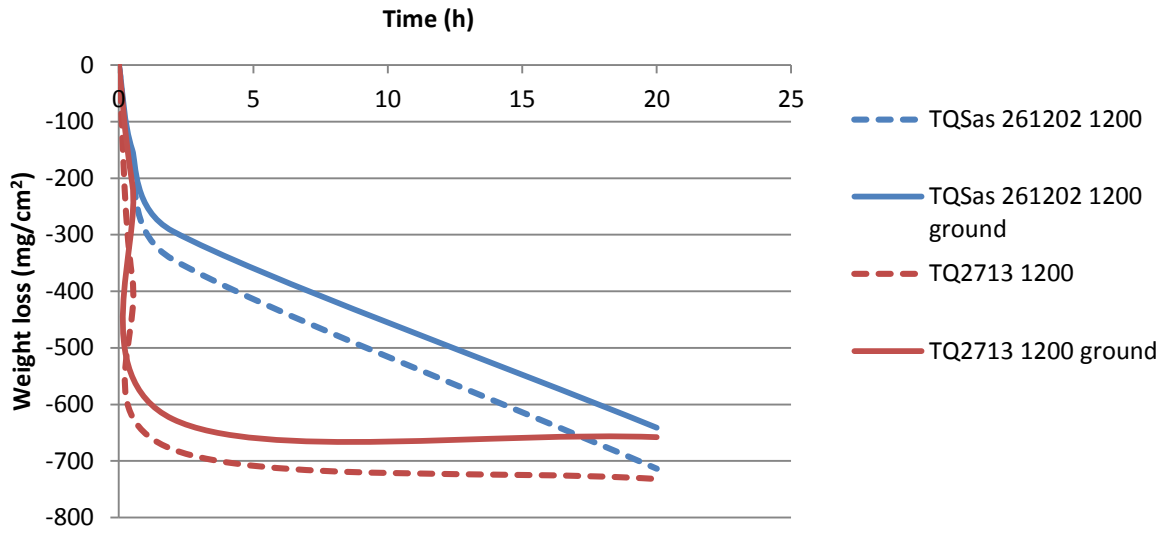

Figure 5.29: Comparison of weight loss from TQSas261202 and TQ2713 in ground vs. unground cases at 1200°C

5.3.2.2.2. Short Term Oxidation

To examine the mechanisms of oxidation, BST041523 samples were oxidized at shorter times. Samples were cut and polished and oxidized in air at 1300°C individually for times of 1, 2 and 10 minutes so that the formation of the coating during the initial transient phase could be observed microscopically.

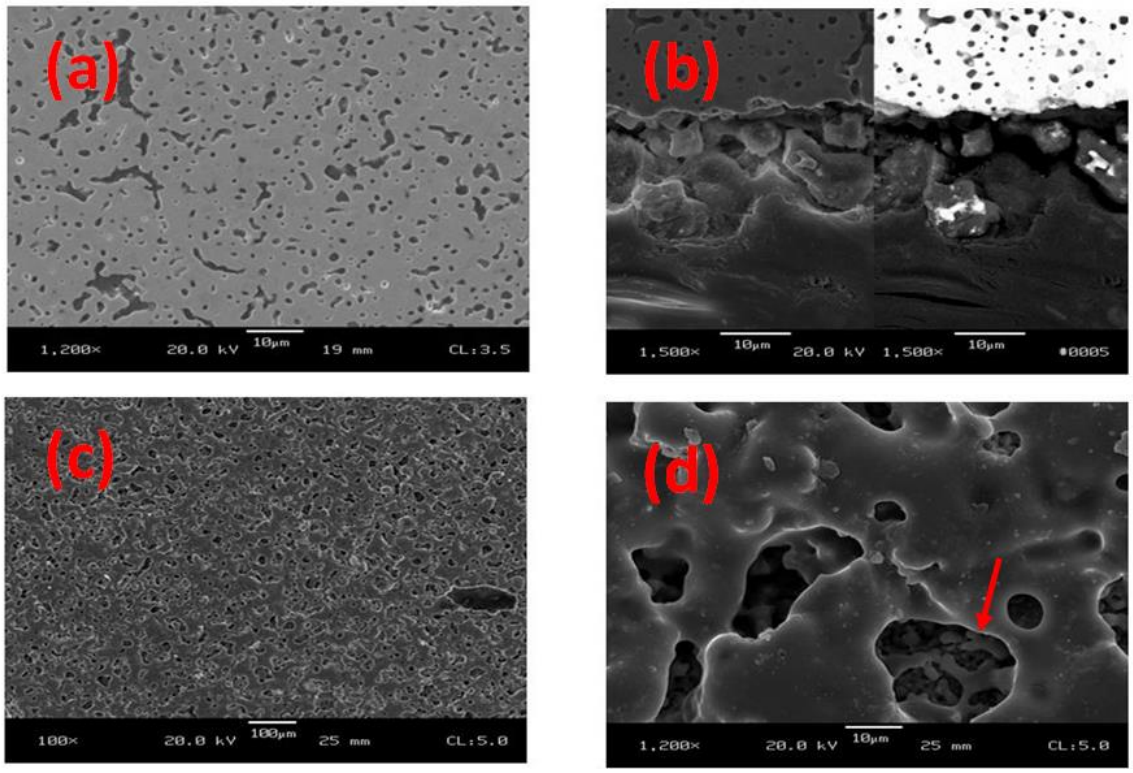

Figure 5.30: Oxidation of BST041523 after 1minute in air at 1300°C, top right (a) shows the bulk microstructure, top left (b) shows the oxidized layer's cross section in secondary electron (right) and backscattered (left), bottom right (c) shows the oxidized surface, and bottom left (d) is a close up of the oxidized surface at the same magnification as a and b.

Figure 5.30 shows the results of the oxidized samples. The bulk microstructure (a) contains approximately 10-15% glass. After 1 minute of oxidation, the surface is as shown in the bottom left (d). There are a large number of pores and now close to 60-70% of the surface is coated by glass. The magnification of the images are the same, but scale of the glass is much larger than the bulk microstructure; the 1-10um glass regions of the initial microstructure have grown to a fully interconnected but porous glass layer, with pores between 10 and 50um. Borosilicate is forming and coalescing. Within the holes in the bottom right image (red arrow) there can be seen new glass forming on the approximate size scale of the initial microstructure indicating that this is likely a new

fresh surface at the base of the bubble. In the top right (b) is shown a cross section of the layer of around 20µm depth. The BS image in the right half of (b) decreases depth of field and exhibits the much smaller fraction that exists on a single plane. Image analysis suggests about half of the volume of the oxide layer is empty. It appears that the surface is very volatile and dynamic, with rapid formation of glass alongside gaseous MoO_3, which is creating bubbles and holding/blowing open these pore channels.

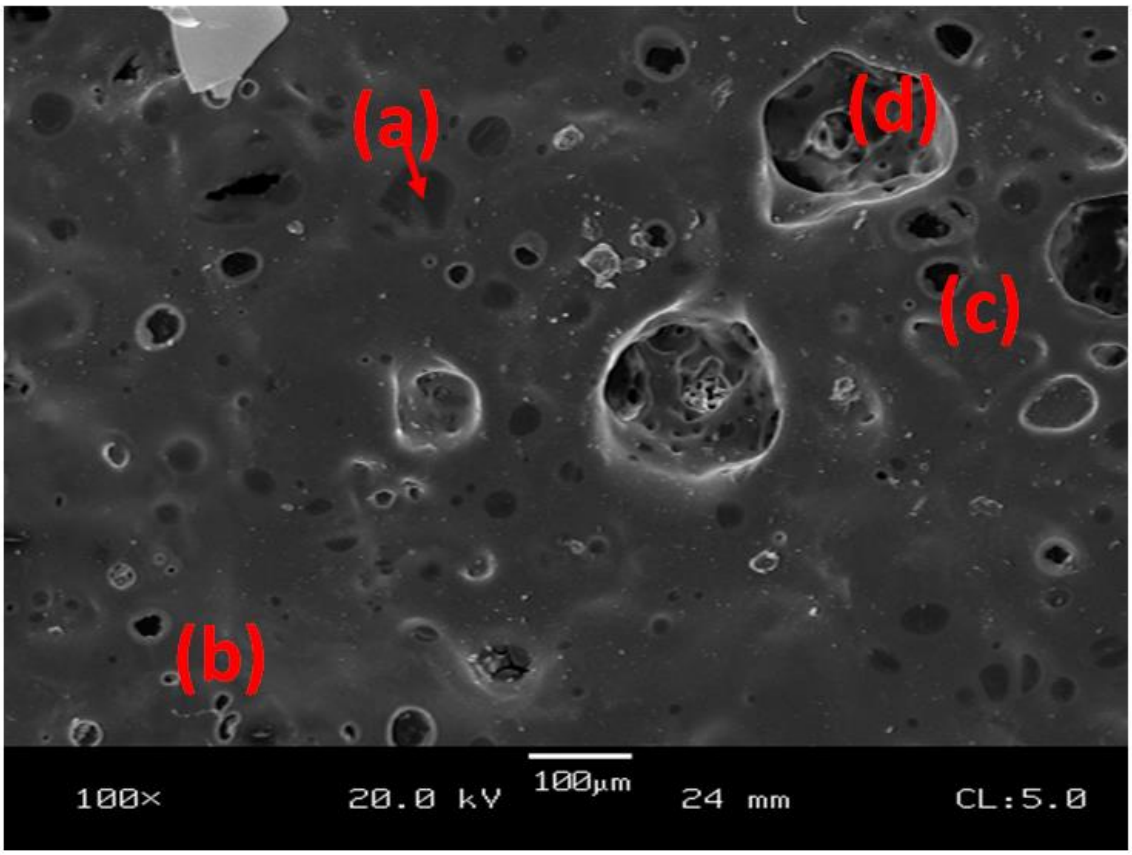

Figure 5.31: Close up SEM image of the oxidized surface of BST041523 at 10m in air at 1300˚C showing the various types of surface features.

As time continues the type of surface remains the same but the scale changes. The depth of the scale and size of the bubbles increase, but fewer bubbles are apparent. As

shown in Figure 5.31, there are numerous smaller bubbles within the scale even after just 10m. As the borosilicate depth increases it becomes more effective at sealing the bubbles, however the high rate of MoO_3 production forces others open. This leads to a coarsening effect of the bubbles. Meanwhile, MoO_3 formation is still rapid enough to nucleate new smaller bubbles separate from the large channels. Sealed bubbles are apparent (a) where the glass is now significant enough in volume to close off more of the smaller pores. Bubbles are still forming and escaping through the glass to the surface (b, c) and the larger pores remain with rapid MoO_3 formation from exposed surface at their base (d).

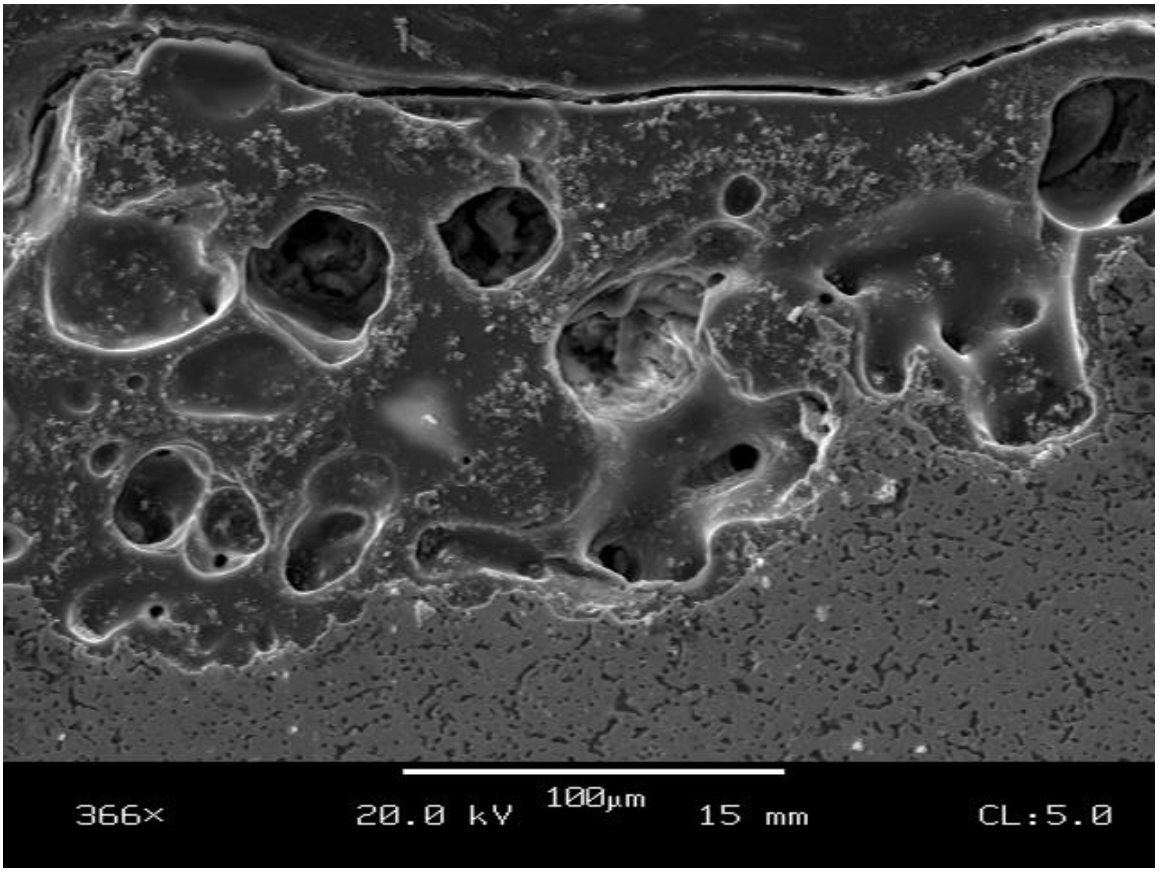

Figure 5.32: SEM cross section of the oxidized layer on BST041523 at 1300°C in air for 10m.

In the cross section image (Figure 5.32) the bubbles seen in Figure 5.31 are more apparent. They're mostly on the same size scale as the surface bubbles observed after 1min, however the depth of the glass is significantly greater and the bubbles are now entrapped. At the 1 minute time bubbles of the same size would span the full depth of the glass. If there is a stable bubble size, the glass thickness must be greater than that or no protection is possible. Also bubbles can join into larger void regions which if grown large enough would leave open-channels for fast track oxidation upon rupture. The oxide behavior appears to be that of a very dynamic series of bubble formation, coalescence and collapse. The Mo oxide is present throughout the glass and is moved around as the glass flows and bubbles. In this case the oxidization has not leveled off to the parabolic diffusion controlled rates, but is instead controlled by a more rapid fluid flow and mixing through bubbles and pore channels.

5.3.2.2.3. Si:B Ratio

A TS1520 composition, which is a low volume fraction of glass formers and a low Si to B ratio also exhibited rapid violent bubbling. The oxidation was good at 1000°C and 1100°C and full of bubbles and nonprotective at 1200 and 1300°C. It appears that at the higher temperatures where the MoO_3 vapor pressure is greater than 1atm, the low viscosity which aids sealing at low temperatures is too low at higher temperatures. The higher temperature further reduces viscosity, but also there is the now greater than 1atm partial of the MoO_3 vapor which forms bubbles. The bubbles act to disrupt the already poorly protective low viscosity glass, and can act also to stir and move the oxygen through by convection as well as diffusion.

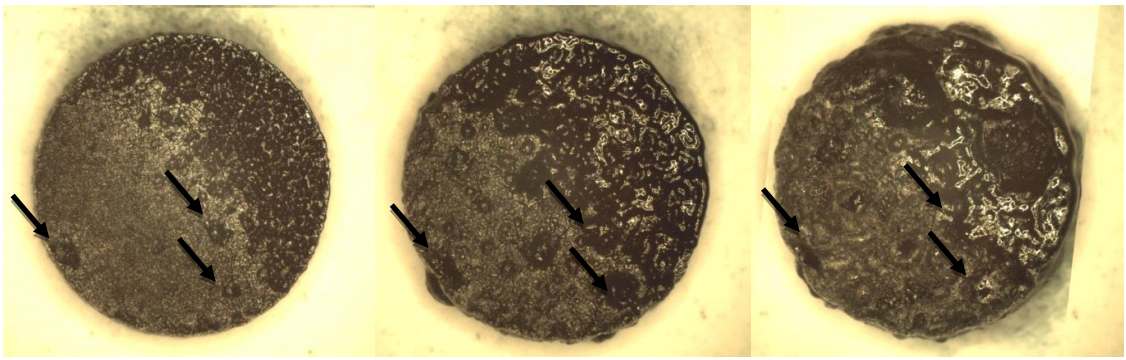

Figure 5.33: TS1817 pellet oxidized at 1300, from left to right 10m, 30m and 90m. Arrows indicate consistent features maintained through the time frame

Oxidation of other samples also supports the need for higher viscosity. Figure 5.33 shows TS1817 at 1300˚C after 10, 30 and 90 minutes and you can see features and bubbles maintained but only slightly growing (red arrows) in the better performing bottom left side. There are regions, such as those maintained features, which have a good coating, whereas the rest – especially the top right– is too low viscosity (or too high diffusivity) and is responsible for the poor oxidation overall. This is likely due to uneven depletion; however the better performing section is most likely the greater depleted so the behavior is not representative of the composition which was batched for. Consistently the higher viscosity is better for oxidation in the long term, and required to passivate.

Furthermore, many of the better protected samples such as BST052021exhibited friable white oxide layers at 10m, the result of B depletion leaving behind a high SiO_2 high viscosity layer. The images and proposed mechanisms, as well as evidence of better performance from the B-depleted surfaces, suggest that this system would benefit from a higher viscosity of glass. A lower viscosity glass would be more effective at sealing pores and channels, but also allows new bubbles and pores to form more easily. In the previous compositions it appears that the glass is capable of sealing itself but not maintaining that

seal due to rapid MoO_3 formation and bubbling, which then creates open pathways for oxygen and prevents oxidation protection from being achieved. A more viscous glass should require less depth to be protective by limiting transport and making bubbles more difficult, but would also lose more weight initially due to its reduced ability to flow and fill pores. The mechanism for failure here appears to be less about initial flowability, and more about ability to suppress bubble formation. Without the same stirring flow effects from bubble motion the depth required to achieve parabolic protection should be much less. Also MoO_2 can form below the glass which further restricts oxygen transport. A more viscous glass would create a scenario where the system would proceed toward truly diffusion controlled parabolic oxidation limited by oxygen mobility through a stagnant homogenous glass rather than the volatile low viscosity glasses seen so far.

5.3.3. Higher Viscosity Compositions

The evidence of better performance from the B-depleted surfaces suggests that this system would benefit from a higher viscosity of glass. The performance in the TS, TQ and BST samples is acceptable at 1100°C, but when held at 1300°C the glass is too fluid to prevent oxidation from continuing. This is not surprising however because the composition of the glass was designed to match that of the 3:1 Mo-Si-B, which is optimized for oxidation protection at 1100°C. In an attempt to increase the viscosity of the glass and prevent the rapid loss by bubbling through the oxide coating, a third set of higher silica compositions was prepared. Figure 5.34 shows viscosity curves for borosilicate glasses of varying boron contents as a function of temperature from Doremus[55]. A composition was chosen so that the viscosity at 1300°C matches that of 3:1 Si:B glass at 1100°C. The $\ln(\eta) = 13$ (red line) for the 30 mol% B_2O_3 at 1100°C falls

nearest to a composition of 25 mol% B_2O_3 at 1300°C. The revised composition consisting of 23 vol% T2 and 22 vol% amorphous SiO_2 (TS2322) produces the desired 25 mol% B_2O_3 in the borosilicate, and should possess the higher viscosity needed to provide oxidation protection at 1300°C.

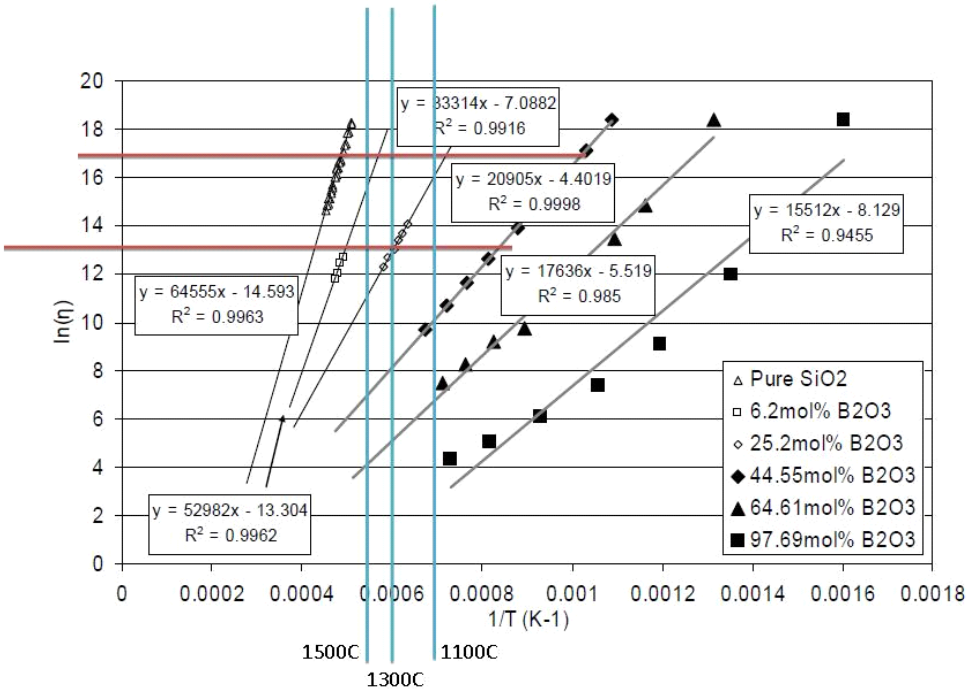

Figure 5.34: Viscosity of borosilicate glass as a function of boron content and temperature, with relevant viscosities and temperatures highlighted.

5.3.3.1.Firing

The TS2322 fired to full theoretical density t 1550°C. The high density may be in part due to depletion however. The depleted layer on the TS2322 was very significant and obvious and extends to a depth of 200µm or more, Figure 5.35. Crescents of silica also remain an issue in the microstructure.

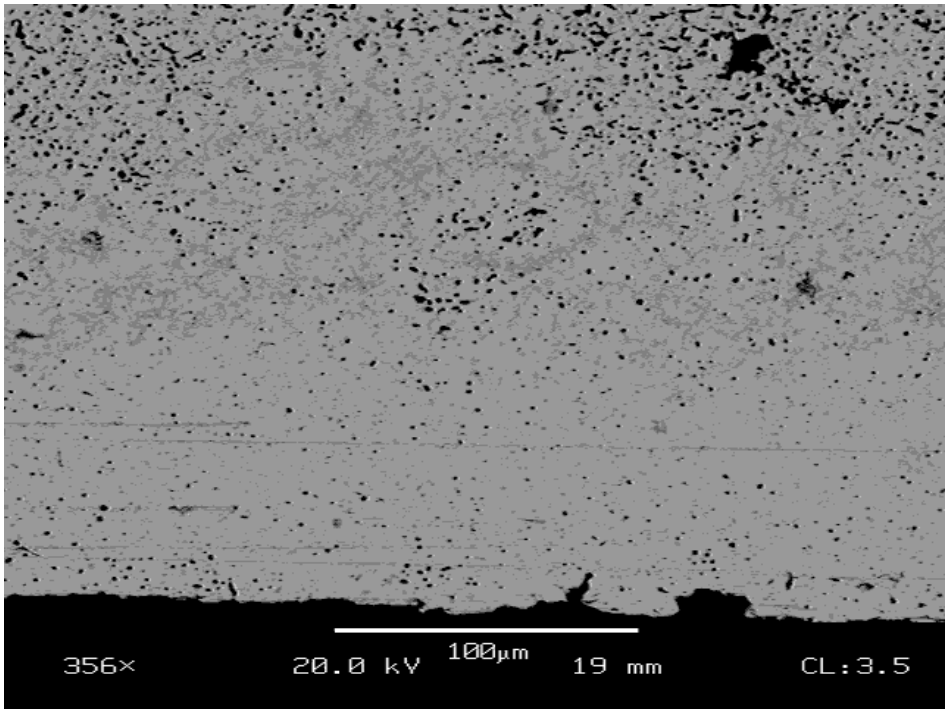

Figure 5.35: As-fired cross section of TS2322 microstructure and surface depletion

5.3.3.2.Oxidation

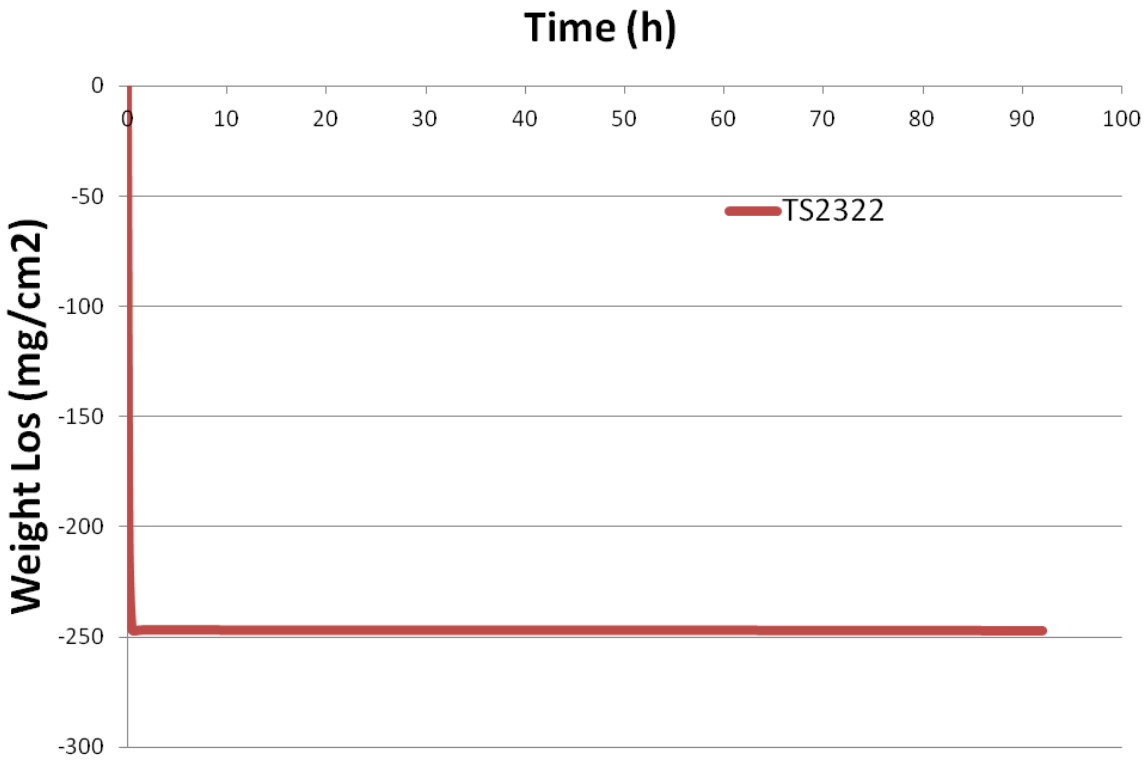

Figure 5.36: Weight loss of TS2322 vs. time at 1200°C in air.

The new higher viscosity TS2322 was oxidized at 1200°C for 100h and oxidation was very good; however initial losses were still high. The weight loss curve is shown in Figure 5.36. It lost 225mg in just the first 10m, but leveled off after 30m at 250mg/cm which it maintained out to 100h of oxidation. The long term loss had an exceptionally low rate of only -0.0038 mg/cm^2*h. An initial crust was formed, while the bottom center maintained a much glassier looking coating without evidence of bubbles or protrusions.

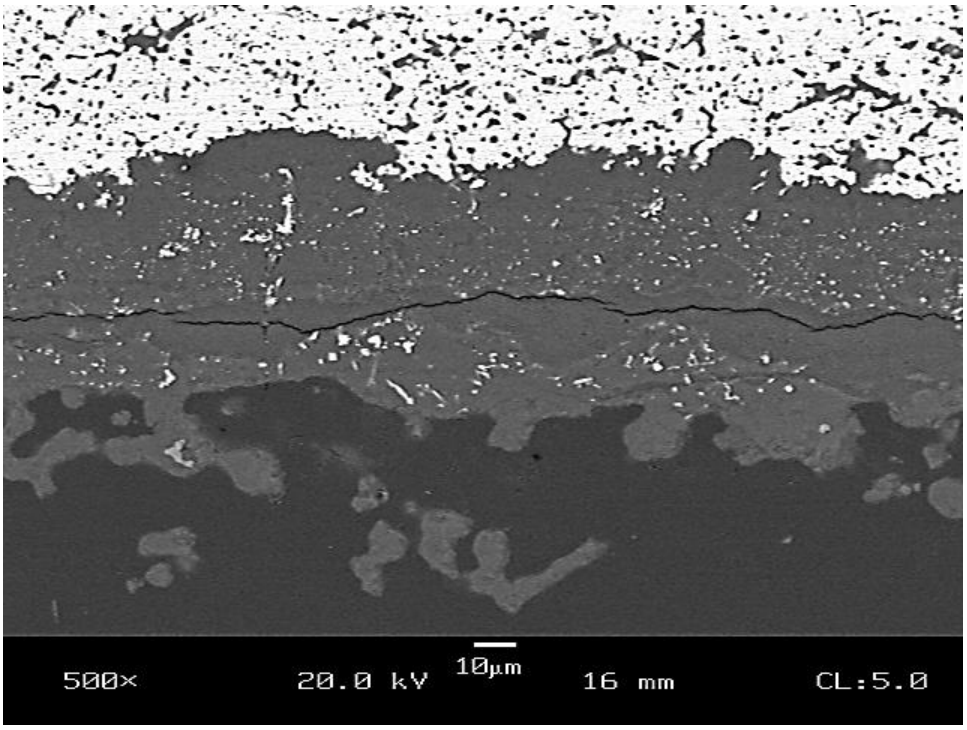

Figure 5.37: TS2322 pellet oxidized in air at 1200°C for 100h

The cross section of the surface after 1200°C 100h oxidation in the Keith is shown in Figure 5.37. The friable outer layer along the bottom of the image is noticeable as the isolated regions separate in the epoxy mount. The porous outer layer is presumably due to a much more viscous glass initially which is unable to coalesce and flow together because of boron depletion near the sample's surface. The effective coating is only 50-100µm deep and appears to limit oxygen very well. There is no obvious MoO_2 layer at the interface of the coating and substrate; however some MoO_2 exists within the coating.

The high initial weight loss and the initial high-silica crust could both be due to B depletion as seen in Figure 5.35. Grinding as seen previously would significantly reduce the high initial losses. The depletion must also have resulted in an even higher viscosity

than initially planned for, and might indicate that the ideal viscosity should be even greater still.

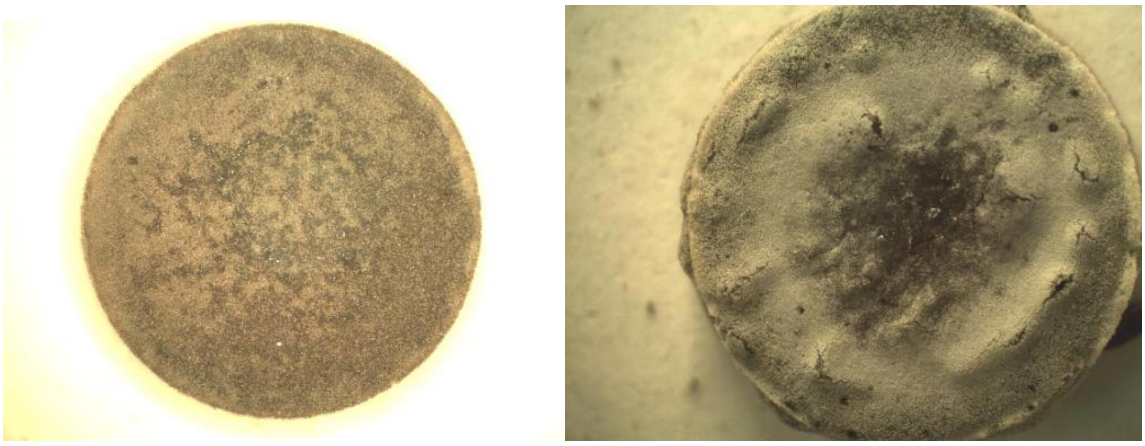

Figure 5.38: Oxidized TS2322 at 1300°C pellet after 30m (left) and 20h (right)

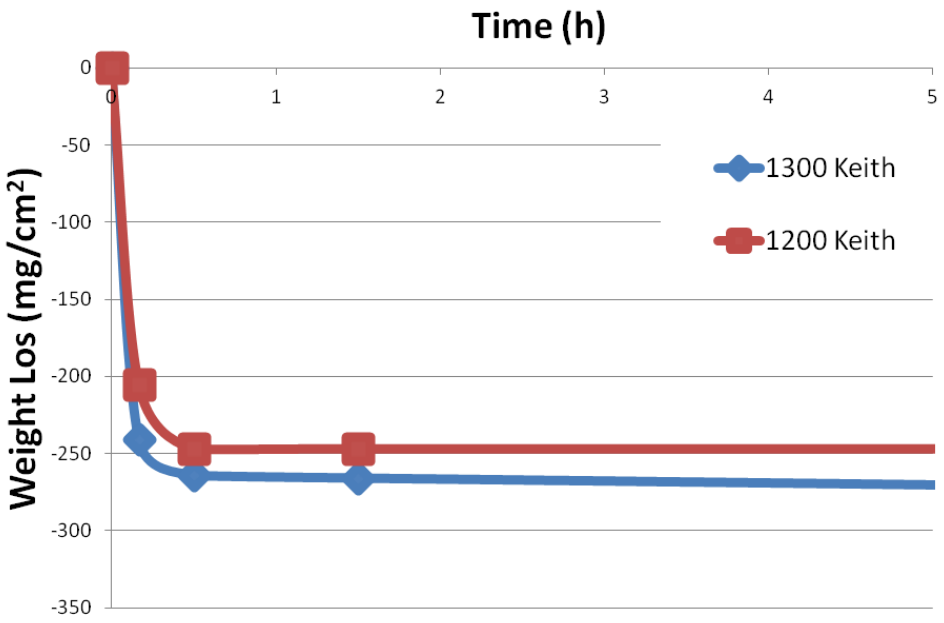

Figure 5.39: Chart of 1300°C oxidation weight loss results for TS2322

At 1300°C the oxidation protection was also improved compared to the previous compositions (Figure 5.39). Initial weight losses were high, around 250mg/cm^2 but level off after about 30m with nearly constant weight out to 20h. The figure shows the TS2322 sample oxidized at 1300°C for 90m compared to the weight loss at 1200°C and is only slightly greater loss, but also a slightly higher parabolic loss rate.

Initially porous Si foam exists from the high silica regions exposed as the Mo is removed similar to the 1200°C case which has been linked to B depletion during firing from the surface of the samples. A porous high Si region remains on the outside of the coating with glass underneath. After 30m the borosilicate has mixed enough that the foam sinters and coalesces at the bulk surface into a protective coating underneath the porous high silica crust. After 20h, there is some rippling and bulging of the coating due to large bubbles beneath the coating as seen in Figure 5.38.

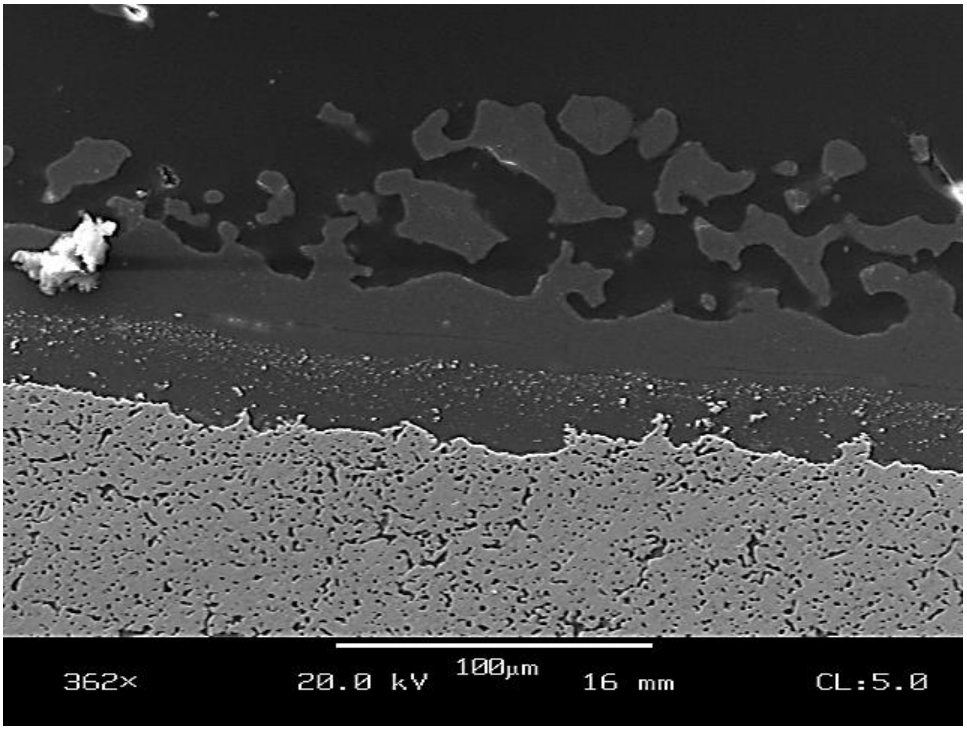

Figure 5.40: TS2322 oxidized at 1300°C for 20h in air.

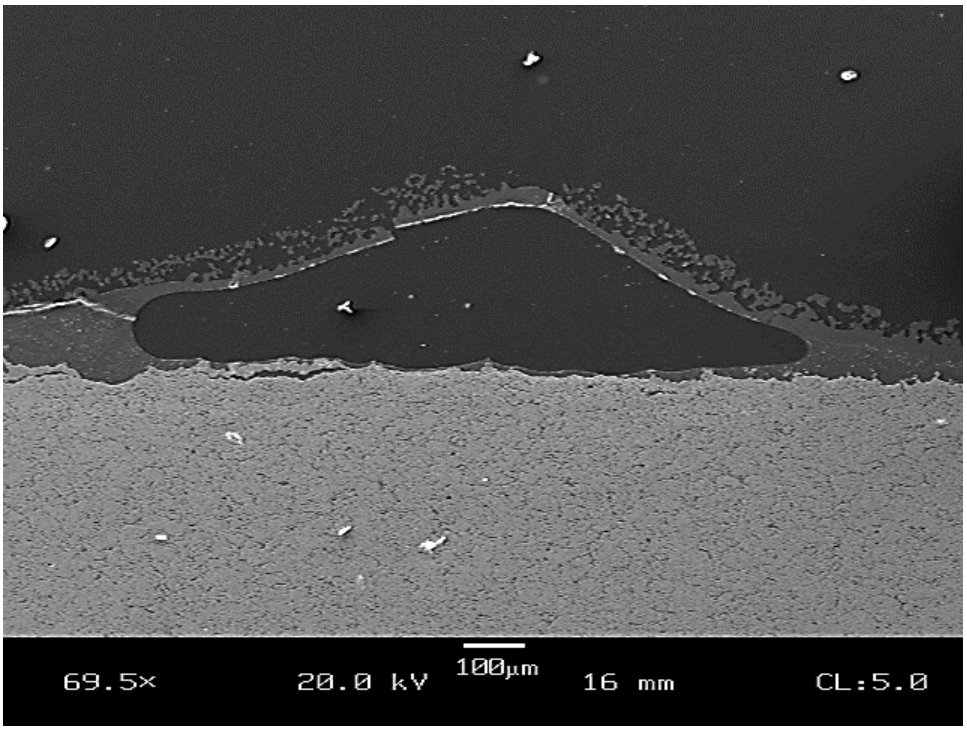

Figure 5.41: Detail of bubble in the surface coating of TS2322 oxidized at 1300°C for 20h in air

Looking at the cross section of the 1300°C oxidized layer in SEM (Figure 5.40), again we see the friable outer layer presumably due to the depleted layer. Some of the surface had a very good even protective coating present. Figure 5.41shows the cross section of one of the bubbles observed in the coating after 20h at 1300°C, it'd formed a coating much like the rest and seems to have formed a bubble on the inside. Of note is that in all of the above images we have a multilayer type effect in the glass scale, the friable outer layer connected to a clean glass top layer, but under that is a very definite interface where oxides appear in the glass. The bubble in the above image exists on this interface, with the oxide glass below it (and seen aligned with its edges) and clearer glass above. There is also a layer of apparently MoO_3 solidified on the top surface of the bubble suggesting that it was blown by MoO_3 vapor which then condensed at the outer surface upon cooling.

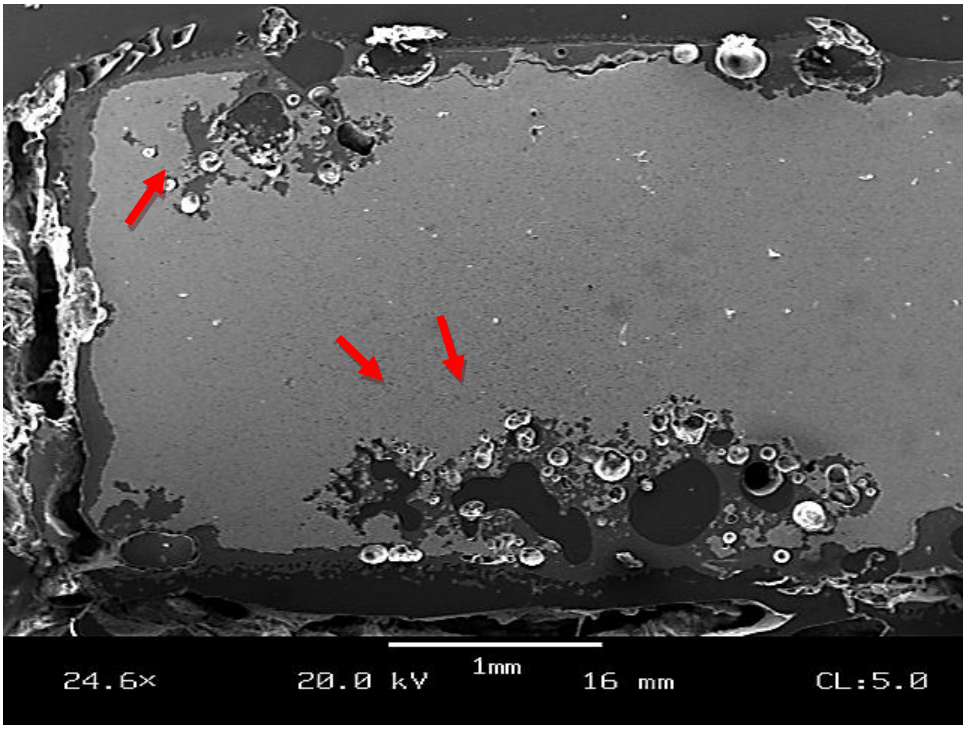

Figure 5.42: Surface coating and cross section of a second TS2322 pellet oxidized at 1300°C for 20h in air, red arrow indicates region of heightened penetration.

A second batch of TS2322 samples were prepared which after firing were observed to have less depletion and also slightly lower density. These were also oxidized at 1300°C, and performed less well than the first set. In some places large penetration zones exist with very significant bubbling shown in Figure 5.42. The glass may be low viscosity to contain bubbling at 1300°C because of the much higher vapor pressures. In these poorly performing locations, large scale local penetration by a bubbling mechanism is present. Likely this is also an artifact of the depleted layer and the protective coating is more representative of the depleted layer's composition, but once the oxidation front reaches into the bulk, the glass composition is no longer protective. The depletion of T2 was to a greater extent than SiO_2 depletion. This leads to a high silica outer layer with the

high viscosity on the outside where protection was good, and a low viscosity in the center.

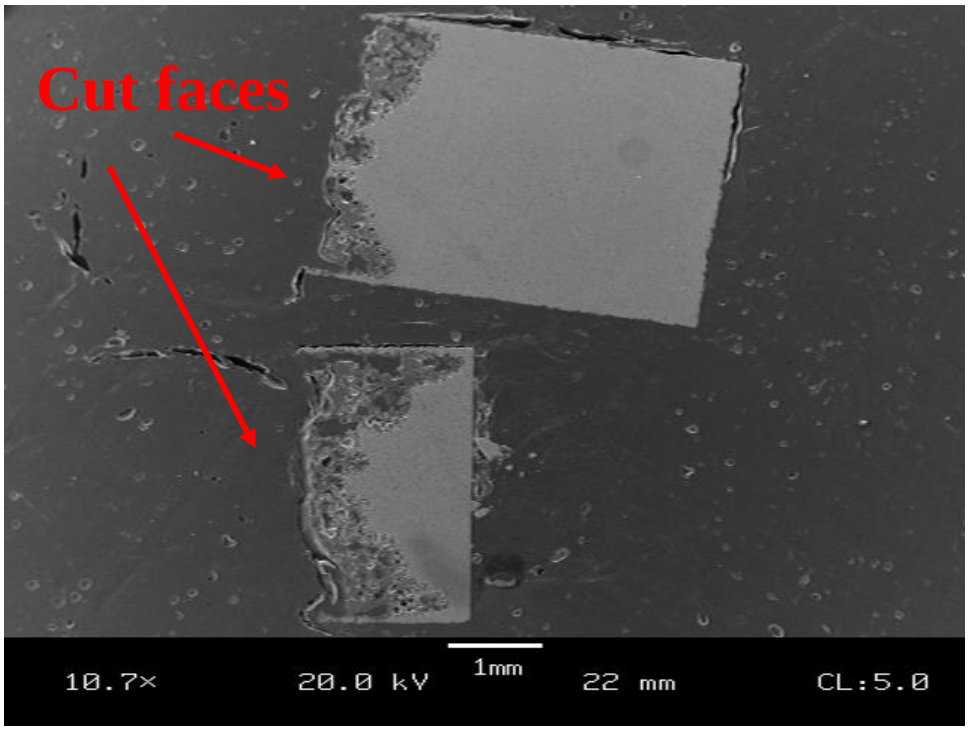

Figure 5.43: TS2322-2 half pellets after oxidation at 1200°C in air for 30m.

In order to investigate further, a pellet of TS2322-2 was cross sectioned to look for differences across the cut face between the bulk and surface-depleted compositions. The sample did well everywhere except the cut face, where protection was poor, which supports the argument that the ideal viscosity is not that of the bulk, but rather the higher viscosity of the B-depleted outer layer. Again we see evidence that a still higher viscosity is beneficial for good performance. Oxidation at 1100°C was similar to 1200°C and showed a friable outer layer consistent with those at other temperatures.

In all of the samples a higher degree of oxidation was present at the center of one surface. The bottom surface of the pellets during firing would sit in direct contact with the alumina boats. On the bottom surface, there is the least exposure to firing atmospheres and as discussed in section 5.3.1.3.4 the depletion is a gas phase phenomenon. Therefore on the bottom surface and more so at the center of that surface, the depletion of evaporate components would be least. Further, there's an additional possibility for chemical interaction with the alumina boat. These both could lead to a lower viscosity coating at the center of one side of each pellet's surface, which would then allow enhanced oxidation and bubble formation as exhibited in both of the images above.

5.3.4. Mechanical Results

5.3.4.1.SiO_2-Containing 4 point Bend Tests

In addition oxidation resistance, the mechanical properties must be sufficient, and the expected increase in room temperature toughness when removing Si from Mo solid solution is the primary motivation for shifting to SiO_2 containing compositions. Results of the 4-point bend tests of silica containing bend bars compared to previous frit samples is shown in Figure 5.44. Multiple tests were done for each composition but failed very similarly, and only one representative curve is shown for each. Stress strain curves from the mechanical testing of the frit and Quartz containing samples showed no measurable ductility at room temperature. Consistently no silica-containing compositions have shown any room T ductility.

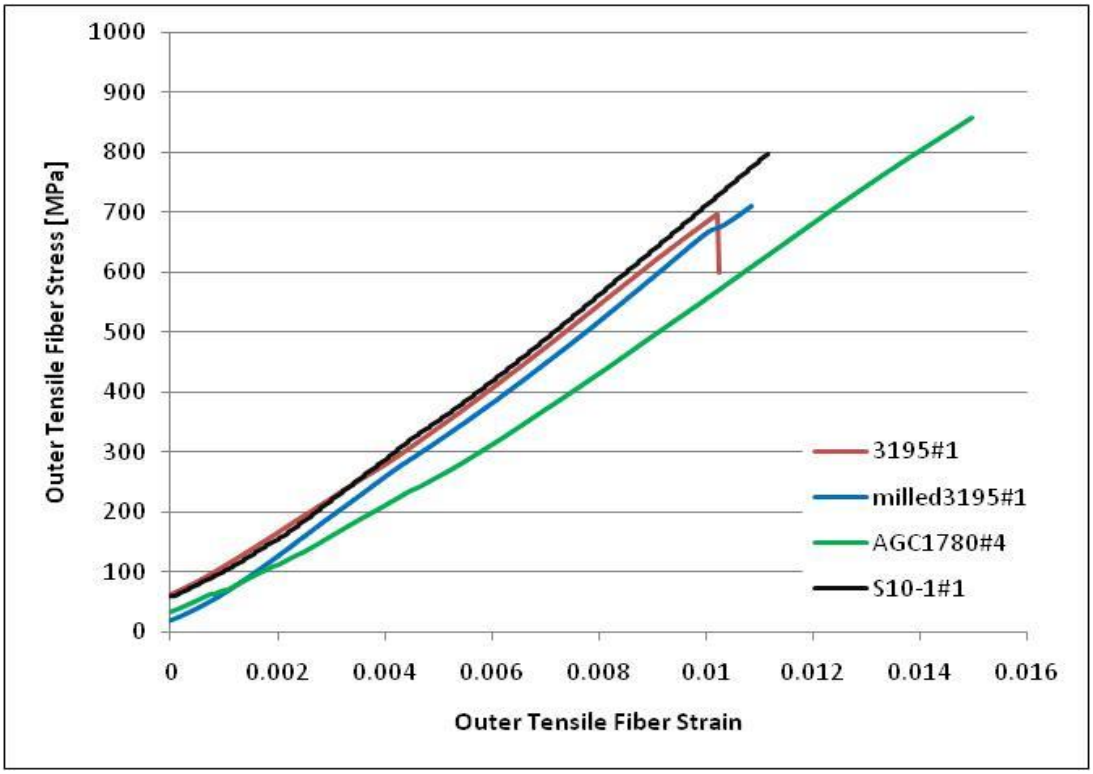

Figure 5.44: 4 Pt. Bend Bars: Outer tensile fiber stress-strain at room temperature of Mo containing 20 volume % glass frits (3195 or 1780) and Mo with 10 volume % amorphous SiO_2 (S10).

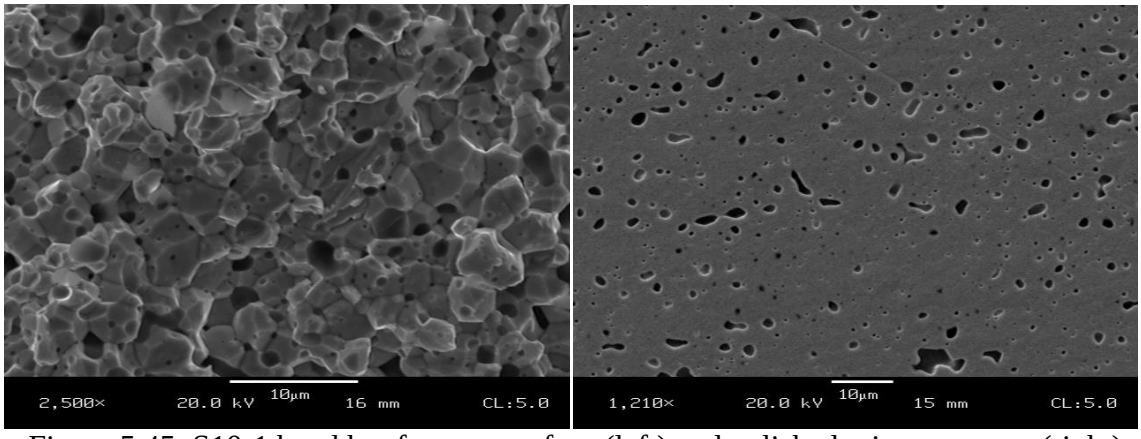

Figure 5.45: S10-1 bend bar fracture surface (left) and polished microstructure (right)

Examining the S10 sample which contains only 10 vol% SiO_2 and should be ductile, we see fully brittle failure at room temperature. The fracture surface reveals entirely intergranular failure and pockets on the grain boundaries associated with the SiO_2 (Figure 5.45). This does not mean that the DBTT has not been significantly reduced, but it is still higher than room temperature at which these tests were done.

During firing and reduction, SiO_2 may reduce to SiO, and the SiO may then be re precipitating on the grain boundaries leading to embrittlement. Dimples which may have been pores or pockets of SiO_2 can be seen on the grain boundaries; although possibly more is there as a fine coating as well.

SiO_2 embrittlement could also be due to the glassy regions acting as stress concentrators. For one, there is a thermal expansion mismatch. In addition the silica is already acting as stress concentrators in the matrix. Combined with the residual tensile stresses from thermal expansion the SiO_2 could give increased brittle behavior; yet the DBTT is the crossover between temperature dependant yield strength and stress for crack propagation. If the SiO_2 were merely acting as stress concentrators, the stress for crack propagation would be lower and would cause a lower total strength in addition to higher DBTT. Instead we see an increase in strength; the ultimate outer fiber tensile strength fails near 700 MPa whereas pure Mo does not typically exceed 600 MPa before yielding. This does not mean that the DBTT has not been significantly reduced however; the DBTT of the samples may be much lower than the 800°C minimum seen in the MoSiB system, but only room temperature tests were performed.

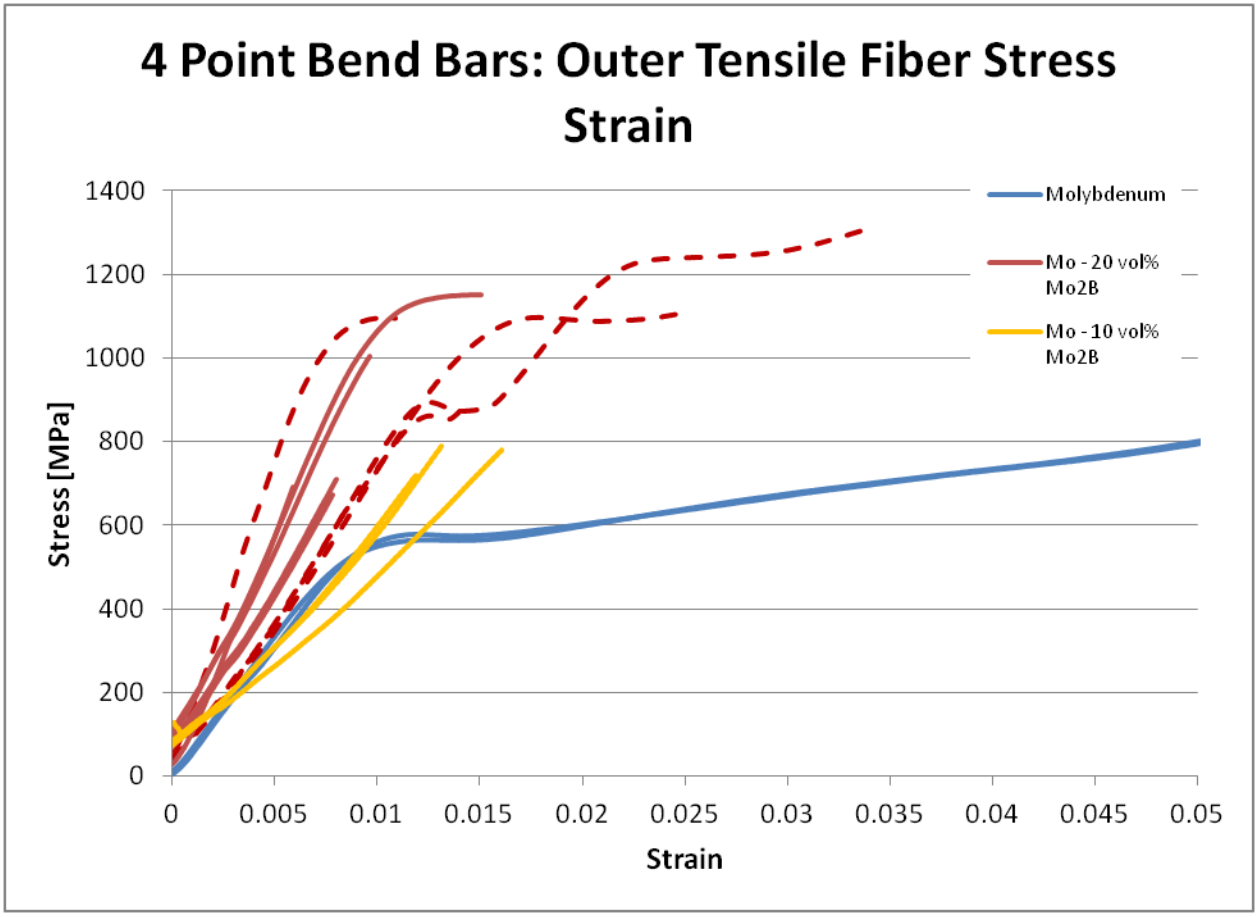

Figure 5.46: 4 Pt. Bend Bars: Outer Tensile Fiber Stress-Strain at Room Temperature for Mo and Mo+Mo_2B compositions

Figure 5.46 shows the stress strain curved measured from bend bars with 10 and 20% Boride with the remainder pure Mo, tested in 4 point bending at room temperature. The ones with only 10% boride did not fire to full density, and thus fail at lower stresses while the 20% Mo_2B samples exhibit measurable ductility and high strengths nearly twice that of the pure Mo. It's presumed that were the 10% Mo_2B bars fully dense, they would've also shown ductility, but the high porosity caused them to fail before reaching their yield strength.

This shows that good mechanical properties and usable strength and ductility are possible in the presence of the Mo boride even at room temperature or below. The boride does not embrittle Mo the way A15 does. Also, the fact that the 20% Mo_2B samples reached over 1000 MPa before failing could suggest that the silica containing sample also have increased yield points, and with greater strength and control over the microstructure it may be possible to increase their strength and thus allow yielding at room temperature.

5.3.4.2.Vickers Hardness

Vickers indentation was used to look for indications of fracture toughness, however at the loads possible (2kg) no cracking was observed. This shows that toughness must be greater than the minimum for that load; however that only indicates toughness is at least greater than ~3.0 MPa√m. The Vickers toughness is a highly unreliable empirically based test even when cracks exist and can be measured, but without cracking, no fracture toughness estimates can even be made.

There is possibility to check any relationships between hardness and toughness. Hardness measurements were taken by Vickers indentation. An increase in solid solution strengthening should raise hardness as well. The hardness values for A15 containing MoSiB were compared to those with only T2 and silica. The A15 values are softer, contrary to the solid solution strengthening expected to occur for Mo_{ss} with A15. Additionally there does not appear to be a significant difference in grain size nor porosity, and the raw materials, firing and preparation were similar enough to exclude other impurity differences. Instead it's most likely that the hardness difference is caused by depletion and wholly unrepresentative of the bulk properties. The XRD and SEM of

the A15 sample does indicate some Si depletion has occurred, giving possibly higher Mo phase fraction at the surface where indents were made.

5.4. Conclusions from T2-Silica compositions

The ability to create composites of molybdenum containing SiO_2, Mo_2B and/or T2 has been demonstrated. Further, the ability to control and create microstructures with fine grained continuous Mo for these composites is apparent as shown in Figure 5.35. The composites are able to be sintered to suitably high densities above 90% of theoretical and room for further improvements exists by changing process parameters and by using isostatic pressing. In the future better raw materials, better lubrication and pressing for higher green density, better dispersion of the slurries and hot isostatic pressing will lead to even finer grained, better sintered and better dispersed microstructures which should give improved properties in terms of both strengths and oxidation resistance.

Strengths have been shown for these materials which are higher than others in the literature and ductility at room temperature has been demonstrated for Mo-Mo_2B alloys. These composites show promise in extending the ductility range for oxidation resistant Mo alloys to room temperature without compromising high temperature strengths or oxidation resistance.

Finally, oxidation protection was observed for samples based on these compositions. The formation of the protective coating mimics that of MoSiB and follows the same optimization schemes. Further improvements to processing will focus on removing the cracks and possible preoxidation and could lead to composites with better oxidation resistance than their MoSiB counterparts. Ultimately the effects of fluid silica during processing, which must be the result of B_2O_3 reacted from residual oxygen, limit

the connectivity of the Mo matrix and also convolute and disrupt the self-healing coating near the as-fired surfaces. These remain the most significant issues affecting the usability of these alloys.

CHAPTER 6. ALTERNATIVE SILICATES

6.1. Introduction

The Mo-T2-SiO_2 alloys unfortunately have suffered from issues which arise due to incomplete de-oxidation of the starting powders. When the starting Mo powders are reacted, some O remains, which may be in part due to the processing and also due to the powders themselves, but it appears to be unavoidable that some surface oxygen will be present in the samples. During the firing the oxides are reduced by H_2-Ar atmospheres and the oxygen is ideally driven off. O can severely embrittle Mo, however after reduction-firing very low O contents in the final Mo are measured and ductile bars of pure Mo have been produced. On the other hand, it seems that during the firing and before the reduction can complete, some of the O has reacted with the boron to form boria. The liquid boria fluxes the silica internally and permits it to flow into the regions between the pressed granules. Typical final microstructures are filled with large crescent shaped regions of glass, on the size scale of the spray-dried particles and, as a result, the non-uniform microstructure has easy fracture paths through the brittle glass phase resulting in poor mechanical properties. Furthermore, if the silica is fluxed internally and able to flow, the presence of amorphous silica could create problems with high temperature creep resistance. The same problems are seen whether using silica powders of initially amorphous nature or crystalline as quartz or cristobalite.

It has proven to be impossible at this time to fully de-oxidize or prevent the internal glass flow by avoiding or gettering oxygen. Silicate additions such as mullite may provide a more stable source of silica that will not be fluxed or flowable internally, and may also benefit oxidation resistance by contributing alumina (aluminum oxide,

Al_2O_3) or other glass modifiers. Alumina in the glass could act to increase viscosity and reduce the oxygen permeability. Alumina is added to commercial glass batches to help improve chemical resistance and mechanical strength, and to increase viscosity at lower temperatures. The entrapment of boria by Al_2O_3 and SiO_2 has also been shown to delay boria volatility. [106]

In addition to modifying the glass, more stable silicates could prevent the depletion of silica. In the batches containing SiO_2 there is depletion from the surface of both silica and boron. Since the oxidation begins at the surface, and the depths and severity of the depletion can only be loosely measured, the actual composition of the glass forming is uncertain. It also changes with depth due to competing and unequal depletion of each of the main glass formers. Using a more stable silicate should stop the evaporation of silica in processing and help make the composition of oxidation-formed glass consistent and also more easily known.

Another issue observed with the SiO_2-containing samples is interaction with the nitrides. The Mo-T2-SiO_2 system replaces the reaction-formed A15 with a pre-mixed SiO_2, eliminating the need for most of the Si_3N_4 which is used to form the A15 phase in GTRS processed MoSiB alloys, but some Si_3N_4 is still required to react alongside BN to form the T2 phase. Reactions which are not problematic in traditional MoSiB case have been identified in the Mo-T2-SiO_2 system, most importantly; SiO_2 can react with silicon nitride.

Silica and silicon nitride form an oxynitride at high temperatures when in contact, which is well established in the phase diagrams[107] and a known issue regarding the

interface of SiO_2 on Si_3N_4 ceramics[108]. The oxynitrides in turn react to form volatile SiO in the presence of excess nitrogen by the reaction:

$$Si_2N_2O + SiO_2 \rightarrow 3SiO_{(g)} + N_{2(g)}$$

In our system, the volatilization of SiO leads to increased depletion of the Si and SiO_2 from the sample surfaces during firing.[109]

Additional benefits include reduced grain boundary mobility which beneficially limits both creep and grain growth. Grain boundary mobility can be limited by solute segregation at grain boundaries; however solute impurities cause embrittlement in this system. Instead dispersed inert particles such as the refractory silicates act as Zener pins which would pin the boundaries and limit the grain boundary mobility of the molybdenum. A greater fraction and better dispersion of the pinning phase should have greater effect. This would limit high temperature creep as well as any grain refinement that could potentially reduce strengths by the Hall-Petch assumption. This is similar to the effect of the refractory intermetallics in MoSiB. While silica is nearing its melting point at the use temperatures and has lower strength and reduced creep resistance, more refractory silicate additions may prove advantageous to creep resistance.

6.2. Mullite

The first option pursued for a more stable glass former was mullite. Mullite is a stable alumino-silicate refractory compound which will not contribute any of its elements to the molybdenum. Mullite will limit the grain boundary motion by pinning boundaries which restricts creep and grain growth of the molybdenum. Also, Mullite has a thermal expansion of 5.4 μm/mK which closely matches Mo (4.8 μm/mK) and forms strong, clean interfaces with Mo as in the work by Bartolome and Sivakumar[99, 100] it should also contribute beneficial alumina to the silicate melt.

Mullite can be added directly or reacted during firing from alumina and silica powders. The desired result is a composite consisting of a ductile Si-free Molybdenum matrix phase with finely and evenly dispersed Mo_2B and SiO_2 for self-healing oxidation resistance similar to that of MoSiB alloys, and with finely distributed mullite for high temperature strength and to modify the glass.

There have been a number of studies regarding Mo-mullite composites; however these all focus on using Mo as a secondary phase in a mullite matrix to add toughness to mullite refractories. Our approach is radically different but is based on some similar principles, mostly the closely matched thermal expansions.

6.2.1. Mullite Mechanical Results

The primary goal of using mullite is improving toughness, so in order to evaluate the effects of adding mullite bend test bars were spray dried and pressed of Molybdenum containing 10 and 20vol% Mullite. 4-point bend tests were conducted to look qualitatively for ductility, with possible further 3 or 4 point bend tests to get valid strength and fracture toughness values. As outlined in Chapter 3.6, 0.65 gram bars were

pressed to 2500psi in with 1x .125in bar die. Green densities were improved with addition of the stearic acid. They were fired and tested in an MTI mechanical tester using a 4 point bend apparatus with an outer diameter of 17.65mm and 6mm inner diameter and a rate of 0.3mm/min. The results are plotted in Figure 6.1.

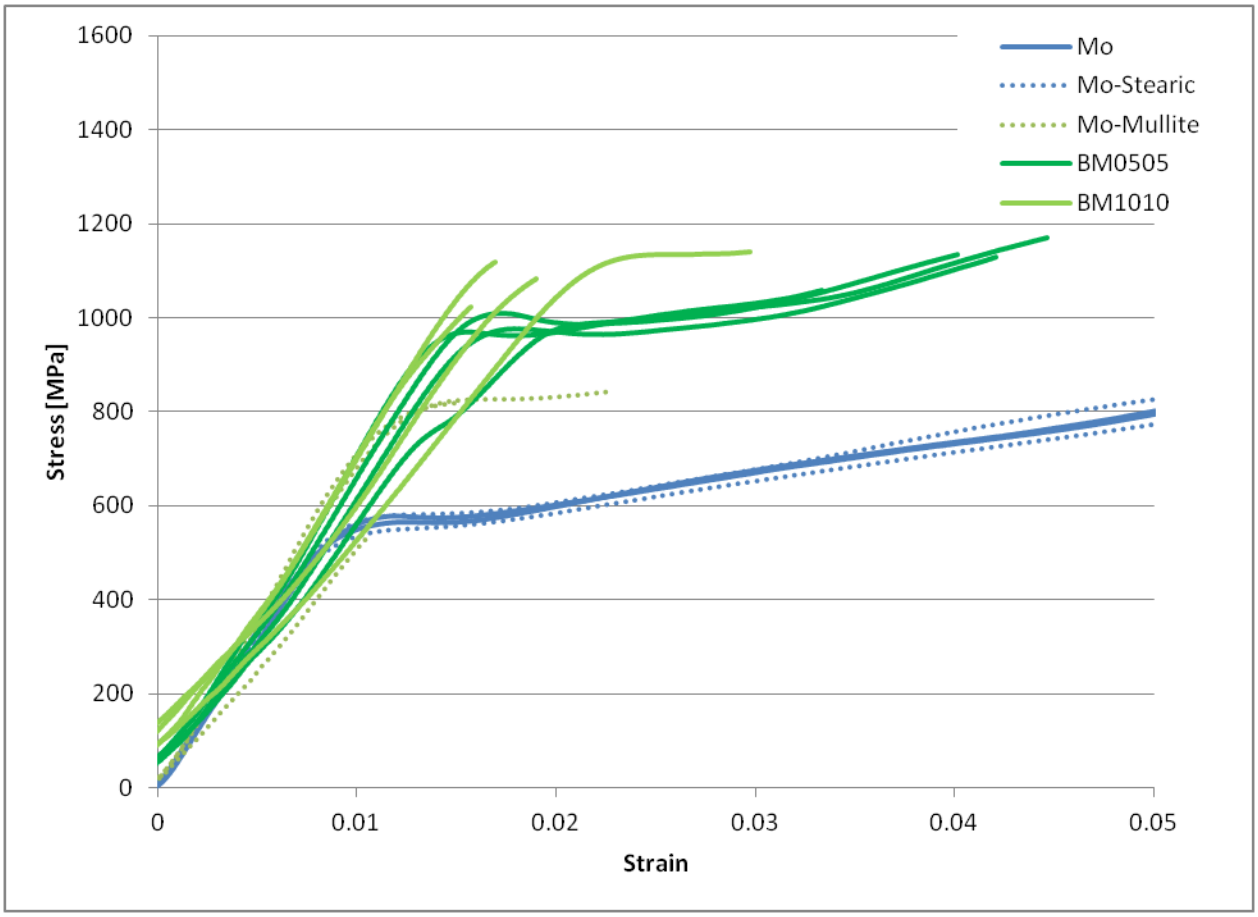

Figure 6.1: Stress strain curves from 4 point bend tests of pure Mo and Mo with mullite and Mo_2B (BM), prepared by the GTRS method.

Mullite increases the ultimate strength which may be due to the lower Mo fraction and in part also due grain size reduction from pinning by the mullite. The mullite acts similarly to oxide toughening and restricts some dislocation motion. While the elongation

is lower than for pure Mo, it is still measurable and yielding is observed which shows that ductile composites can be achieved with a Mo matrix containing silicates such as mullite.

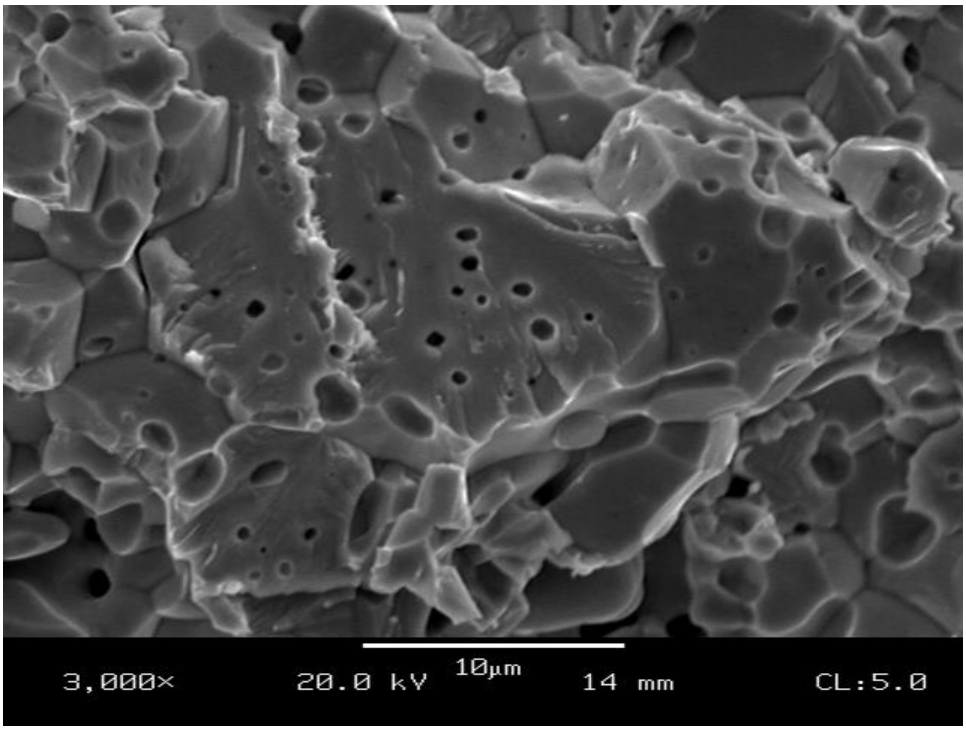

Figure 6.2: Fracture surface of Mo with 10% Mo_2B and 10v% mullite showing some transgranular ductile cleavage.

Samples containing a mixture of Mo boride and mullite were also prepared for bend testing. The results are also shown in Figure 6.1. Room temperature yielding and limited ductility were seen in all of the samples which contain up to 20 v% brittle phases. Examination of the fracture surfaces (Figure 6.2) showed mixed mode fracture and indications of ductile transgranular failure. Usable strength and yielding are possible for samples with alternate silicates in conjunction with boria forming Mo_2B intermetallics to room temperature and below, whereas embrittlement of Mo by A15 limits MoSiB to purely brittle behavior until over 800°C. The final microstructure is also consistent

throughout, all the way to the edges, and the mullite does not appear to be volatilizing. No depletion or crescent lenses are seen.

6.2.2. Mo-Mullite Oxidation

As a matter of course, a boride and mullite containing Mo sample, BM1010-1 #1 (10v% mullite, 10v% Mo_2B) was prepared and oxidized at 1300°C in static air in the Keith furnace. The pellet lost 341mg/cm^2 in 10 minutes, roughly the same rate pure Mo, minus the 10v% mullite that is not evaporating. Not surprisingly it was nonprotective and within 2 hours only white powder remained. The powder was loose, non glassy and unsintered and no Mo metal remained.

Unfortunately mullite doesn't flux well to form a glass with boria. Work by Griesser[110] indicates that you can get up to 20mol% Boria incorporation into mullite without phase transformation. After that, additional B_2O_3 begins to form aluminum borates, but not any glass.

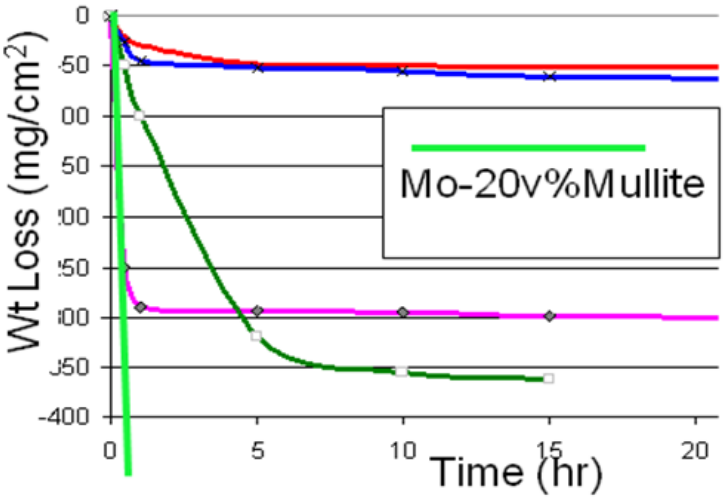

Figure 6.3: Oxidation behavior of mullite samples.

6.3. Alkaline Earth Aluminosilicates

6.3.1. Justification for Aluminosilicate Additions

Because of the inability to form a stable glass with mullite, further alternative silica sources were pursued. Any alternative silicate must satisfy the requirements of:

- high T_m to remain solid to 1300°C and above
- ability to react/flux to a fluid glass with B_2O_3 at 1000°C or below
- no devitrification
- minimal volatilization
- closely matched thermal expansion
- chemically stable and not contribute Si nor otherwise embrittle the Mo

Other possible Silicates include those of MgO, Cr-, K-, Na-, Sr-, Ba-, or Ca-oxides. The alkaline earths have good high temperature stable silicates with high melting temperatures. For the refractory silicate phase, the alkaline earth 1:1:2 aluminosilicates ($RO\text{-}Al_2O_3\text{-}(SiO_2)_2$) of Ca, Ba, and Sr were selected. These are sufficiently refractory, with melting temperatures near 1600°C and stable single-phase regions over wide composition ranges. They are also compatible with the powder processing used and thermodynamically stable with boron nitride and molybdenum boride, so as not to form boria during sintering. The alkaline earth oxides are commonly used glass-modifiers and, with the lower alumina to silica ratio, this system is not expected to form aluminoborates upon mixing with boria. Additionally the Ba and Sr aluminosilicates have found use in environmental barrier coatings of SiC-SiC composites. [111-113] Specifically, the

monoclinic Sr 1:1:2 aluminosilicate (henceforth referred to as SAS) was selected due to its higher melting point than the Ca analog and lower toxicity than Ba. It remains monoclinic without phase transformation, doesn't' melt until 1650°C and forms a low viscosity glass with B_2O_3.

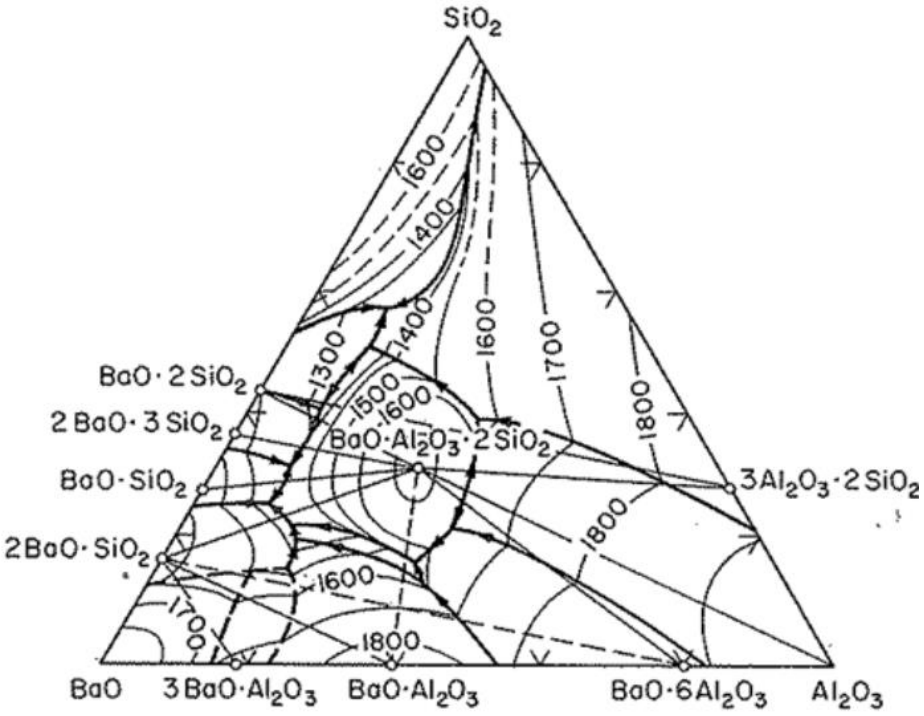

Figure 6.4: Representative Alkaline Earth oxide BaO ternary phase diagram with SiO_2 and Al_2O_3.[107]

Spodumene is another possible alternate silicate. The lithium aluminosilicate is another feldspar mineral which is also monoclinic and on a molar basis consists of 1 mole Li_2O, 1 mole Al_2O_3 and between 2 and 6 moles of SiO_2. The 1-1-4 Li_2O-Al_2O_3-SiO_2 is henceforth referred to as 4Spod and the 1-1-6 as 6Spod. Spodumene has a minor transition to tetragonal system at 900°C and has a glassy softening point at 1421°C for the 4Spod ($LiAlSi_2O_6$) and is assumed to be similar for the 6Spod. It forms a low

viscosity glass with B_2O_3 but is solid at 1300°C by itself. The Li spodumene may have advantages over the SAS because it contains a higher fraction of SiO_2 compared to the other oxides, even more so for the 6Spod.[114] A final option was Sr metasilicate ($SrSiO_3$) referred to here as "Sms" which also has higher Si content and additionally avoids Al.

6.4. Alternate Silicate Results

6.4.1. Pre-reacting Alternate Silicates

A powdered strontium aluminosilicate was prepared by spray-drying and firing the precursor SrO, Al_2O_3 and SiO_2. XRD verified presence of the target Sr-feldspar compound, $SrAl_2Si_2O_8$, a monoclinic 1-1-2 celsian-type Strontium aluminosilicate (SAS) a.k.a. slawsonite (Figure 6.5). XRD indicated after firing to 1500°C either slawsonite (00-038-1454) or the feldspar analog (04-011-6763). They're not exactly the same phase, but both are monoclinic 1Sr-1Al-2Si strontium aluminosilicates stable at ambient T & P and thus are indistinguishable by XRD, and functionally the differences are negligible.

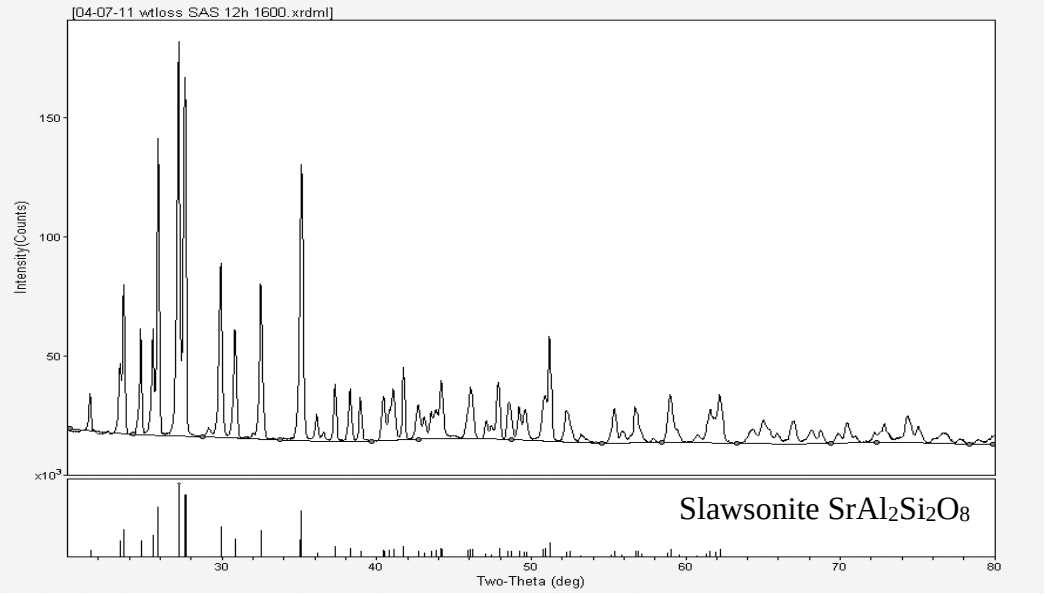

Figure 6.5: XRD profile of SAS powder after reacting confirming presence of pure slawsonite (the monoclinic 112 SAS Sr-celsian.)

Before preparing any composite batches with Mo, powders of boron oxide and SAS, and boria and 6Spod were prepared and fired to 1200°C to verify that they would form a glass, and both did. Next the 6Spod and SAS were mixed as powders and fired for 3 hours at 1300 °C to see if either or the combination of both were forming glasses on their own, without the presence of boria, at that temperature.

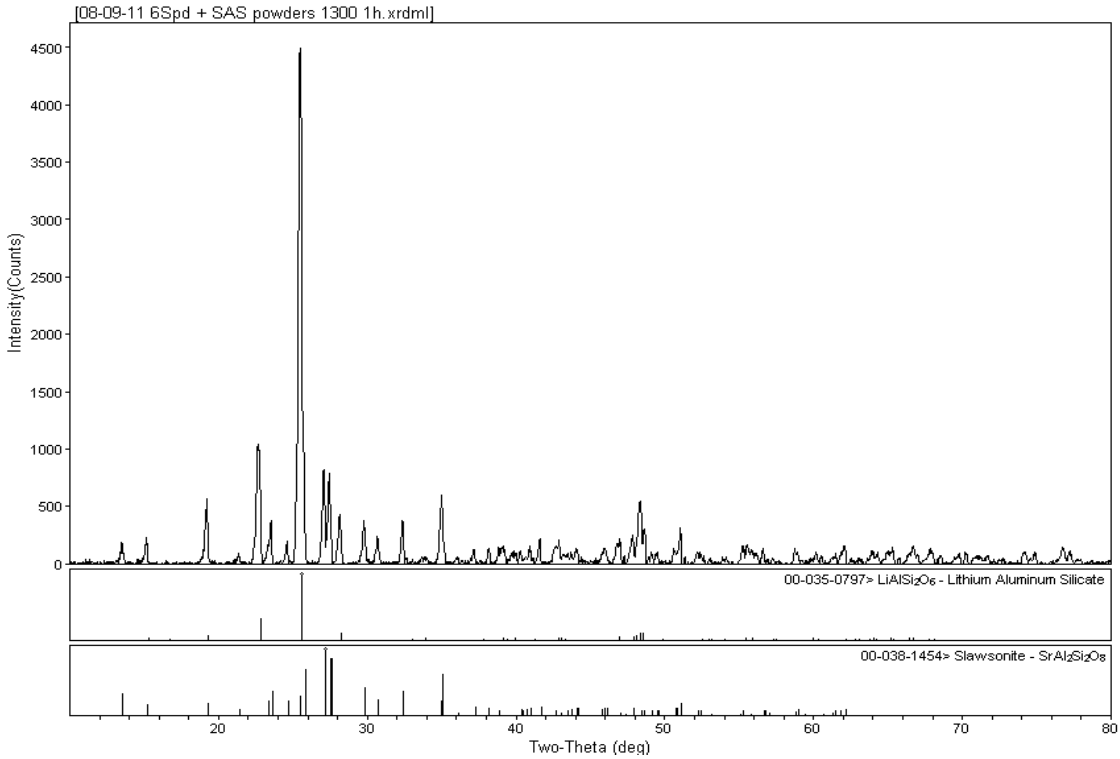

Figure 6.6: XRD scan of 6Spod and SAS powders fired to 1300°C in air without B.

The XRD scan of the fired 6Spod and SAS powders is shown in Figure 6.6. Every peak could be identified as either the Spodumene or SAS, with no glass phase observed. The powder remained an easily friable white powder after firing identical to its

appearance before firing and it was confirmed that these are stable solids at the use temperatures unless fluxed by boria. No significant weight changes were observed.

6.4.2. Firing

Table 6.1: Sr and Li aluminosilicate containing compositions tested

	Final Volume Fraction								
Batch	Mo	Mo2B	Mullite	Silica	SAS	T2	6Spod	Sms	Nd apatite
BSr0505	90	5	0	0	5	0	0	0	0
BSr2020	60	20	0	0	20	0	0	0	0
BSr0515	80	5	0	0	15	0	0	0	0
BSms0510	85	5	0	0	0	0	0	10	0
B6Spd0510	85	5	0	0	0	0	10	0	0
BSr6Spd090918	64	9	0	0	9	0	18	0	0
BSr6Spd091809	64	9	0	0	18	0	9	0	0
BSr6Spd4.51020	65.5	4.5	0	0	10	0	20	0	0
BNd0510	85	5	0	0	0	0	0	0	10
BSrNd151812	55	15	0	0	18	0	0	0	12
TSr1531	54	0	0	0	31	15	0	0	0
TSr2027	53	0	0	0	27	20	0	0	0
TSr2720	53	0	0	0	20	27	0	0	0
TSr2323	54	0	0	0	23	23	0	0	0
TSr2323+Nd	51.5	0	0	0	23	23	0	0	2.5
TSr2720+2.5Nd	50.5	0	0	0	20	27	0	0	2.5
TSr2720+0.5Nd	52.5	0	0	0	20	27	0	0	0.5

Table 6.1 shows most of the batch names and final volume fractions of compositions examined in the alternate silicate system. “Sr” and “SAS” are used interchangeably to refer to the 1-1-2 Sr-celsian, “Nd” refers to addition of Neodymium apatite ($Nd_{9.33}(SiO_4)_6O_2$) discussed at the end of the chapter, and “_Spd” refers to the lithium spodumene. Two compositions were investigated first from the system containing Mo, Mo_2B and SAS; one containing 5 volume percent each of the boride and Sr aluminosilicate (BSr0505 a.k.a. BSAS0505) and another containing 20 volume percent of each (BSAS2020); with the remainder being molybdenum.

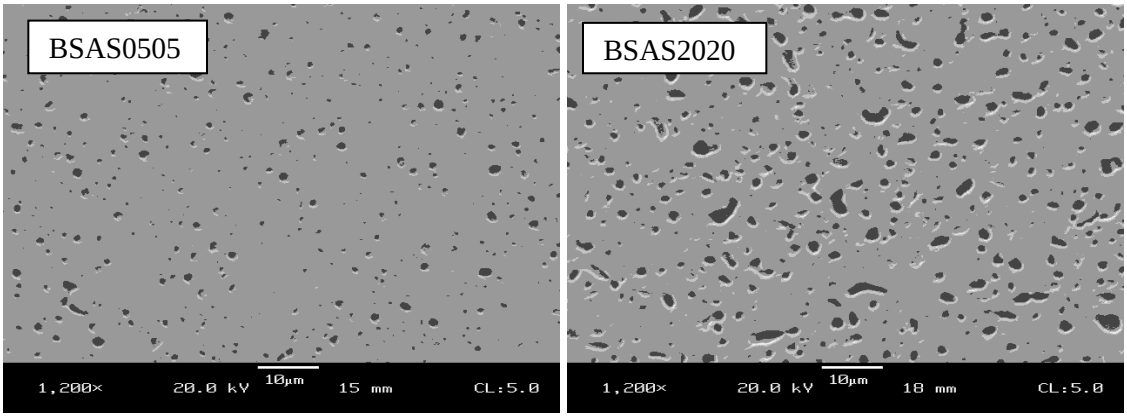

Figure 6.7: As-fired microstructures of Mo with 5v% each Mo2B and SAS (left) and 20v% each of Mo2B and SAS (right).

The samples both fired to over 95% dense. Figure 6.7 shows the as-fired microstructure of the 5-5 and 20-20 v% Mo_2B and SAS samples. In addition to the fine, homogeneous, and mostly isolated distribution of the SAS particles, these samples were near fully dense (>99% theoretical) with no measurable open porosity indicating good compatibility with the process employed. The crescent shaped regions are not observed in either case.

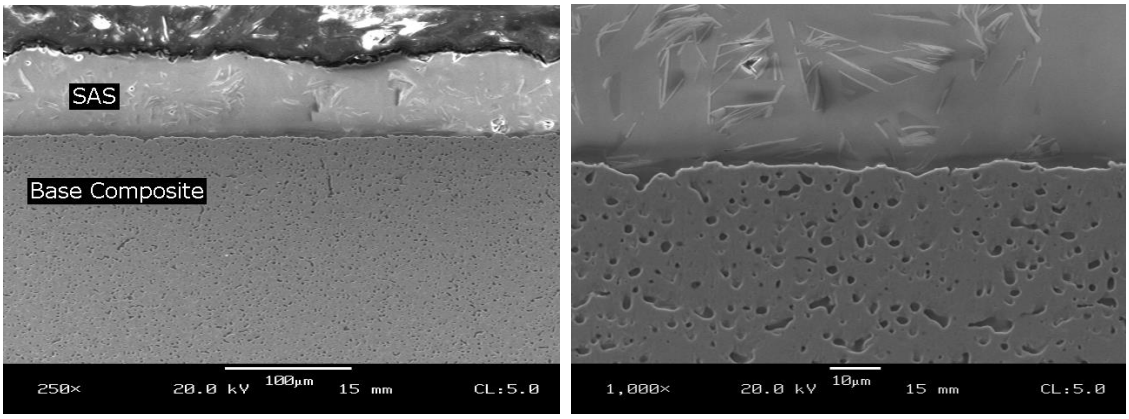

Figure 6.8: SAS coating formed during sintering for Mo with 20v% each of Mo_2B and SAS. The interface is shown in more detail on the right.

After firing, samples of the 20-20 v% Mo_2B and SAS composition were observed to have formed a coating during firing, Figure 6.8. The coating was identified by XRD as being crystalline monoclinic SAS. On two of the four samples this was observed to form a nearly complete coating while on the other two the coating was wicked away to the side of the alumina boats. The flow of the SAS to the surface indicates fluidity in the firing, these samples were fired to 1600°C and the melting point is uncertain but had been reported to occur between 1500 and 1600°C. The presence of an even coating implies a good wetting.

An expelled coating forming during firing was something we'd seen before with the glass frit compositions. We also notice much better sintering perhaps due to this, maybe caused by liquid phase. Liquid in firing may enhance sintering through faster diffusion, at the same time improved sintering may expel the liquid.

In order to address the issue of expelled SAS pooling on the surface after densification, three alternate firing schedules were attempted; one with a 10h hold at 1500°C, one with a 6h hold at 1600°C and finally 6h hold at 750 and 1600°C . All had a ramp rate of 3°C /min in flowing Ar/10%H_2. The fired samples were very different, but the one which reached only 1500°C showed very few crystals on the surface, unlike the others which have a nearly complete covering of SAS. This is consistent with the reported melting point of SAS being somewhere between 1500 and 1600°C.

6.4.3. Alternate Silicates Mechanical Results

As-fired bars were tested under four point bending at room temperature to investigate the fracture behavior and plasticity, if any. The 20-20 v% Mo_2B and SAS composition showed no ductility at room temperature, similar to the amorphous silica

containing and the Mo-Si-B compositions. The 5-5 vol% Mo_2B and SAS did show a yield point and failed at a strain higher than the equivalent Mo_2B and mullite composition. Figure 6.9 shows characteristic stress strain behavior of samples which showed a room temperature yield point.

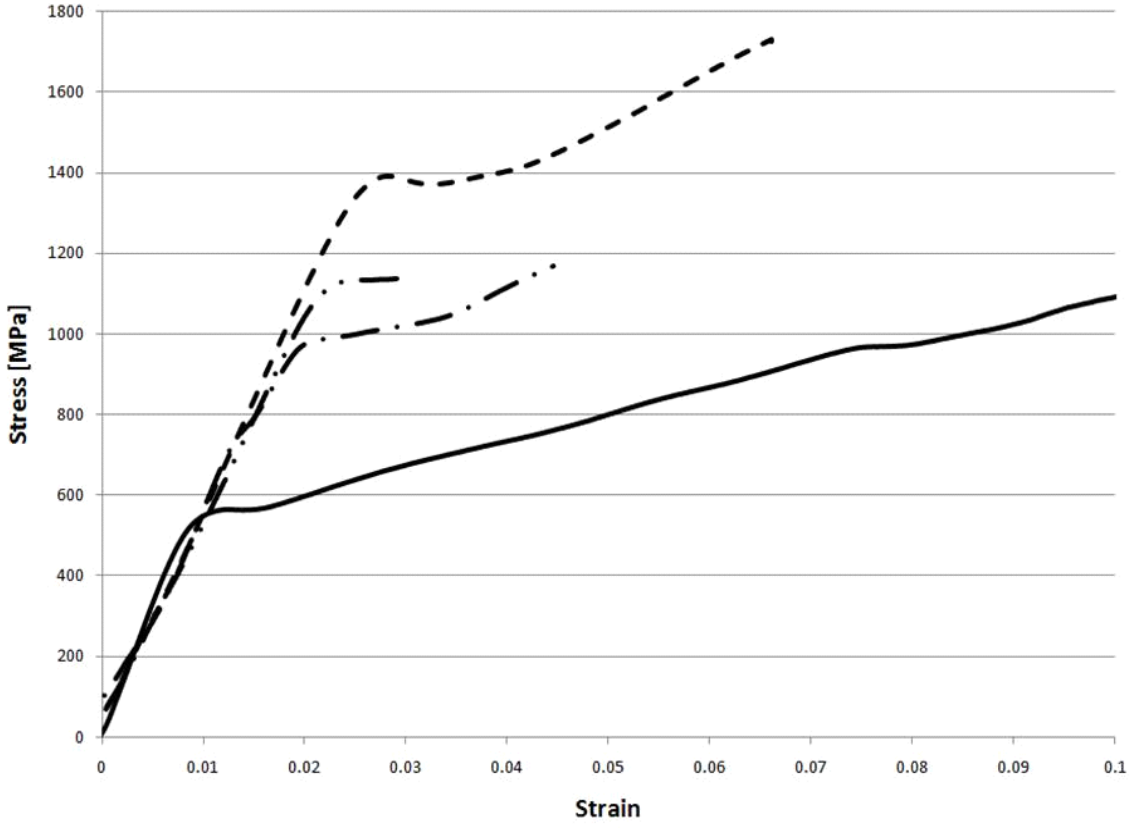

Figure 6.9: Outer tensile fiber stress strain during four point bend testing at room temperature. Solid line: pure molybdenum, dot-dash: 5 v% Mo_2B and 5v% mullite, dot-dot-dash: 10v% Mo_2B and 10v% mullite, and dash: 5v% Mo_2B and 5v% SAS.

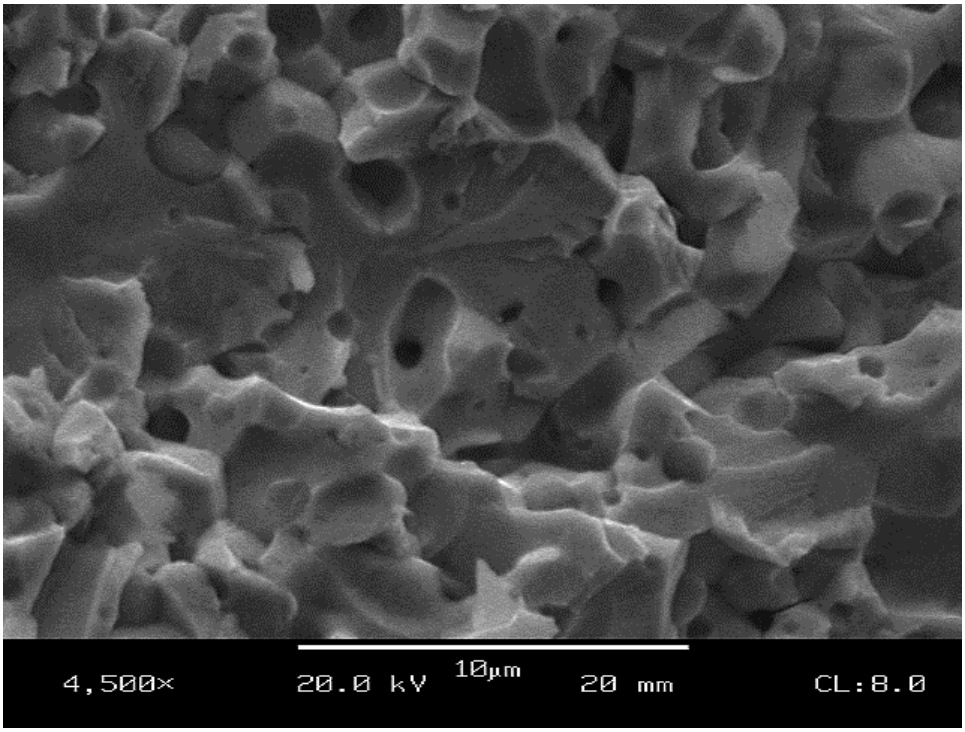

Figure 6.10: BSAS2020 Fracture surface.

The fracture surfaces for 5-5 and 20-20 vol% Mo_2B and SAS show mixed transgranular and intergranular fracture, Figure 6.10. The brittle samples all exhibit completely intergranular fracture. The mechanical behavior of primary interest here is the room temperature fracture toughness which goes hand in hand with the presence of plasticity. In molybdenum, brittle failure is typically intergranular, and plasticity is dominated by the relative magnitudes of the critical resolved shear stress versus the grain boundary fracture stress. Due to Si solid solution and segregation in Mo-Si-B and to silica locating in crescents and along boundaries in the amorphous silica composites, the grain boundary fracture stress is reduced and the critical resolved shear stress may be increased such that at room temperature the grain boundaries fracture prior to observable plasticity. Composites of SAS, Mo_2B, and mullite have shown yielding, implying that the

grain boundary strength remains high enough for slip to occur and thus these systems can be expected to have significantly higher fracture toughness. The presence of some transgranular cleavage also indicates relatively high interfacial strengths.

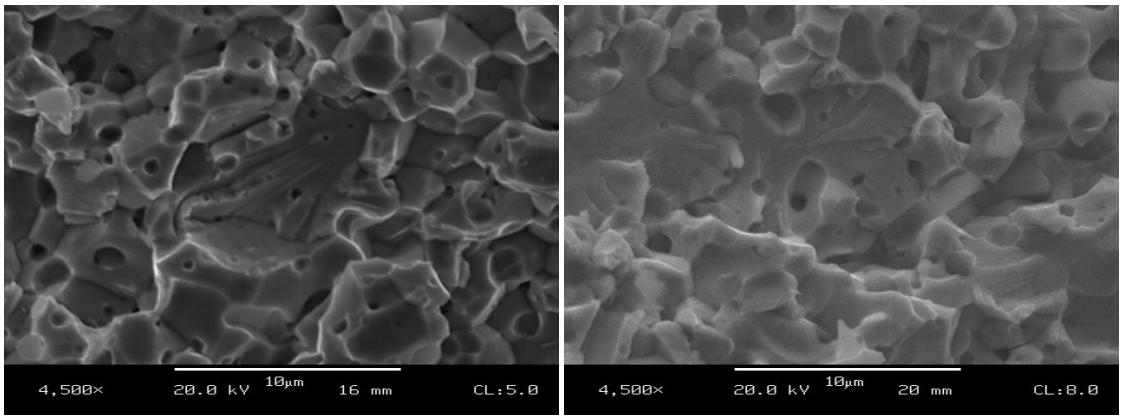

Figure 6.11: Fracture surfaces of 5-5v% Mo2B-SAS (left) and 20-20v% Mo2B-SAS (right) centered on regions of transgranular fracture.

6.4.4. Alternate Silicate Oxidation Results

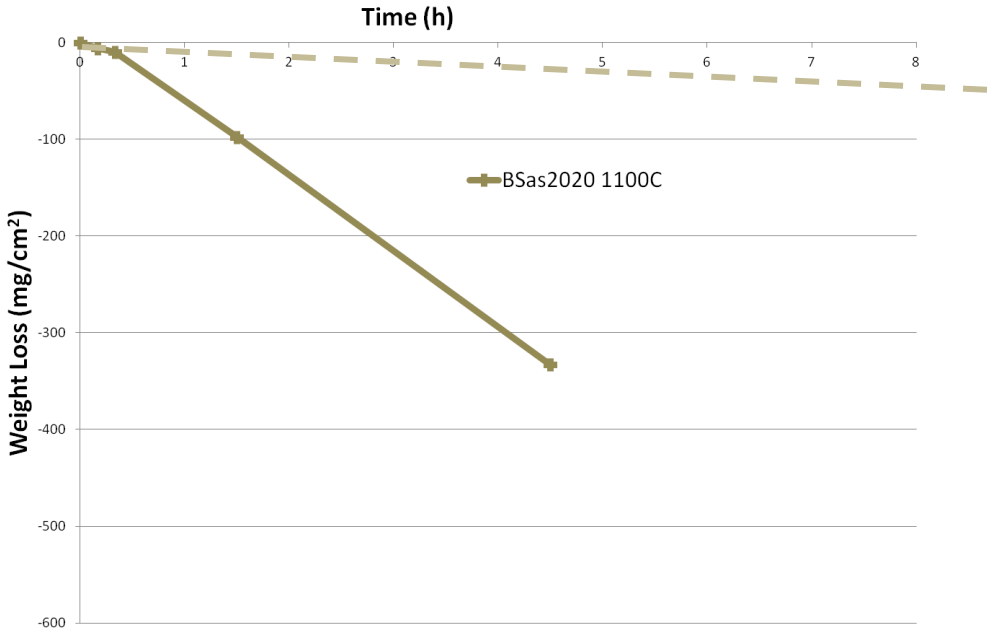

Figure 6.12: Weight loss of BSAS2020 oxidized in air at 1100°C. Weight loss rate for the first coating plotted as dashed line.

The 20-20 v% Mo_2B and SAS samples were subjected to oxidation tests in air at 1100°C for periods of 10, 30, 90 and 360 minutes. The 10 and 30 minute samples were those which had already nearly complete coatings resulting from initial firing, while the 90 and 360 minute samples did not. The results are plotted in Figure 6.12. The 10 and 30 minute samples exhibited very low degrees of oxidation, their rate plotted as a dashed line indicates the loss rate predicted if all of the samples had the initial coating present. It was seen in some places that the initial coating was incomplete, and under these locations where the initial coating was compromised, some oxidation had occurred but a new coating appeared to be forming. For the 90 minute sample, no coating existed from firing, but in oxidation a coating had formed above on the exposed Mo surface. The coating was identified by XRD to consist of a glassy phase with some crystalline $Sr(MoO_4)$. As the oxidation proceeded the exposed silicates were forming a fluid glass which was coating most of the surface but the glass seems to have been wicked toward the areas where some initial coating had existed and left behind areas of unprotected material. After 360 minutes further oxidation had occurred in much the same manner. Large hemispheric pits existed with a glassy coating that grew thinner towards the trough of the pits and allowed oxidation to continue at the base of these pits. It was clear that the coating was not passivating. Lower boron content for a higher viscosity glass should be beneficial to prevent excessive flow that seemed to be allowing the very fluid glass to roll around on the surface without a good wetted coating.

Of the pellets #2 and #3 which had the pre-existing coating formed during firing exhibited very low weight losses, shown as the dashed trendline in Figure 6.12. However any places where the as-fired coating was compromised lead to holes which were

expelling MoO_3. SEM Images of the microstructure and coating before and after oxidation are shown in Figure 6.8 vs. Figure 6.13 and generally good cohesion between the bulk and coating was seen.

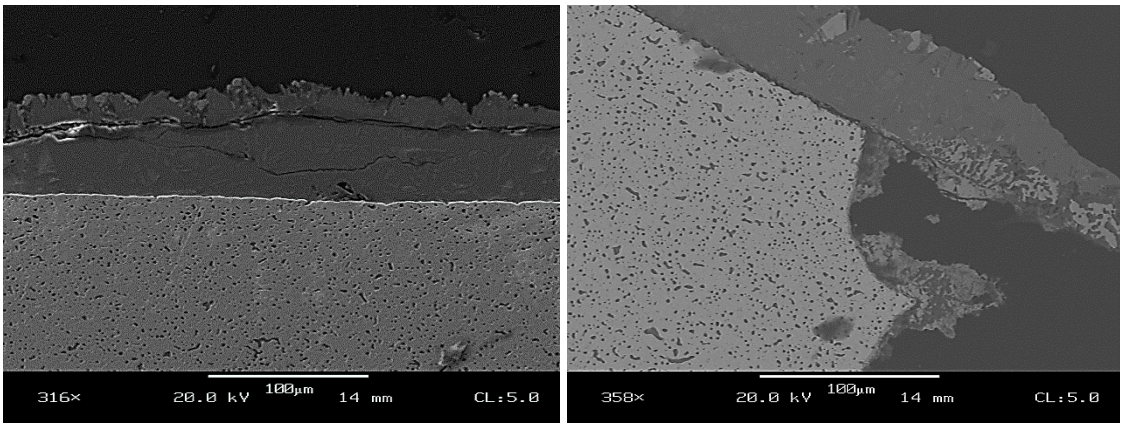

Figure 6.13: BS 2020 cross section after 10m at 1100°C oxidation in air, right close-up at corner.

While the pre-existing coating was effective at preventing oxidation, any places it was compromised lead to failure. The Figure 6.13 images of BSas2020 oxidized at 1100°C in air show definite alternate phases already occurring after 10 minutes and also some debonding/reaction from the interface in places like the corners (right). The attack of the underlying material does not form a protective coating. From the EDS and XRD scans it's apparent that the Mo and oxygen are reacting with the existing SAS at the surface to form a phase-separated $SrMoO_4$.

The other two pellets, # 4 and 5 didn't have a coating to start and represent a very different data set. The data in the chart are difficult to interpret because of the different mechanisms between pellets 2 & 3 and pellets 4 & 5, as the latter two were forming their own coating in-situ.

XRD scans of the oxidized surfaces of the pellets were taken and the plot is shown in Figure 6.14. The pellets which had the initial coating of SAS were observed to maintain the SAS coating, and could be seen both microscopically and in the X-ray data. However the presence of $SrMoO_4$ strontium molybdate was also identifiable as early as 10 minutes exposure in air at 1100°C. Molybdenum in binary oxide is already reduced to metal at about $-\log PO_2 \sim = 11.5$, the hexavalent molybdenum is strongly stabilized in the sheelite-type oxides, such as $SrMoO_4$, under a very low oxygen partial pressure ($<-\log PO_2 = 13$).[115]

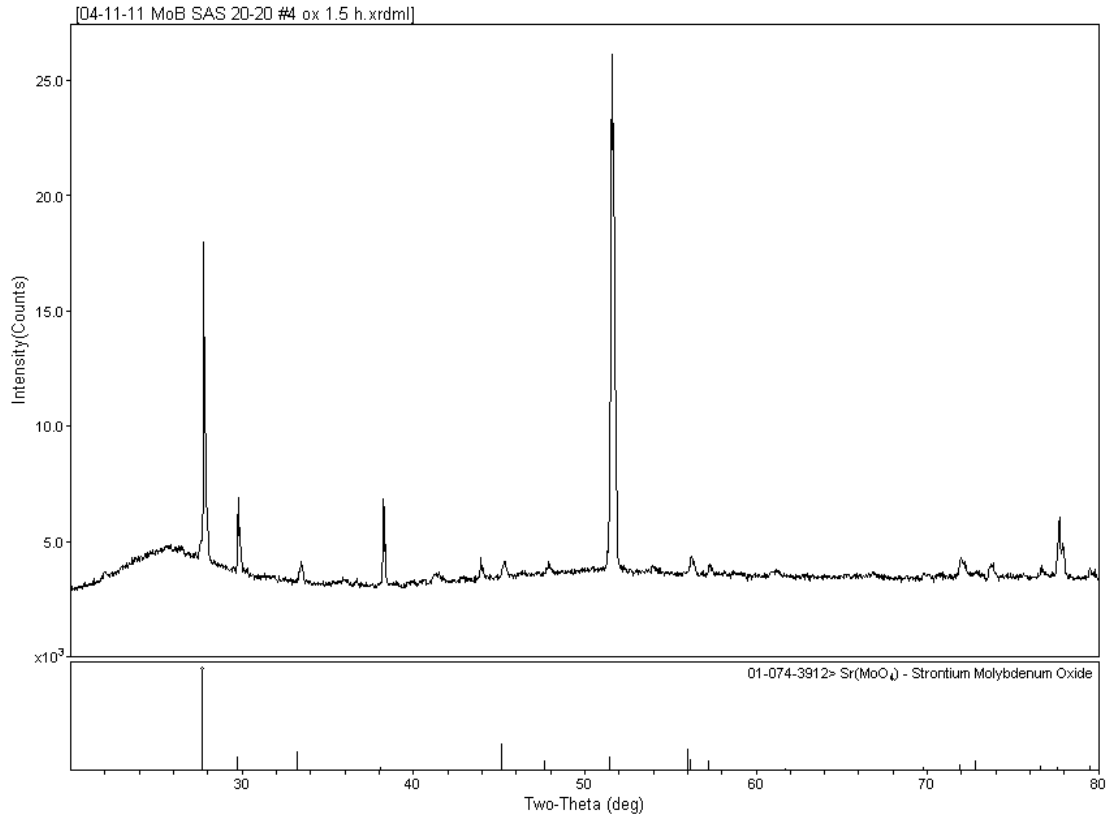

Figure 6.14: XRD scan of the surface of BSAS2020 #4 after 90m oxidation at 1100°C.

The images show what appears to be a step-wise failure of the material when exposed to air. The exposed material reacts to form a glass from B_2O_3 and SAS and coats the surface as expected, however before it completely passivates $SrMoO_4$ crystallizes within the glass and prevents it from flowing further. The few unprotected spots lead to more oxidation below while it's too rigid to collapse and re-seal. This results in a nonprotective series of broken layers as seen in the micrographs.

The sample #3 exposed for 90 minutes in 1100°C air was similar and images are presented in Figure 6.15. The pre-existing BSAS coating maintained complete protection except in areas where the coating was originally compromised, such as the corners.

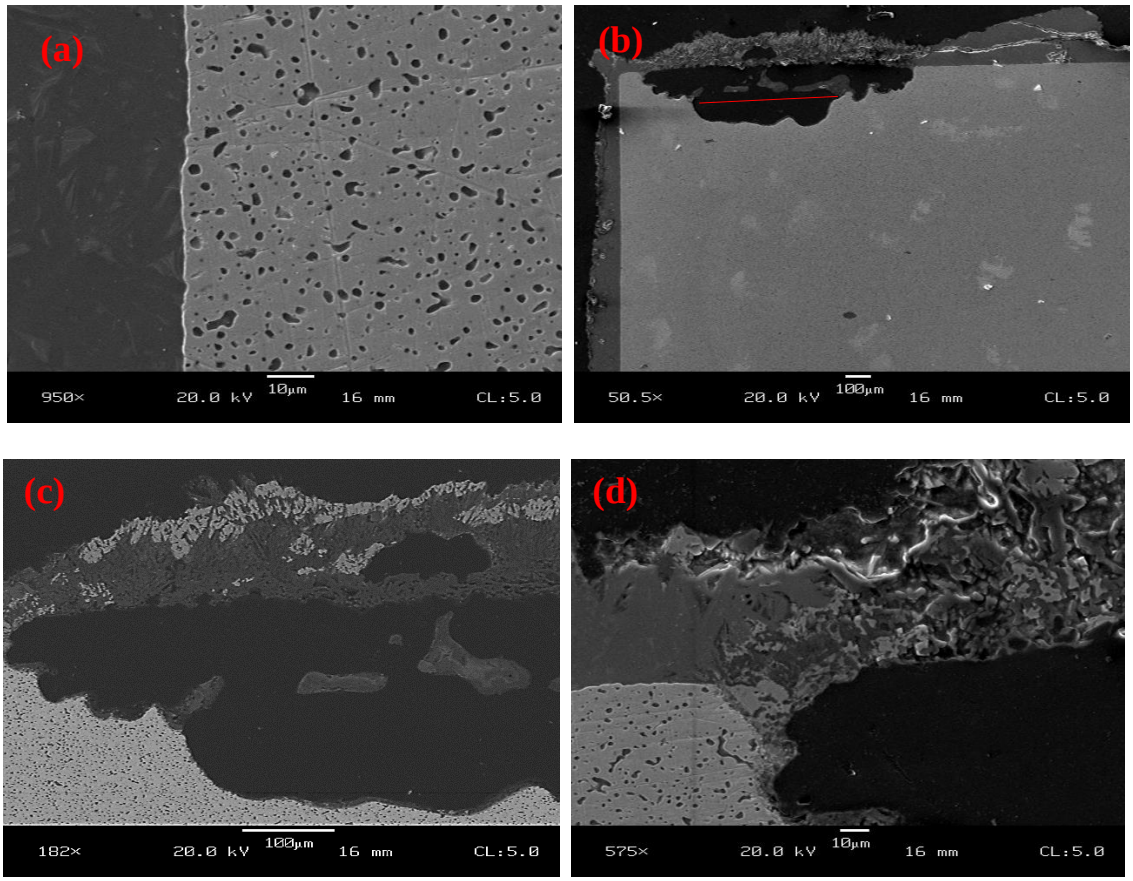

Figure 6.15: SAS Coating after oxidation for 90m at 1100°C. (a) showing good edge coating, (b), (c), and (d) detail of failed section near corner.

Again in Figure 6.15 we see a layered effect of the remaining coating that had formed over the eroded substrate. The red line in (b) shows a coating which had formed, then subsequently crystallized and eroded away, and the detail of that layer is shown in (c). In the image (d) the phase separation can be clearly seen. Backscatter electron imaging again shows the location of the $SrMoO_4$ forming over the eroded areas and separating and crystallizing at the surface.

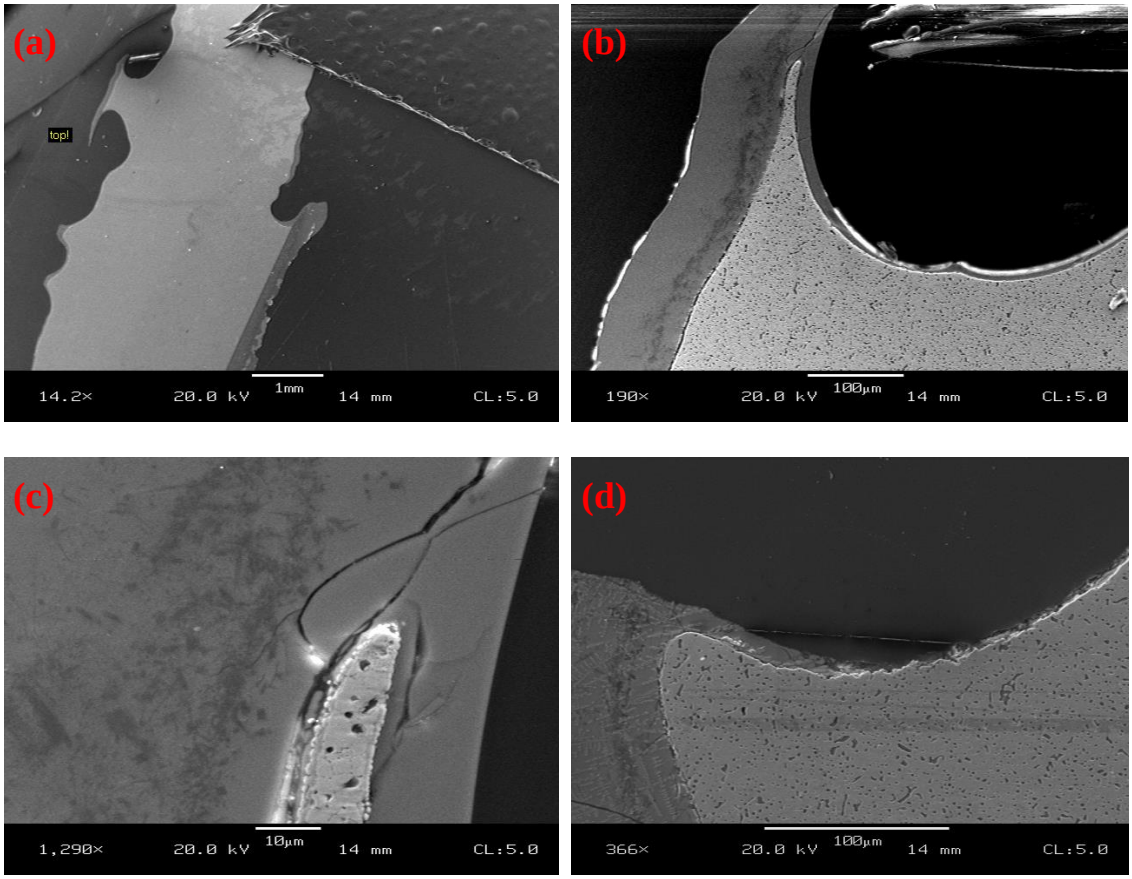

Figure 6.16: BSAS2020 Oxidized 6h in air at 1300°C.

Figure 6.16 shows the BSAS2020 sample after oxidation for 6h at 1300°C. Optically the surface consisted of a series of cloudy peaks and large (~0.5-1mm) wells with exposed Mo at the bottoms. The cloudiness indicates crystallization and solidification. Fine, tooth-like MoO_2 is seen in the cross section under the outer surface showing that in these places oxygen transport is limited enough to lower the pO_2 and promote formation of the lower molybdenum oxide. There is a large degree of phase separation, especially in the thickest sections of coating on the bottom of the sample. The glass is quite fluid and flowing by gravity to the bottom implying, at least initially, a low viscosity, however the persistence of overhanging lips of coating suggest it's solidifying due to $SrMoO_4$ crystallization. Crystallization is obvious in the images, and also there are sections where the coating thins out or is not coating such as in the (d) image, the thinned out sections may be due partly to crystallization and/or reduced wetting.

It's been reported that glasses containing MoO_3 opacify and form precipitates with alkaline earths (e.g. Sr).[51] It's also worth considering that MoO_3 significantly reduces surface tension and can be used as a wetting agent in glazes even at small amounts. The formation of molybdates with the alkaline earths could remove MoO_3 from the glass and may be partially responsible for the poor wetting.

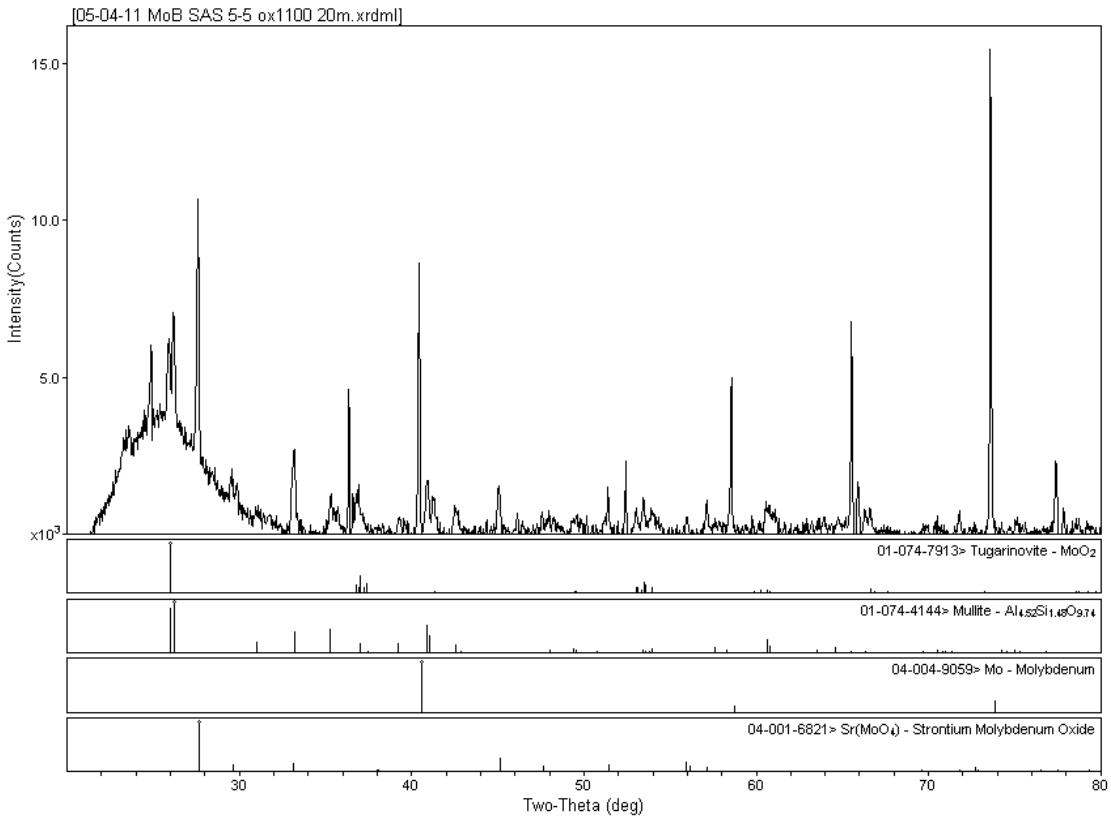

Figure 6.17: XRD Pattern of the oxidized surface of BSAS2020 after 20m oxidation in air at 1100°C

The XRD pattern in Figure 6.17 shows the oxidation products after 20m oxidation at 1100°C and has been treated and the background removed. A pronounced amorphous hump around 20-30° 2θ indicates significant glass fraction. The crystalline phases are split between the Sr molybdates from reaction and some Mo and MoO_2, which may be exposed or seen through the glass which is thin and has low x-ray absorption. The presence of mullite indicates a shift towards excess Al and Si ratios, perhaps due to the Sr leaving SAS and forming molybdates.

Additional compositions including T2 and SAS in varying ratios were also oxidized and in all cases performed very poorly. The samples suffered from apparently

poor wetting and significant crystallization, leading to hardened crystalline cage around outside of evaporated pellet. TSAS 1531, 2027, 2720 were oxidized all for 12h at 1300°C. After 90m, in all cases the glass had begun to form but was pooling up and not wetting well, and thicker sections became hazy. The flow was poorest for the higher SAS fractions. After 12h, in all cases the glass had crystallized to a mix of $SrMoO_4$ and cristobalite, which remained as an empty shell with most or all of the molybdenum eroded away. Figure 6.18 shows this effect for the pellets of TSAS2720 at 90m and 12h.

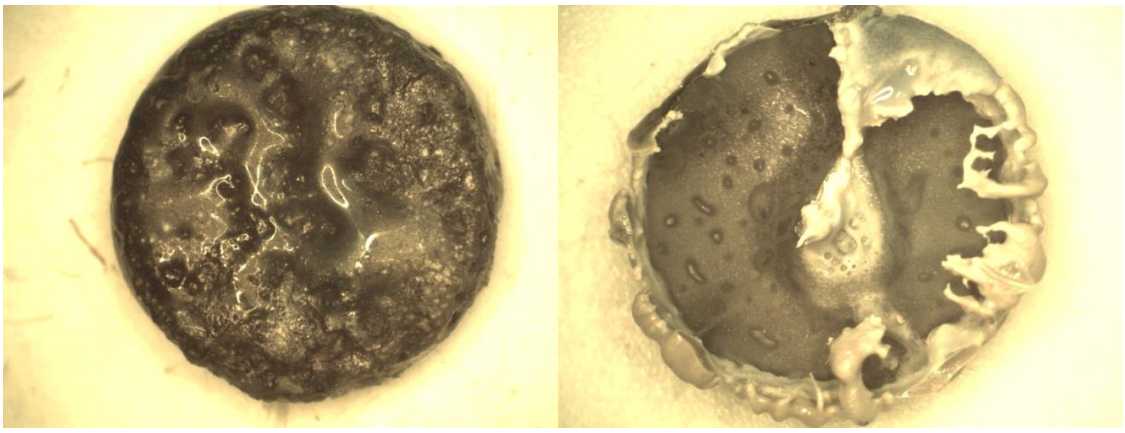

Figure 6.18: TSAS2720 pellet oxidized at 1300C at 90m (left) and 12h (right.)

6.4.5. Spodumene Oxidation Results

When using SAS as a silica source, the Si to Al ratio is fixed by the SAS stoichiometry, yet the poor wetting and crystallization problems may imply a higher Si fraction could greatly improve oxidation resistance, In order to address these issues, the next set of samples included both the SAS and spodumene in hopes of increasing the silica fraction. The spodumene has a higher ratio of silica to alkaline earth and alumina. These consisted of varying ratios of SAS to spodumene to Mo_2B and investigated the

differences. The compositions tested were BSAS6Spod 090918, BSAS6Spod091809, BSAS6Spod4.51020 which are named with the same convention as before, for example BSAS6Spod4.51020 has 4.5 vol% Mo_2B, 10 vol% SAS and 20vol% of the 6-Si Spodumene.

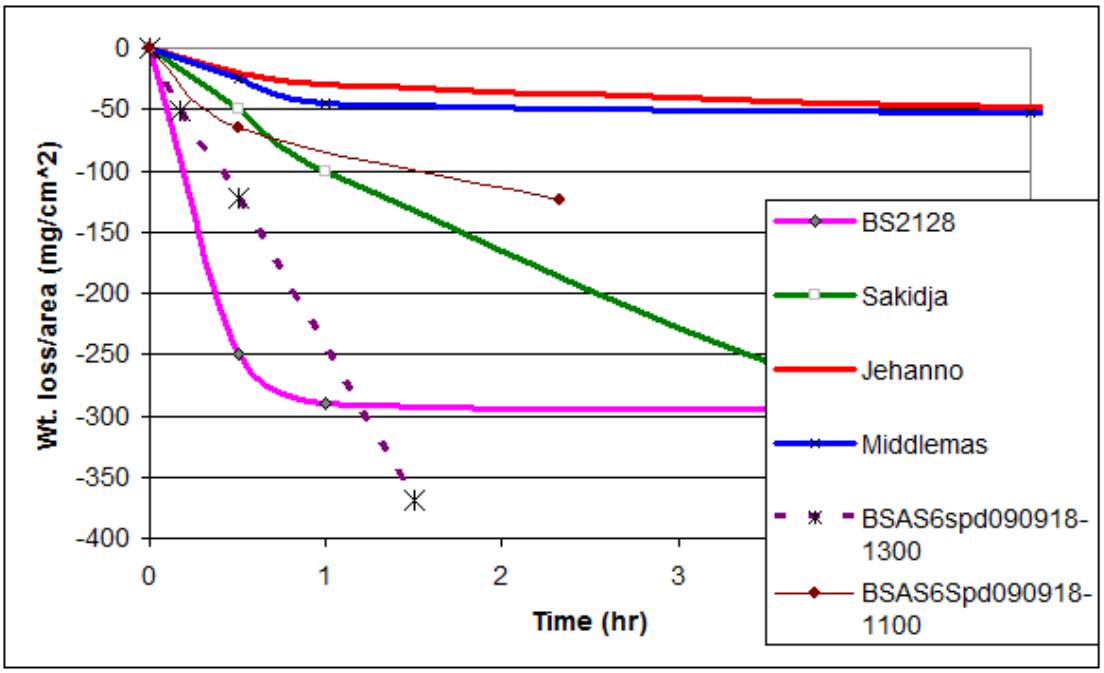

Figure 6.19: BSAS6Spd compositions' oxidation results at 1100°C and 1300°C in air.

The oxidation results are shown in Figure 6.19. The weight loss remained rapid and linear. It was slightly improved with a slower rate than for other poor compositions but it never leveled off to usably low parabolic loss rates.

After 10 minutes at both 1100°C and 1300°C, XRD of the BSAS6Spd 091809 with highest SAS fraction had the largest amorphous hump indicating a higher fraction of glass, as well as peaks from $SrMoO_4$, Mo and MoO_3. After 20h only crystalline phases remained. The BSAS6Spd 4.51020 had the lowest B and highest Li silicate content. After

30m oxidation XRD showed a combination of glass, lithium molybdate, MoO_3 and small peaks which could be identified as possibly mullite and Sr-molybdate. After 20h however, there were again only crystalline phases; identified as the 1:1 aluminosilicate Sillimanite (Al_2SiO_5) and some $SrMoO_4$. The BSAS6Spd 090918 had the highest spodumene contents and XRD of the oxidized surfaces showed amorphous humps from the glass, as well as peaks for $SrMoO_4$ and $LiAlSi_3O_8$ which is a crystalline aluminosilicate with higher Si than the 6spod. This is likely formed by the shifting glass compositions as Sr from SAS is incorporated into the molybdate.

All three cases appeared to have issues of initially too low viscosity and were likely excessively fluxed by the presence of Li and Sr. It builds up in pools rather than flowing over the whole surface, The surface morphology and XRD data suggest that between 1h and 20h the fluid glass then transitions to an almost fully crystalline coating made up of Sr and Li molybdates, and the coating is unable to flow or provide adequate protection. They have slower oxidation rates than without a coating, but still much too rapid to be usable.

6.4.6. Neodymium Additions to SAS

We have seen that Alkaline earth aluminosilicates show promise; the mechanical properties are improved versus pure SiO_2, while presence of the alkaline earth silicates can form a fluid liquid phase unlike like in the mullite case. The aluminosilicates with the presence of a flux can create flowing glassy coatings on the surface to prevent oxidation. Further, Mo and Mo-Borides have been shown to have both high strength and measurable ductility when combined with Sr-Celsian (SAS).

The oxidation resistance of this system is not complete however. Initially a coating and glass does form, but the glass phase-separates and $SrMoO_4$ crystallizes from the glass, while B_2O_3 evaporates away. As a result of both boria loss and devitrification, the glass loses flowability, and in areas where the coating is compromised the glass is unable to fill in and pesting beneath the coating is observed. In an attempt to alleviate this problem, higher silicate compositions and the addition of alkali earth oxides were investigated. Li Aluminosilicates are too fluid initially and also too reactive and suffer from phase separation and devitrification. In these cases as well it was shown that while oxidation rates are limited, no complete glassy coating is formed and long term oxidation resistance is poor. In almost every case a porous layer of glass and molybdates was observed after oxidation, and this incomplete coating in all cases was allowing continued oxidation of the underlying exposed Mo. Attempts were made to adjust the composition of the glass to higher B contents for greater flowability, however no balance could be struck and the low viscosity glasses either were not completely wetting and/or were too fluid, and allowed rapid transport of oxidation products and reactants through bubbling and the pore channels which remain after rupture of said bubbles.

The suspected problems with using alkaline earths are the issues surrounding precipitation of molybdates. MoO_3 has a limited solubility in silicate and borosilicate glasses. In solution under neutral and oxidizing atmospheres, the Mo is present in MoO_4^{-2} tetrahedra. Based on bond valence considerations, Mo-O-Si bonds cannot exist, so the MoO_4 must be disconnected within the silicate network and as a result they would then be located in regions of the glass structure which are high in non-bridging oxygens (NBO). These regions would also be rich in alkaline-earth cations, in our case Sr^{2+}, based

on considerations of charge balance. Consequently, the alkaline earth cations and MoO_4 groups would be in close proximity and electronically in favor of crystallization of the alkaline earth molybdate ($SrMoO_4$).

Neodymium in glass is known to break up the Si-O-Si bonds and form NBO's. Nd^{3+} have a high field strength and are surrounded in the glass structure by 6 to 8 NBOs while a fraction of the low field strength cations, such as alkaline-earth ions, locate in the second coordination sphere of the Nd^{3+} cations to maintain charge neutrality. Chouard et. al.[116] suggest that the Nd^{3+} cations depolymerize and disperse the silicate structure and effectively fix the locations of the alkaline earth cations, and would also act in some part to charge compensate for the MoO_4^{-2}. In effect it would separate the MoO_4^{-2} groups and the alkaline earth cations from one another which would make crystallization more difficult. Further the depolymerization of the glass by Nd allows for more NBO-rich regions to which the MoO_4^{-2} would locate and thus increase solubility of the molybdenum oxide. Chouard's group successfully showed that addition of Nd_2O_3 to a Mo-oxide-containing alkaline earth aluminosilicate glass composition induces a strong decrease in the tendency of molybdates to separate and crystallize for additions of up to 8 wt.% Nd_2O_3. Based on this it is expected that additions of NdO_4 to our composition will effectively limit phase separation and molybdate formation in the glass and ultimately lead to improved oxidation performance.

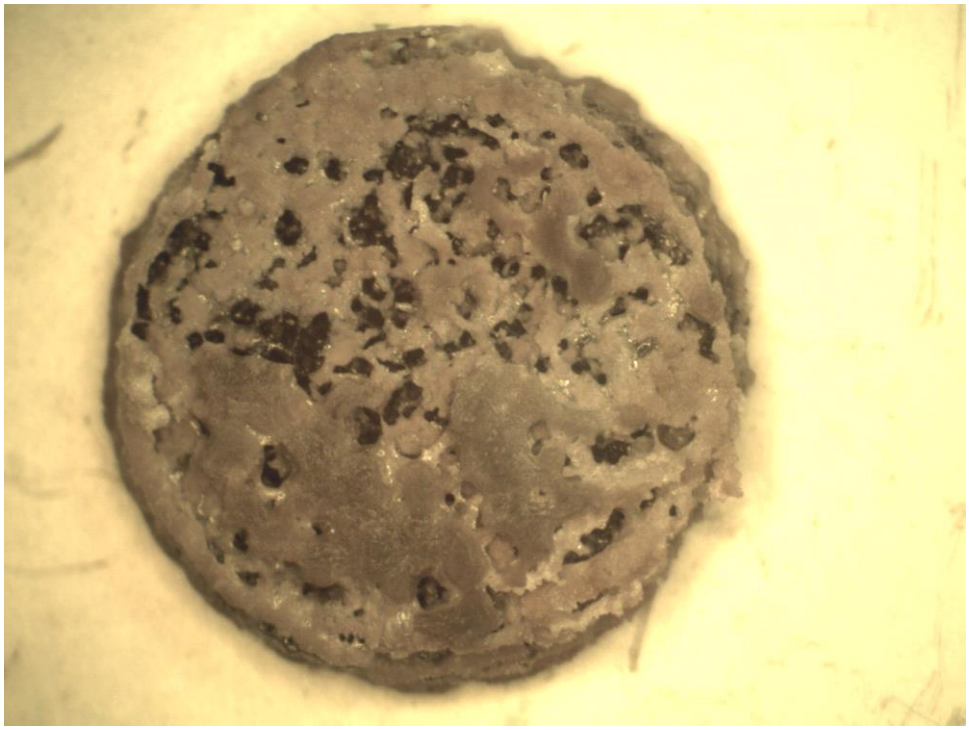

Figure 6.20: BSASNd151812 after 6h oxidation in air at 1100°C

The first Nd containing composition (BSASNda151812 – where Nda refers to vol % Neodymium apatite) had an added Nd apatite volume fraction of 12%, corresponding to a glass composition which had been identified by Chouard as within the usable Nd contents for preventing devitrification. Upon oxidation at 1100°C however, an opaque and nonprotective scale did form (Figure 6.20), with perhaps even worse devitrification than before. A pink hue to the crystalline phase was also observed which is known to be an effect of Nd additions to glasses. At 1300°C the glass still devitrified but instead was very fluid and poorly wetting. The crystallization and poorly wetting pools of glass can be seen in Figure 6.21.

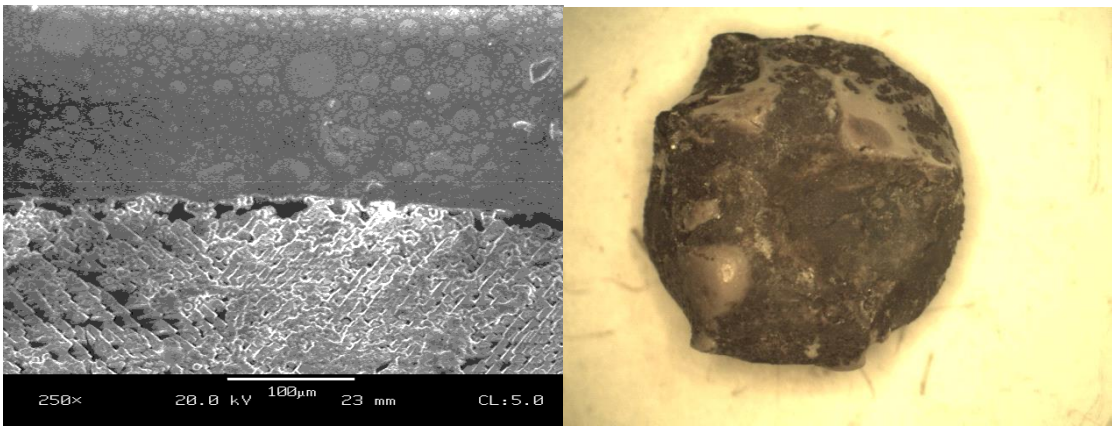

Figure 6.21: BSASNd151812 oxidized for 1h at 1300°C.

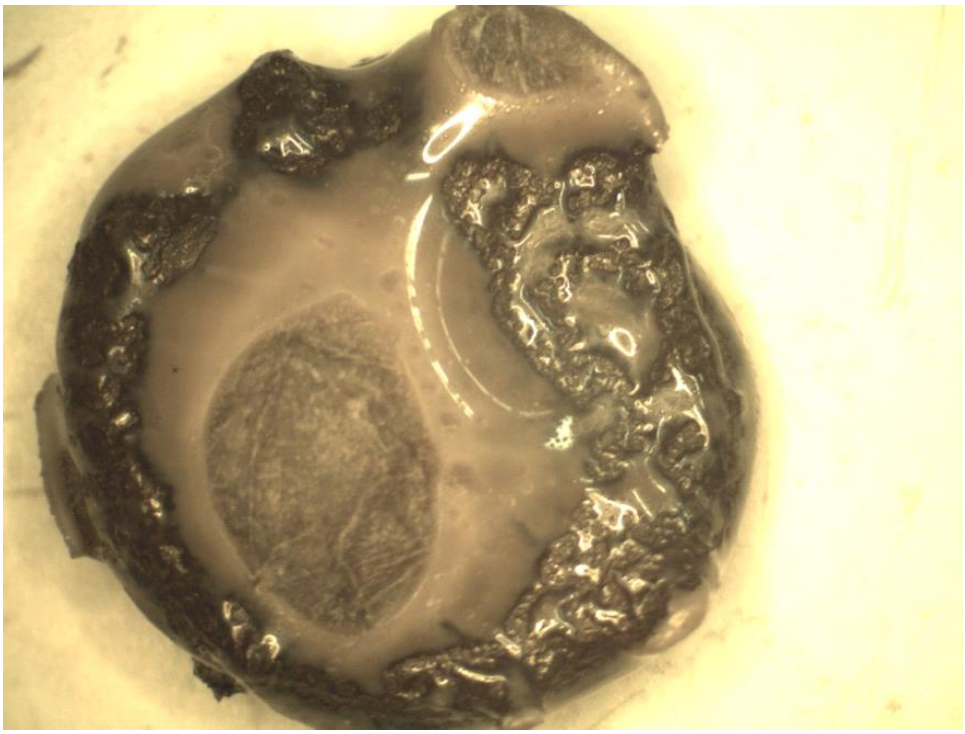

Figure 6.22: BSAS2323 +2.5 Nd. Oxidized at 1300°C for 90m.

Another higher B composition with less Nd (2323 +2.5 Nd) was prepared and oxidized at 1300°C. Nd was added at low levels to investigate any potential advantages to retaining Sr and preventing molybdates from devitrifying. The low levels should help

avoid the drastic viscosity reduction that led to poorly wetted fluid glass which was nonprotective in the prior BSASNda case at 1300°C. The pellet surface after 90m is shown in Figure 6.22. In the BS2323+2.5Nd case the wetting is reduced still further, significant phase separation and devitrification is obvious, even optically. The opaque low viscosity liquid silicate phase had a final pinkinsh/purple hue due to Nd additions.

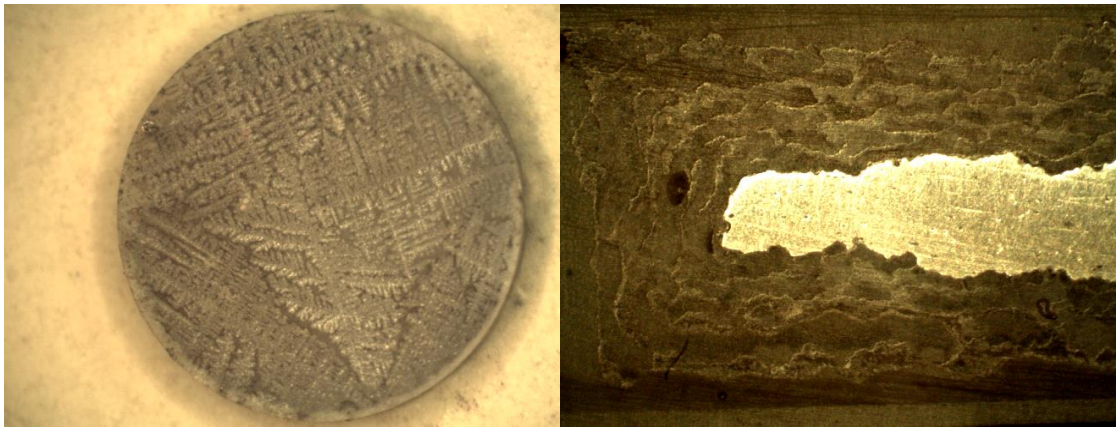

Figure 6.23: TS2720+0.5Nd after oxidation 1300°C, 90m surface right and left is cross section after 20h.

Following the BSAS samples with Nd apatite, T2 containing samples were prepared with T2 in place of the Mo_2B to reduce the boria levels and increase Si and thereby reduce fluidity and prevent the nonwetting fluid glass seen in the BSASNda samples. When TSAS2720 with 2.5wt% Nd was subjected to oxidation at 1300°C the devitrification was actually worsened by addition of the Nd. An image of the oxidized pellet is shown in figure above and large dendritic crystal growth is readily apparent over the entire surface. After 20h the cross section is shown on the right of Figure 6.23. It fails again by the same stepwise erosion and crystallization typical of the devitrifying samples.

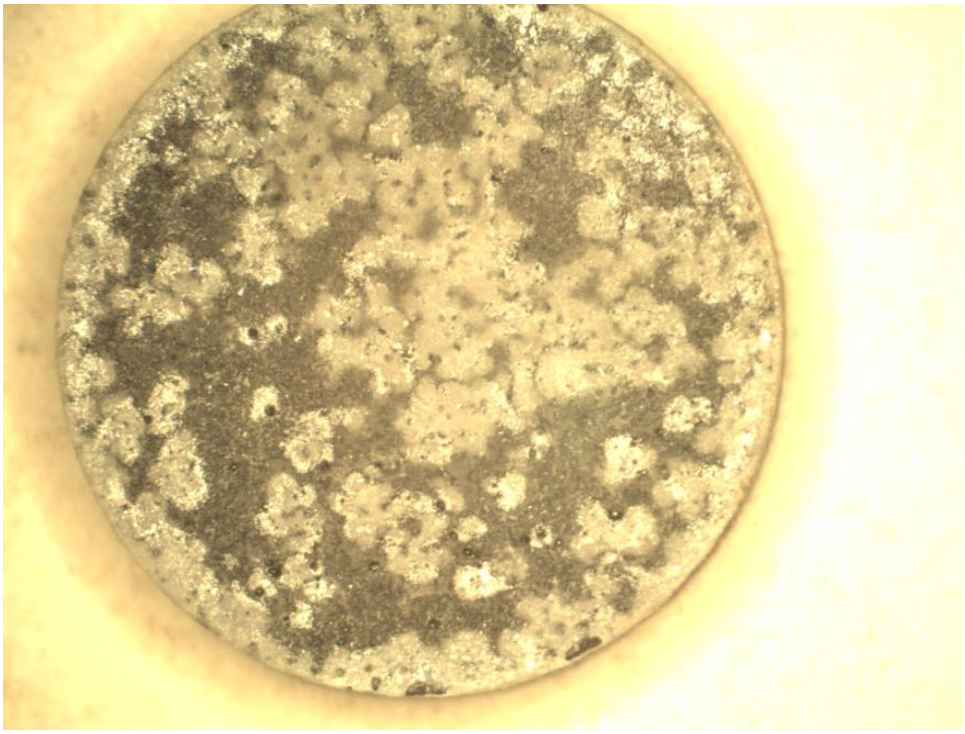

Figure 6.24: TSAS2027+2.5 Nd oxidized at 1200°C for 30m.

At lower temperatures also, the TSAS 2027 _+2.5 Nd failed from devitrification, Figure 6.24. The samples failed in a stepwise scenario of forming a coating, then the coating devitrifies and becomes solid, and the underlying material is eroded beneath through pinholes. In the above image, the whiter spots are not due to spreading heterogeneous nucleated crystals, but rather places where pinholes have allowed erosion of the substrate beneath the coating, while the coating remains as a shell. This results in lighter spots, in contrast to the darker areas where the substrate is still in contact beneath the coating.

6.5. TQSAS

Because of the failures of the lithium and other alkali silicates to increase the silica ratios, and the probability that the boria formed from Mo_2B alone is too volatile, we

began to look back at including the T2 phase along with silica, and including the alkaline earth silicates as glass modifiers instead of the primary glass source. Many commercial glass batches, including borosilicates, rely on presence of alumina and other oxides to stabilize the borosilicate and create homogenous glasses.

In previous tests, the TQ2713 composition containing only Mo, 13v% quartz SiO_2 and 27v% T2 behaved well in oxidation at 1300°C, but poorly at 1200°C. It formed a glossy black scale after 30m, and had visible porosity/holes in the scale, and was wholly consumed within ~10h. For the same composition we added small amounts of SAS.

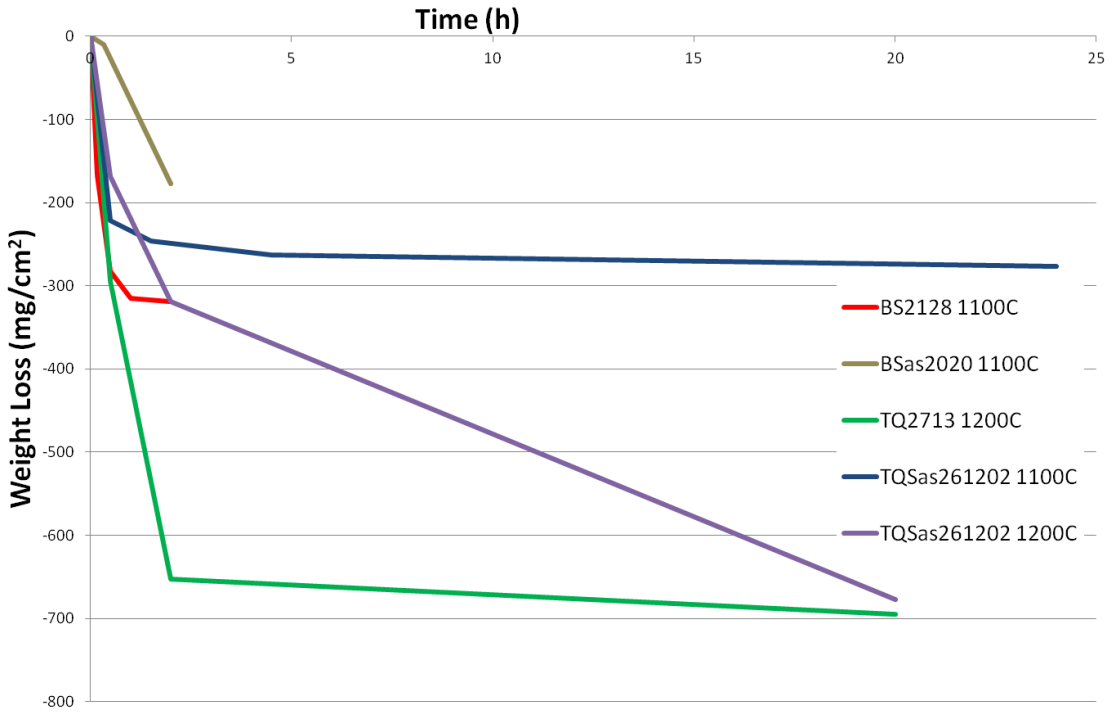

Figure 6.25: Oxidation results for small SAS additions compared to prior TQ and SAS containing samples.

The TQSAS compositions fired without issue and samples were oxidized and results are shown in Figure 6.25. TQsas261202 hoped to achieve a balance of oxidation enhancement via some slight Sr addition to the traditional TQ 2713 composition; however viscosity again appeared to be too low, in the end all that remained after 20h at 1200°C was a porous devitrified puck with numerous Mo oxide inclusions, with some of the pores filled with a separated fluid black glass. The TQ with 2% SAS did result in some improvements to the oxidation resistance however. Porosity or channels can still be observed in the glass scale; but they were much finer, possibly due to lower viscosity and thus finer bubbles (easier to form, smaller critical size, rise faster, etc.) The TQSas performs better at 1200°C yet in the long term no protection was maintained and the sample failed within 20h. Again the cross section of the oxidized sample looked much like the failed TQ2713 at 1300°C, with a large degree of MoO_2 surrounded by glass and small islands of Mo within. This type of coating morphology has been linked to too low of a glass viscosity.

At 1100°C the glass did offer some protection, again supporting that it has overall too low of a viscosity for higher T use. The addition of SAS helped develop a partially crystalline glassy coating and the oxidation rate appears to level off effectively. The crystalline nature of the coating is effective at reducing oxygen transport to much slower rates than through glass alone and has very low long term loss rates, and gave the best oxidation performance of any of the tested compositions to that point at 24 hours and 1100°C. It's apparent that a balance may be met between the problematic crystallization that prevents oxidation protection in the high SAS and the potential for beneficial reductions in oxygen permeability such as was seen here for small SAS fractions at

1100°C. If it crystallizes too early it becomes unable to form a complete coating, but without any crystallization the diffusivity of O through the scale remains high. Crystallization of the coating can offer large benefits to the overall performance so long as it can be controlled. It also should retain its ability to self-heal, as the glass under a crack in the coating would have the same composition as the initially exposed glasses, and would form and crystallize in the same manner. It could thereby re-heal cracks or flaws with more crystalline oxidation protective coating. It appears that the glass coating can benefit most from small additions of aluminosilicates to act as modifiers to the glass and perhaps encourage a delayed crystallization, but in general the glass sources are best left to SiO_2 and T2 in order to prevent excessive crystallization and undesirably low glass viscosities.

6.6. Alternate Silicate Conclusions

Silica can be used as a replacement for the A15 phase in MoSiB alloys and thus avoid the issues of Si in solid solution in the Mo matrix to benefit toughness while maintaining a sel-healing oxidation resistance. Residual oxygen which is unavoidable in the system leads to issues of depletion of boride and silica, as well as internal crescent shaped glass regions throughout the microstructure, and as a result the strength and toughness suffer. Instead more stable silicates were proposed as alternate sources of Silica.

The addition of mullite gives excellent density and microstructures, and the ductile to brittle transition is lowered to below room temperature, evident by measurable plastic deformation in room temperature bend tests. Mullite however cannot form a

suitable glass even with a boria flux, and further aluminosilicates including Sr metasilicate, Sr-aluminosilicate, and Lithium spodumenes were examined.

It appears that additions of SAS and other alkali or alkaline earth silicates instead of silica are incapable of maintaining the fluidity necessary to create a permanent protective coating, and lose their self-healing ability by crystallizing. Despite their promising effects on the microstructure by removing the detrimental crescents seen with the silica samples, and the improved mechanical properties showing both high strengths and measurable ductility at room temperature, the SAS and alternate silicate approaches were discarded. The positive mechanical results in the system do indicate however that ductility should be possible for the T2 and silica compositions, provided the crescent defects in the microstructure could be corrected. Further, some evidence of improved oxidation has been shown which uses the devitrification of the coating to benefit the oxidation resistance. A controlled devitrification could limit oxygen diffusivity once a coating has formed and result in significant improvements to the long term weight loss rates.

CHAPTER 7.

ELEMENTAL ADDITIONS

7.1. Introduction

Other elemental additives may be incorporated into MoSiB alloys and numerous reports have been made on the inclusion of various additives. These take two main paths; first are additives for mechanical improvement, which may either affect microstructure and phase arrangement or affect the properties of the individual phases. The second opportunity for elemental additions would be to affect the oxidation performance, either by forming other oxides to prevent lower temperature pesting, or by affecting the properties and kinetics of the borosilicate protective coating.

7.2. Mechanical Additions

The additions of silica to T2 and Molybdenum were able to provide suitable oxidation resistance, but they also suffered from problems with non-ideal microstructures. Specifically, large crescent regions of silica were present in the microstructure. These are caused by flow of the silica into the regions that exist between the pressed spray-dried granules prior to the completion of sintering. Flow of the silica should not be possible unless something is acting to flux it, and the non ideal crescents have been linked to the presence of B_2O_3 during firing which forms from residual oxygen on the Mo.

A second microstructural hurdle has been the depletion of the secondary phases from the surfaces, leaving a Mo-rich zone near the outside edges. This drastically increases the initial weight losses during oxidation and complicates the formation of an oxidation resistant coating, as well as our understanding of the coatings. This also is

believed to be the result of residual oxygen on the Mo which permits formation of volatile boria during firing and also forms H_2O rich atmospheres when reduced by the flowing H_2. H_2O vapor can react with both boron and silica and enable their volatilization from the near surface of the material.

Both of these problems are accredited to residual oxygen during firing; however adjustments to the process, raw material purity, and firing schedules were unable to resolve the issues. Attempts were then made to improve the stability of the silica by adding alternate silicate phases with greater stability such as mullite and strontium aluminosilicate (SAS). These still were unable to meet the requirements of suitable oxidation resistance and mechanical properties.

The next step taken was to investigate elemental additions to the Mo-T2-SiO_2 system while leaving the silica present as SiO_2. Similar to TZM alloys, trace additives with high oxygen affinity could be used to getter residual oxygen. This could improve ductility of the Mo by gettering any O in the final piece but should also potentially eliminate the causes of the crescents in the microstructure and depletion from the surfaces.

7.2.1. Gettering Additions

A first set of quaternary elemental additions to the Mo-Si-B system were made to getter residual oxygen and improve mechanical properties. In order to recreate some of the mechanical strength of TZM alloys, a portion of the Mo was replaced with pre-alloyed powders of Mo-Ti, and Mo-Zr. After firing however, the pellets were instantly rejected because of severe cracking and deformation during firing caused by thermal

expansion, liquefaction and other issues which arise during the high T 1600°C processing.

A next set of samples considered additions of Aluminum. As mentioned previously with the mullite case, aluminum could potentially enhance oxidation resistance, and its high oxygen affinity allows it to act as a gettering agent to absorb unwanted oxygen. The additions were made to a traditional 3:1 Mo-Si-B alloy since Al additions can't be used in the Mo-T2-SiO_2 system due to reactions with SiO_2 to form mullite or other aluminosilicates.

An A15 analog exists between Mo and Al (Mo_3Al) similar to the Si A15 (Mo_3Si). In the Mo-A15-T2 system with Al, the Al occupies some of the Si sites in A15 shifting it to smaller lattice parameter. XRD scans showed presence of only the expected Mo, A15 and T2 phases, and the expected shift of the A15 to a smaller lattice size was also observed. EDS maps also confirmed that the silicon and aluminum occupy the same locations, that is, the A15 analog ($Mo_3Si_xAl_{1-x}$).

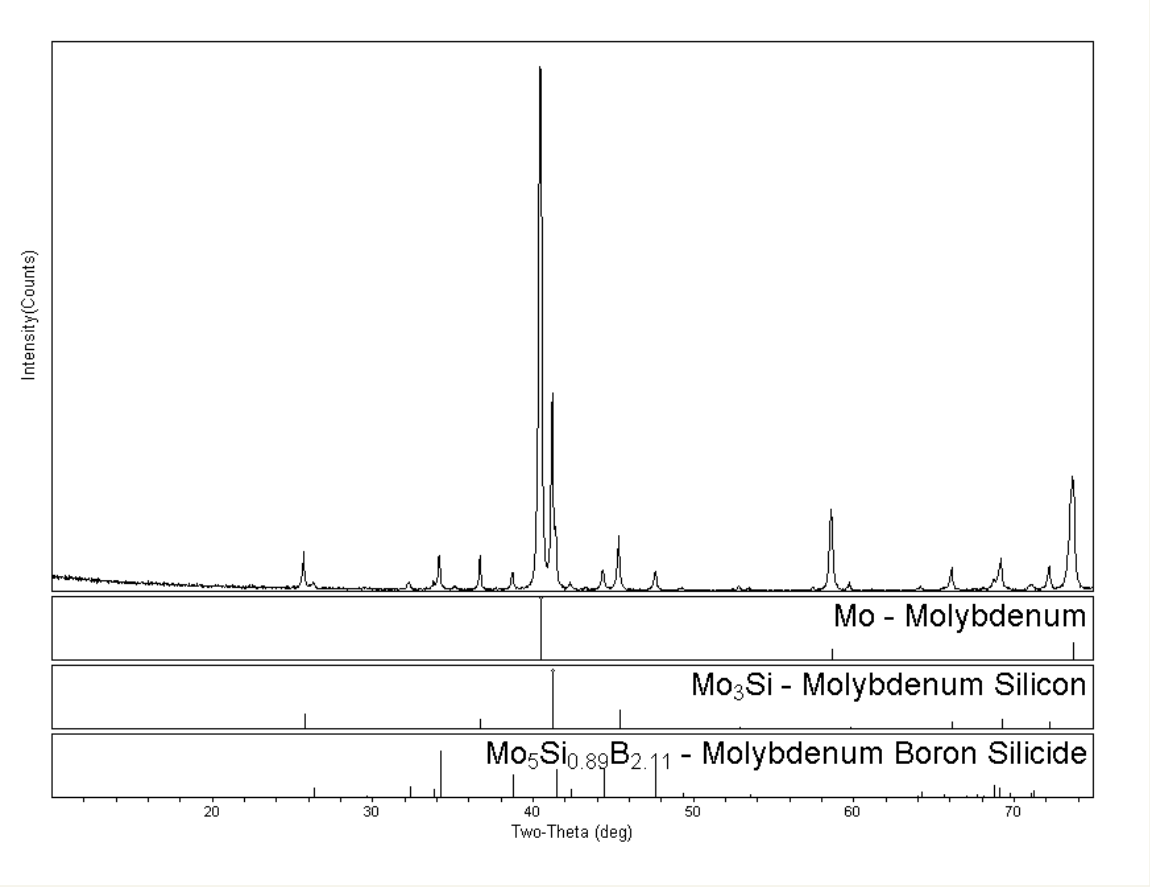

Figure 7.1: Fired TCAln201210 XRD pattern of the polished pellet cross section.

To examine effects of Al on TC samples, AlN was added for its higher temperature stability with SiO_2 and to avoid brining in additional O on pure Al powder. A TC2012 composition was fired with 10v%AlN – TCAln201210. The XRD scan however shows presence of neither silicon nor aluminum oxides (

Figure 7.1.) XRD revealed that the aluminum had reacted and reduced the SiO_2 to form a MoSiB Mo-A15-T2 alloy. Reitveld analysis gives weight ratios for Mo: A15: T2 of 56: 28: 16. Al can form A15 and fit nearly completely in place of the Si, with full mutual solubility between the Mo_3Si and Mo_3Al analog. If all of the batched Si for the T2 as well as the added Al were all going to form the $Mo_3(Al,Si)$ A15, those values still

indicate an excess in the A15 which must be from additional silica liberated by reduction of silica. There's no cristobalite or crystalline SiO_2, nor any Al or Al-Si oxides apparent. Assuming complete reduction of SiO_2 with all available AlN, less than 20% SiO_2 would still remain; meanwhile liberated Si can be contributing to Mo embrittlement.

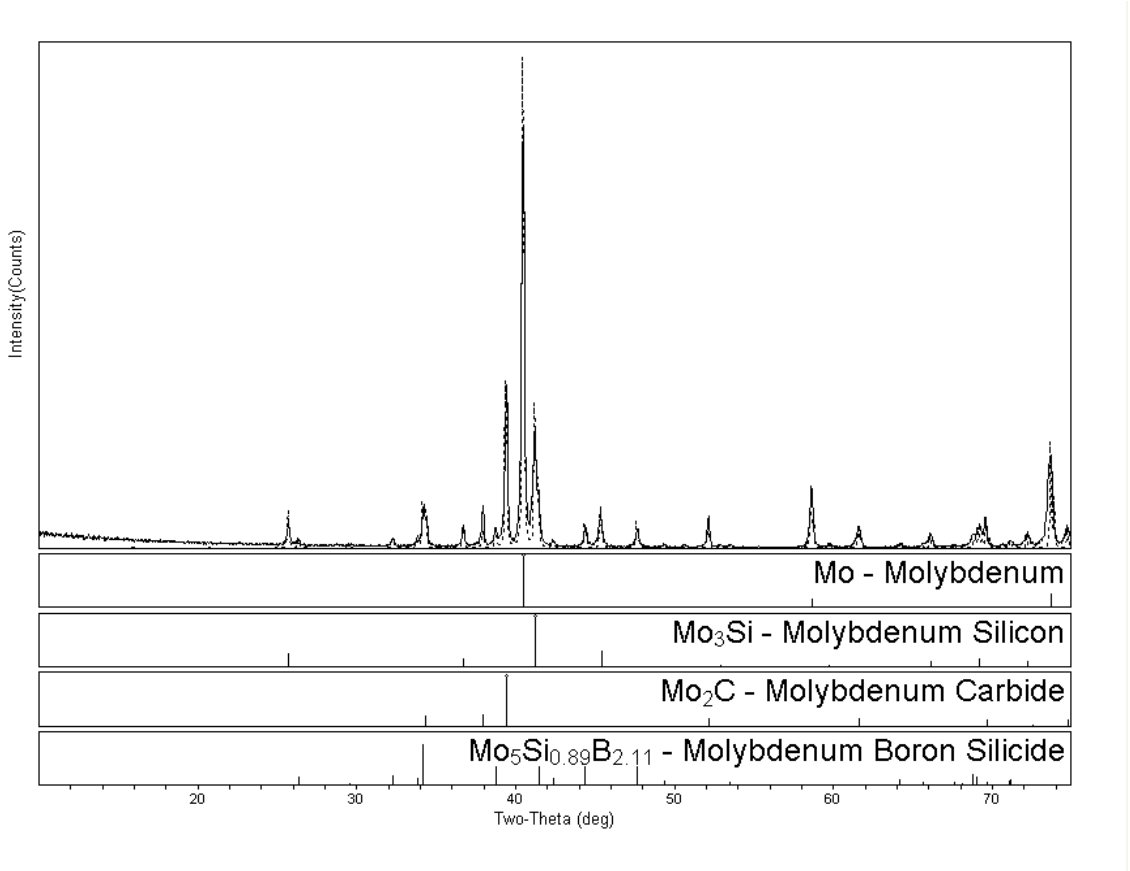

Figure 7.2: XRD Phase identification of TC2017 with added carbon for gettering oxygen after firing to 1550 for 6h in Ar/10%H_2.

TC2017 was also fired with carbon black. The carbon should also act as a gettering agent to reduce anything that might be vitrifying the cristobalite; however an excess could also reduce silica. Not surprisingly the XRD in Figure 7.2 shows that it resulted in formation of Mo carbide and A15. Weight fractions of the crystalline phases suggests a ratio of approx: 44% Mo, 21% A15, 18% Mo_2C, and 17% T2. If none of the

carbon reacted to leave as CO or CO_2, but instead remained to form molybdenum carbide, there would be around 22wt%. The measured carbide fraction is only slightly lower, allowing that some C may have reduced SiO_2. This would result in free Si which explains the A15 seen in the above scan; meanwhile no cristobalite peaks are seen.

Unfortunately none of the gettering or mechanical modifier additives were successful in creating usable pieces, nor in preventing vitrification of silica. Further the higher oxygen affinity additives reduce the silica resulting in free Si which forms unwanted A15 but also will enter into the Mo_{ss} resulting in embrittlement.

7.3. Oxidation Modifying Additives

Quaternary additions to affect the gettering of oxygen proved unsuccessful and create more issues than they correct, yet opportunity also exists for trace additives to act as glass modifiers and improve oxidation resistance. Previous attempts by other researchers are recounted in Chapter 2.9

7.3.2. Fe Additions

Following the compositional guidelines in the Pratt & Whitney patent[92], samples were prepared with small additions of Fe, TC2421+1.5 Fe. The batches prepared were a previously well behaved TC2421 composition and another with the same composition but adding 1.5wt% of the Mo as Fe. These were prepared according to the GA Tech powder processing technique and fired to 1500°C for 6h in flowing Ar/10% H_2 to form final oxidation coupons of roughly 10mm diameter and 3mm thickness. Oxidation tests were performed in laboratory air in a bottom loading Keith furnace held at 1300°C. As with previous tests, the samples were laid on Pt wire stretched across Al_2O_3 boats and raised into the furnace at temperature. It's been noted regarding Fe-containing glasses that Pt

can catalyze reduction of ferric to ferrous oxide in contact with it at high temperatures. The samples were checked for any noticeable differences at the Pt contacts of the Fe containing sample, but no indication was seen of different behavior at the Pt contact. The pellets were removed and weighed at 10m, 30m, 90m and 20h. X-ray diffraction and SEM were used to identify the mechanism and products of oxidation.

Fe Oxidation Results

Initial tests were contradictory to the long term excellence shown in the patented work and showed that while there was indeed a reduction in initial transient loss and a turnover to slow parabolic loss rates, it was followed by collapse of the oxidation protection at longer times (Figure 7.3). During the first 30 minutes at 1300°C oxidation loss with Fe (red) was reduced to one fifth of previously recorded losses without Fe (blue) from ~300 mg/cm^2 to only 60 mg/cm^2. At 90m however, the coating is no longer as protective – marked by a downturn in weight vs. time. The second downturn in oxidation appears to be caused by phase separation and crystallization within the glassy coating which occurs on a slightly longer time scale than the initial formation of the coating.

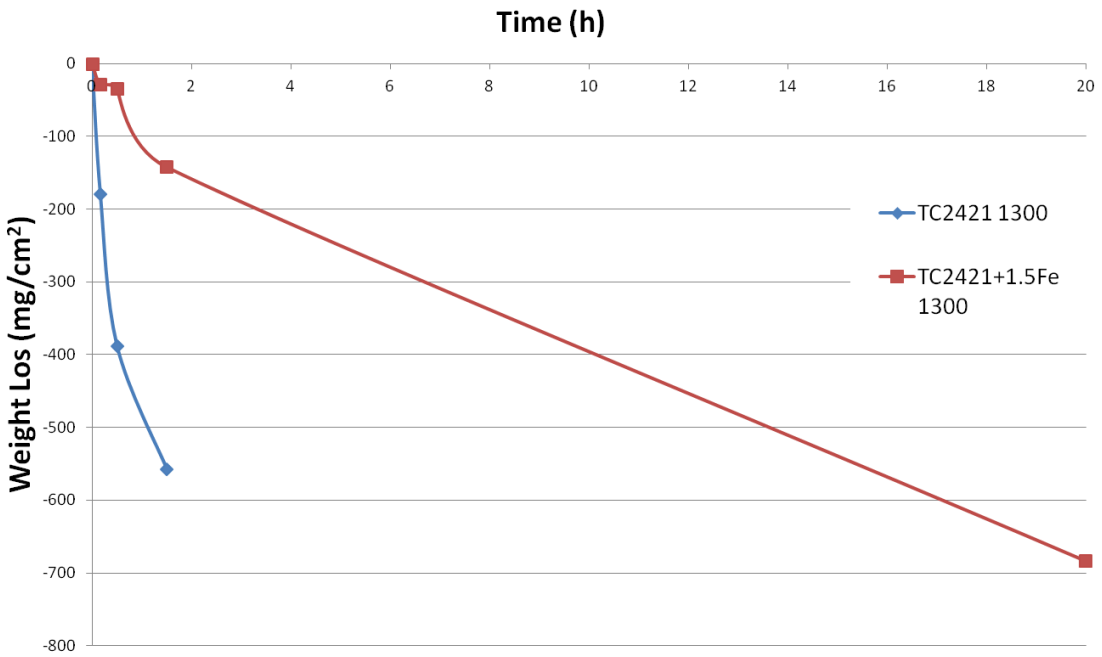

Figure 7.3: Image of Fe containing oxidation curve.

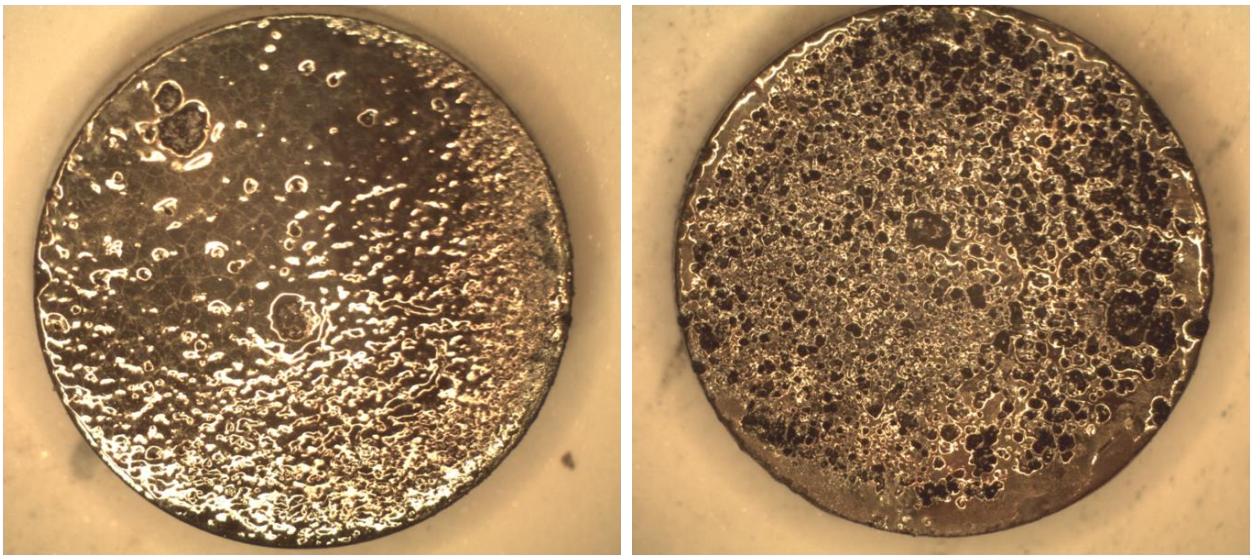

Figure 7.4: Sample TC2421+1.5Fe after oxidation at 1300°C: 30m (left) and 90m (right)

The surfaces of the pellets formed a very fine thin glass initially which nearly evenly coated the pellet up to 30 minutes (Figure 7.4- left). At longer times however

bubbles appear through the thin coating from volatilization of MoO_3, meanwhile the glass thickens and loses its ability to collapse and fill in the channels left by bursting bubbles, evident in Figure 7.4- right.

After 90m the coating had begun to phase separate similar to the effect seen in Figure 7.5. On the outermost parts of the coating some of the glass has fully crystallized to cristobalite as identified by XRD. Long term oxidation resistance suffered and proved to be insufficient.

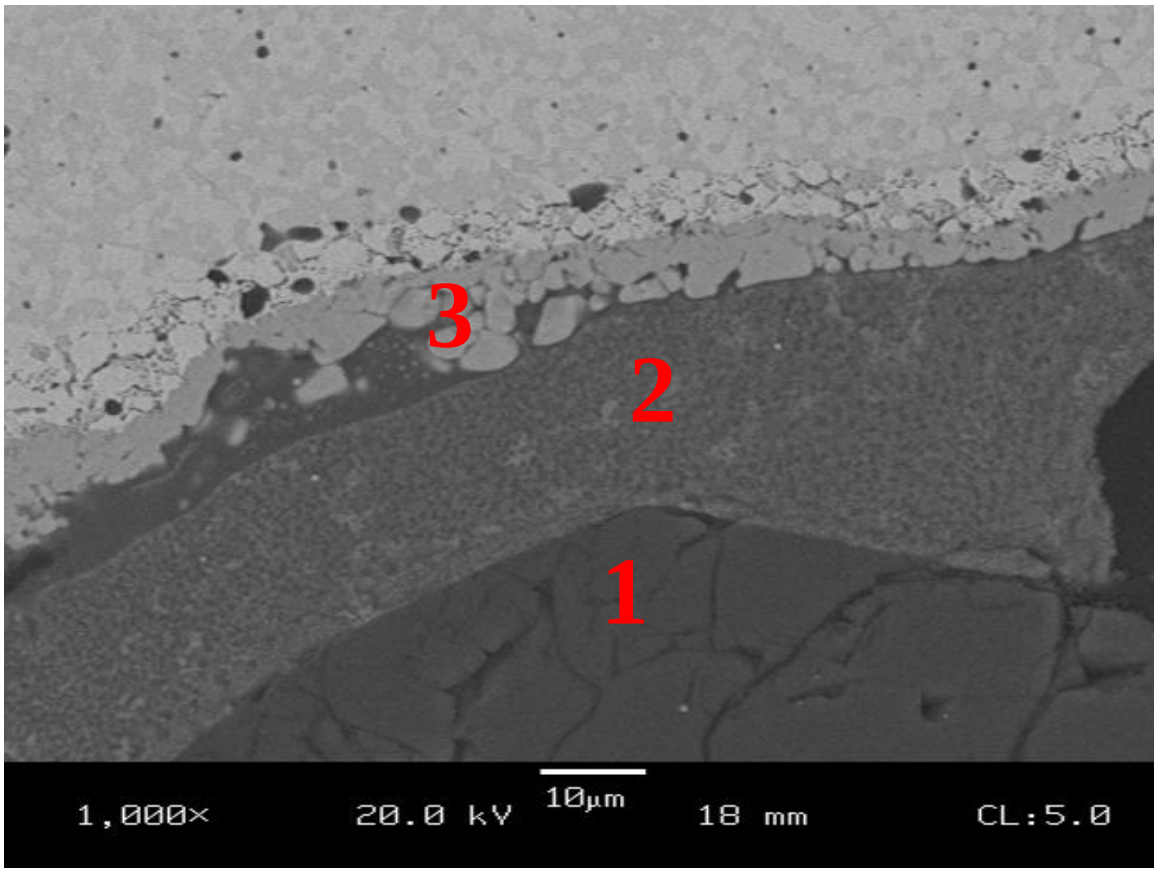

Figure 7.5: SEM polished cross section of oxidation layer of a similar 3:1 MoSiB containing 1.5 at% Fe after 20h oxidation at 1300°C

In the cross section of the oxidation layer, distinct phase separation is obvious. Simultaneous oxidation testing was done of a 3:1 composition with 21v% A15 and 27% T2 which also failed in the same manner. The TC2421+1.5Fe had the same issues, but the 3:1 image shown in Figure 7.5 better illustrates the mechanisms. We see three layers, a clear but cracking glass (1), a finely phase separated region (2) with a spinodal type separation into a presumably crystalline and amorphous phase, and beneath that a homogenous scale layer (3) similar to previously seen MoO_2 layers. The glass at (1) is a homogenous mixture of the individual components but is not stable and begins to separate into iron rich and iron poor regions (2), which then crystallize into fayalite (Fe_2SiO_4) and possibly iron molybdate, and an outer layer of crystalline SiO_2 (cristobalite).

The XRD scans of the TC2421 + 1.5 Fe oxidized in air at 1200°C and 1300°C show Mo, Iron Molybdate $Fe_2(MoO_4)_3$, cristobalite and Fayalite (Fe_2SiO_4). The background was also very significant, implying presence of a large amount of glass as well. The pure Mo peaks can be seen possibly through the coating, and also parts of the coating spall off and expose some underlying Mo.

After 20h a hole had been eaten through the center of the sample seen in Figure 7.6.The XRD scan in Figure 7.7 showed strong hematite peaks (Fe_2O_3) and reddish crystals were observed growing from the surface, while the center remained a fluid glass, and no protection was maintained.

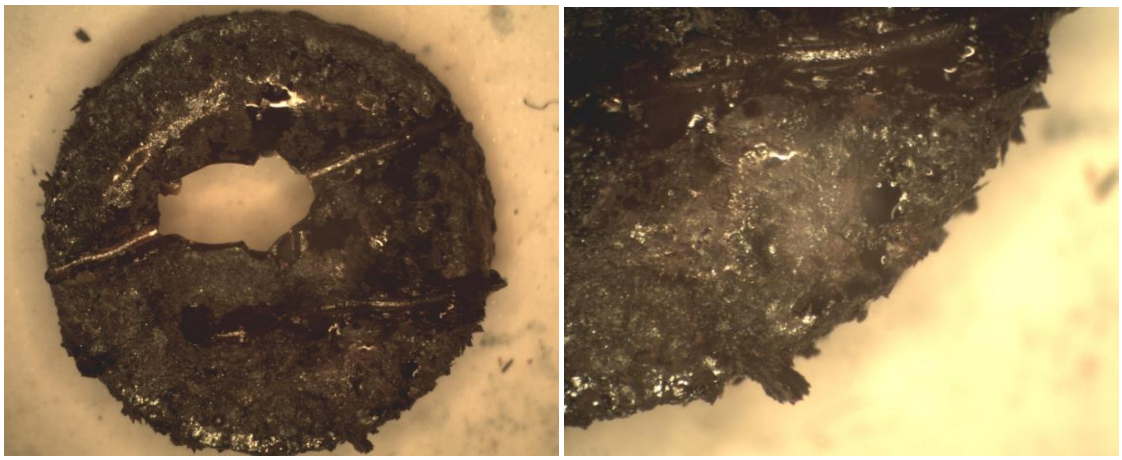

Figure 7.6: Surface of TC2421+1.5Fe after 20h oxidation at 1300°C

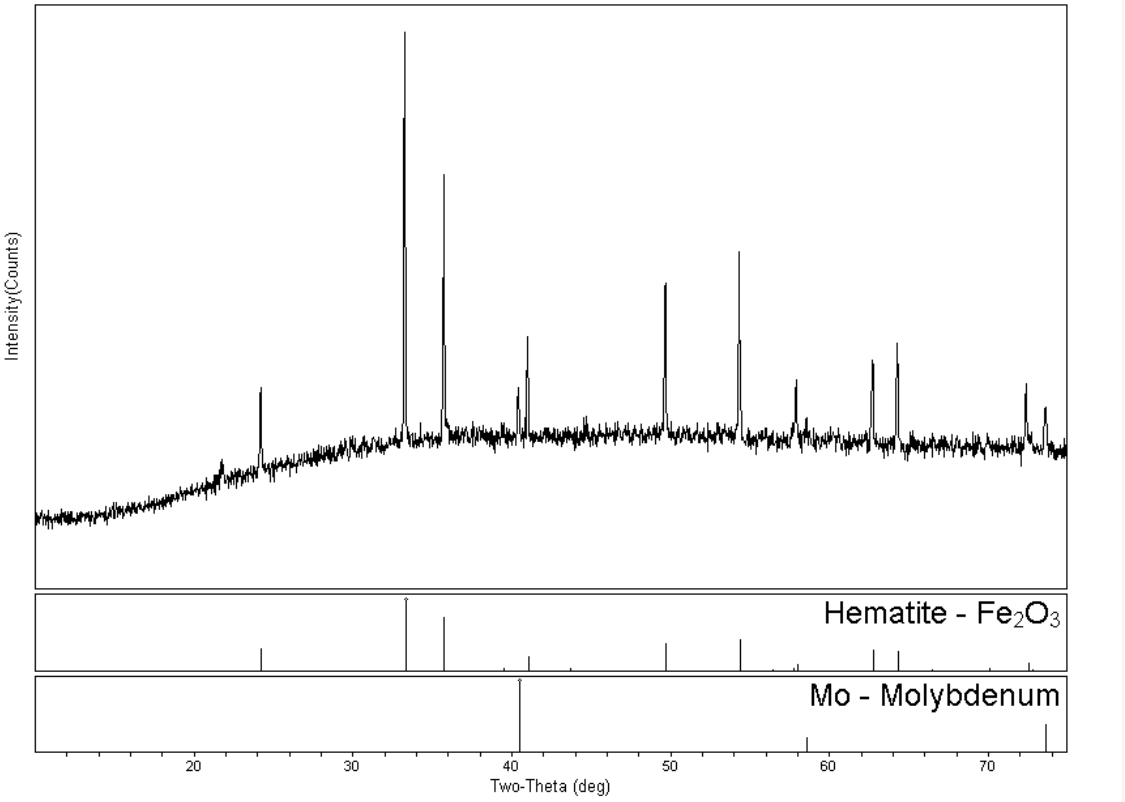

Figure 7.7: TC2421+1.5Fe after oxidation for 45m in air at 1200°C XRD scan.

In conclusion, addition of Fe gives an initial coating which forms quickly and nearly completely and oxidation rate slows and becomes nearly flat within the first 10m. However, as time proceeds the glass becomes nonprotective and after 20 hrs, the sample is nearly totally annihilated. The failure of the coating appears to be caused by the phase separation and subsequent devitrification of fayalite, iron molybdate, hematite and cristobalite within the glass.

7.3.3. Co, Cu, Cr, Ni and Mn

It has been reported in two publications that additions of Fe have promoted oxidation resistance at 1300°C,[92, 93] however our attempts at addition of Fe to compositions in both 3:1 and T2:Silica were less successful. In the T2:silica system the glass was non-protective due to iron oxides phase separating and devitrifying and in the 3:1 case a process of phase separation and devitrification leaves the glass too rigid to collapse and seal, allowing the continued stepwise formation of layers and erosion of the material beneath them. While initial loss was reduced, the samples all suffer from a subsequent downturn and increasing oxidation rates as time goes on.

The Pratt & Whitney patents also mention benefits from adding Co, Cr, Cu and Ni. Manganese was also chosen because its behavior in glasses is similar to iron. It has not been previously investigated for oxidation resistance however because Mn metal becomes highly volatile at the melting point of Mo, making Mn addition accessible only through powder processing routes such as ours.

Samples containing similar transition metals (Cr, Co, Ni and Mn) alongside additional samples with lower Fe contents were produced next to explore the effect of minor additions on oxidation scale formation including the behavior of molybdate,

silicate, and borate species, variations in glass viscosity, phase separation, and the formation of complex, multi-component scales.

Co, Cr and Mn all should have roughly similar reactions with Mo, T2 and A15 and should affect the bulk microstructure and mechanical properties nearly equally, however they do different things in glass. Alloying MoSiB with varying degrees of these additions should elucidate some differences in reactions in the glass, phase separation, and other effects on oxidation resistance. Furthermore, while the effects of Mn are similar to Fe in the glass, in the MoSiB system Mn does not occupy sites in the A15 as Fe does, and in this way allows us to investigate whether the Fe-fluxed SiO_2 formed on A15 is actually responsible for improved oxidation resistance as suggested by Sossaman[56, 93], or if instead it is more affected by the change in overall glass properties with transition metal additives like Mn or Fe.

Table 7.1 gives the compositions of the batches prepared and relevant atomic % of the additives in the glass. All additives were added to prepared base compositions with the previous naming convention, and the additives are batched as a fraction of the Mo, for instance 1%Mn has 1wt% of the Mo fraction replaced by the Mn additive. As an example; TCSas202101+1.5Mn has a base batch with 20v% T2, 21v% cristobalite, and 1v% SAS and the remainder Mo, and of the molybdenum 1.5 wt% is replaced with Mn. This convention was adopted because the additives do not form a separate phase and thus have no volume fraction, but they do exist exclusively as a fraction of the Molybdenum solid solution. An additional batch TCSas171601+0.5 Mn was also prepared to investigate microstructure effects of higher Mo fraction, but not for oxidation testing.

Table 7.1: Batches and Fired Densities.

Name	Firing (C)	Green (g/cc)	Fired (g/cc)	Theoretical	%TD
TC2421+1.5Fe	6h@1550	4.71	7.87	8.23	95.6%
TC2421+1.5Co	8h@1500	4.59	7.86	8.20	95.9%
TC2421+1.5Cr	8h@1500	4.65	7.73	8.20	94.3%
TC2421+1.5Mn	8h@1500	4.51	8.14	8.20	99.3%
TC2421+1.0Mn	6h@1550	4.62	7.58	8.23	92.1%
TCSAS222101+0.5Mn	6h@1550	4.62	7.43	8.19	90.7%
TCSAS222101+0.25Mn	6h@1550	4.57	7.55	8.19	92.2%

The samples were fired, the schedules and final densities are also given in Table 7.1. The presence of crescent regions of silica as well as depletion layers remains an issue. An attempt to deal with the crescents and depletion was approached by pre-reacting the T2 vs reacting it in situ because possible reactions between the Si_3N_4 and SiO_2 were identified. The two samples were TCSas171601+0.5 Mn and denoted "-1" and "-2". "-2" is prepared with pre-reacted T2, whereas "-1" is reacted during firing from BN, Si_3N_4 and SiO_2. These compositions are also higher volume % Mo than previous batches in order to investigate the effects on microstructure.

The crescent shaped regions are noticeably fewer and the microstructure appears more homogenous (Figure 7.8), but this may be due in part or wholly, to the higher Mo fractions.

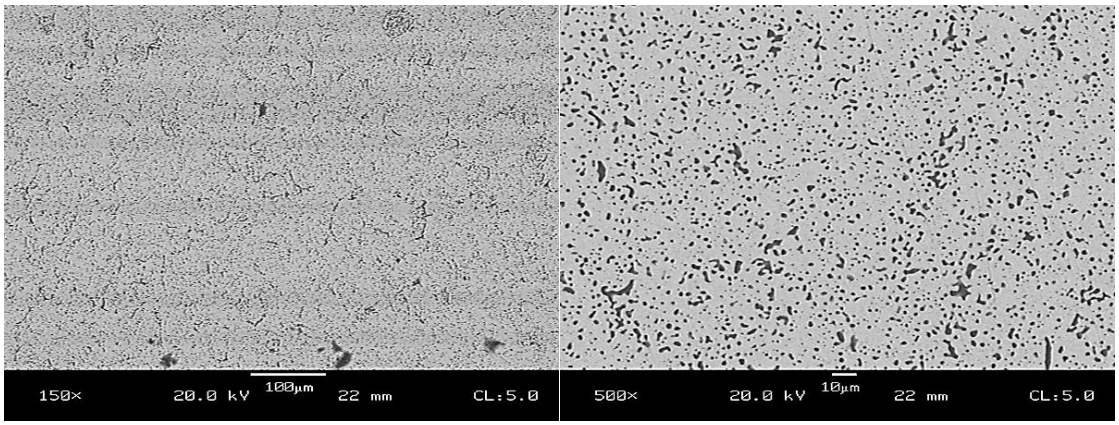

Figure 7.8: SEM of Microstructure of TCSas171601+0.5Mn with T2 reacted during firing (-1) on left and using pre-reacted T2 (-2) on right.

For the firing reacted "-1" sample, depletion of T2 extends to ~ 60 µm, with no visible silica depletion. The pre-reacted "-2" had slightly less but still ~50-60 µm T2 depletion and also nearly no depletion of silica. Measuring a volume fraction from images show slightly more SiO_2 in the pre-reacted case at 17.15% vs 15.5% for the as-reacted sample. This may be due to some SiO_2 reacting with the Si_3N_4 in the as-reacted case, or instead could be that there is more oxygen in the system reacting with Si during firing in the "-2" case, or it may just be experimental error.

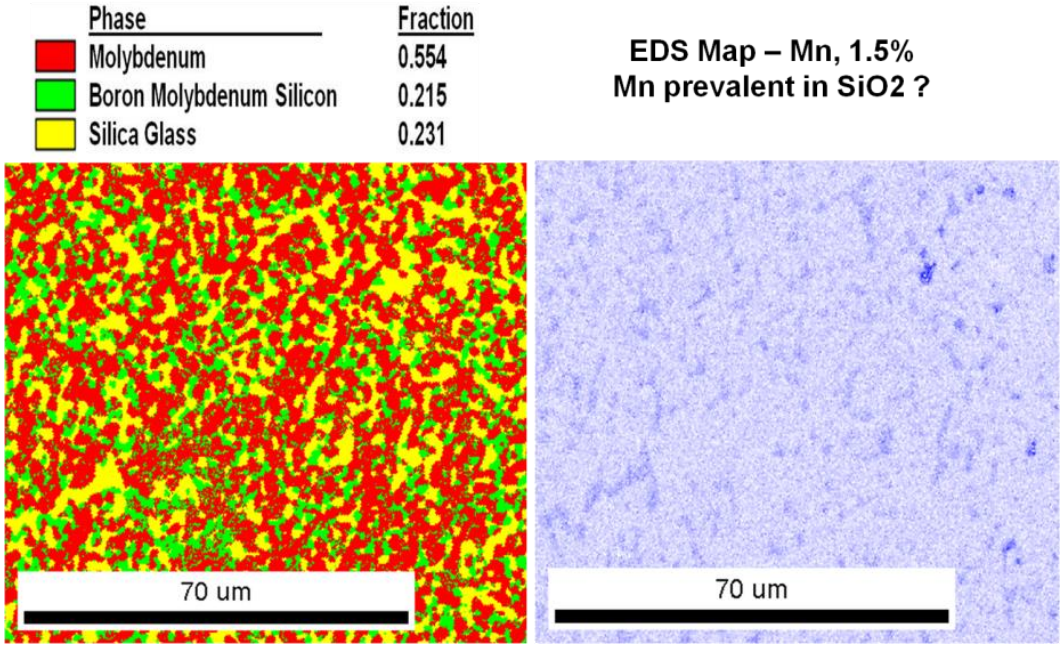

Figure 7.9: EBSD map of Mo-T2-SiO_2-Mn showing phase distribution and Mn concentration. Molybdenum Boron Silicon refers to the T2 phase.

The EBSD map shown in Figure 7.9 confirms the desired fine and homogenous distribution is achieved. In the figure the same red, yellow, green color scheme is used as for Figure 3.4 but here the yellow is the SiO_2. The measured volume fractions are also given and are close to the expected values for a TC2421 sample. Shown at the right is the Mn distribution as measured by EDS since it is not a unique crystalline phase. Much of the Mn is in the Mo phase which is expected for their high mutual solubility however high concentrations of Mn also exist in the SiO_2. The Mn concentration is so low however that the EDS may not be accurate, and may also be misled by the Si to Mn vs. Mo to Mn peaks which would over exaggerate Mn content in the lower molecular weight SiO_2 phase.

7.3.3.1.Oxidation Results

The oxidation resistance of the additional transition metals (Cr, Co, and Mn) added to Mo-T2-Silica (TC2124) was compared to Fe. The general trends are shown in Figure 7.10 and Figure 7.11 and individual elements discussed in greater depth following.

At 1200°C (Figure 7.10) Fe can be seen resulting in the lowest initial losses however the previously observed downturn in oxidation resistance appears again resulting in poor long term protection. Ni also adds improvement over the base material. At 1300°C, (Figure 7.11) Fe provided improved oxidation resistance for both AT and TC compositions but long term oxidation rates of 30 mg/cm^2-hr were obtained which are too high for practical use. Ni also showed greater improvements at 1300°C than at 1200°C and long term rates near 10mg/cm^2 show promise. Both Cr and Co additions did provide a small measure of improved oxidation resistance but were consistently unable to escape the rapid transient loss regime. Mn provided the best improvements at 1300°C in both short and long term performance.

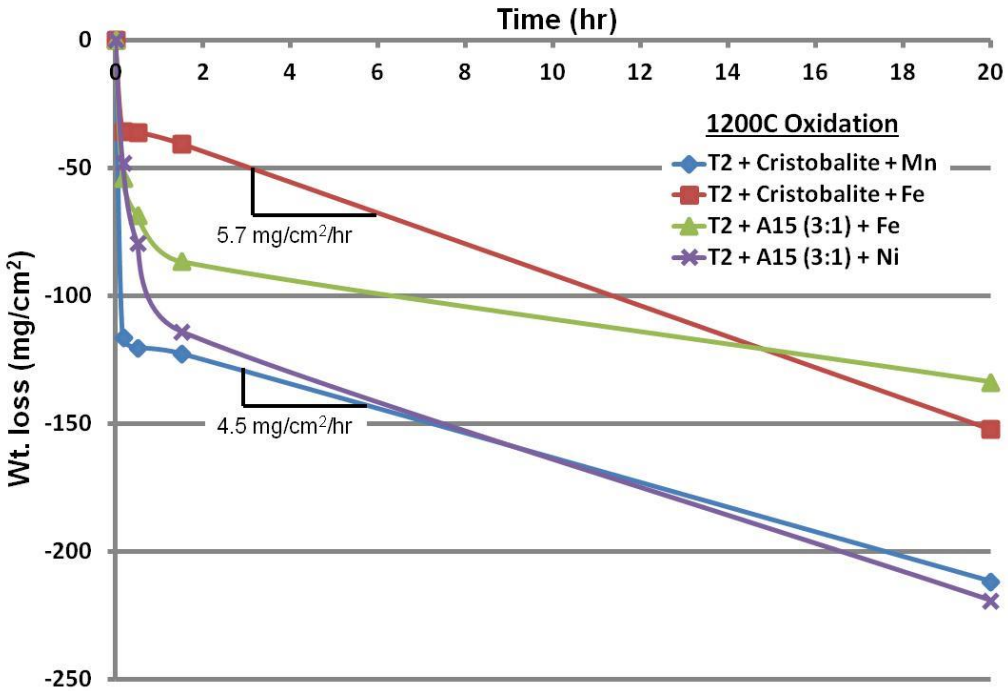

Figure 7.10: Effect of Mn, Fe and Ni on Oxidation of Mo3Si1B and Mo-T2-Silica at 1200°C.

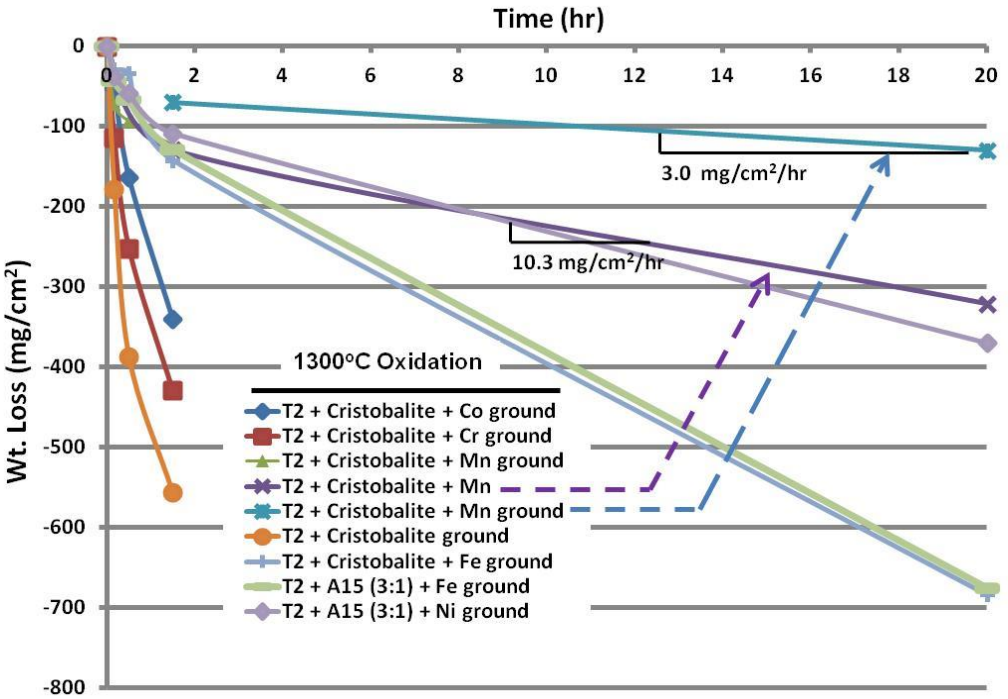

Figure 7.11: Effect of Mn, Fe, Ni, Co, Cr on Oxidation of Mo-T2-Silica and Mo-3Si-1B at 1300°C.

Also for the samples tested in Figure 7.11, grinding of the surfaces removes the effects of boron depleted layers from the surfaces, and unground versus ground cases are considered indicated by the arrows on the figure. The long term rates are comparable, however consistent with previous grinding tests, the grinding reduces overall loss most strongly during the transient portion.

7.3.3.1.1. Nickel

Addition of Ni compared to Fe provided overall better oxidation at 1200°C and 1300°C when added to 3:1 MoSiB samples. The oxidation rates were still high however. Oxidation of samples containing Ni form NiO and Ni_2SiO_4 as crystalline phases. Ni created other issues also because it has a very low solubility in α-Mo and reacts to MoNi. This forms a thin layer of MoNi which can be seen on Mo grain boundaries and which causes significant embrittlement and removes all ductility.

Vicker's hardness has been used to compare the various compositions and the observed increase in hardness with Ni over the base 3:1 is large and supports that the liquid δ-MoNi phase is forming on grain boundaries.

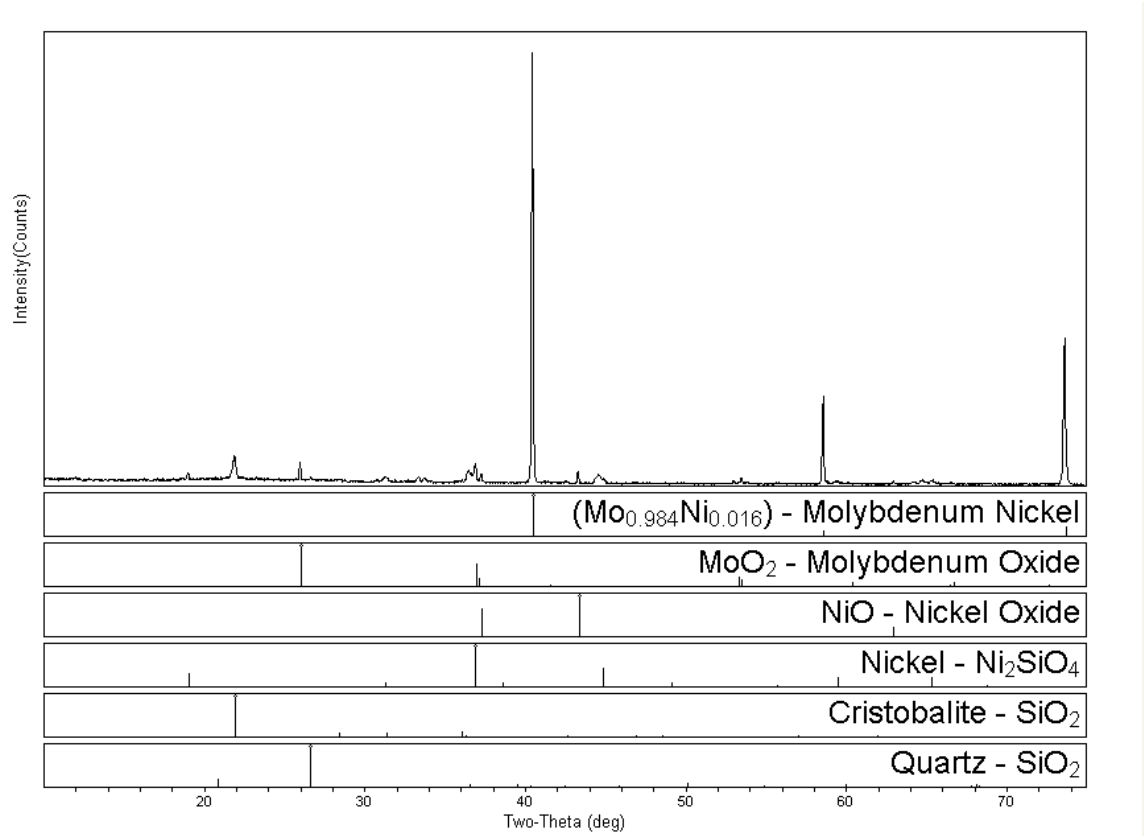

Figure 7.12: XRD Scan of 3:1 + 1.5 Ni after oxidation in air at 1300°C for 45m.

XRD of the 3:1 + 1.5 Ni in Figure 7.12 shows Nickel oxide and silicate phases, with a decreased amorphous hump. This suggests a similar phase separation and devitrification scenario to the Fe case, and results in insufficient long term oxidation protection.

7.3.3.1.2. Cobalt

The oxidation rate for the Co sample was both fast and linear. The optical images of the oxidized Cobalt sample are given in Figure 7.13 and the pellet cross section is shown in Figure 7.14. The surface had formed a nonprotective and very porous bubbly glass. Upon removal from the furnace the surface was visibly bubbling quite violently. There is no question that the viscosity was much too low. Co has been identified as a very

effective flux. It does not appear to have readily formed any molybdates however, and XRD was unable to identify any crystalline phases besides underlying Mo and MoO_2.

Co oxide is less stable than MoO_2, and would be reduced by Mo in this system. Cobalt can form a cobalt silicate, similar to the iron silicate fayalite (Fe_2SiO_4). There is also a cobalt molybdate, which may be liquid at 1300°C. These phases may phase separate and crystallize, and also promote the devitrification of the glass to cristobalite.

The optical images at 10 and 90 minutes in Figure 7.13 show large spalled sections of glass and evidence of the severe bubbling. At 90 minutes the bubbling was so fierce at the coating and bulk interface that it interrupted the connectivity such that the thermal expansion mismatch upon cooling caused spallation of large regions of the glass coating.

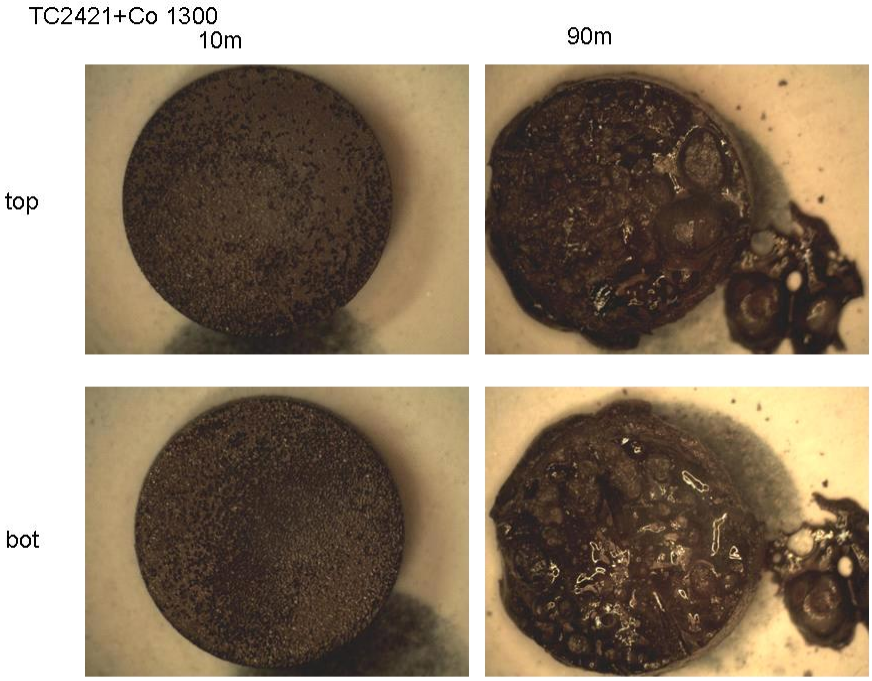

Figure 7.13: Optical images of the TC2421+1.5Co after oxidation at 1300°C for 10 and 90m.

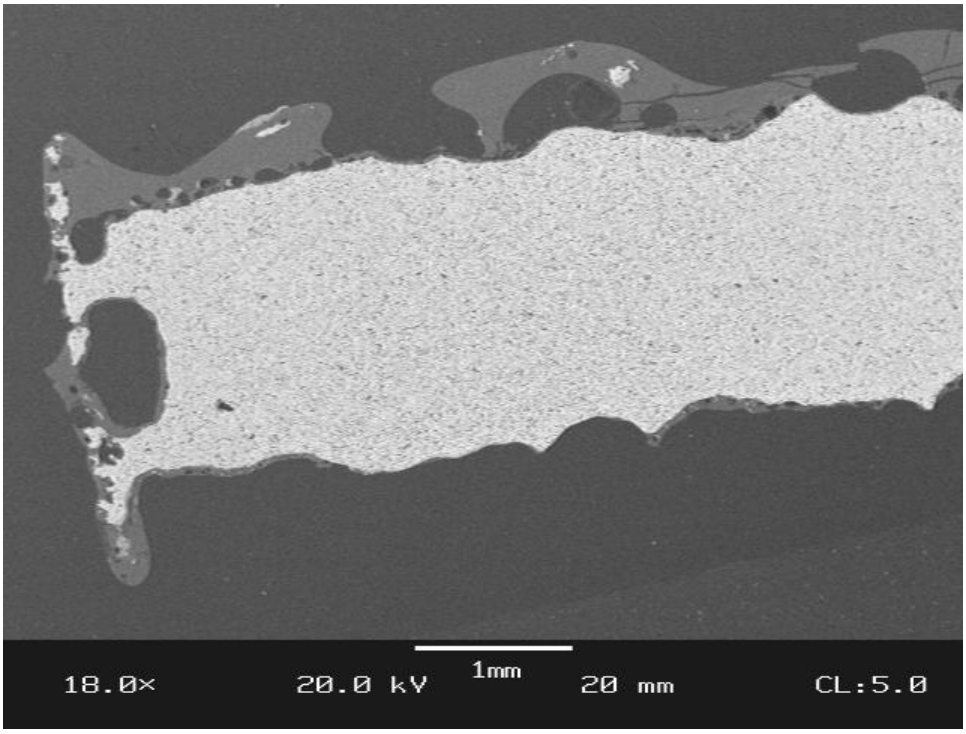

Figure 7.14: SEM cross section of the TC2421+1.5Co after oxidation at 1300°C for 90m.

The SEM image in Figure 7.14 shows the Co sample after 90 minutes. A much larger amount of glass is observed on the top surface because poor adhesion of the glass to the sample caused the glass which would have been seen on the bottom to spall away. The rapid formation of bubbles along the glass/bulk interface weakens the adhesion, and coupled with the mismatch in thermal expansion we see spallation of the coating.

One interesting feature is the line along the edge at the left of the image which seems to have lasted fairly well. The position of the remaining Mo gives a marker of the depth of recession from the faces, which is roughly the same ~500μm on both the top & bottom. Also interesting is that at the center of the edge is a cavity where oxidation proceeded more rapidly than at the surface of the edge. The original sample had been

ground on the faces prior to oxidation, but not ground on the edges. The inconsistent behavior is likely related to a greater protection provided by the depleted zone's chemistry. Preferential depletion of viscosity-lowering modifiers like B from the edges could increase viscosity and offset the fluidity that caused failure on the ground faces; while the B depletion at the edge is actually benefiting that area.

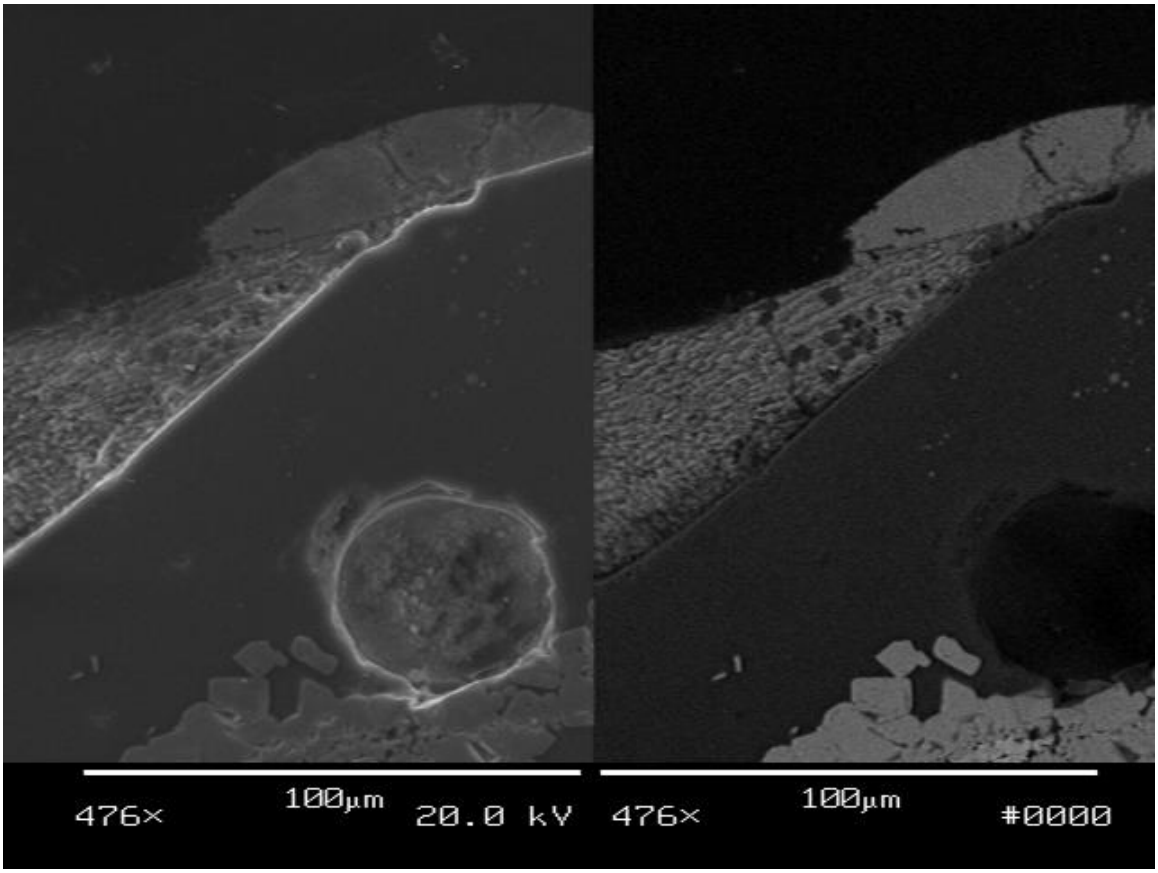

Figure 7.15: SEM detail of the cross sectioned TC2421+1.5Co after oxidation at 1300°C for 90m.

Many bubbles such as the one visible in Figure 7.15 were seen positioned directly at the interface of the bulk and the glass and in many instances MoO_2 could be seen at their bases. In some few places it did appear to be devitrifying at the surface as well, also

visible in Figure 7.15. XRD didn't show any oxide phases besides MoO_2, but the secondary devitrified phase at the surface is most likely a Co molybdate. Lipsch and Schuit[117] investigated phase stability in the Co-Mo-O ternary and showed presence of stable Co molybdates.

As noted previously the edge had an improved behavior versus the ground surfaces. However in a comparison of ground versus unground Co samples, the grinding on the surface doesn't appear to have had any effect. In both the unground and ground cases the bubbling was significant enough to prevent a well adhered glass and spallation of the coating prevented adequate protection from being achieved.

7.3.3.1.3. Chrome

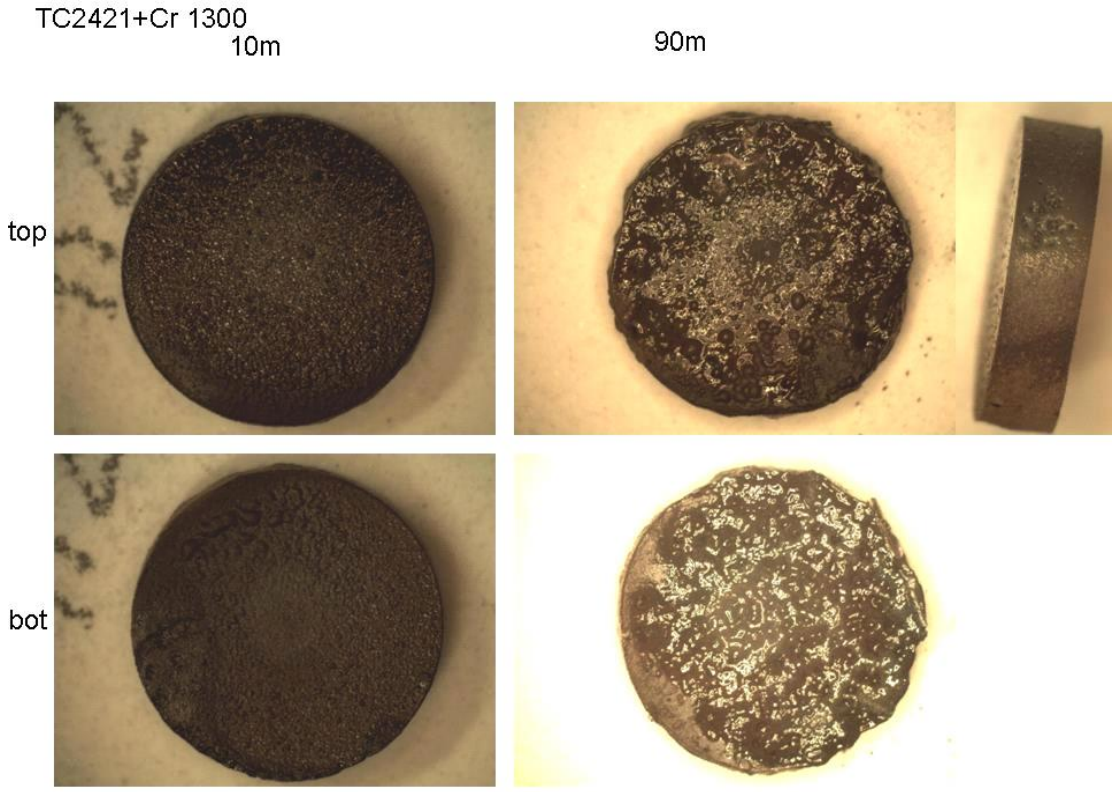

Figure 7.16: Optical images of the TC2421+1.5Cr after oxidation at 1300°C for 10 and 90m.

The Cr sample after 10 and 90 minutes of oxidation at 1300°C is shown in Figure 7.16. The Cr sample followed a very similar linear oxidation rate to the Co sample, but apparently for different reasons and not so much a dramatically low viscosity. After 10m there were some bubbles appearing but not the sort of rapid, constant and violent bubbling seen with the Co. The Cr also developed a green color which was attributed to the green cobalt oxide Cr_2O_3. XRD identified some glass, cristobalite (SiO_2), Cr_2O_3 and some MoO_2 also. A high intensity of Cr_2O_3 peaks relative to its expected fractions in the surface XRD analysis suggests it's forming on the surface of the glass. In this case we're forming a fluid glass which is phase separating and/or crystallizing and increasing in viscosity leaving some channels open. The microstructure is one of a simultaneously formed mixed oxide and glass. Cr also exhibits phase separation and devitrification to cristobalite similar to what we'd previously seen with Fe.

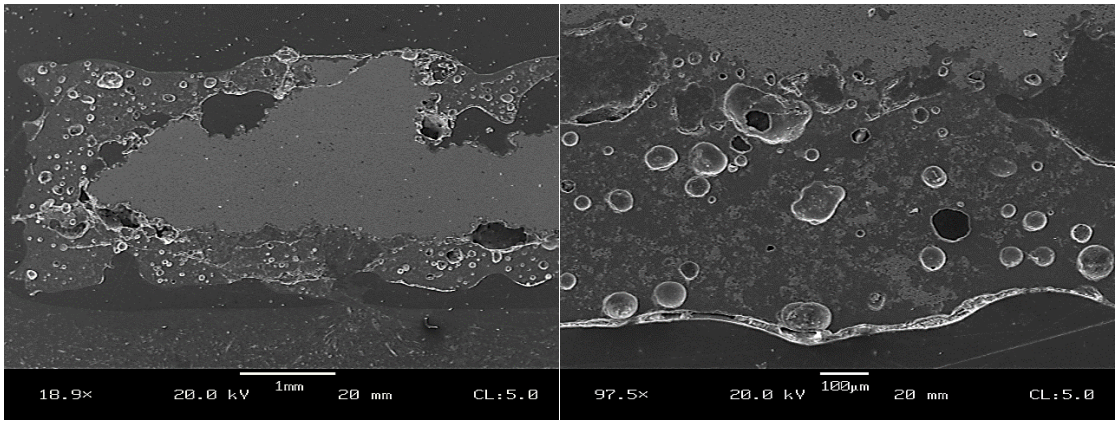

Figure 7.17: SEM of the cross sectioned TC2421+1.5Cr after oxidation at 1300°C for 90m.

Looking at the SEM cross section (Figure 7.17); bubbles are stabilized in the glass which can be seen optically from the surface also. In addition to MoO_3, the Chrome oxide is also volatile at these oxidation temperatures and may be adding to the total combined vapor pressure and aiding bubble formation. Cr_2O_3 is not dissolving into glass, and it looks like much of the Cr_2O_3 is built up on the surface, which gave it an optically visible greenish hue and a high fraction of chromium oxide was seen in XRD.

Burk[27] had in his thesis taken Cr containing MoSiB to 1300°C and also saw a lot of Cr_2O_3 in the glass but did not identify it as contributing to blowing bubbles, however it does contribute if only slightly to the total excess gas pressure there. The Cr was deemed unviable as an oxidation modifier since it does not benefit the glass, it forms separate oxides, and also may contribute to bubble formation.

7.3.3.1.4. Manganese

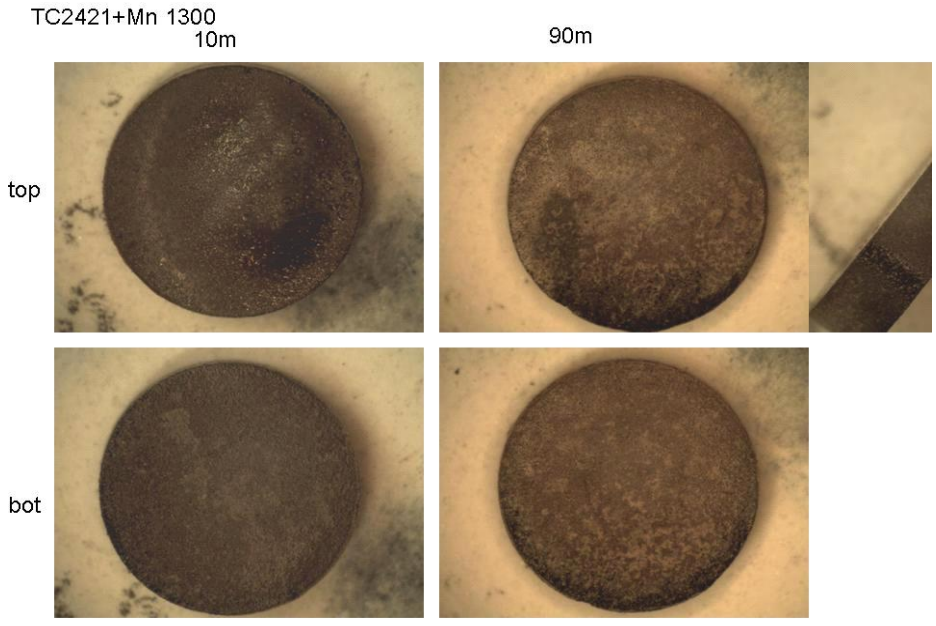

Figure 7.18: Optical images of the TC2421+1.5Mn after oxidation at 1300°C for 10 and 90m.

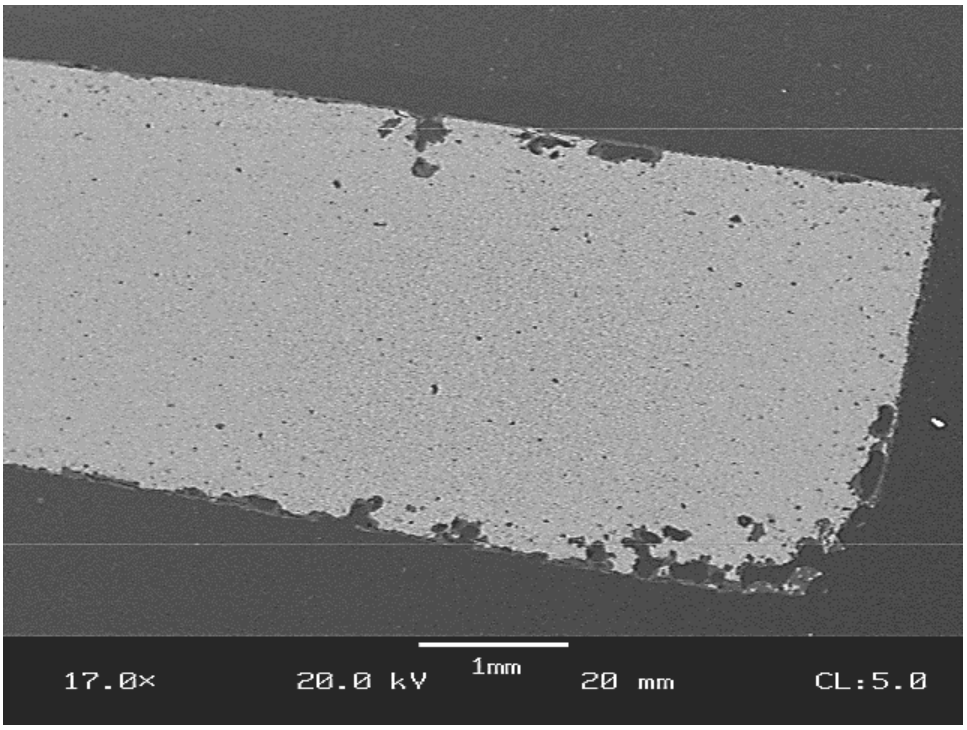

Figure 7.19: SEM of the cross sectioned TC2421+1.5Mn after oxidation at 1300°C for 90m.

Mn added at the 1.5 at% level to Mo-T2-Silica gave some of the best performance when tested, both at 1200°C and 1300°C for up to 20 hours. At 1200°C there was an initial weight loss ~ 120 mg/cm^2 which is higher than for iron, but likely due to a greater depletion layer. Afterwards the loss rate was nearly linear at 4.5 mg/cm^2/hr which is slightly lower than for Fe; which had a weight loss rate of 5.7 mg/cm^2/hr during the same time period.

The effects of Mn in Mo-T2-Silica were nearly as impressive at 1300°C as seen at 1200 °C. At 1300°C, the loss rate was 10.3 mg/cm^2/hr in the as-sintered pellet which is higher but reasonable compared to 1200°C. Further, when the depletion layer was ground, the initial oxidation loss was almost halved to only 70 mg/cm^2, and the long term rate was also improved to only 3 mg/cm^2-hr; an excellent rate compared to previous TC

materials. Images of the oxidized TC2421+1.5Mn pellets are shown in Figure 7.18, Figure 7.19 and Figure 7.20.

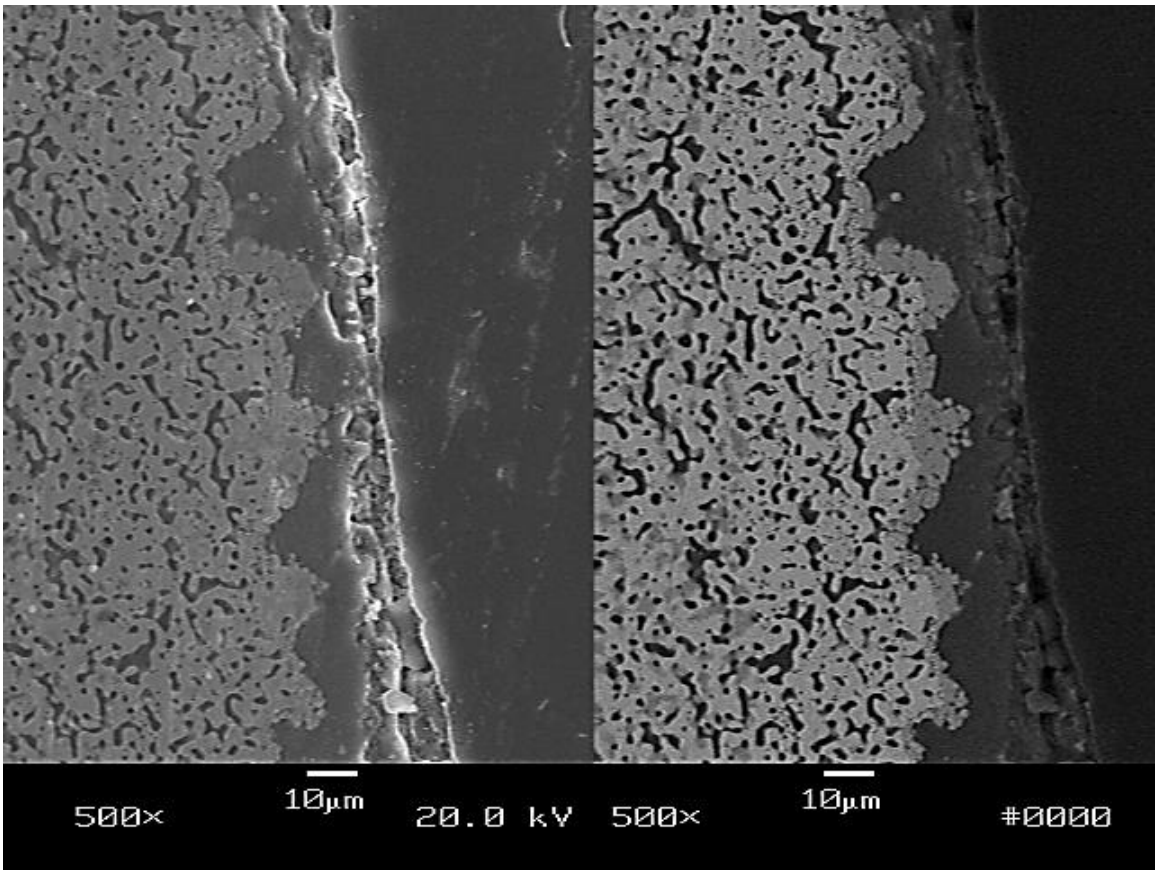

Figure 7.20: SEM detail of the cross sectioned TC2421+1.5Mn after oxidation at 1300°C for 90m.

In the cross-section shown in Figure 7.20 there's a good glassy coating and this was replicated on much of the surface. The coating is only around 10µm thick with some evidence of crystalline molybdate at the surface. Also cristobalite is observed at the surface, either nucleating on the molybdates or separating out when the Mn and Mo are removed. It can be seen in Figure 7.19 however that some spots were prone to internal erosion, despite the excellent protective coating that existed on much of the remaining

surface. In those few spots, bubbling and penetration are occurring; yet even in these there appears to be a reasonable coating still forming and a MoO_2 layer beneath. Optically the deeper penetrated regions appear as pinholes on the surface, and likely exist where the local composition was different enough to permit penetration.

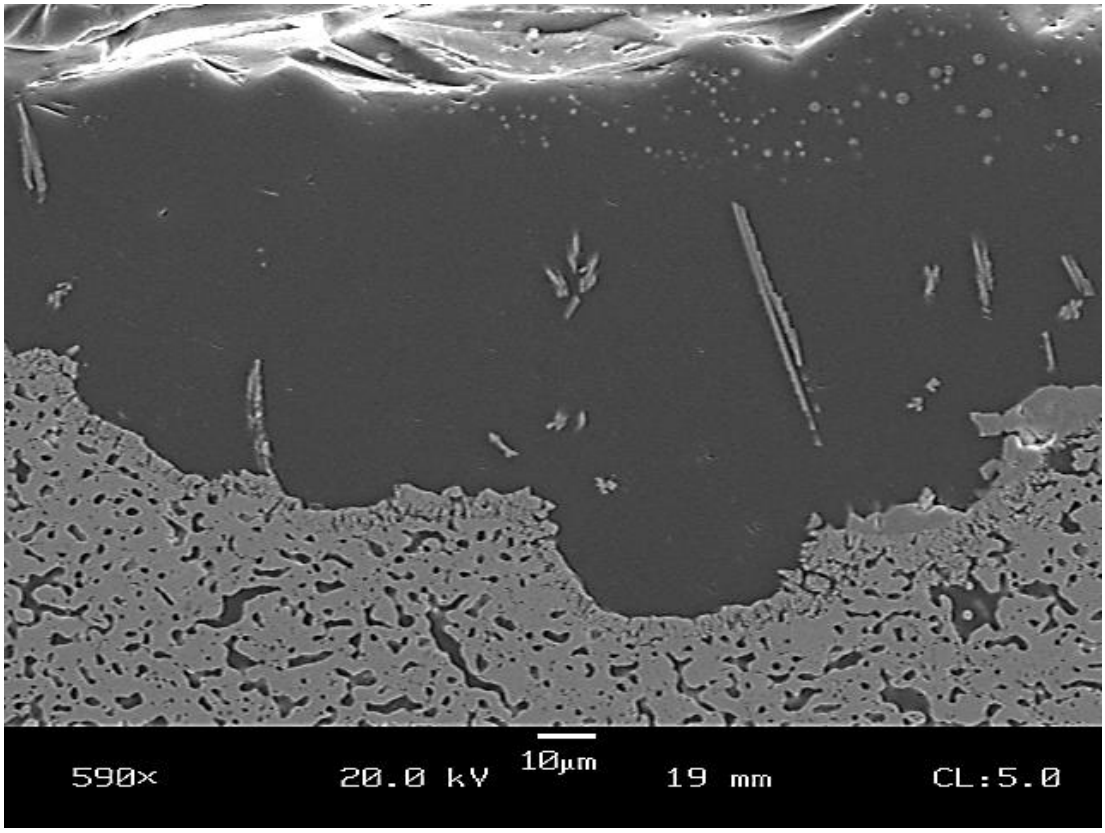

Figure 7.21: SEM detail of the cross sectioned TC2421+1.5Mn after oxidation at 1300°C for 20h.

Above in Figure 7.21 is shown another view of the TC+Mn sample after oxidation for 20h at 1300°C in air. The surface had not been ground. There are a few noticeable traits. First, round spherules can be seen near the surface. They're sub micron up to about 2 or 3 µm in diameter, and bright in backscatter indicating they contain Mo, likely they're MoO_3. MoO_3 has also been identified as spheres in other works including

those by Helmick, who proposed they were due to condensed MoO_3 vapor along the inside of pore channels which exist during formation of the glass layer. They differ significantly from the needle like crystals in the lower glass which also appear to be Mo oxides. They are crystalline with needle or plate-like morphology, unlike the spherical Mo oxide at the surface. These could be due to Mo oxide saturated in the glass and precipitating on cooling or growing as the pO_2 profiles change within the glass over time. These structures are also seen in micrographs of other oxidation samples by other researchers but never commented upon.

The phase separation of the MoO_3 spheres within the glass are also concentrated more near the outer surface implying buildup of MoO_3 is greatest near the surface. In that case diffusion of MoO_3 may be fast but it's not being adequately removed from the surface. This could be due to stagnant environments leading to buildup of MoO_3 gas near the surface which causes a backup of MoO_3 within the glass near the surface. Alternately the MoO_3 may be present and diffusing out but the glass is most viscous near the surface due to boria evaporation resulting in reduced mobility in that zone.

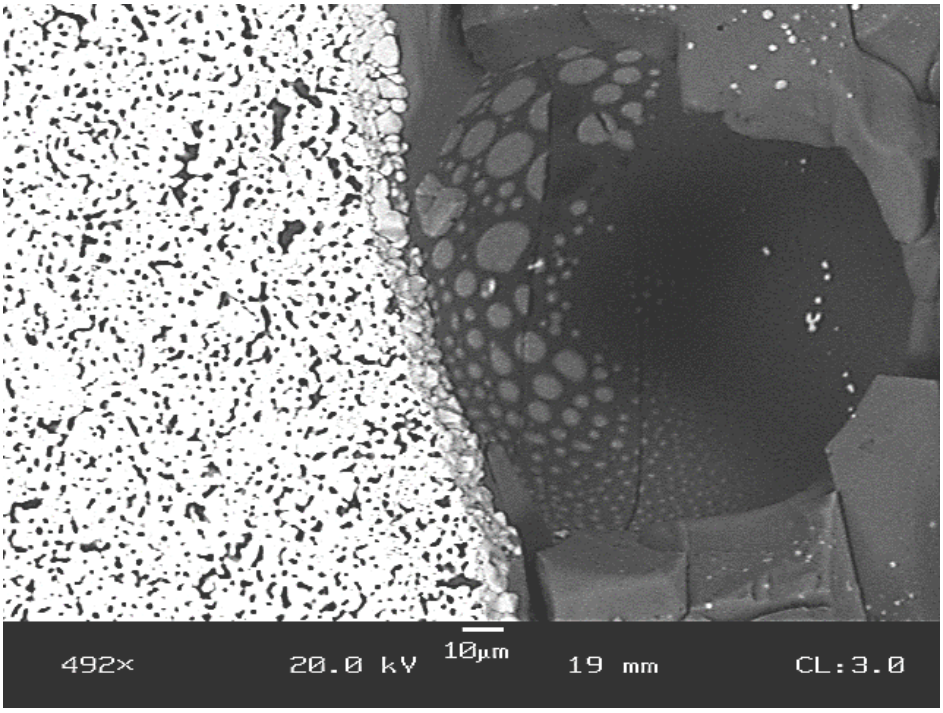

Figure 7.22: SEM detail of a bubble in TC2421+1.5Mn after oxidation at 1300°C for 90m.

A bubble is shown in Figure 7.22. Apparent liquid-liquid immiscibility can be seen occurring at the base of the bubble; possibly between $MoO_{3(l)}$ and glass. Since the temperature was well above the boiling point for MoO_3, the vapor must be saturated within the bubble and condensing upon cooling.

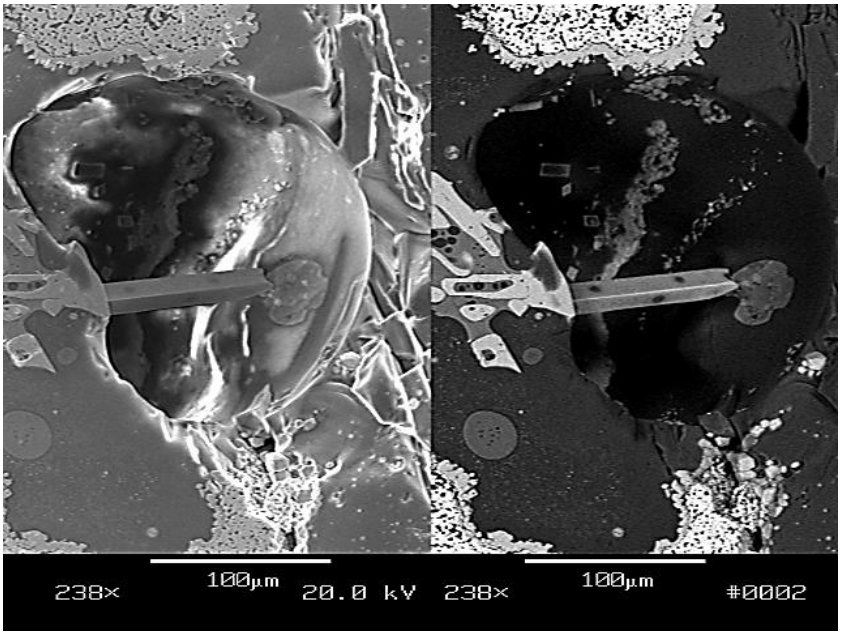

Figure 7.23: SEM detail of a crystalline needle growing in TC2421+1.5Mn after oxidation at 1300°C for 90m.

We also observed a large single crystal growing into a void (Figure 7.23). To have grown to such a large size, (it's even macroscopically visible) could not have happened during cooling. The needle must either have grown in the glass and the void formed around it, or it grew by a slow steady vapor transport mechanism. If it were the second case, the void must have been present and stable for a long time. In the background extended from its tip is a region of phase separated liquid, and at its base there's a lot of liquid-liquid phase separation occurring.

Also in the background some similar rectangular crystals are growing. There are at least 3 separate liquid phases; molten phases may include MoO_3, $MnMoO_4$, MoO_2, and/or various compositions of glass such as B-rich vs. Si rich separation. The high brightness on the background crystals and in the large crystalline needle implies that they are Mo containing, and probably $MnMoO_4$. There's also a row of MoO_2 crystals visible

along the surface of the bubble which may be oxidizing to volatile MoO_3 and would be supporting the bubble/void.

The images and oxidation show a strongly crystalline nature, and formation of cristobalite and manganese molybdates, along with MoO_2 being present. The glass is not cutting off oxidation; instead it is limited to a slow diffusion through fine pores in the crystallized coating. It did form a glass at first but that seems to have mostly crystallized by 90 minutes.

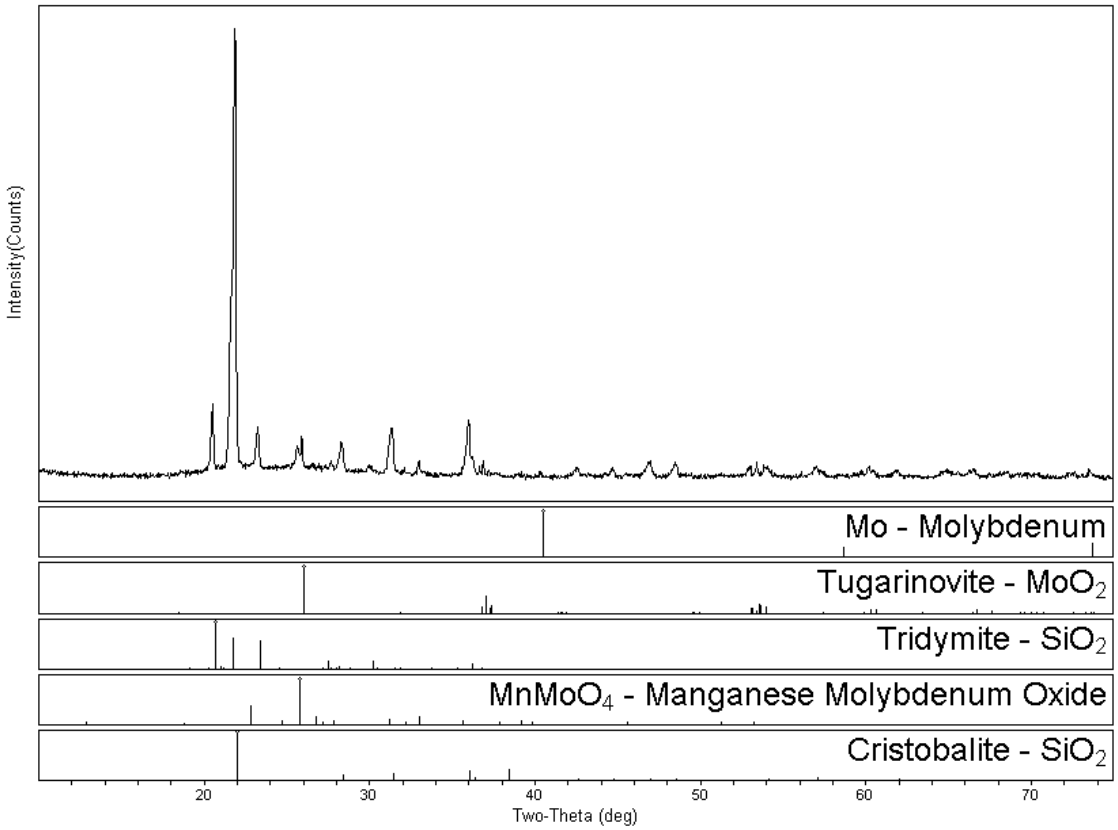

Figure 7.24: TC2421+1.5Mn XRD scan of oxidized surface.

XRD (Figure 7.24**)** shows the usual Mo and MoO_2 peaks, as well as Mn molybdate ($MnMoO_4$). Devitrification of crystalline peaks for cristobalite is also evident, but it doesn't seem to affect the performance as detrimentally as for the Fe-containing case. Also interesting, there's definite tridymite peaks in addition to cristobalite.

Of the Mn, Fe, Co, Cr and Ni samples Mn showed the most promise, but still has issues of phase separation and devitrification. The varied problems in each case however may each be avoided at lower loading contents. Because the oxidation protection provided by Mn was very good (weight loss of 3.0 $mg/cm^2/hr$ at 1300°C), this work was expanded. To reduce devitrification and molybdate formation, the Mn contents were reduced from 1.5 wt% of the molybdenum to 0.5 and 0.25 wt%.

In industrial glass batching, alkaline earth and transition metal oxides and alumina modifiers are frequently added, especially in borosilicate glasses. These act to partially counter the viscosity reduction from fluxes and also to stabilize the glass.[55] In the previous chapter we added various alkaline earth silicates as glass sources which proved unsuccessful, but they may be beneficial to stabilize the glass when added also in small amounts. 1 wt% of SAS was added and an equal amount of T2 was removed for the compositions with 0.5 and 0.25 wt% Mn.

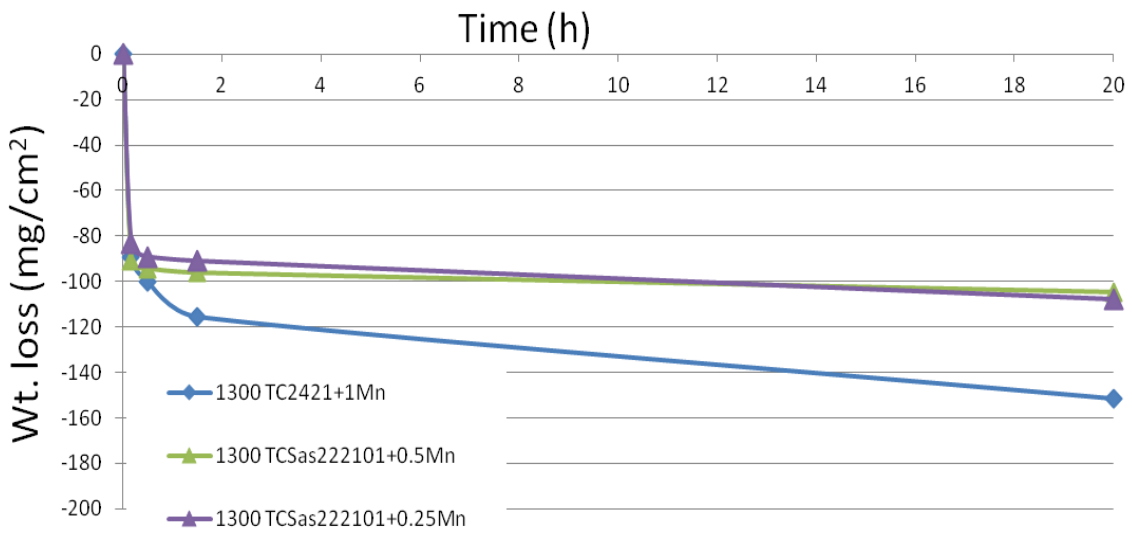

Figure 7.25: Weight loss curves for TC samples with trace SAS added in addition to Mn

The oxidation results of these samples in air at 1300C are shown in Figure 7.25 . The reductions in Mn content and additions of SAS produced much improved oxidation rates. In each case around 100 mg/cm^2 is lost from the surface to produce the protective glass layer. All have rapid but short transient losses near 100mg/cm^2 and after forming a protective glass layer oxidation rate reduced dramatically. The short term rates between 10 and 30 minutes and long term rates between 30 and 90 minutes are given in Table 7.2. At 0.5at% and for 0.25at% Mn + SAS, long term oxidation rate was reduced to only -1.8 mg/cm^2/hr. The best performance was achieved for the sample containing 0.5 at% Mn + SAS, for which the 30/90 rate improved further, to an oxidation rate of only -0.4 mg/cm^2/hr between 90m and 20h. This is an order of magnitude better than the previous best oxidation protection and excellent protection compared to any in the literature for in-situ oxidation protection of MoSiB type alloys.

Table 7.2: Weight loss rates for TC samples with Mn, comparing initial loss between 10 and 30 minutes, and long term rates measured between 30 and 90 minutes. Rates listed are calculated linear rates in mg/cm^2*hr.

T (°C)	#	10/30 rate	30/90 rate
1300	TC2421+1Mn	-32.82	-15.57
1300	TCSas222101+0.5Mn	-10.70	-1.82
1300	TCSas222101+0.25Mn	-17.17	-1.83
1200	TC2421+1Mn	-7.47	-1.74
1200	TCSas222101+0.5Mn	-16.55	-0.80
1200	TCSas222101+0.25Mn	-27.22	-2.39

It should be noted however that the microstructure still contains a silica glass distribution in the Mo matrix with a number of lens shape morphologies. The connected glass will reduce ductility and needs to be addressed before further mechanical testing is pursued.

Metallographic examination of the ground surfaces of the two Mn/SAS samples at 1300°C showed that the glass layer covered the exterior of the pellet with a thickness of ~ 10-20 um. The glass layer on the ground surfaces for samples with 0.5 and 0.25 w/o Mn, plus SAS, are shown in Figure 7.26. The glass layer is quite ideal, it has a thin layer of glass on the surface above a layer of MoO_2 and internal oxidation is present as well indicating very low pO_2 below the protective glass layer.

(a)

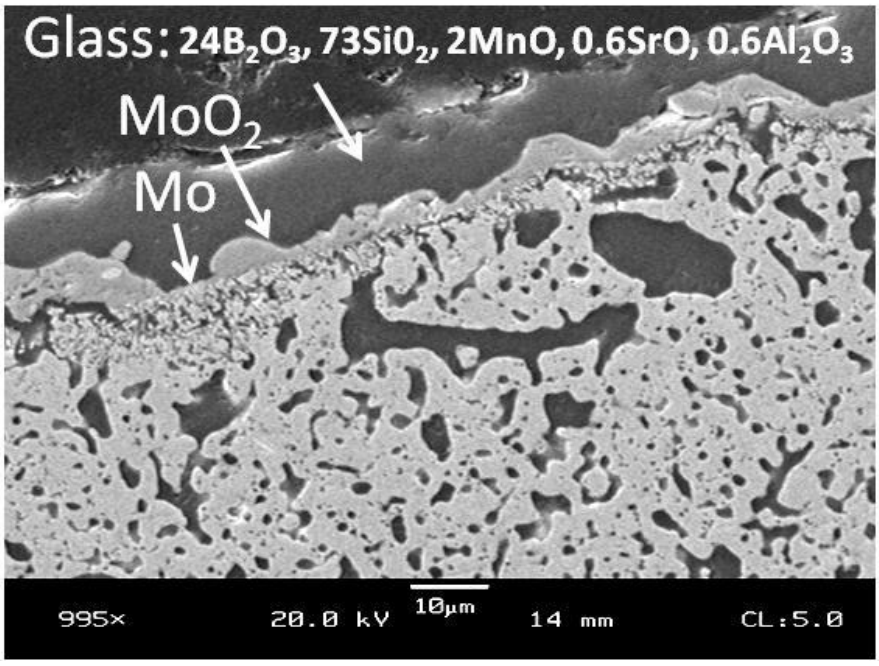

(b)

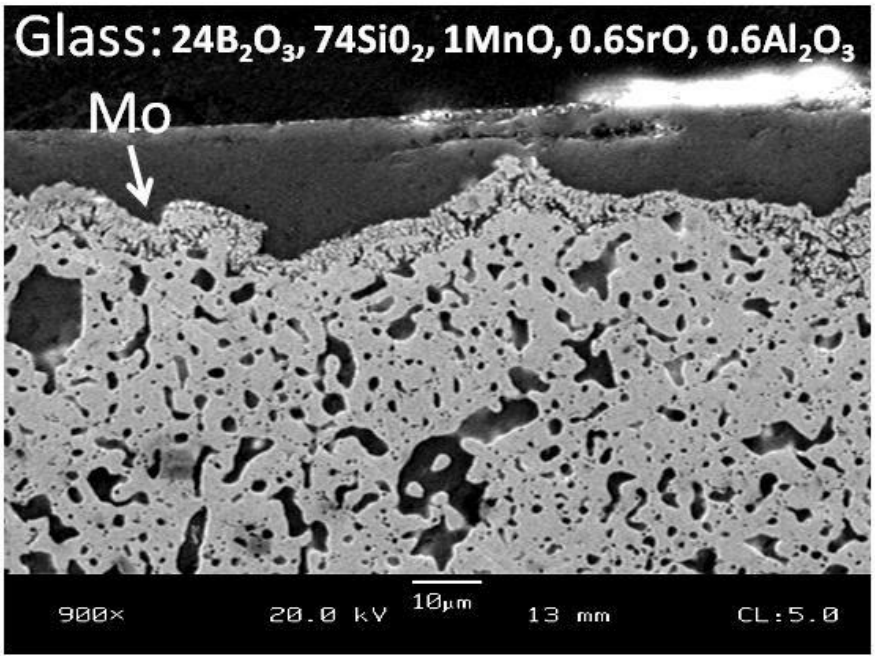

Figure 7.26: Metallographic examination of the ground surface of Mo-T2-SiO_2-Mn-SAS pellets with (a) 0.33Mn & 1.0SAS and (b) 0.17Mn & 1.0SAS.

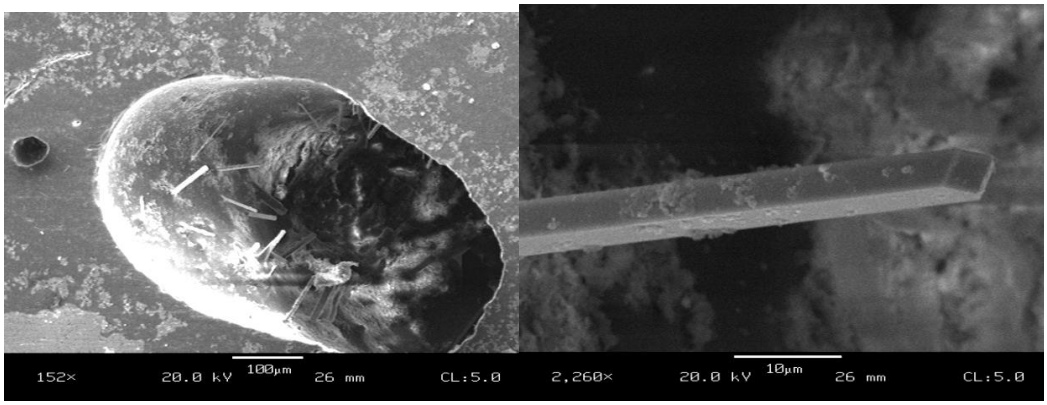

Figure 7.27: Detail of whiskers growing within a void in the glass coating of TS with Mn and SAS

Again in voids within the glass we saw needles growing into the voids; nice monocrystalline whiskers. We only see those with the Mn, and only growing into voids in the glass. The $MnMoO_4$ and MoO_3 phases are monoclinic which could grow into that sort of needle shape, and may be growing by vapor deposition or possibly within the glass which has receded around it, so that they are only visible in the voids even if they're present throughout. The shape and lack of visible needles elsewhere suggests that the needles grow into the bubble, which would imply that the bubbles are stable for a long time.

7.3.4. Discussion of Oxidation Additives

The alternate behavior of Mn may be due to its reaction in the glass, and its similarity to Fe seems to imply that the differences between the quaternary additions is not dependent on the location of the addition (Fe in A15 vs Mn, Co, Cr in Mo_{ss}) but rather their relative and varied effects on the glass properties. In all cases there is phase separation and crystallization which may be moderated by simply lowering the additional

element's fractions. The Mn fraction may also be lower than intended in the fired samples, due to its well-known volatility issues.

The transition metals added (Fe, Ni, Mn, Cr & Co) unlike the alkaline earths added previously with the high SAS compositions don't appear to have the same effect on reducing Mo contents in the glass nor the corresponding reduction in wettability. In fact the Mn-containing samples formed molybdates and still showed excellent surface coverage.

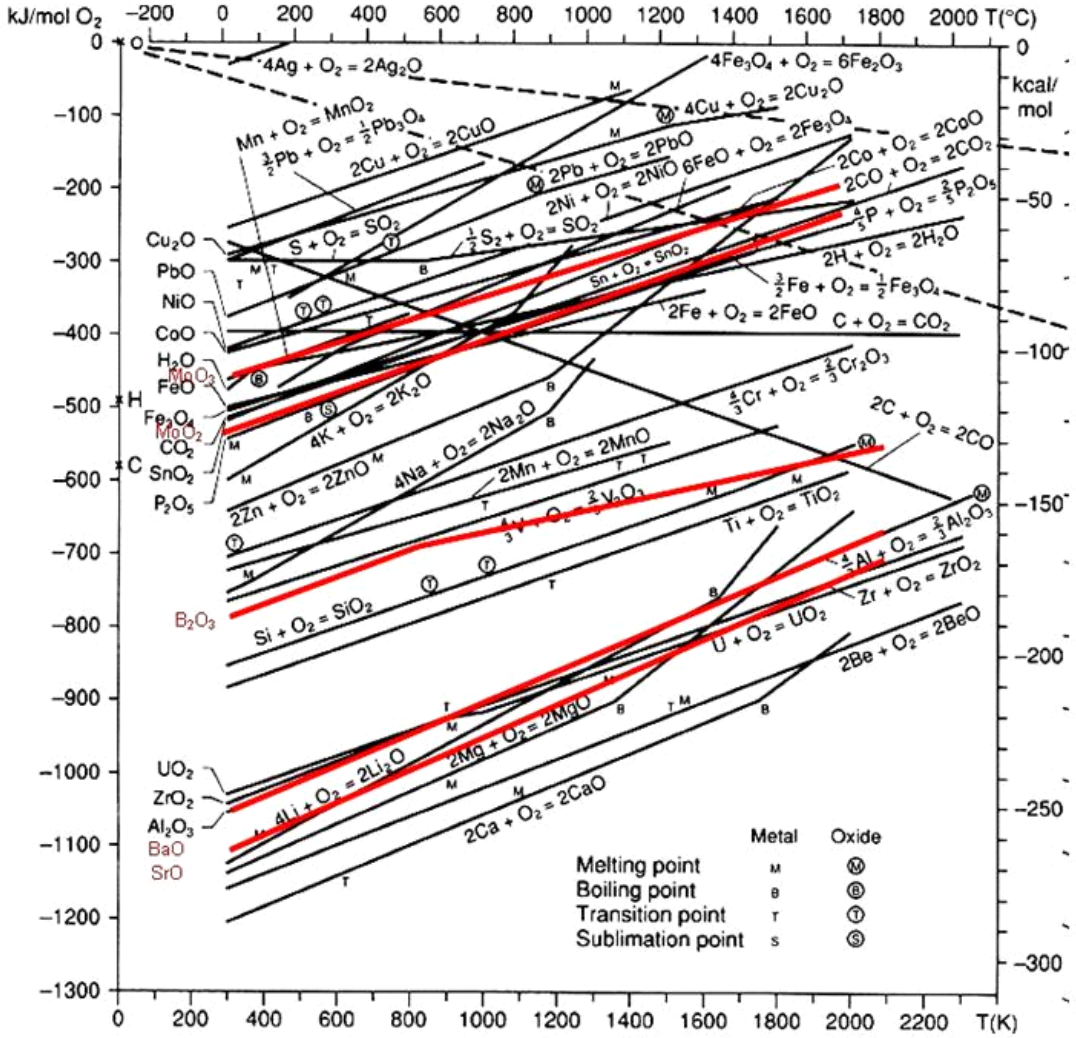

Figure 7.28: Ellingham diagram of relative stability of oxides.

Perhaps we can begin to understand the effects of added elements by studying their relationship with oxygen partials on an Ellingham Diagram (Figure 7.28). If we look at the Alkali and alkaline earths, Li, Ba and Sr metal form more stable oxides and will reduce even the silica, likewise they readily form stable molybdates. The transition metals fall closely around Mo in terms of their oxidation equilibrium, and they affect the glasses differently.

Cobalt oxides are less stable than the Mo, so Mo oxide should form before cobalt oxide. Cobalt also acts as an effective flux. We saw a very violent bubbling as mentioned above, and presence of cobalt oxide. For Ni, the Ni oxide is also less stable than the Mo oxides, and only forms in the higher pO_2 regions at the surface of the glass, which we have seen.

For Fe and even more so Mn and Cr, the Mo oxides are similarly or more stable, and you get the oxides forming within or below the glass at the surface; either just above the MoO_2 interface, or just below in the case of Cr and Mn. For Cr and Mn, the oxides were seen in the XRD patterns in relatively high weight fractions and appear to be forming on surfaces. MoO_2 and Cr_2O_3 were both present and detectable in the Cr containing alloy. The green tint on the surface is caused by the green Cr_2O_3 oxide and shows crystallization from the melt, diffusion and oxidation of chrome to the surface, and possibly volatilization and reprecipitation of Cr_2O_3. There is also a lot of Cr_2O_3 in the glass. In ceramic glaze chemistry Cr is added only in low amounts; Cr should be less than 1 mol% to avoid adversely affecting and devitrifying the glass. Additional Cr above 1 mol% forms Cr_2O_3 within the glass rather than contributing Cr ions modifying the glass.

7.3.5. Lower Co Compositions

More samples of Mn and SAS were prepared to investigate possible further improvements in oxidation protection, and to begin trying to improve the microstructure and remove crescent shaped silica regions. The later compositions surrounded the best Mn + SAS compositions and tried both higher and lower Mn and higher or lower SAS contents; however each one was vastly inferior to the previous good Mn+SAS samples tested before. We then tried to recreate the original 0.5Mn + SAS composition, yet every later sample containing Mn lost the excellent protection we'd seen before.

It was noticed that the shift to poor oxidation performance for identically batched samples corresponded directly with the use of a new tube in the firing furnace. It is expected that the prior tube had leaked and allowed a depleted surface that gave lower B contents at the surface. The TCSas222101+0.5Mn successes appear to be due to artificially increased Si: B levels, and afterwards we had gotten much better atmosphere control in firing which lead to a disappearance of these successes. The newly repaired tube will require re-examining a broad range of compositions to recreate the good results. The unbroken tube does give much better consistency in the results and allows reproducible results with an actual composition rather than trying to predict a depleted composition or relying on grinding to remove the altered surface layers, which itself introduces inconsistencies.

Unfortunately with the improved atmosphere, the Mn, which previously had probably at least been partially oxidized and thus stabilized, is now present as the elemental metal. In order to be stable, Mn metal must react and enter the Mo_{ss}, a slow process controlled by slow diffusion in Mo. Otherwise it melts as Mn metal and

volatilizes away. Measuring the dewpoint gives a measure of the oxygen partials during firing, and with the new tube our dew points have been lowered to levels where the Mn oxides are reduced to pure metal. This is causing uncontrolled loss of Mn, which prompted a move to Co instead as the quaternary glass modifier.

Co was examined before with the initial investigations into quaternary additions, and is one of the additions addressed in the Woodard patent. It had been added at a level of 1.5at% and discarded for the excessively dramatic reduction in viscosity observed, in favor of the much better performing (and not patent protected) Mn. Co in lower levels should be able to provide the same longer-term reduction in viscosity necessary to provide the protection seen with the first Mn samples, those before the atmospheric controls were optimized. The Co is not volatile and should be less irregular and allow good control and reproducibility.

Co was brought back into focus at only 0.5at% instead of the previous 1.5. The first composition examined was a traditional Mo-A15-T2 AT3315, one which had seen optimal performance previously with Mn. Further compositions proceeded toward higher and higher Si contents which saw consistent improvements. It makes sense in light of the first Co and Mn samples where we saw large reductions in viscosity with Co that the new Co samples will require a higher viscosity borosilicate to be successful.

So far many of the samples have shown promising improvements but none have been as good as the original Mn samples. The cobalt appears to be suffering from crystallization and failure as well, and possibly phase separation. In many samples a fine initial coating with blue tint develops over the surface and looks good, but a bubble/pore filled appearance slowly grows across it. Within a half hour the surface becomes pocked

with collapsed bubbles and is no longer flowing. The coating is inadequately protective, and the long term rate settles around 10-50 mg/cm^2*h.

This prompted another comparison of polished vs unpolished and ground vs unground samples again. The ground samples so far have been uneven and perhaps the depleted layer and depletion regions exist at uneven depths and this has led to surfaces still not truly representative of the bulk. After grinding ~100μm of each of the surfaces there is very little change except in the very first transient losses. Generally the differences are all resolved within half an hour and the final performance is mostly unaffected by surface treatment.

7.3.6. Flow/Furnace Effects

In addition to grinding and surface effects, during the last set of oxidation testing a surprising effect was noticed. Another researcher was using our furnace between our oxidation testing. When oxidation tests were run after he had used the furnace, the weight losses were lower than for samples tested consecutively of our oxidation samples. This has been attributed to the buildup of MoO_3 in the furnace environment, which as it builds up it negatively impacts the ability of samples to form adequate oxidation protection. The Keith furnace that had been used was a bottom loading box furnace with a space of ~1.5 ft^3. It has a nearly 20mm opening at the top for the thermocouple which also acts as a sort of vent. During oxidation testing, MoO_3 vapor could be seen as a hazy yellow smoke escaping from that hole, and MoO_3 needles were growing where the vapor met the cooler lab air. This had been largely ignored until it was noted that the previous furnace uses affected the oxidation properties.

It was proposed that between consecutive MoSiB oxidation tests in the stagnant box furnace, MoO_3 would build up within the furnace to a point that MoO_3 pressures were becoming excessive around the samples. This could lead to condensation of MoO_3 in the glass, which disrupts the sealing ability of the borosilicate. A certain amount of MoO_3 must be removed in order to create a glass of sufficient depth and continuity to move into parabolic oxidation kinetics. Condensed $MoO_{3(liq)}$ could hold open the pores and channels in the glass while $MoO_{3(gas)}$ forms a diffusion barrier for oxygen coming in and the oxygen available in the furnace is used up. B_2O_3 continues to evaporate but little additional glass is able to form because of the decreased oxygen availability, and so the glass stiffens before it is able to seal. As a result we see an inability to form a good coating in the closed box furnace. Further the box furnace is much less representative of the end-use environment which would be flowing and open in a turbine rather than the limited stagnant air in the oxidation furnace.

Test samples were then made and tested using a tube furnace which has much better flow and consistently the same compositions would perform better in the tube furnace vs. the box furnace. Two T2 + cristobalite samples modified with manganese and strontium-aluminosilicate were compared for the bottom loading Keith box furnace versus samples in the tube furnace under different air flow conditions, the results are shown in Figure 7.29 below. Since the sample is cooled slightly the furnace hold temperatures were adjusted for the changes associated with moving air. In the image "1250 Moderate" had a moderate air flow around 100cc/min and a set point of 1250°C, which results in thermocouple readings at the sample location between 1200 and 1250°C. The other two were adjusted to give thermocouple readings as near as possible to

1300°C, “1350 Slow” had a setpoint of 1350°C and a flow rate of 10cc/min, and “1375 Fast” had a flow rate of 500cc/min and required a 1375°C setpoint to keep sample temperatures near 1300°C.

The worst oxidation resistance was seen in the bottom loading box furnace set to 1300°C, labeled as “1300 Static”, which has very limited air flow. Sizable improvements in oxidation rate are seen in the three flowing conditions: a sample temperature between 1200 and 1250°C under moderate air flow, sample temperature between 1250-1300°C under slow air flow, and sample temperature between 1250-1300°C under fast air flow. Under the more aggressive oxidization conditions, higher temperature and faster air flow, both samples show a significant increase in initial transient loss but, surprisingly, a greatly reduced long-term rate between 90m and 20h and onward. This occurs in MoSiB materials because the increased initial weight loss is associated with a thicker borosilicate surface layer that will slow the oxidation during parabolic behavior.

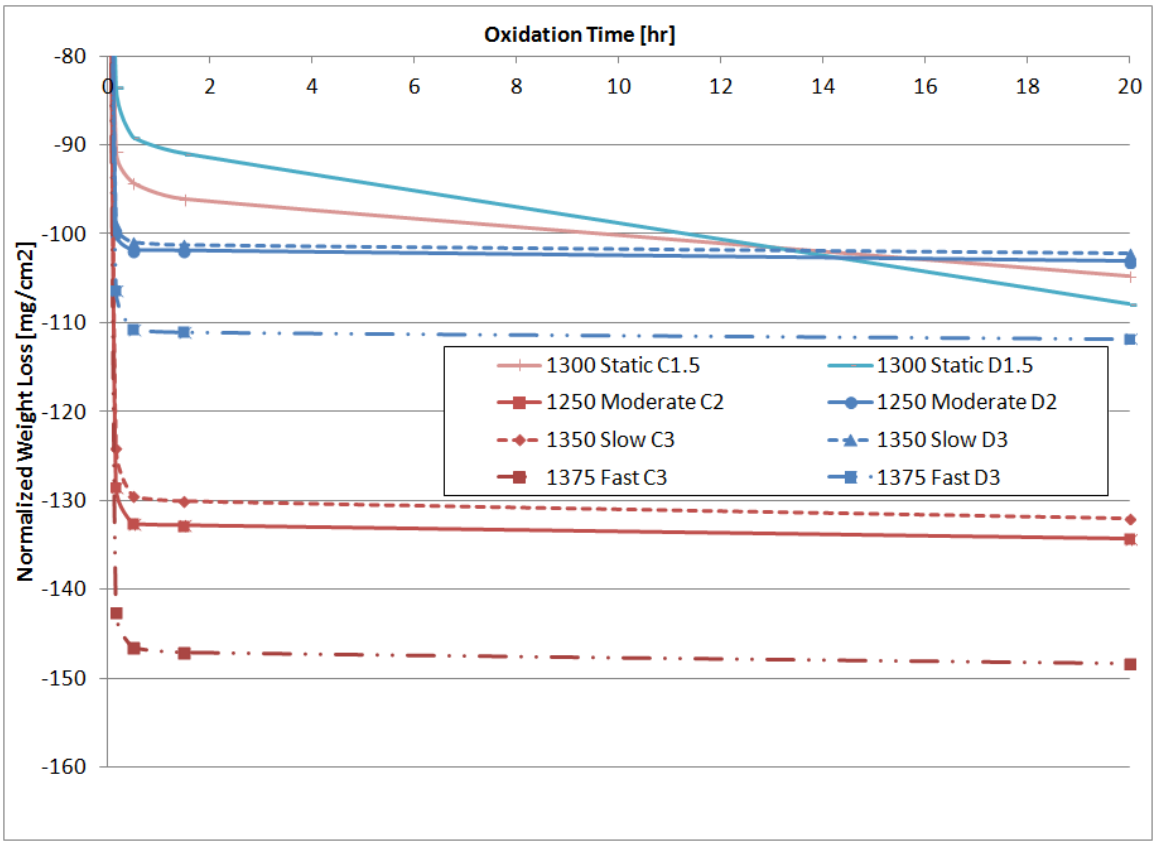

Figure 7.29: Weight loss during oxidation of two Mo-T2-Cristobalite samples under various air flow conditions. The furnace temperature was adjusted to keep the samples close to 1300°C in spite of forced air cooling effects.

The oxidation testing in flowing air was also done for 12 samples of the T2 + A15 type. These samples covered a composition range of Si/B atomic ratios from 1.4 to 3.7, and modification with cobalt, yttria and manganese at levels of 0.3 to 1.5 mol% in the equivalent glass. In these tests, a moderate air flow was used with the furnace heated to 1375°C to counteract the forced cooling and achieve a steady state sample temperature of nearly 1300°C. In all samples other than the lowest Si/B yttrium modified composition, the oxidation in a flowing atmosphere resulted in higher initial weight loss but greatly reduced long term oxidation rates. Previously cobalt and yttrium containing samples were

only able to be oxidized for 90 minutes due to the onset of devitrification and spallation. The improvement under flowing air allowed for surviving up to 20 hours and beyond.

CHAPTER 8.

OXIDATION DISCUSSION

One of the biggest hurdles in the MoSiB system, and one which we've repeatedly tripped over is the oxidation resistance. When comparing to other oxidation resistant alloys, protection can rely on a number of options. Some metals form stable oxide coatings themselves which protect the surface, others such as stainless steels rely on added elements in the system which provide a protective oxide layer. The Molybdenum silicide systems are most nearly of this sort, but differ in a number of ways.

8.1. Wagner Theory of Oxidation

The Wagner theory of oxidation discussed in Chapter 2.2.6.2 is one of the simplest explanations of oxidation of a scale forming metal. In the Wagner theory, chemical equilibrium is established at both interfaces of the scale, and thus establishes an activity gradient across the scale of interposed oxygen and metal cations which then migrate in opposite directions and form an electric field mitigated by the opposing migration of electrons. Cation, anion and electron migration must be balanced so no net charge transfer occurs.

This gives different possible oxidation modes which apply generally to silicide intermetallics. If inward diffusion of Oxygen in is greater than diffusion of silicon out, both silicon and metal are oxidized internally and there is total oxidation of both metal and silica. However if Si transport out through the scale is faster, it results in selective oxidation of the Si which forms SiO_2 scale from the surface as seen in the $MoSi_2$ case.

The Wagner theory can be used to understand oxidation in many scale-forming metal/metal-oxide systems, but falls short in the Mo systems on a number of counts. It

assumes a perfect even and compact scale, ion/electron migration is rate controlling, equilibrium is established at both the oxide/metal and oxide/air interfaces and locally throughout the scale, no deviation from stoichiometry, and neglects oxygen solubility in the metal.

The MoSiB scale cannot be treated as a perfect, even, compact and perfectly adherent scale. This is because the scale is formed not from the surface of the metal itself, but rather from reaction of the secondary phases, which must then flow over the other surface and takes time to form a scale. Additionally the concurrent evaporation of MoO_3 from the bulk as well as from reaction of the intermetallics must be considered. Instead of a homogenous bulk metal oxidation, local inconsistencies in phase distribution do not inherently meet the criteria of an even and perfectly adhered scale. Also as oxidation proceeds, bubbles and pores may exist in the scale thus interrupting the requirement of a compact scale.

Also in the MoSiB case, ion/electron migration is not fully understood. It's assumed to be the case that the oxygen migration is rate limiting, at least once the scale has formed neatly. Migration of MoO_3 out and its subsequent evaporation and gaseous diffusion from the surface are also very important.

Further, the gas/oxide interface may nearly approach equilibrium, but the environment of the gas/oxide interface also varies. For example, changes in flow rate can drastically change oxidation kinetics by affecting supply of new oxygen and removal of MoO_3 vapor. At the metal/oxide interface the equilibrium takes some time to be achieved as the scale spreads and growth is inhomogeneous. Migration of Oxygen can in certain cases be greater than MoO_3 out, resulting in nonequilibrium excess of MoO_3 which may

then form vapor bubbles, condensed liquid pockets, or an oxide layer under the silicate scale. The formation of a MoO_2 interlayer which disappears with longer times indicates a changing equilibrium state as well.

Additional difficulties exist due to the variations in glass composition throughout the scale from differences in distribution of B and Si containing phases, the reaction and homogenization between the high B and low B glass, volatilization of B_2O_3, oxygen excess or deficiency, and liquid phase separation occur. Also the solubility of oxygen in molybdenum is significant, and the internal oxidation and reaction of the Si and B in the second phases below the metal/scale interface is non-negligible and contributes to the overall oxidation behavior by forming new glass internally.

As a result, Oxidation is very difficult to approach because of the very convoluted inter-relations between the many many variables affecting its behavior. It's well understood that the glass viscosity is important, and has repeatedly been noted that viscosity should be low enough to flow in order to form a complete coating, but high enough to limit oxygen diffusion once formed. Further it's also well known that the viscosity is directly dependent on the composition – which in the simplified borosilicate system here can be described as a ratio of Si:B. While these assumptions may hold generally, there is a much greater complexity that's being ignored, for example, the viscosity changes obviously with temperature, but nonlinearly. The composition and thus viscosity also changes with time due to evaporation of boria, and the rate of that viscosity change also changes with temperature. Beyond that, the actual compositions are difficult to gauge because of uneven loss of B and Si from the surface in processing, not to mention the relatively large local inhomogeneity inherent in the microstructure. Partial

pressures of the combined volatile MoO_3 and other vapor species reach 1atm around 1150°C which could lead to bubbles. The formation or suppression of bubbles varies as the partial pressures of the gas phases change, and in turn these factors affect and are affected by the changes in viscosity and composition. There are complications regarding devitrification at varying temperatures and under the repeated heating and cooling cycles that these pieces undergo and spallation may occur as well.

8.2. Viscosity Estimation

Attempting to estimate the behavior of a glass based on viscosity and composition, we find the chemical dependence of viscosity is extremely complex. Minority components and impurities, humidity and water, and even the redox state of the furnace atmosphere can have significant effects. We typically disregard these when examining our various MoSiB compositions and assume they remain essentially constant; however this may not be a valid assumption.

Considering viscosity changes with temperature, molten glass flow can generally be taken as a transport process within a non-associated liquid, activation energy for flow based on Frenkel's equation can be assumed, and Arrhenious behavior is followed. On cooling however as the liquid becomes a more and more associated glassy network, the activation energy for viscous flow strongly increases in its temperature dependence. The Arrhenius behavior deviates from linear and the widely accepted Vogel-Fulcher-Tamann (VFT) models deviate from actual behavior due to the effects of time dependence and viscoelastic relaxation, and there is no comprehensive model based on principles. Instead, many calculators and models exist based on experimentally derived fits for various compositions relevant to glass production. Unfortunately the composition ranges rarely

include anything free of soda (Na_2O), which is not a viable additive in our system, nor do many allow for boria contents as high as we typically use. Further the additional minor elements we add introduce distinct changes in viscosities that are not represented in any empirical models to date.

We see repeatedly that the initial losses are affected simply by the grinding of the outer layer and behavior across cut faces compared to the fired surface varies. This illustrates the difficulty in estimating the properties based on batch composition, since only with the later samples were we observing a ground or cut-face response representative of the bulk. In the others what we observe is an initial response that reflects the outer surfaces' depleted composition. In some cases it oxidized well past and into the bulk, but in others the varied glass composition may have persisted even once the oxidation front had receded into the bulk composition. It's not even possible to apply relative correction factors because the depth of depletion and ratio of depleted phases varied by sample. On some the silica depletion may have been higher or lower than the boron so the effects are not even consistently in the same direction; some had higher viscosity depleted layer than the batch while others were lower. We must then consider the mechanisms of oxidation using what we do know, and look beyond just defining behavior by composition alone.

Measuring actual viscosity directly is also not a valid option because the temperatures of interest are high for many typical viscometers, and in order to recreate the as-formed compositions for viscometry the composition could only be estimated considering loss rates of volatile molybdenum and boron oxides is uncertain and because of the varied depletion of glass formers (borides, T2 and silica) from the surface. In

practice it's much simpler to observe the effects of composition changes on actual samples and relate that back to viscosity, and to approximate values from the equations despite the errors involved.

Composition still remains one of the simplest descriptors of expected oxidation properties. Specifically the overall Si:B ratio at least generally defines the viscosity of the melt which forms the protective coating. As previously discussed, a specific balance must be met of high viscosity for long term protection and low enough viscosity to coat the surface, and it must suffice to estimate the properties from what we can remove from the variables (such as grinding surfaces to remove depletion) and what we can know of the processes and the many variables involved including temperature, environment and more.

8.3. Transient Oxidation

When we observe the oxidation of the test pieces, we look at weight loss versus time with the goal being to minimize the initial transient losses and hasten the shift to nearly flat parabolic loss rates, and also to minimize the long term parabolic rates. Most often when adequate protection is not achieved, it's not due to insufficient long-term rates but rather an inability to escape the transient losses. Example weight loss curves are shown in Figure 8.1. Often the transient oxidation mechanisms dominate the lifetime of a piece, yet they are not well understood and are typically ignored; in most cases the aim is only to shorten the transient regime as much as possible without much effort involving the understanding of how it occurs.

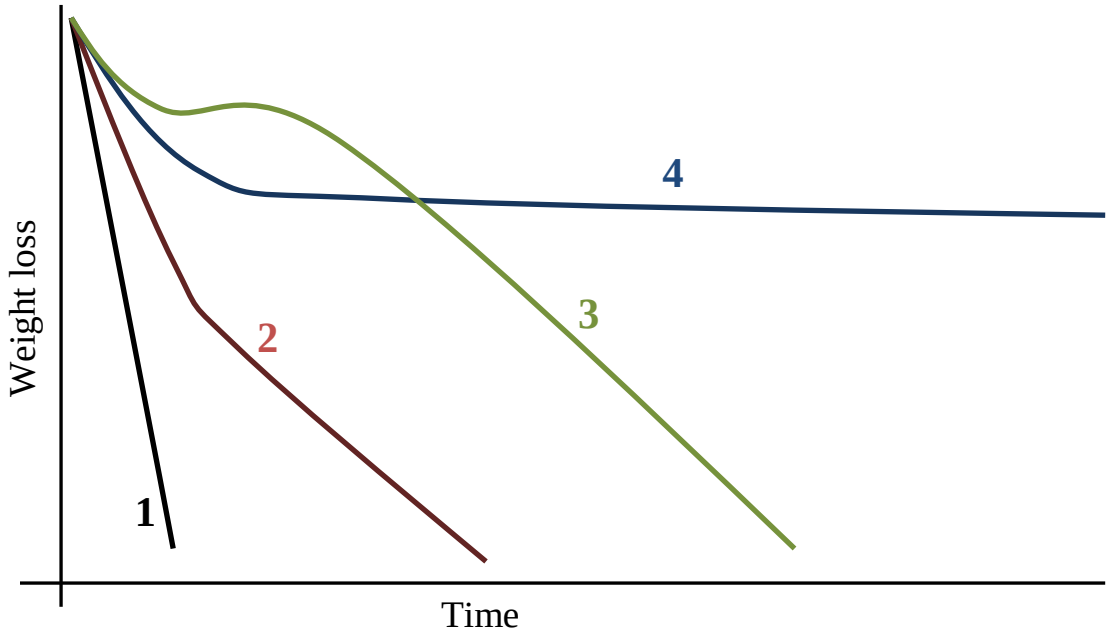

Figure 8.1: Schematic of possible oxidation curves of weight loss versus time.

In many test cases we never see a complete transition to parabolic long term oxidation kinetics. Instead the transient just shifts to a different but still linear oxidation rate which is much too high for long term use. Essentially a complete protective coating is not forming and the transient regime is never fully escaped, leading to a slower but still rapid and linear loss.

Four general cases of oxidation behavior are illustrated in Figure 8.1. Number 1 is the case where no protection is given, and weight loss remains rapid and linear. This is the case for pure Mo, or samples with too little glass or wholly nonprotective glass. The slope can be affected somewhat, with increased flow generally making the rate more rapid or in other cases a nonprotective glass might slow the rate but still remain fully linear. Curve number 4 shows the ideal behavior of a steep initial loss which transitions into a much slower flat long term rate. The transition between transient rapid losses to a

parabolic diffusion controlled rate occurs once a complete protective coating has formed. The curve numbered 2 shows a case where a coating is forming, but the transient regime is not fully escaped. It does not reach an acceptably low weight loss in the long term, but rather continues at a slower but still rapid and nearly linear weight loss with time. This type of curve is often accompanied by either bubbles or channels which disrupt the coating and allow continued oxidation, or a crystallization or devitrification which prevents the flow and sealing of the glass to reach completion. Another possible oxidation scenario is illustrated as curve 3. In this case, a complete coating does form and transitions into a low weight loss parabolic type rate quite quickly. The curve then takes a second turn down however, and loses its protection. This may happen for example, when the initial coating was too thin to prevent further formation of vapor underneath, and there is a spallation of the coating. More often the downturn is associated with time dependant reactions from phase separation as occur with minor transition metal additives such as Fe. The initial coating is rapidly formed within the first 10-30 minutes but phase separates into crystalline silicates or molybdates, and to cristobalite.

In order to transition properly between high initial loss and low parabolic loss like the ideal curve #4, initial protection is formed only if the glass has low enough viscosity to flow over the surface, and if that glass is thick enough to provide a sufficient oxygen barrier. The depth and severity of the oxidation in the scale would depend on surface microstructure, simply by the effects of the different scale formed over each individual phase and local inequality in compositions.

The depth is an important factor to consider, while generally the transient oxidation is treated with the goal of absolutely minimizing it, a certain depth and weight

loss must occur in order to form any glass at all. As the coating becomes complete the partial pressure of oxygen decreases parabolically through the glass layer based on the diffusivity of oxygen inward (Figure 8.2). It develops a pO_2 gradient moving inward, and a MoO_2 layer is formed beneath the glass coating at a depth indicated by the equilibrium pO_2 for MoO_2 formation. The MoO_2 layer is commonly observed in other MoSiB in the literature as well. Through the MoO_2 layer, oxygen partial decreases further until it is so low that Mo is no longer oxidized. The borosilicate thickness grows slowly by diffusion of oxygen inward to react internally with B and Si in the borosilicides. The advance of the internal oxidation front can be observed microscopically which can be seen in the results. The coating is nonprotective until it has reached sufficient depth that the partial pressure of oxygen is no longer sufficient to form molybdenum oxides, as dictated by the equilibrium partials between Mo, MoO_2 and MoO_3.

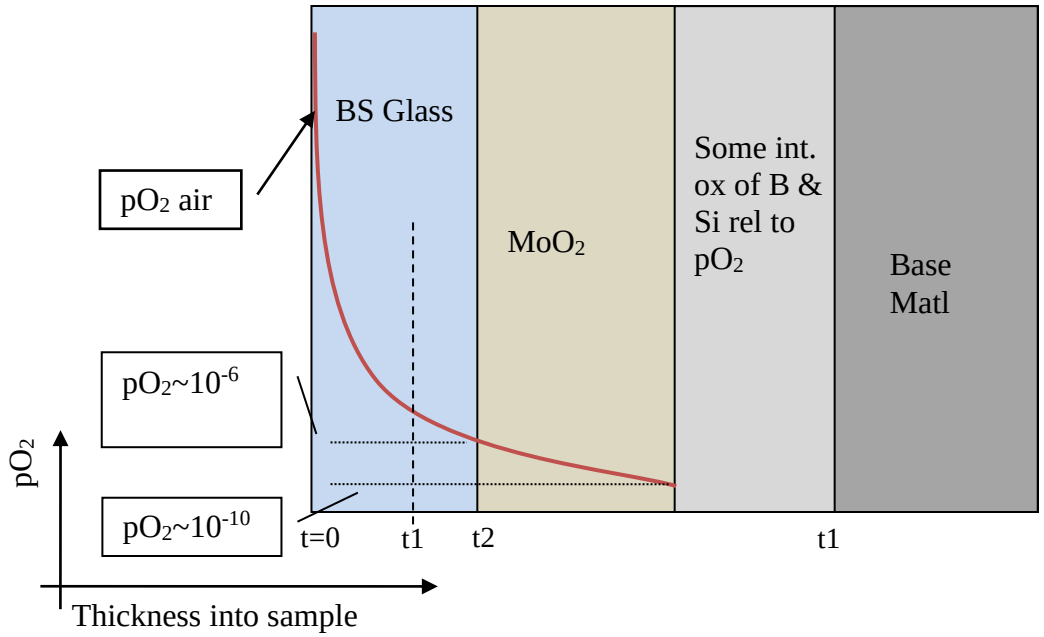

Figure 8.2: Example of the relation between decreasing pO_2 gradient through the borosilicate coating, from the atmosphere to bulk right to left and the internal layers' depth and thickness dependant on the equilibrium pO_2. Equilibrium pO_2 of the interfaces at 1300°C are indicated.

Assuming a coating is formed and complete and oxidation has reached the parabolic diffusion-controlled state, the result will be a multilayered oxide scale. From the outside moving in, you first have the MoO_3-SiO_2-B_2O_3 equilibrium through the glass. As you move inward the pO_2 decreases parabolically according to the oxygen diffusivity of the glass. At the surface, pO_2 is defined by the atmospheric pO_2, as you move inward pO_2 decreases until it is below the equilibrium value for MoO_3 and MoO_2 is the stable oxide phase. The diffusivity changes through this MoO_2 containing layer but maintains still a parabolic decrease in pO_2. As you get further in pO_2 drops to where Mo, B_2O_3 and SiO_2 are in the stable phases, which results in an internal oxidation zone of SiO_2 and

B_2O_3 within the unoxidized Mo. Finally oxygen drops so low that nothing is reacting and no oxides are present.

In the representative Figure 8.2 above; the diagonal line represents the pO_2 moving inward through the scale. As glass forms and reaches thickness t1 from the interface, some coating exists but is not thick enough yet to reduce pO_2 to equilibrium levels between O and Mo or MoO_2. The excess O oxidizes Mo or MoO_2 to MoO_3, which either forms liquid or gas. Once the borosilicate is fully saturated or the vapor pressure is great enough, bubbles may begin to form within.

When the borosilicate is at or greater than thickness t2 it should reach stable oxidation, where all incoming O is converted to MoO_2 at the glass/bulk interface and there's a slow stable recession related to O/Mo transport through the glass.

If T is raised or viscosity otherwise reduced, diffusion of oxygen is greater and its concentration (activity/partial pressure) decreases more slowly, leading to greater excess O at the same thicknesses, and a greater thickness required for equilibrium. Increased oxygen diffusivity increases the thickness required to drop into the next lower regime; for the same glass thickness there would be a higher rate of MoO_3 formation. Also if the diffusivity through the MoO_2 is high enough, you have a shallow decrease in pO_2 and a large thickness before you get to the internal oxidation regime. Likewise a higher pO_2 at the surface will also lead to greater excess O at the same internal depths, and a greater thickness required for equilibrium.

Anomalously however, lower temperature sometimes results in worse failure, for example as was seen with the TQ2713. The viscosity should be higher at lower temperatures and oxidation resistance should improve assuming that a coating has

formed, which at both temperatures a coating had formed. It would be expected that the glass layer thicknesses and MoO_2 content should be less at lower T. This is not what we observed however, and can possibly be attributed to the much higher B evaporation at 1300°C. As a result, after a short time has passed, diffusivity at lower temperatures may actually be higher due to the higher B which remains present in the glass.

In support of that possibility, we notice in the cross-section figure for the TQ at 1300°C (Figure 5.40), the bottom side has thicker glass and MoO_2 layers. Since it was against the oxidation basket, gaseous diffusion is restricted on the bottom side. This would keep B_2O_3 in the glass and lower the viscosity on the bottom side, which is consistent with the B_2O_3 volatility being an important factor in the viscosity, especially so at 1300°C.

The linear diffusion schematic is important in understanding the equilibrium partial pressures through a consistent layer of homogenous glass, but is not representative of the dynamic and incomplete equilibrium in the glasses forming during the change from transient to parabolic weight loss. The glass does not often form an even layer, and the depth and composition (and thus diffusivity) all depend on the local distribution of the bulk phases. It's possible that even once a coating has formed over most of the surface, in some locations the glass thickness is too small or diffusivity of O too high to reduce pO_2 to equilibrium established by the Mo/O_2. Excess O_2 would oxidize Mo or even MoO_2 below the glass which could lead to formation of MoO_3 vapor. This can lead to channels which form through the thin glass over pure Mo regions which may be farther from the intermetallic glass sources, as well as erosion of pure Mo that hasn't been coated yet. Preferential loss of larger pure Mo regions can undercut sections of material. Internal

oxidation of the B and Si below regions of Mo also has a volume expansion that can push out and create isolated islands of Mo and Mo oxides within the glass, which slowly oxidize and disappear as oxidation continues.

When MoO_2 is present as isolated islands within the glass it may indicate that the viscosity is so low and the diffusion so high that the Mo is being undercut and large volume of glass is formed but not protective. Clusters of Mo are left trapped in the glass and MoO_2 layers form around the larger Mo regions. The MoO_2 provides a diffusion barrier and the Mo islands are stabilized while oxygen is readily accessing the bulk Mo via diffusion through the nonprotective glass. In a very fluid glass the movement of oxygen may also be enhanced by convective flow or flow driven by bubble movement instead of just linear diffusion of O inward through the scale.

In addition to being thick enough and of proper viscosity once formed, the completion of the coating itself is often an issue. In many samples we observe channels or pores in the scales. As the coating forms it seals last over the molybdenum phase. This can lead to pore channels, and especially at higher temperatures the vapor pressure of MoO_3 may be high enough to keep the channels open, or to form bubbles underneath. Grain boundaries also can act as fast track diffusion sites and lead to even more MoO_3 production.

Helmick also observed these in his works with MoSiB, and attributes it to the channels left from the evaporation of Mo which are last to fill at grain boundaries. These channels also allow undercutting and regions of much deeper penetration. The image in Figure 8.3 shows a row of bubbles along a grain boundary.

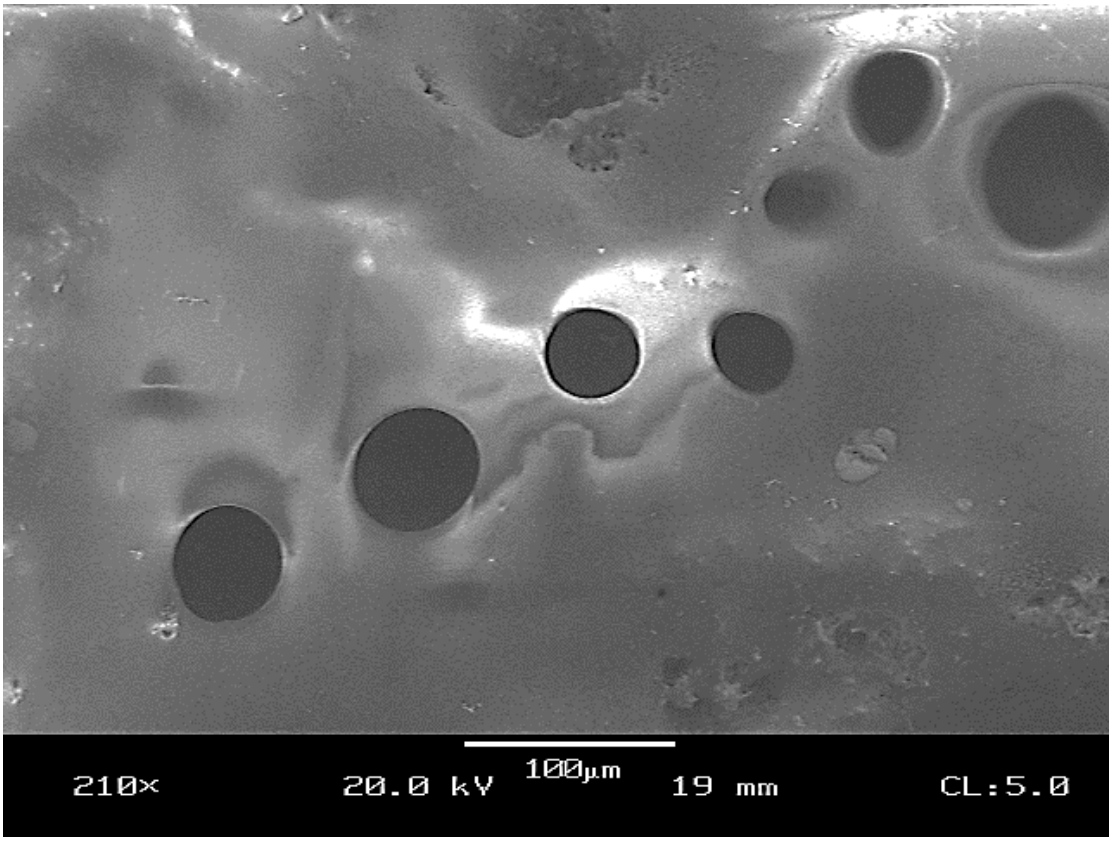

Figure 8.3: Bubbles through the silicate on the surface of BST041523 along a Mo grain boundary.

8.4. MoO_3 Condensation

The formation of channels pores and bubbles often dominate oxidation behavior by preventing a complete coating. Only recently we've also noted the very important effects of furnace atmosphere. It's often said in reference to the transient regime that the "oxidation kinetics are limited only by gaseous diffusion of the reactants in and products out." Typically this is used dismissively referring to how rapid the oxidation is during the transient regime and the actual gaseous diffusion scenarios are just assumed to be more or less instantaneous, however the implications are significant. In the oxidation results of the failing samples, the loss is never getting out of the transient regime; in some

cases the transient region is prolonged or sometimes reaches a slower but still too rapid loss, but never gets fully into the slow steady parabolic state. Atmosphere must then of course be very important in those scenarios. D_{O2} in the glass isn't rate limiting in the transient regime, only in the parabolic, wheareas in the transient regime the oxidation rate is dependent on the exposed area, sealing production of glass and perhaps most importantly, gas diffusion.

Once MoO_3 vapor begins to form it builds up rapidly around the material. When the gaseous diffusion is limited through a thick MoO_3 vapor cloud, the oxygen partial at the surface could dip low enough that the MoO_2 oxide is formed, or the high MoO_3 partial could lead to condensation of liquid MoO_3. These can disrupt the coalescence of the borosilicate glass and prolong the transient regime.

Burke noted the thin layer of MoO_2 which forms under the glass over all of the MoSiB phases and proposed that the MoO_2 forms over the entire surface and is then converted to the MoO_3 vapor, and that the MoO_2 layer's thickness depends on how rapidly the MoO_3 forms and how rapidly the borosilicate can coat over it. Specifically he notes that the more rapidly MoO_3 can be removed from the surfaces, the sooner the borosilicate develops continuity.

Burke suggested that there are simultaneously present MoO_3 and borosilicate liquids, and the high vapor pressure of MoO_3 requires the borosilicate to seal quickly within seconds. In this scenario, MoO_3 is trapped beneath as liquid and forms inclusions and bubbles and eventually leads to the metastable MoO_2 layer. This suggestion may explain why sometimes a thick MoO_2 layer exists under the glass which is thicker than would be expected from growth beneath the glass. Diffusivity of O through solid MoO_2

should be lower than through a low viscosity glass, and MoO_2 should not easily grow under the glass. When we see a thin glass region then thick layers of MoO_2 it may imply that MoO_2 forms early in the oxidation process and is slowly reduced or oxidized away.

As Mo evaporates away, it can quickly saturate the immediate area and MoO_3 liquid begins to condense on the surface. Meanwhile Si and B are oxidized and form a Mo-rich BS glass that must coat over the Mo and any exposed liquid MoO_3. Once it does, it shuts down oxidation and limits oxygen transport; MoO_2 diffuses through the glass as MoO_4^{2-} and leaves the surface as MoO_3 vapor.

. If the glass doesn't seal over it a rapid oxidation continues within and the vaporization of the liquid holds open channels. The glass needs a low viscosity to coat over, but thick enough to prevent turbulence from MoO_3 vaporization. The MoO_3 would also be forming along with the new glass and their ability to separate (or the MoO_3 to leave completely) is important.

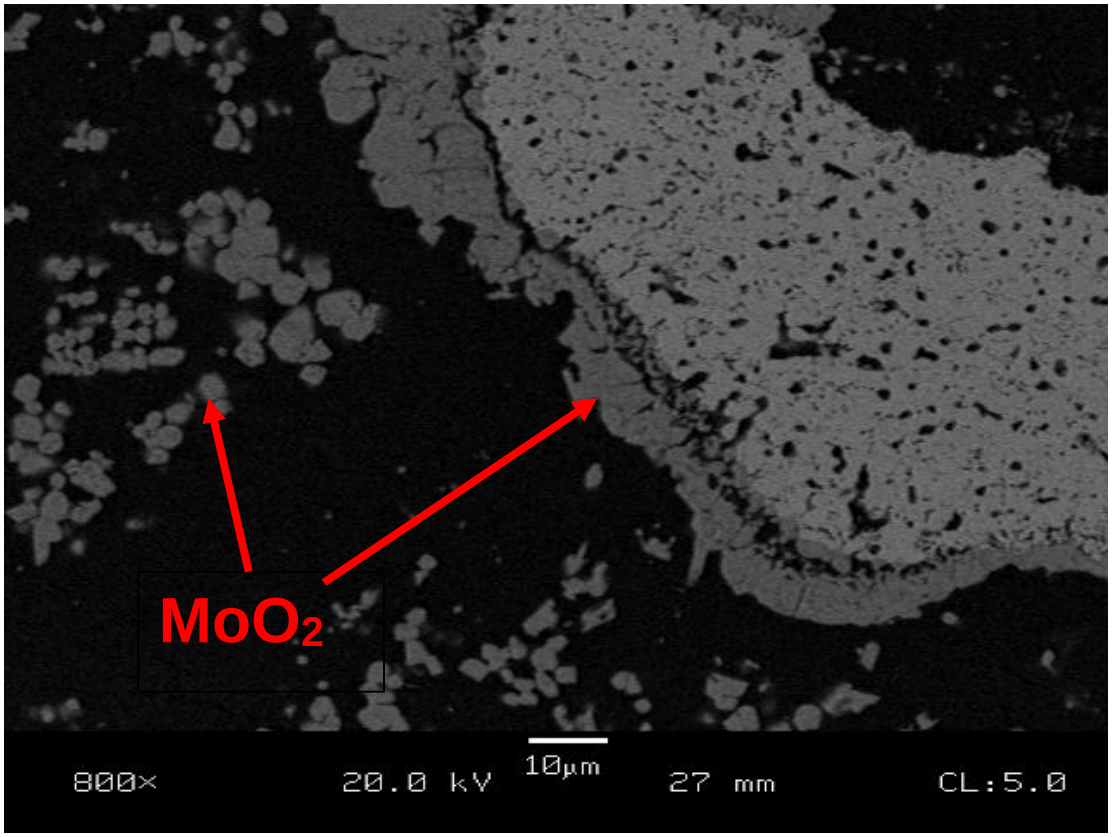

Figure 8.4: Oxidation products showing MoO_2 in the glass and along the bulk interface.

Figure 8.4 shows the MoO_2 layer as well as Mo oxides within the glass. Some MoO_3 may also diffuse into the glass and become supersaturated when cooled. We often see needles and crystallites within the glass. Helmick attributes these Mo oxide inclusions to trapped or condensed Mo oxides, however the needle formation implies growth from within the melt, such as from reducing solubility upon cooling. At any rate there appears to be a significant Mo-oxide content in solution in the glass.

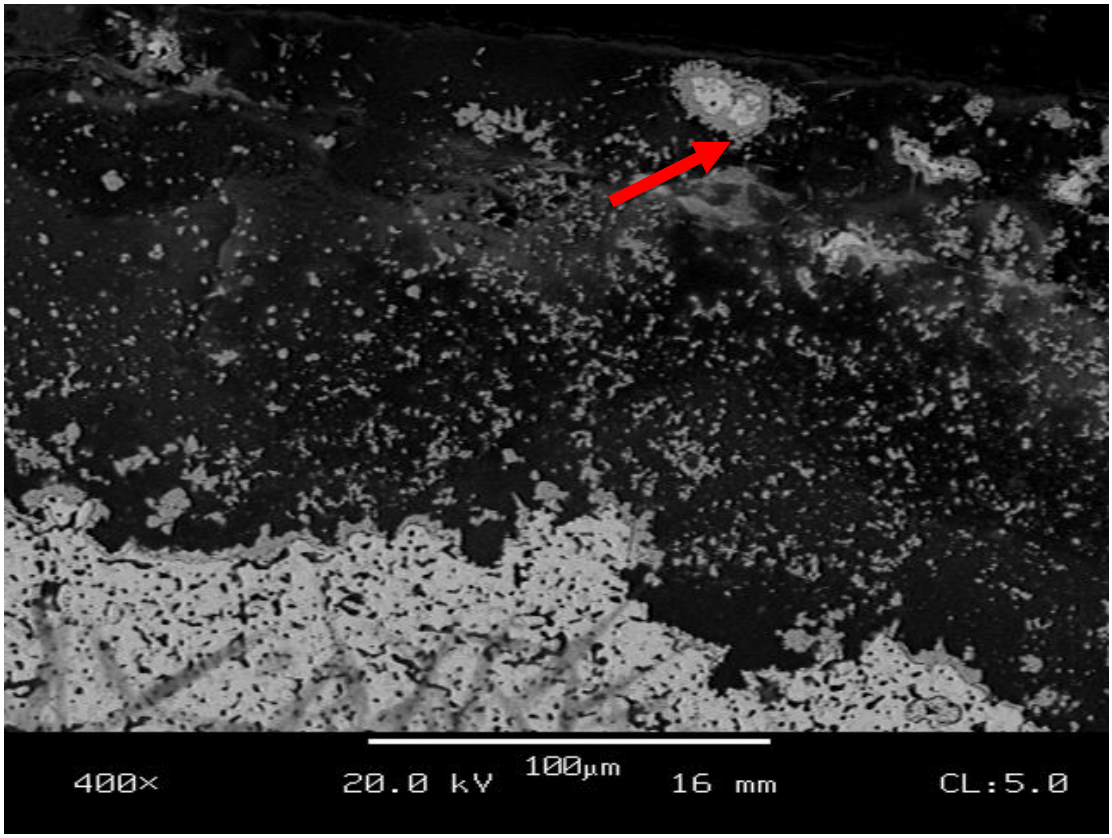

Figure 8.5: Isolated Mo island surrounded by glass which is rich with MoO_2 inclusions

In Figure 8.5 an isolated Mo segment can be seen which is being attacked on all sides. This illustrates the mechanisms of undercutting oxidation which is believed to be responsible for the isolated MoO_2 in the glass.

There are also sometimes MoO_3 spheres in the glass on certain samples Such as the TC2421+1.5Mn in Figure 7.21, apparently caused by phase separation in the borosilicate liquid. These may have been saturated vapor bubbles which condensed on cool down, or the proposed liquid-liquid separation. There are also whispy regions visible in many of the oxidation-formed glasses which appear lighter in backscatter, possibly due to local inhomogeneity and excess MoO_3 concentrations. Convection may in some cases be playing a more significant role than diffusion directly. Some Mo oxide may also be

incorporated into the glass as MoO_4^{-2} units: the limit of Mo in glass should be low, but has been reported to be as high as 7at% Mo in glass.[118] It is also possible that enough MoO_3 is building up to condense as a liquid, especially in the reduced gaseous diffusion which occurs within the pore channels. The liquid has a high vapor pressure over it would be very effective in maintaining a pore channel and preventing glass coalescence, and would evaporate away as soon as the high MoO_3 vapor pressure at the surface can diffuse away. This leads to continuous oxidation through channels in the glass and the channels can be held open by the rapidly forming liquid and vapor Mo oxide. If vapor pressure on the inside of the channels was greater than ambient it could prevent them from sealing.

Also, at very low pO_2 (cite low partial pressure paper) MoO_3 builds up as a solid oxide on the surface and does not permit the BS glass to seal. This indicates the importance of removing MoO_3 in order to form a continuous glass.

In a related experiment Helmick et al oxidized MoSiB again in flowing gas, and noted trapped spherical bubbles at the leading edge, but at the trailing edge, where the atmospheric gas was enriched in MoO_3 vapor, the bubbles were forced to the surface and kept open. This suggests then that the MoO_3 gas pressure must be low in order for channels to close.

Looking back again to the work of Bartlett and Williams on oxidation of pure Mo, it was found that the oxidation is dependent on gas flow rate. In a static environment, Mo reacts at the surface to form MoO_3 vapor, which remains near the surface forming a gaseous diffusion barrier and limiting further oxidation. In flowing air, weight loss is maximized by minimizing $pMoO_3$ vapor near the surface such that the oxide forms, vaporizes and is swept away while a ready supply of oxygen is brought to the surface.

Flowing air should decrease the saturation of MoO_3, but only if it's MoO_3 evaporation which is rate limiting. The excess O at the Mo interface will lead to higher and higher driving force to form MoO_3. Higher flow rate should decrease bubbling, but too high may be detrimental because oxygen supply is faster and stiffening of the glass by B_2O_3 evaporation is also accelerated.

Helmick[56] also did a series of oxidation tests on a 3:1 MoSiB in varying atmospheric flow conditions. He found that at 1000°C, flowing air did not have a great effect. At 1100°C however flowing air improved oxidation resistance if flowing at a slow rate (1cm/s). Both the initial and long term weight losses were reduced. At a faster flowing rate of 10cm/s however, the alloys were unable to form a protective coating and oxidized catastrophically in both dry air and pure oxygen. This was attributed to the loss of B_2O_3 due to the higher flow rate, and also increased availability of oxygen.

While removal of MoO_3 to allow channels to seal is one possible scenario, another possible scenario involves bubbling formed by the greater than atmospheric pressure of MoO_3 vapor in the scale. This would also be accelerated if the MoO_3 isn't leaving quickly enough at the surface. Further, as they bubbles and protrusions grow to the point of collapse, craters form which act as fast track diffusion sites. We sometimes see evidence of this, both in the form of bubbles growing beneath the scales and hooked type edges on the scale possibly related to a recently collapsed bubble. This bubbling can occur whenever the pO_2 below the scale is high enough to form MoO_3 such as if there is high DO_2, possibly due to a thin scale. A finite depth of SiO_2 is required to prevent formation of oxides, but early on and under craters there is not enough of a coating to sufficiently reduce pO_2 at the glass/bulk interface.

For the successful flowing air samples in Chapter 7.3.6., the samples under static air had coatings which spall off, whereas under flowing conditions the initial losses are much more drastic but completely manage to turn over to nearly flat excellent protective long term rates. The spallation was caused by bubble formation between the glass coating and the bulk surface which disrupts the connection between the two. Upon subsequent cooling, the thermal mismatch leads to cracking along the weak bubble-filled interface between the glass and the underlying sample.

The lack of spallation in the flowing air case may be due to a stronger thicker and more adherent glass. It's been stated in the literature that removal of MoO_3 is an important part of developing continuity of the glass; meanwhile Gulbransen had shown oxidation of pure Mo is most rapid in high flowing air. The flowing air scenario allows much more rapid formation and removal of MoO_3 but also forms more of the borosilicate quickly, and before the boria evaporates enough to stiffen the glass. This results in a thicker glass more quickly, which can coalesce into a much more protective and thicker coating. Furthermore the partial pressure of MoO_3 vapor is minimized which prevents condensation and reduces bubble formation – both of which could contribute to poor adherence of the glass.

In other cases the spallation is not of a bubble-dominated mechanism but instead is cause by devitrification of the glass, the devitrified crystalline coating then cracks and spalls off during coating. This type of failure is discussed later in the chapter.

8.5. Bubbles

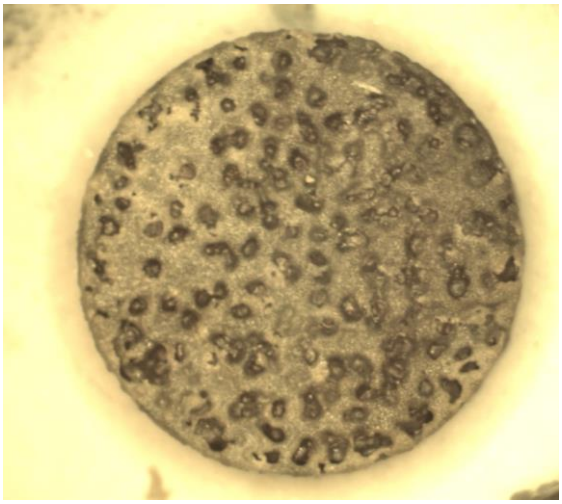

Figure 8.6: Burst and solidified bubbles on the surface of BLANK oxidation at BLANK

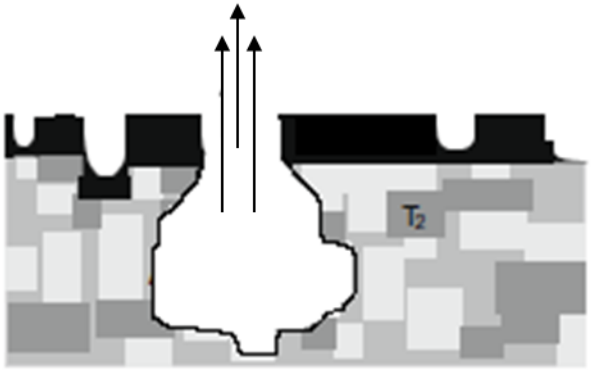

Figure 8.7: Schematic of oxidation failure by bubbling, following the ideal protection illustrated in Figure 2.12

Bubbles are observed for many samples especially with lower viscosities. Bubbles may form in the glass if the viscosity is low enough and the partial pressure of volatile oxides is high enough. If we look at the free energy of reaction for the formation of MoO_3;

$$Mo + 3/2\ O_2 \rightarrow MoO_{3\ (g)}$$

And of vaporization of the liquid

$$MoO_{3\ (l)} \rightarrow MoO_{3\ (g)}$$

The free energy of reaction can be calculated from:

$$\Delta G_{rxn} = RT\ln K_p$$

Assuming ideal gasses, activities are related to partial pressures and K_p is a function of pO_2 versus $pMoO_3$. As ambient $pMoO_3$ increases, the reaction is less favorable both for increased $pMoO_3$ and lower pO_2. Oxygen availability becomes less at the surface when $pMoO_3$ is higher.

Regarding Gulbransen's seminal work on MoO_3 vaporization the enthalpy of sublimation has been found to be between 80 and 90 kcal / mol vapor, while enthalpy for evaporation was 35.2 kcal / mol. MoO_3 melts at 795°C and boils at 1155°C.[25] MoO_3 vaporizes when its partial pressure exceeds the ambient levels and boiling of $MoO_{3(liq)}$ occurs when $pMoO_3$ = 1atm. Polymers of MoO_3, $(MoO_3)_x$, additionally exist. The trimer is known to be prominent in the vapor and possess the higher vapor pressures. Gulbransen gives the following equations:

$4.576 \log P\ (MoO_3)_3 = -75{,}400/T + 62.3\ (+/-0.2)$ for sublimation, and

$4.576 \log P\ (MoO_3)_3 = -35200/T + 24.6$ for vaporization of the trimer,

P in atm. The equations suggest that sublimation and evaporation begin to occur well below the boiling point and the total pressure of the Mo oxides can exceed 1atm below 1150°C, and also that condensation of MoO_3 is possible in saturated atmospheres.

Bubbles can form even at temperatures below 1100°C, but become more significant above those temperatures and cause significant disruption in the borosilicate. The growth of a bubble can be estimated as a balance of flux from a bubble. A negative outward flux, that is, more gas going into the bubble than going out, indicates the bubble will grow. Flux (*J*) maybe be given by:

$$J = ((c_e-c_i)D/R\ )(1+(R_o/(piDt)\text{^}0.5))$$

c_i is the internal concentration of the gas in the glass set by the equilibrium and rates of gas forming versus evaporating away. c_e *i*s the gas concentration at the bubble interface, and the bubble radius (*R*) grows from an initial size R_o depending on the diffusion coefficient of the gas (*D*).

Equivalently, rate of shrinkage of a bubble in a melt could be used to calculate the diffusion coefficient of the gas.

$$J=(ce-ci)D/R\ *(1+(R_o/sqrt(pi*D*t)))$$

If we assume $c_i>c_e$, that is: the gas concentration in the melt is greater than the equilibrium concentration of gas in the glass at the bubble surface, then the bubbles grow since flux out of the bubble is negative (i.e. positive flux into.)

Bubble nucleation on a simple case is driven by excess pressure and the energy released (ΔG_v) of forming a new volume, countered by the energy required for creating a new interface (surface tension - σ). For a spherical volume of radius *R*:

$$\Delta G = (4/3*\pi*R^3)*\Delta Gv + (4*\pi*R^2)*\sigma$$

Since the terms are dependent on size, a critical radius can be calculated where smaller bubbles have positive free energy and thus collapse, while larger bubbles are stable and grow.

Critical radius $R_c = (-2*\sigma)/(\Delta Gv)$

Alternately free energy of forming a critical nucleus (ΔG_c) can be calculated as the balance of excess pressure released by forming the volume against the surface energy increase:

$$\Delta G_c = 16\sigma^3 / 3(\Delta P)^2$$

ΔP is the excess pressure; the difference between the vapor pressure of the gas and the ambient pressure. A small critical energy or critical radius means many bubbles can grow, and bubble formation depends on nucleation. Nucleation rate is strongly dependant on the gas pressure, much more so than on the gas species or the total pressures.

To rearrange; bubble growth follows an Arrhenius type relation:

$$2\gamma/R_c = K\, C\, p_o \exp(-\Delta G_v/RT)$$

where ΔG_v is the activation energy for the vaporizing species. K is the activity of the solute gas, and since the dissolved gas is a very dilute solute, we can assume Henry's Law for the vapor pressure, which states that the activity K is independent of concentration for small concentrations.

As the gas content changes, so does the critical radius:

$$dR_c/R_c = -(1/C + \Delta G_{v/RT^2} * dT/dC)dC$$

Thus the change in the critical radius depends on the activation energy of the dopant vaporization, not the absolute vapor pressure.

Murase and McBirney[119] propose activation energies for bubble formation in silicate melts to be around 1-5eV, but only investigated limited temperatures and pressures and did not evaluate internal gas pressures.

Furthermore, regarding the rates of glass/gas interactions, the amount of gas dissolved in glass is proportional to gas pressure, even when the pressures far exceed the maximum saturation of surface adsorption sites. In other words, once all of the surface sites would be fully saturated, the gas pressure relationship remains indicating that the kinetics are not dependant on adsorption/desporption or reaction. Thus it seems the gasses dissolve nearly directly into (or out of) the glass. Solubility of gasses also decreases at higher T, which increases saturation pressure.

It is also important to consider that MoO_3 is known to significantly reduce surface tension in glazes and can be used as a wetting agent in glazes even at small amounts.[51] Considering this, since critical radius for homogenous nucleation of a bubble is directly proportional to surface energy, Mo in the glass makes bubble formation even easier.

As a result, for temperatures of 1100°C and above formation of bubbles can occur homogenously within the glassy scale if sufficient $pMoO_3$ is present and the glass must have great enough thickness and/or viscosity to prevent the necessary inward diffusion of O to form MoO_3. Further, bubble formation can in many cases be possible for much lower temperatures still, despite not exceeding individual vapor pressures of 1atm.

8.5.1. Bubble Removal

Bubble removal is something studied extensively for commercial glasses. Arsenic is used in fining of glass batch in manufacture to aid removal of bubbles. The mechanism is believed to proceed by increasing solubility and allowing the O in bubbles to dissolve

into the glass, however our bubbles are not oxygen-filled as in the commercial glass case. Sulfates are also used in fining but in MoSiB glasses these will react with Mo. Unfortunately our bubbles are driven by high Mo fractions and excess volatile oxides, and occur on a much smaller size scale and higher temperature range than is applicable to commercial processes.

When considering removal of bubbles, the rise rate for bubbles to reach and dissipate at the surface is important. Bubbles rise at a rate:

$$dh/dt=(2\rho gR^2)/9\eta$$

where g = gravity, ρ is density, η is viscosity, and R is the bubble radius.

In our case the rise-rate is not important because the glass depth is so small; its total thickness is on the order of the ideal stable bubble size. The compromise of the scale is not by rise of bubbles through it, but the creation of craters and channels by growth and bursting bubbles within it. The bubble formation occurs outward from all sides, independent of gravity. Formation and growth of bubbles are both energetically feasible and responsible for the disruption of the scale. If the rate of bubble growth were to be slowed enough that the glass grows more quickly, or if the oxygen availability can be lowered by thickening glass and stiffening by B_2O_3 vaporization, then it may stop bubbles from growing and the difficulties of bubbling can be minimized. A delicate balance must be met which is high enough viscosity to prevent bubbles and high $pMoO_3$ from keeping pores and channels open or forming new ones but also still fluid enough to be able to grow to the required thickness and to fill in such holes and channels as may form.

8.6. Crystallization / Phase separation

Bubbles and open pore channels can become a much more significant concern when the glass thickens or crystallizes and holds them open. B_2O_3 volatilization is constant and reasonably fast at 1300°C. If the glass can flow over to fill in the pore channels they cease to be a concern, however the filling of the pore may be impossible if the boria loss has resulted in too high of a viscosity for flow by the time there is enough glass available to fill the pore.

The glass can also lose its ability to flow if it devitrifies. The formation of crystalline phases restricts its flowability, as is seen in many of the results presented in the previous chapters. The crystallization of the glass seems to be driven in most cases by phase separation, which us then followed by reaction to form molybdates or possibly SiO_2-rich regions which devitrify to cristobalite.

Tendency to phase separate can be expressed as width of immiscibility gap at a given temperature (i.e. the size of composition range where two separate liquids coexist) or height of the consolute temperature – the temperature above which the liquids are fully miscible. The width of the immiscibility gap has been show to follow, and thus can be approximated generally, by the ratio of the charge/radius of the ion in the glass. A larger cation radius or lesser charge is more stable and will be less likely to phase separate. For example, for equivalently charged alkaline earth oxides in silicates, immiscibility increases with decreasing cation size from Ba<Sr<Ca<Mg.[55] This puts Sr being less likely to phase separate than Ba, and Fe which has a high charge (trivalent) and small radius (Z/r~5) as having high tendency towards phase separation.

Crystallization was observed primarily in Sr-containing samples which were identified as forming $SrMoO_4$. A glass forms initially but as boria leaves and phase separation proceeds within the coating, it becomes too rigid to seal any further. This leads to a step-wise deterioration as a coating forms incompletely, loses its capacity to flow over the last exposed areas, and is eroded away beneath. It then forms a new layer, but again incompletely and the stepwise oxidation proceeds in this manner leaving behind a series of crystalline layers. A schematic of this is shown in Figure 8.8 based on the Rioult schematic. The glass is crystallizing and becomes rigid and material erodes beneath it. An actual example of this is shown in Figure 8.9, where a rigid crystalline coating is formed but is nonprotective and eroded away beneath.

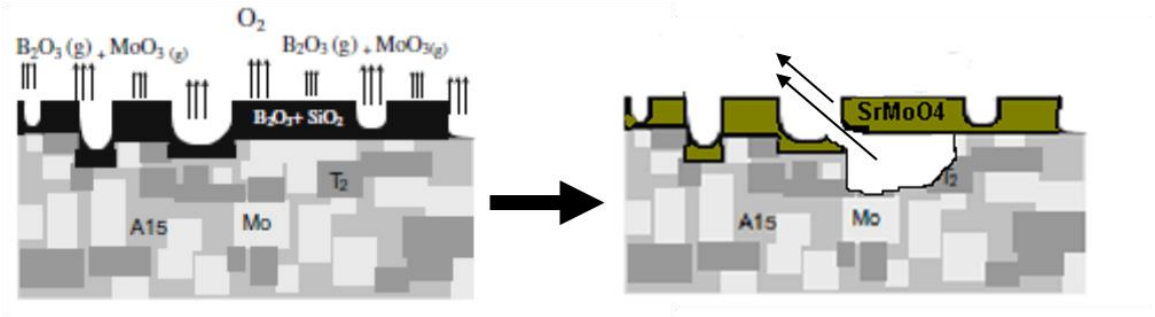

Figure 8.8: Schematic of oxidation beneath a crystallized coating.

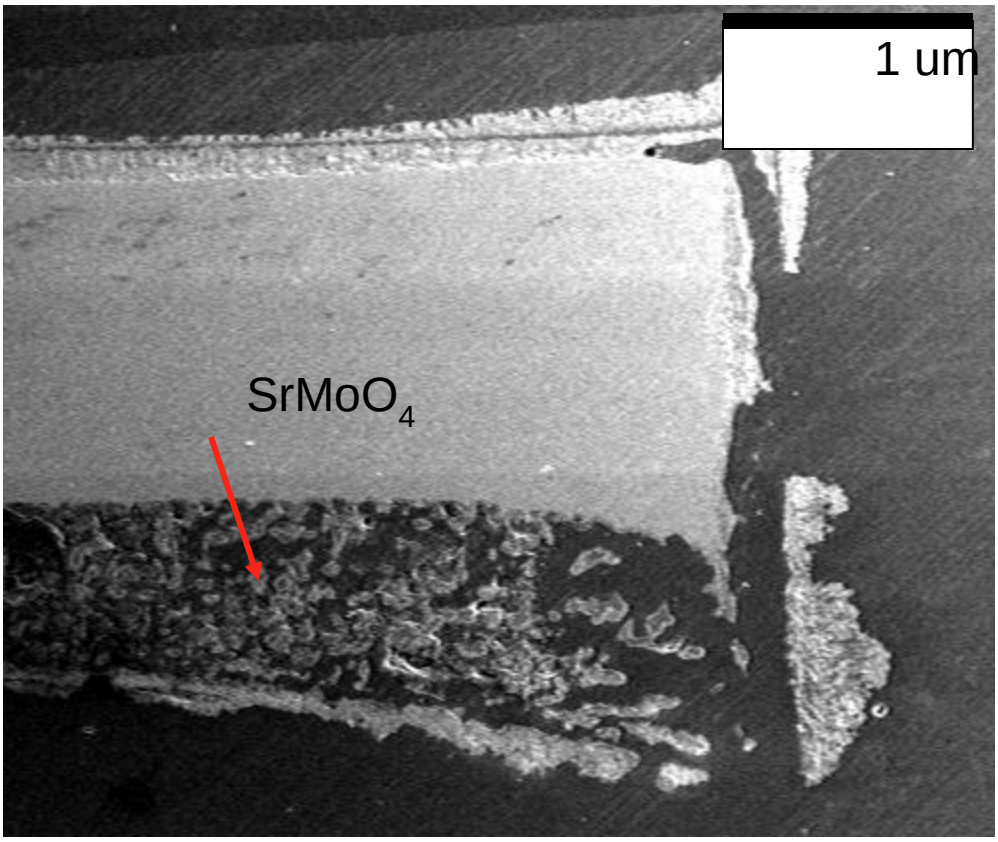

Figure 8.9: Failure by crystallization during oxidation of a BSAS2020 sample.

When forming the Sr molybdates, bonding is partially ionic and partially covalent. The covalent contribution of the bonding involves competition between the A and B cations dependent on their coulombic potential and in turn inversely related to their ionic radii. Coulombic potential is defined as Ze^2/r where Z is the valence and r is the ion radius. So the bigger alkaline earth cations have lower coulombic potential and thus allow a greater contribution of the anion electron cloud to be involved with the Mo. Thus there is a larger overlap of electron clouds between Mo and O; i.e. more covalent bonding. This leads to stable molybdates and also stabilizes the MoO_x in the system and limits its vaporizations, and also may remove MoO_4^{-2} tetrahedra from disrupting the glassy

network. As a result Sr may be beneficial or harmful and a balance of crystallization must be optimized.

The ionic tolerance factors for the molybdates can be calculated using Shannon's ionic radii, which gives 1.03 for $BaMoO_3$, 0.98 for $SrMoO_3$ and 0.95 for $CaMoO_3$. The deviations from one are proportional to the distortion energy, a lower distortion energy allows distortion and permits wider solubility ranges, so Sr is the easiest, it has the least deviation from 1, i.e. lowest distortion energy, and can accommodate the widest composition range around stoichiometry.

Work by Bahat[120] looked at heterogenous nucleation in glass ceramics with addition of nucleating agents for Cr, Ba,and Sr aluminosilicate glasses. It was observed that Iron in aluminosilicate glasses acts as an effective nucleating agent, which is consistent with the devitrification and subsequent loss of protection we see in the glasses formed on Fe-containing samples. In Bahat's work, wide variations in FeO to Fe_2O_3 ratios in the glass were seen but with no effect on the heterogenous nucleation. This indicates that the devitrification is not due to epitaxial nucleation and growth on a specific mineral structure (i.e. heterogenous nucleation and growth from hematite or magnetite seed crystals). Instead it is surmised that iron leads to phase separation which promotes local compositional variations that enable nucleation, in the same manner as we've proposed in our system.

Fe containing silicates phase separate into Fe-rich areas which precipitate magnetite (Fe_2O_3) or fayalite (Fe_2SiO_4) and Fe-poor areas which then crystallize into cristobalite. The breakup of the silicate structure by iron helps to promote the reconstruction of amorphous silica to crystalline cristobalite. The devitrification of the

glass and crystallization of cristobalite expels any remaining iron to the growth front, further enabling the reconstructive transformation and is marked by spheres of cristobalite in the glass surrounded by red rings of iron which has been expelled and oxidized. The same sort of behavior is also seen in other samples such as the later Co-containg ones, in which the growth of the devitrifying cristobalite is driven by the transition metal additives which build up at the growth front. Again the devitrification is a problem when it prevents sealing, but in other cases may be beneficial by reducing diffusivity, but only for a complete scale.

In this type of failure as well, the higher flow rates seen in Chapter 7.3.5. may be also beneficial by aiding removal of boria from the glass. This causes the glass to reach higher viscosity quicker, and limits rearrangement and devitrification. The effect of boria volatility on increasing the melt viscosity is well established and would certainly be enhanced by the flowing atmosphere. Flowing air removes boria vapor at the samples' surfaces and may be further increased on humid days by water vapor present in the laboratory air forming the even more volatile HBO_2.

8.7. Wetting

Another final mechanism of failure in the oxidation coatings is poor wetting. This is generally seen in cases of excessively low viscosity, but also occurs concurrently with formation of molybdates. The poor wetting seen in those cases means that a large volume of glass which would otherwise neatly coat the surface can form, but the surface tension prevents it from spreading over the metal. This is shown schematically in Figure 8.10, and Figure 8.11 shows this effect on an oxidized surface where some coating is present

but large areas of the surface remain bare.

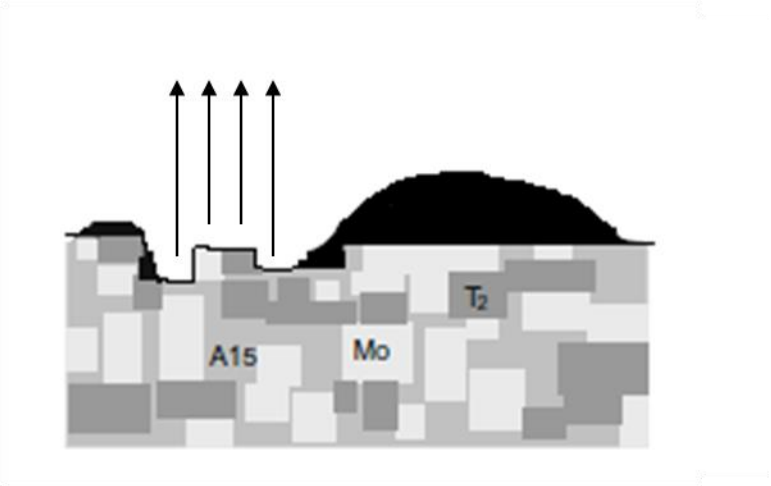

Figure 8.10: Schematic of continued oxidation due to poor wetting despite a glass being present (black)

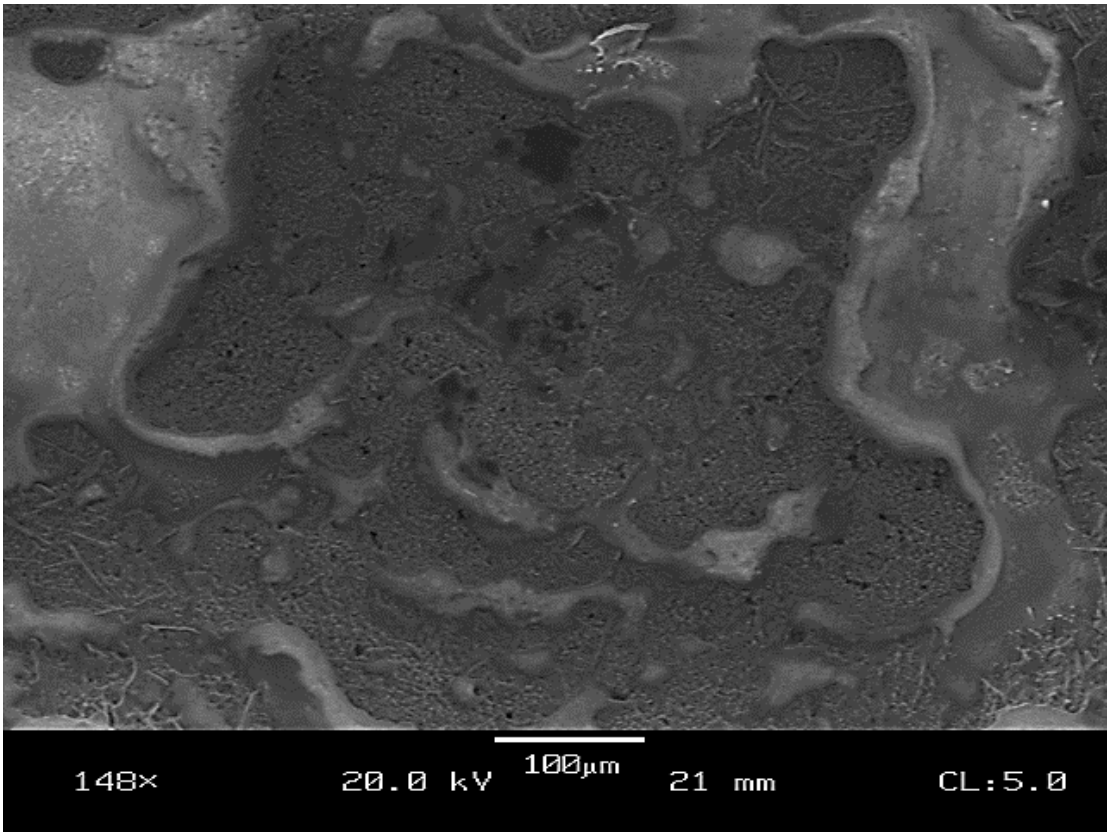

Figure 8.11: TQSAS261202 Detail of non-wetting section of the surface after 10m oxidation at 1300°C

Wetting can be simply understood from Figure 8.12 and Young's equation for surface tension:

$$\gamma_{SG} = \gamma_{SL} + \gamma_{LG}\cos(\theta)$$

If solid and gas remain unchanged, reducing surface tension decreases the contact angle and gives greater wetting.

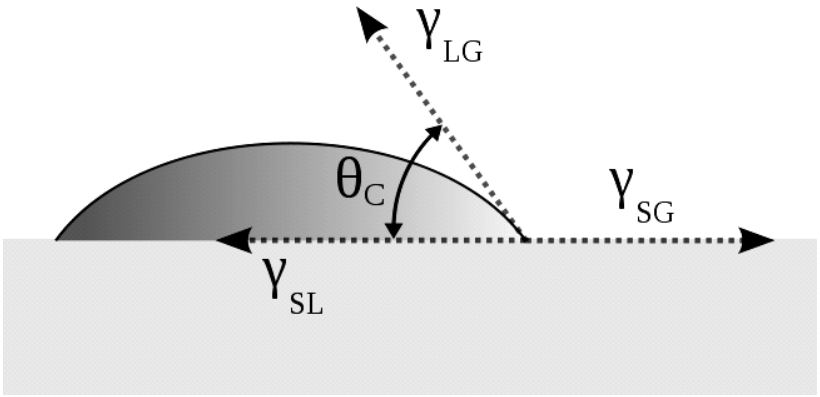

Figure 8.12: Schematic of the relation between surface tension differences and the contact angle (θ_c) for a liquid droplet on a solid surface

Mo improves wetting of silicate glasses significantly by a reduction in surface energy. In the case of Alkaline and alkali earth additions, there is a strong tendency towards phase separation in the glass and also for formation of molybdates. We saw this in the case of Li and Sr additions which lead molybdates forming in the oxidation layers and has been discussed in the previous section.

Tying Mo up in the molybdates however reduces Mo content in the glass and consequently increases surface tension and the contact angle. As a result the reduced wetting would inhibit spreading and the formation of a protective coating, and this was observed on some SAS samples. Nd was added to increase Mo solubility and stability in

the glass. Effects were not quite as expected however and the poorly wetting low viscosity remained in some cases, while in others the glass readily phase separated and crystallized into molybdates. Figure 8.13 shows the combined effects of poor wetting and phase separation, which has then devitrified leading to very poor oxidation resistance.

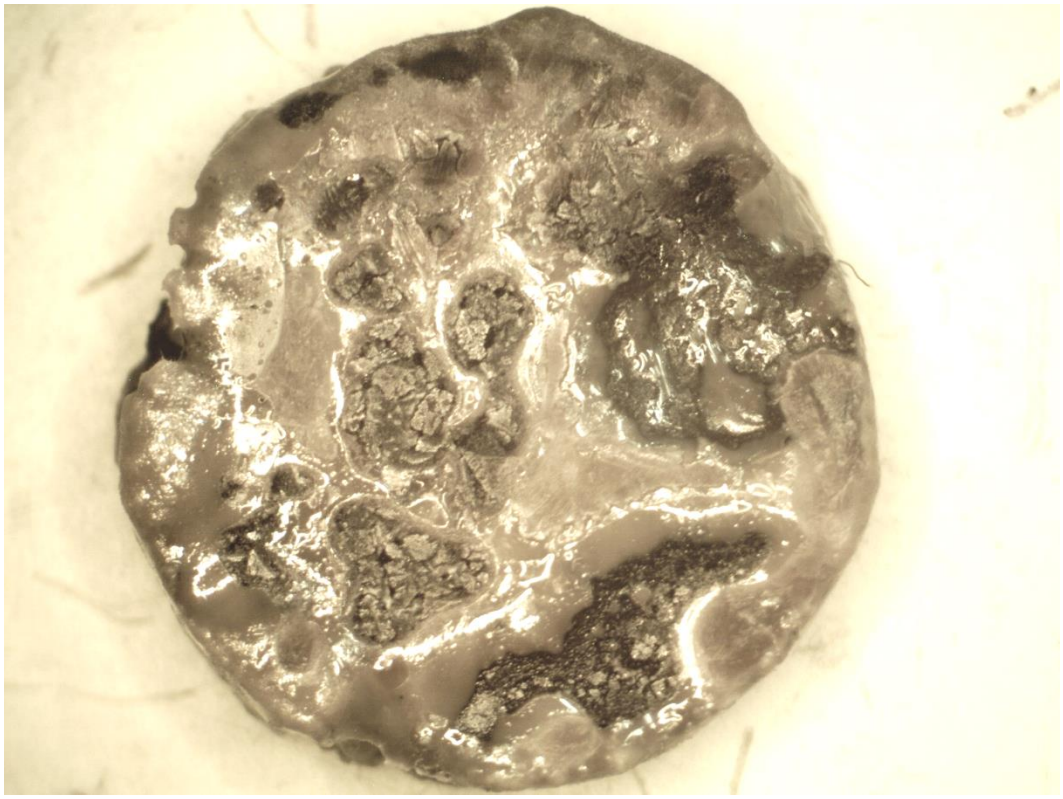

Figure 8.13 TSAS2027+2.5 Nd oxidized at 1300°C for 90m illustrating the combined difficulties of phase separation, poor wetting and crystallization.

8.8. Oxidation Conclusions

The proposed scenario is one in which upon very first exposure to oxygen rich environments and high temperatures ~1300°C, MoO_3 forms uninhibited as a vapor over the pure Mo phase. Simultaneously very fluid droplets of borosilicate form over the T2, and the exposed SiO_2 exists as rigid islands. As the Mo recedes, more of the T2 is

exposed and converted to borosilicate, which flows and fluxes the SiO_2. The resulting borosilicate mixes and flows by wetting over the surface. This step may be aided by Mo oxides or possibly also by the transition metal additives in the glass, and is complicated in some cases by poor wetting. During this stage MoO_3 may saturate the atmosphere and form MoO_2 or condensed MoO_3, which disrupt the coating from becoming connected.

The rates transition from the rapid initial loss to a slower but potentially still rapid loss following a complete coating. The borosilicate prevents contact between Mo and air, but is too thin to prevent inward diffusion of O forming MoO_3 underneath. The positive combined partial pressures of the vapor phases lead to nucleation and growth of bubbles. The bubbles grow and expand the glass around them until the glass flows away and the growing bubble bursts. This leads to a fast track open crater through which new oxygen can more easily be brought to the surface. If the glass is too fluid, the high oxygen diffusivity and continued bubbling keep oxygen supplied to the Mo, possibly also aided by fluid stirring from bubble motion. MoO3 may also condense at the bottom of the pore channels and keep the fluid glass from joining. The thickness of glass required to prevent bubbling is greater than the piece itself, and eventually all of the Mo is oxidized. If instead the glass becomes too viscous at this point, either by boron loss or devitrification, the voids created by bubble collapse do not seal and remain as fast track oxygen sites. Erosion beneath the solidified coating may also occur, and the piece fails in a stepwise manner. But in between, as long as the glass has achieved great enough depth and remains fluid it should then flow into the void. At some point the glass thickness is ideally great enough to prevent further MoO_3 from building up the pressure to form bubbles, and a stable connected glass coating is achieved. The details of this transition

between the rapid initial transient loss and long term parabolic loss regimes is rarely regarded in detail but ultimately defines the success or failure of many of the samples and compositions tested.

After this point, the system transitions again into the final parabolic regime. The coating thickens with time due to slow oxidation of silica and boron internally, and may also reduce intermediate MoO_2 to form more borosilicate internally. The glass is thicker and has lower oxygen diffusivity due to boria loss, and a lower partial pressure of oxygen is available to form the volatile oxide coupled with higher pressures now needed to nucleate bubbles. If the coating then devitrifies it is benefitted further by even lower oxygen diffusivity.

A lower viscosity should permit glass to coat faster, but a thin low viscosity glass allows more bubble formation, less protection as bubbles form and more rapid bursting and turbulence, and could result in a situation where adequate protection is never achieved. A higher viscosity is needed in order to restrict formation of bubbles and channels and to provide a sufficiently permanent glass protective barrier.

On one end of the spectra of thee failures we see, a common scenario is a series of craters on the surface from general creation and collapse of bubbles due to high MoO_3 volatility coupled with too low of a glass viscosity. This is most predominant in glasses with high boria content and/or low modifiers. On the opposite end, we see a nonsintering porous silica matrix when silica is too high. With slightly more boria, a still very high viscosity coating can form but may be prone to spallation from bubbles beneath the coating, or spallation and flaking from thermal stresses and inability for rearrangement due to its rigidity.

In between we see combined effects. Higher boria content allows the glass to coalesce but diffusivity is high enough that MoO_3 is still forming beneath resulting in bubbles, whose size is dependent on surface tension and the glass viscosity. These form and grow rather slowly with concurrent boria loss from the surfaces, but if the rates of the competing crystallization, thickening by boria volatility, bubble formation, and glass joining are all optimized, excellent protection is possible and has been demonstrated.

The balance of mitigating the various failure mechanisms is a difficult one to achieve. The low surface tension that promotes wetting also enhances crystallization and bubble formation, meanwhile a balance of viscosity must be met for low enough viscosity to flow but high enough to stop bubbles and keep glass from pooling or dripping away. This balance is a tricky one which depends not only on the effects of composition which itself is difficult to control, but also the atmosphere and temperature. It is affected by differently with time depending on the rates at which the composition changes due to reactions or phase separation within the glass and also volatilization of the glass components such as boria. Furthermore, within an otherwise identical sample there may be regions of great success and regions of complete failure due to local effects of composition and depletion effects, as well as variations in atmospheric conditions.

CHAPTER 9.

RECENT WORKS AND RECOMMENDATIONS

Mo-T2-SiO_2 alloys have yet failed to meet the desired balance of strength and oxidation resistance. The use of T2 and SiO_2 as an alternative to the A15 phase circumvents the issues of Si embrittlement in traditional MoSiB alloys. The new type of alloys without A15 have been shown to have measurable ductility, even down to room temperature in some cases, and they have also been shown to be able to provide comparable or even superior environmental resistance when subjected to oxidation testing at 1300°C in air. They have not been able to achieve both of these properties in the same sample. The failure to achieve both properties together however is not intrinsic to the alloy system itself, the way that it is for Si-embrittled Mo in equilibrium with A15. Instead the lack of low temperature ductility in the oxidation resistant samples is due to processing issues, specifically the flux and flow of glass internally during firing. Simply by improving the processing to avoid the crescent shaped silica regions should greatly improve the ductility of the composites. Improved processing should also benefit oxidation resistance as well if the depletion of glass formers and glass modifiers from the samples can be controlled and minimized.

9.1. Hot Isostatic Pressing

A new approach to processing with Hot Isostatic Pressing was recently investigated. Hot Isostatic Pressing (HIP) is a common procedure in high performance powder-processed ceramics and metals. The HIP process uses high pressures combined with high temperature to drive the free energy reduction that leads to sintering of powders, and is able to create fully dense samples more reliably, more quickly, with less

grain growth and at lower maximum temperatures than with traditional pressure-less sintering. Typically a sample of powder is encapsulated and evacuated in a steel or similarly deformable metal can, which is held at temperatures up to 1400°C and pressures from 40-60ksi.

HIP should benefit the Mo-T2-SiO_2 system in a number of ways. The main goal is minimizing or removing the presence of the crescent regions of glass in the microstructure cause by glass flow in firing. The HIP uses pressure in addition to temperature to drive sintering, and the high pressure process should stabilize the crystalline SiO_2 phase quartz over amorphous, while also the lower temperature should also significantly limit flowability of the silica. HIP may also benefit oxidation resistance by eliminating the depletion of Si and B from the surface since the closed and evacuated cans don't allow the constituents to volatilize. The traditional MoSiB system with A15 and T2 may also benefit from HIP by the reduced maximum temperature for complete densification. At 1300°C the Si solubility in Mo is nearly zero and shouldn't contribute significantly to the embrittlement of Mo.

Our system has some unique difficulties compared to the typical HIP processing. First and foremost is the reaction process we employ which requires the reaction of silicon and boron nitride precursors to form the desired final phases. The reaction generates and requires removal of N_2 gas, which would disrupt a HIP run. Further we require strong reducing atmospheres to reduce any oxides, to drive the intermetallics' reactions and to prevent reaction with any residual oxygen on the samples. Finally we also require precise compositional control; the final pieces must be free of impurities which could arise from contamination of samples in contact with the HIP can material.

We designed a set of HIP runs to investigate the benefits of HIPing and adapt the process to our system. An initial run was done in which samples were spray dried and dry pressed into 13mm pellets by our usual procedure (Chapter 3). The binders and dispersants were removed at 400°C in a tube furnace with flowing Ar gas to prevent contamination in the cans themselves. Afterwards they were pre-fired in the typical tube furnace setup but only to a maximum temperature of 1300°C, in order to complete the reaction of the nitrides but without significant sintering and with no opportunity for the solubility of Si in Mo to exceed the limits set by the 1300°C max. Next the samples were loaded into steel cans with a protective Mo foil barrier layer to prevent reaction with the steel cans, and the cans were pinched closed under vacuum and welded hermetically. The evacuated welded cans were sent to American Isostatic Presses (AIP - Canton, OH) to be pressed in and 8hr cycle with 6hr hold at a temp of 1300°C and pressure of 45ksi.

When returned from AIP the cans were removed by cutting and peeling. Figure 9.1-a shows good silica distribution. The Mo foil also bonds to the underlying material but no interdiffusion between the foil or the Si or B from the bulk was seen (Figure 9.1-b). The compositions and densities after pre-reaction and after HIP are given in Table 9.1 and show that HIP could be used to create fully dense samples while never exceeding 1300°C. XRD indicated the desired final phases in the expected fractions, except that the crystalline silica is not present. Issues with residual oxygen remain, however the first run was to verify if fully dense pieces could be achieved, and they were, while subsequent runs work towards fully eliminating oxygen contact from reaction to the final piece.

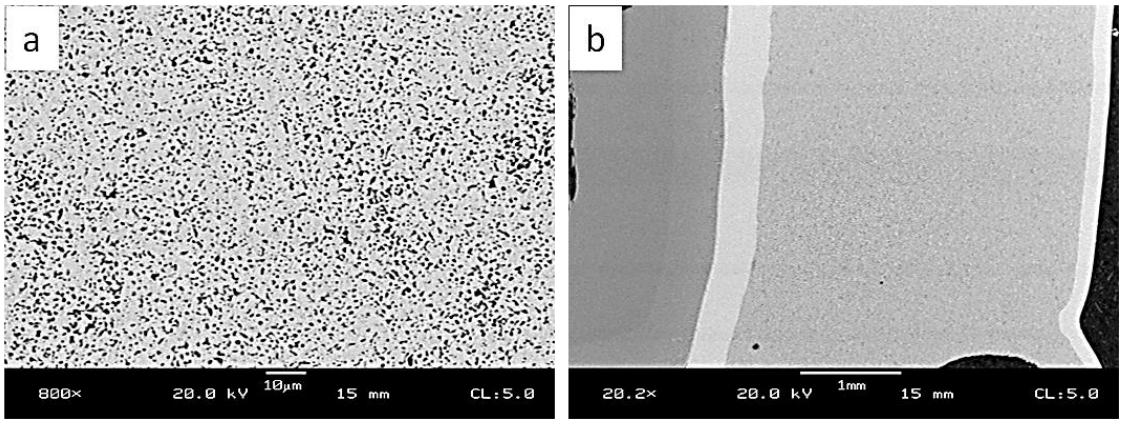

Figure 9.1: May HIP Can 2. TC sample showing (a) good silica distribution in the microstructure and (b) cross section of the effective Mo foil barrier (solid vertical line) between the steel can on the right and the composite allot on the left.

Table 9.1: Fired Densities of HIP batches

	Composition	TCSas171601 + 0.5Mn	TCSas171601 + 0.5Mn
	TD [g/cc]	8.651	8.651
Green	% TD	56.9%	55.1%
Reacted	% TD	57.5%	76.2%
	Bulk ρ	8.59	8.77
HIP'ed	Relative ρ	99.3	101.3
	Open Porosity	0%	0.1%

In order to prevent negative interaction with oxygen between firing and HIP, a second can design was developed. In the second set of HIP samples, the powder was a loaded directly after the 400°C hold to remove the PMMA, into a steel can lined with Mo foil. The can was designed for the reducing Ar/H_2 gas to flow through the powder during firing in the can. ¼ in. steel tubes were welded onto either end of a larger ¾ in. diameter, 5 in. long can. The powder was then reacted in the can and using a hygrometer to measure the dewpoint of the effluent gas in order to monitor completion of the

deoxidation reactions. After completion of the reaction firing run with reaction hold 1300°C, the can was evacuated to below 50 millitorr and again welded hermetically. In this method the samples never come in contact with any oxygen between the reduction in firing and the final HIP stage. These were also sent to AIP to be HIP'ed using the same schedule as before.

When the second set of samples were returned the cans had ruptured, along the edges and at the sharp points where the can had to deform around the samples inside. Steel is known to embrittle with H gas at temperature, and the de-oxidation by Ar-10%H_2 gas in the cans had led to embrittlement of the can such that under pressure in the HIP it was unable to deform evenly around the can.

After the failure of the cans because of H embrittlement, a third set was prepared. The samples had to be de-oxidized in the cans in order to prevent oxygen from defeating the usability of the final pieces; however the H embrittlement in the steel also needed to be avoided. The diffusivity of H in steel is high at 1300°C and is only needed during the deoxidation portion of the firing, so the approach was to only use the H_2 gas through the first two hours of the 4h hold at 1300°C. After that, two subsequent approaches were investigated. In one case the atmosphere was switched to vacuum, and the other case to pure Ar. This should allow the H to diffuse back out of the steel enough to allow it to properly deform in the HIP later. As a secondary consideration, Alumina powder was used to pack the empty space in one can. Alumina is inert with our system and applies the pressure from the can to the samples. It is common use in many commercial HIP practices. The Alumina powder is used here in order to fill empty space and minimize the

deformation of the cans required during HIP in order to reduce hard edges where the previous cans had failed.

After HIP, the removal of H proved successful in preventing the rupture of the cans. Unfortunately the alumina-filled cans did not densify, the loose alumina powder was unable to be adequately contained in the can between the reaction and the crimp and weld steps and some powder remained on the weld site which prevented a hermetic seal. Without a completely sealed can a HIP sample does not sinter. The remaining cans on the other hand both sealed and deformed without H embrittlement and produced usable, fully dense samples. shows the deformed can.

Figure 9.2: Fully deformed and densified can after HIP pressing.

9.1.1 HIP Microstructure

The total measured dewpoints of the prior pressed pellets however suggested poor and uneven deoxidation had occurred. Another set was prepared using loose powder in Mo-foil lined steel tubes after it had been spray dried and the binder evaporated but before deoxidation and reaction. This loose powder should permit more even gas permeation through the samples to assist deoxidation. The flow during firing was restricted by the powder and built up back pressure, where for the pressed pellets flow

was steady. In the pellet case, the reducing environment was likely just passing by the pellets without deoxidizing as effectively.

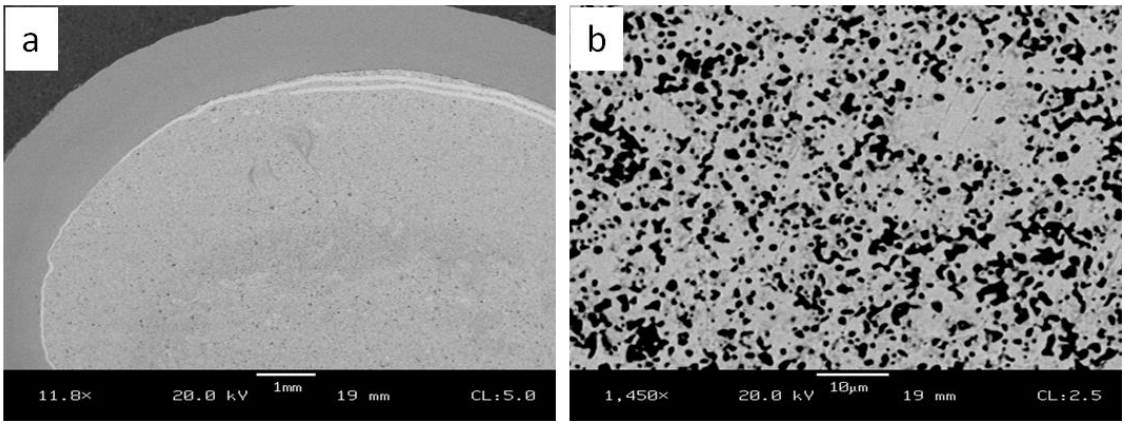

Figure 9.3: September HIP Can #3 cross-section showing (a) the steel can, Mo foil, and sample at the center and (b) the microstructure, grain size and quartz distribution.

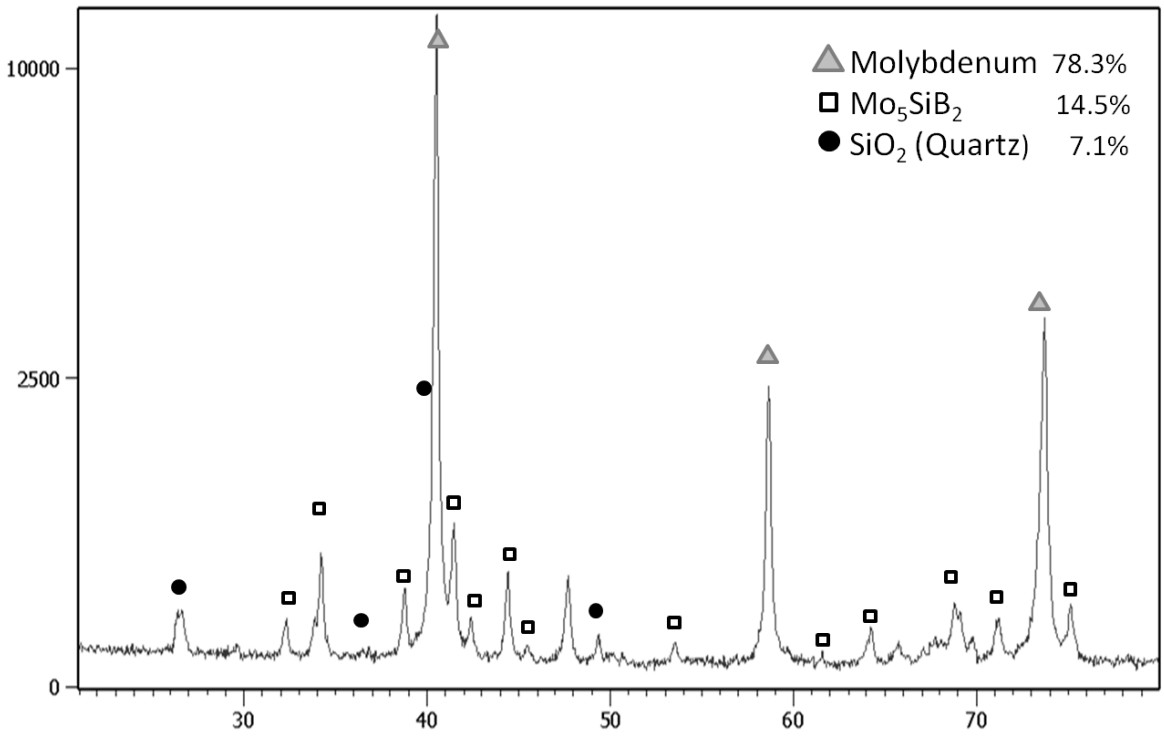

Figure 9.4: XRD Scan of HIP TC sample showing crystalline silica and very nearly the intended weight fractions of the final phases.

The silica, which was added to the batch as cristobalite was found by XRD to be present as crystalline quartz (Figure 9.4). The weight fractions determined by Reitveld had very good match with R values below 2, and are given in the image. These match closely to the expected volume fractions of the batch. This result indicates that no boron nitride was oxidized at any step during the processing as even small amounts of boria have been shown to vitrify any silica. This is a very encouraging result as it confirms the minimization of any oxygen to improve toughness and prevent flowing silica from internally formed crescent-shaped regions.

The HIP can samples were subjected to oxidation testing at 1300°C in flowing air. The behavior was very similar to previous Fe-containing samples; however no Fe was present in the batch. The oxidation was very good initially but began to turn down again after 30 minutes with obvious devitrification in the glass with a red tint identifiable as ferric oxide, which prevented oxidation resistance in the same manner as we had seen when Fe is present. XRD also revealed presence of Fe silicates. The only possible source of the intruding iron was the steel HIP cans, despite the Mo foil barrier. It was previously shown that the foil was an adequate barrier to prevent Fe diffusion through it; however it seems that the reducing hydrogen environment prior to HIP is allowing a gas phase transport of Fe throughout the bulk prior to densification. Remembering the results of alloys which had been intentionally alloyed with Fe, only a very small fraction (>0.5 at% of the Mo) was more than sufficient to negatively impact the oxidation resistance.

The Fe contamination plagued all of the steel canned samples, and in order to achieve good oxidation resistance it must be avoided. Also none of the previous samples,

which had been HIPed as pellets or as loose powders, resulted in samples of sufficient size and shape to perform mechanical tests. To address this a final set of HIP samples was required to produce usable test bars for mechanical bend bar testing, and to investigate alternate can approaches without Fe. Titanium cans were instead chosen. Initial tests of the firing gas through a Ti tube showed possible embrittlement of the Ti by H. Again similar to the Fe case, an extended firing with the H_2 cut off partway through followed by maintained vacuum was used to remove hydrides. The resulting samples were still brittle and showed large grain growth and texture on the tubing and can surface. To remedy the problem, after the initial firing the samples fired in Ti cans were set again into a secondary steel pouch in order to ensure hermetic vacuum for successful HIPing. In this way the Ti acts as a barrier to Fe, and ensures reaction in a non Fe containing can, but the outer steel can protects against possible rupture of the Ti cans during firing.

It is thus possible that fully dense samples can be created with the desired phases and microstructures, provided the processing challenges could be met. These challenges include producing and maintaining hermetic seals in the can design, optimizing the geometry of cans for even fill and ease of preparing without can failure, and better control over the can and material's gas phase relations during pre-firing. This is the strongest approach available to create Mo alloys which are both ductile to room temperature and oxidation resistant above 1300°C.

9.2. Scale-up and Reproducibility

One of the major advantages of the GTRS powder approach is that it can be used to create nearly ideal microstructures using existing well established industrial powder techniques. In order to investigate reproducibility off-site, the process was repeated by a

group at Deep Springs Technology (DST) in Toledo, Ohio. First, T2 powder was formed by reaction from powders of Mo, silicon nitride (Si_3N_4) and boron nitride (BN) in the correct ratios for T2 (Mo_5SiB_2) and reacting the spray dried granules in Ar/10%H2 atmosphere at 1500°C for 6 hours to complete the reaction.

The spray dried granules are shown in Figure 9.5. They are mostly monosize and spherical in a diameter range of 20-80μm and the spray dry process, once optimized, could easily reproduce the granule shapes and sizes we do in our labs. The T2 was pre-reacted at 1300C and after completing the reaction, the T2 crystallites are elongated and ~1-2 μm in size with similar size spacing between the crystallites, Figure 9.5. This creates a microstructure that grinds easily to micron-sized T2 powder for incorporation with Mo powder for fabrication of MoSiB composites.

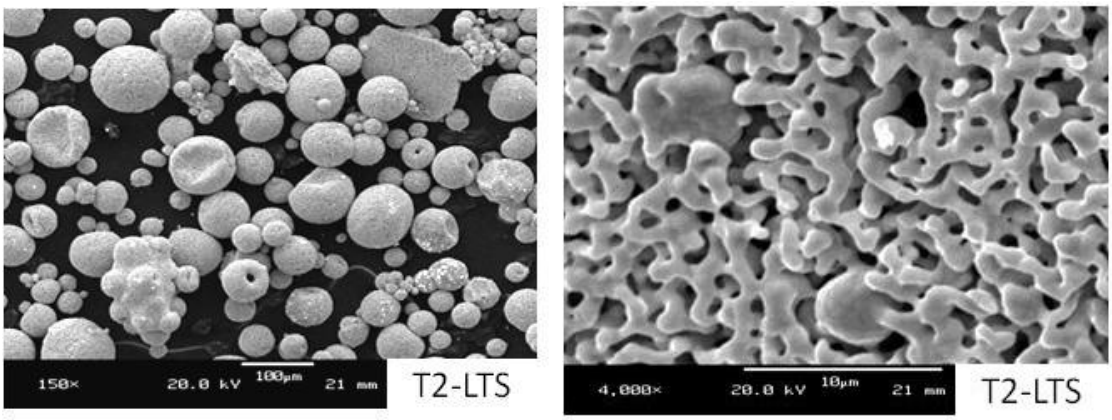

Figure 9.5: T2 granules as spray dried (left) and as-fired (right) both produced off-site by DST using our processing techniques.

Following pre-reaction, samples were made with the granules of T2 added into the batch directly, which resulted in the granule-sized spheres of T2 remaining in the final microstructure (Figure 9.5). As a result the T2, if pre-reacted, must be ground and re-sprayed with the other ingredients in order to achieve a homogenous green distribution, and to produce homogenous final microstructures. A ground T2, Cristobalite and Mo sample was prepared and verified by XRD and SEM to be nearly the same as compositions produced in our labs.

An additional attempt to use powder processing techniques used slip casting of the powders to create a green piece. Figure 9.6 shows one such microstructure of a 3:1 MoSiB alloy. Note there should be no dark spots from silica because this is a traditional Mo A15 and T2 alloy, but illustrates that slip casting may be a viable means to create green pieces. Separation and preferential agglomeration can lead to highly non-ideal microstructures, so high solids loading and good dispersion both must be optimized. The success of this and the dry press routes typically used might also indicate possibility for

other powder forming techniques as well including paste extrusion or additive manufacturing.

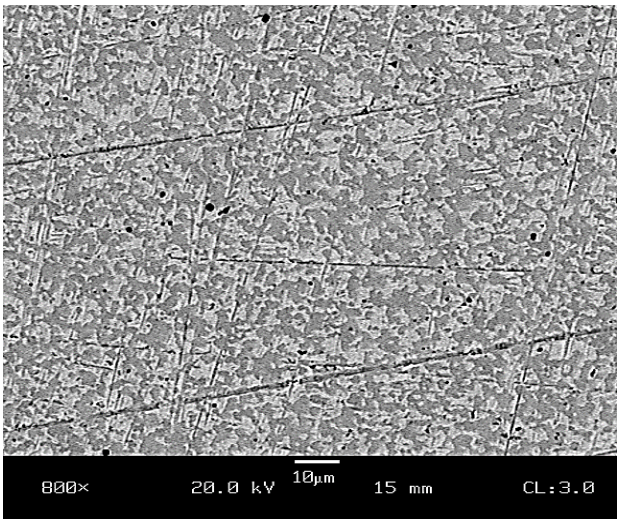

Figure 9.6: Microstructure of slip cast and reaction fired Mo-3Si-1B.

CHAPTER 10. CONCLUSIONS

The efficiency of high performance jet turbine engines is improved by increasing the use temperatures, but this is limited by the materials from which the engine is made. The blades have specific requirements of high strength and creep resistance at high temperatures, fracture resistance at low temperatures and additional considerations of low density and cost. Current Ni superalloy materials have exceeded the base material's limitations through the use of complicated barrier coating and internal cooling systems, but these are costly and complicated, have diminishing returns due to the inefficiencies associated with cooling, and are reaching their maximum usable limits. Alternate materials with higher base temperatures offer potential for significant gains by reducing inefficiency loss while also raising the use temperatures.

Among the alternate materials, alloys of Mo, Si and B are a prominent contender. The excellent high temperature mechanical properties of Molybdenum are traditionally unusable in oxidizing environments because of the formation of a volatile MoO_3 oxide, however alloying with Si and B allows the formation of a borosilicate glass which flows over the material to create a self-healing barrier coating. The success of such materials requires a ductile Molybdenum matrix in order for molybdenum to dominate the mechanical properties, while the brittle borosilicate intermetallics, Mo_5SiB_2 (T2) and Mo_3Si (A15) must be finely and homogenously distributed in order to quickly form a complete borosilicate coating in high temperature oxidizing environments.

Many of the early attempts at creating MoSiB materials focused on melt-based processing, however the incongruent melting and higher $T_{m\ of}$ Mo results in a microstructure of interconnected intermetallics surrounding Mo dendrites, essentially the

opposite of the ideal microstructure. Processing modifications including splat quenching, hot forging, and long anneals can in some cases remedy the nonideal microstructure but the approaches are complex, costly, and difficult to scale-up from a laboratory scale. Instead powder processing and sintering can create homogenous distributions in the green state which remain once sintered, and use established industrial processing methods. These unfortunately suffer from severe impurities which are unavoidable on the fine Si and B powders required. A powder processing method has been developed at GA Tech which uses nitrides (Si_3N_4 and BN) instead of pure elemental powders of Si and B. nitrides are stable in processing and avoid the impurity concerns encountered in the traditional powder processing routes, and when fired in a reducing environment they break down and react to form the desired final phases. This has been shown to produce good usable microstructures and give comparable properties to other processing routes much more simply.

The MoSiB system, specifically those alloys with 3 wt% Si and 1 wt% B so-called 3:1 has been shown to have good high temperature strength and creep resistance and be able to create a protective oxidation resistant coating. The MoSiB alloys however suffer from a very high ductile to brittle transition temperature, and no MoSiB alloys have been shown to possess ductility below 800°C. In order to be usable, ductility should ideally extend to room temperature or below. The primary cause for the lack of low temperature ductility is solid solution of Si in the Molybdenum matrix which has a pronounced embrittling effect. Unfortunately Si solid solution is unavoidable in the Molybdenum when in equilibrium with the Mo_3Si phase, and the Mo_3Si is necessary in order to form SiO_2 during oxidation. Since it is the SiO_2 which is ultimately required

however, the possibility exists to remove the Mo_3Si phase entirely and replace it directly with SiO_2. This is not achievable through melt based approaches however and has not been approached previously, but is uniquely possible through a powder processing route such as the Georgia Tech reaction method.

Initial attempts at approaching the replacement of the A15 phase were made using glass frits as alternate glass sources. These showed that a glass powder could be added to a powder batch and fired using the same processing and firing methods as the GTRS process. A glass coating does form when oxidized as well, but the glass frits are commercial batches designed to be glazes or formed glasses, and as such have low melting points which result in a liquid phase during firing and internally at the final use temperatures. This causes a non-ideal microstructure due to flow while firing and the compositions do not create a high viscosity glass needed to prevent oxygen permeation above 1000°C.

The next approach examined was to use the same reaction of nitrides to form Mo_2B and T2. The Mo-Mo_2B-T2 phase triangle does not have any solubility of B or Si in the Mo phase at our process temperatures of 1600°C. The glasses formed in the boride phase triangle however have too high boron content which forms a glass of too low viscosity. Pure silica can be added to modify the viscosity and reach the same B:Si ratios as the MoSiB system. Pure silica is stable to over 1500°C and should not flow internally as the glass frits had but is too stable to coalesce at oxidation temperatures from 100-1300°C. During oxidation it should mix with the low viscosity borosilicate formed by oxidation of Mo_2B and T2, and in this way form a stable coating in nearly the same way as the MoSiB base system.

Success was demonstrated of the GTRS powder process and reaction for creating composites with a Mo matrix and dispersed Mo_2B, T2 and SiO_2 with relative ease and cost effectiveness. Mechanical tests showed that the strengths are higher than other similar compositions and measurable room temperature ductility could be achieved with the presence of the boride phase; boron is not contributing to embrittlement the way that Si from Mo3Si does. The results of the early oxidation results show promise in meeting the needs of oxidation resistance and compare favorably to prior results for current leading MoSiB systems at 1100°C.

A significant pair of microstructural hurdles was encountered in the Mo-T2-SiO_2 system. First is the depletion of both boride and SiO_2 from the surface. Testing in different firing scenarios revealed that this is a gas phase phenomena resulting from presence of boria which forms from the unavoidable small remnant oxygen that is present on the raw Mo powder surfaces. The oxygen is generally removed during firing in the reducing atmosphere, but the temperatures at which this occurs allows some of the B liberated by decomposition of BN during firing to react and form B_2O_3 which is volatile, and in the H2 reducing atmosphere H_3BO_4 is also possible. SiO_2 is also reduced from the surface by a reduction to SiO, similar to active oxidation of Si, and by reaction with the H_2O resulting from reduction of the other oxides in the H_2 atmosphere.

The second hurdle is also the result of the boria which forms during firing. Crescent shaped lenses were observed throughout the microstructure and are on the same size scale as the spray dried granules. The SiO_2 which should otherwise be totally stable and solid in the microstructure is fluxed by the B_2O_3 and able to flow internally during firing. It occupies the interstices between the spray dried granules and creates an

interconnected web of brittle SiO_2, which destroys the low temperature fracture toughness. The effect is independent of the source of the pure SiO_2, whether it begins as amorphous SiO_2 or crystalline quartz or cristobalite. Consistent with the theory of boria flux being the problem XRD indicated that the crystalline silica was converted to amorphous phase, regardless of starting phase. Numerous tests indicate that the residual O on Mo and subsequent formation of Boria in firing is not avoidable, and gettering agents were unable to prevent the occurrence.

In order to alleviate the issue of internal flow and crescent regions, more stable sources of silica were approached. The first set used mullite instead of silica, and showed none of the non-ideal crescents in the microstructure. The mullite also had measurable room temperature ductility, but when oxidized the boria reacts with the alumina and forms aluminoborides that do not flux to form a flowable glass and no oxidation protection is achieved. Alkaline earth aluminosilicates such as Sr-celsian (SAS), and Lithium 4 and 6-spodumene do form a flowable glass however and like the mullite case do not result in embrittling crescent microstructures.

Unfortunately the oxidation protection in these cases is also incomplete. The alkali and alkaline earth oxides readily react with molybdenum to form molybdates such as $SrMoO_4$. These then disrupt the coating, in some cases they crystallize while the coating is forming which prevents them from flowing further. This results in a stepwise formation and erosion of coating and leads to a series of hollow layers of devitrified molybdate and silicates. In other cases, the glasses are too low viscosity and flow too much even while phase separating and devitrifying, and as molybdenum is removed from the glass to form molybdates, the wettability of the coating is also reduced. Neodymium

was added in order to stabilize the glass and in hopes of limiting the phase separation and crystallization, but these issues remained a significant concern, and focus shifted back towards SiO_2 containing samples.

Oxidation was acceptable but by no means optimized, and much work in other groups had focused on maximizing the oxidation resistance. One successful approach was trace additions of transition metals such as Fe. Fe was added to the Mo-SiO_2-T2 system, and while it did accomplish a reduction in transient losses, the long term protection fell apart due to phase separation into Fe-rich and Fe-poor regions which then devitrify into Fayalite and cristobalite respectively. Additional elements tested include Ni, Mn, Co, Cr, Y, and Nd. Of these, all were observed to form molybdates and oxides which can disrupt the coating. Co was deemed initially to be too effective of a flux and led to excessive bubbling through the low viscosity glass. Cr formed Cr_2O_3, which itself is volatile and may have contributed to problematic bubble formation and also suffered from long term devitrification. Ni showed improvements over the base material but also did not achieve good long term oxidation resistance.

Mn resulted in the best performance and had not been previously examined in the literature because it's volatility below the melting point of Mo makes Mn additions impossible through melt based techniques. The short term losses are reduced, and further reduced by grinding the surfaces, and long term resistance was excellent with near-zero losses to 100h at 1200°C. Unfortunately issues with Mn volatility during firing caused difficulty in accurately estimating and reproducing final compositions. Lower contents of Co additions were also pursued so that their total contribution to reduced viscosity is lower, and they give improved oxidation results also. Small additions of SAS showed

further benefit, in part by stabilizing the glass but also possibly by delaying the crystallization of the glass and allowing a coating to completely form and then devitrify so that the oxygen permeability is greatly reduced and very low long term rates of loss follow.

It was observed that the viscosity of the glass plays a crucial role in forming oxidation resistance. The glass must be fluid enough to flow and coat the surface, but high enough viscosity that the oxygen permeability through the glass is low. The ability to tailor the final phases and their relations by adding or removing SiO_2 allows a wide range of Si:B ratios to be examined. The Mo-3Si-1B composition had been optimized for 1100°C, however the end-use goals for the material are 1300°C or above, and higher Si glasses were observed to be necessary for 1300°C protection.

At 1300°C bubble formation by boiling of the vapor species becomes a serious concern. Channels also exist over the pure Mo phase which is the last to be coated over, and the channels can be held open by condensed MoO_3 and MoO_3 vapor formation. The bubbles disrupt the coating as it forms and the problem is exacerbated when phase separation or devitrification leads to thickening of the glass and prevents it from flowing to fill in after collapse of the bubbles. Boria volatility is also higher at 1300°C, and the glass itself becomes more viscous as boria leaves, which can in some cases be beneficial to long term resistance, but can also prevent filling in of the voids. A finite thickness of glass is required to prevent oxygen permeation, yet in order to expose enough glass-formers a related amount of Mo must be removed. This results in a scenario where some bubbling is necessary but once enough glass is present it must still be able to flow into the void spaces and channels. The boria loss and phase changes are time and temperature

dependent, and the compositions also change through the bulk dependent on initial batch ratios but also affected by depletion during firing. As a result the glass properties are difficult to predict and influenced by a large number of variables, however glasses with excellent protection in the short and long term have been achieved and demonstrated. The ability to tailor the compositions very directly from the initial green batches using the GTRS method allows for these to be further optimized in the future.

A final series of tests involving Hot Isostatic Pressing use pressure in addition to temperature in order to densify the final products. The process has been adapted to eliminate any oxygen presence, and can create homogenous samples which are free of the crescent regions or depletion defects, and also maintain Mn or other volatiles and give much better compositional confidence. Further it stabilizes the quartz phase and crystalline solid quartz was observed by XRD indicating no flux of the silica by boria has occurred. The HIP process is somewhat more complicated and requires more fine-tuning to create final pieces. The HIP runs were limited to only four tests by time and fiscal constraints, and a reproducible and reliable method was not perfected, however with some more work a reliable method could be simply developed. This would allow better compositional control for tailoring the final glass compositions so excellent oxidation protection could be reproducibly achieved for a variety of end-use conditions. Furthermore the HIP'ed materials should have the connected ductile Mo matrix made possible by removing the Mo_3Si phase, though no bend test specimens were successfully made to be tested to date. Using the GTRS nitride powder process method combined with hot isostatic pressing it should be possible to create tailorable composites of SiO_2 and Mo_5SiB_2 in a ductile Mo matrix with excellent short and long term oxidation resistance to

temperatures of 1300°C or above, while also achieving measurable ductility and high fracture toughness at room temperature.

REFERENCES

[1] M. Akinc, M.K. Meyer, M.J. Kramer, A.J. Thom, J.J. Huebsch, B. Cook. "Boron Doped Molybdenum Silicides for Structural Applications", *Materials Science and Engineering A* **261** (1999) 16-23.

[2] D.M. Berczik. *Oxidation Resistant Molybdenum Alloy.* US 5,693,156 5,693,156, 1997

[3] D.M. Berczik. *Method for Enhancing the Oxidation Resistance of a Molybdenum Alloy, and a Method of Making a Molybdenum Alloy.* US 5,595,616 5,595,616, 1997

[4] J.A. Lemberg, R.O. Ritchie. "Mo-Si-B Alloys for Ultrahigh-Temperature Structural Applications", Adv Mater **24** (2012) 3445-3480.

[5] C. Bell, W. Dawes, J. Jarrett, P. Clarkson. "Improving the Conceptual Design of Turbine Rotor Blade Cooling Systems". DS 35: Proceedings ICED 05, the 15th International Conference on Engineering Design, Melbourne, Australia, 15.-18.08. 2005, 2005.

[6] R.L. Fleischer, A.I. Taub. "Selecting High-Temperature Structural Intermetallic Compounds: The Materials Science Approach", JOM **41** (1989) 8-11.

[7] D.R. Lide. CRC Handbook of Chemistry and Physics, CRC press, 2004.

[8] D.M. Dimiduk, J.H. Perepezko. "Mo-Si-B Alloys: Developing a Revolutionary Turbine-Engine Material", MRS Bulletin **28** (2003) 639-645.

[9] B. Bewlay, M. Jackson, P. Subramanian, J.-C. Zhao. "A Review of Very-High-Temperature Nb-Silicide-Based Composites", Metallurgical and Materials Transactions A **34** (2003) 2043-2052.

[10] B. Bewlay, M. Jackson, J.-C. Zhao, P. Subramanian, M. Mendiratta, J. Lewandowski. "Ultrahigh-Temperature Nb-Silicide-Based Composites", MRS bulletin **28** (2003) 646-653.

[11] M. Heilmaier, M. Krüger, H. Saage, J. Rösler, D. Mukherji, U. Glatzel, R. Völkl, R. Hüttner, G. Eggeler, C. Somsen. "Metallic Materials for Structural Applications Beyond Nickel-Based Superalloys", JOM **61** (2009) 61-67.

[12] A. Wronski, A. Chilton, E. Capron. "The Ductile-Brittle Transition in Polycrystalline Molybdenum", Acta Metallurgica **17** (1969) 751-755.

[13] N. Kazakova, N. Morgunova, E. Ageeva, M. Kantor. "Effect of Structure on the Ductile-Brittle Transition Temperature of Molybdenum Alloy TsM-6", Metal Science and Heat Treatment **24** (1982) 479-481.

[14] R.N. Orava. "The Strain-Rate Dependence of Yielding and Flow in Molybdenum", Transactions AIME **230** (1964).

[15] L.E. Olds, G.P. Rengstorff. "Effects of Oxygen, Nitrogen, and Carbon on the Ductility of Cast Molybdenum", Trans. AIME **206** (1956) 150-155.

[16] A. Krajnikov, A. Drachinskiy, V. Slyunyaev. "Grain Boundary Segregation in Recrystallized Molybdenum Alloys and Its Effect on Brittle Intergranular Fracture", International Journal of Refractory Metals and Hard Materials **11** (1992) 175-180.

[17] A. Kumar, B. Eyre. "Grain Boundary Segregation and Intergranular Fracture in Molybdenum". Proceedings of the Royal Society of London A: Mathematical, Physical and Engineering Sciences, **vol. 370**: The Royal Society, 1980. p.431-458.

[18] J.H. Bechtold, E.T. Wessel. Ductile to Brittle Transition in Molybdenum in: Harwood JJ, (Ed.). The Metal Molybdenum. American Society for Metals, Cleveland, OH, 1985. pp. 252.
[19] G. Hahn, A. Gilbert, R. Jaffee. "The Effects of Solutes on the Ductile-to-Brittle Transition in Refractory Metals". Battelle Memorial Inst. Defense Metals Information Center, Columbus, Ohio, 1962.
[20] D. Sturm, M. Heilmaier, J.H. Schneibel, P. Jéhanno, B. Skrotzki, H. Saage. "The Influence of Silicon on the Strength and Fracture Toughness of Molybdenum", Materials Science and Engineering: A **463** (2007) 107-114.
[21] A. Gokhale, G. Abbaschian. "The Mo-Si (Molybdenum-Silicon) System", Journal of Phase Equilibria **12** (1991) 493-498.
[22] J. Shields. "Applications of Molybdenum Metal and It's Alloys", Int. Molybdenum Ass. (2013).
[23] S. Suzuki, H. Matsui, H. Kimura. "The Effect of Heat Treatment on the Grain Boundary Fracture of Recrystallized Molybdenum", Materials Science and Engineering **47** (1981) 209-216.
[24] N. Birks, G.H. Meier, F.S. Pettit. Introduction to the High Temperature Oxidation of Metals, Cambridge University Press, 2006.
[25] E.A. Gulbransen, K.F. Andrew, F.A. Brassart. "Oxidation of Molybdenum 550° to 1700°C", Journal of The Electrochemical Society **110** (1963) 952.
[26] E. Bartlett, D. Williams. "The Oxidation Rate of Molybdenum in Air", Trans. Met. Soc. AIME **212** (1958).
[27] S. Burk. Hochtemperaturoxidation Molybdän-basierter Legierungen unter Berücksichtigung von Einflüssen aus Umgebungsatmosphäre und legierungstechnischen Maßnahmen, Univ., 2011.
[28] L. Brewer, R. Lamoreaux. "The Mo-O System (Molybdenum-Oxygen)", Journal of Phase Equilibria **1** (1980) 85-89.
[29] C. Gupta. Extractive Metallurgy of Molybdenum, CRC press, 1992.
[30] R.S.a.G.R.S. Pierre. Molybdenum in: N.E.Promisel, (Ed.). The Science and Technology of Tungsten, Tantalum, Molybdenum, Niobium and Their Alloys. Pergamon Press, 1964. pp. 289-330.
[31] E.A. Gulbransen, K.F. Andrew, F.A. Brassart. "Vapor Pressure of Molybdenum Trioxide", Journal of The Electrochemical Society **110** (1963) 242.
[32] G.R. Smolik, D.A. Petti, S.T. Schuetz. "Oxidation, Volatilization, and Redistribution of Molybdenum from TZM Alloy in Air ", INEEL/EXT-99-01353 (2000).
[33] J. Berkowitz, M.G. Inghram, W. Chupka. "Polymeric Gaseous Species in the Sublimation of Molybdenum Trioxide", The Journal of Chemical Physics **26** (1957) 842-846.
[34] R.A. Kempe. "Vapor Phase Coating of Molybdenum Articles". Google Patents, 1955.
[35] Y.V. Dzyadykevich. "Protective Coatings on Niobium, Tantalum, Molybdenum, and Tungsten for Increased Resistance to High-Temperature Oxidation", Powder Metallurgy and Metal Ceramics **31** (1992) 313-317.
[36] M. Sundberg, E. Ström. "Molybdenum Silicide Composite Material". Google Patents, 2009.

[37] T. Uchiyama, W. Jiang. "Molybdenum Disilicide Heating Element and its Production Method". Google Patents, 2001.
[38] H. Nowotny, E. Dimakopoulou, H. Kudielka. "Untersuchungen in den Dreistoffsystemen: Molybdän-Silizium-Bor, Wolfram-Silizium-Bor und in dem System: VSi2− TaSi2", Monatshefte für Chemie und verwandte Teile anderer Wissenschaften **88** (1957) 180-192.
[39] C. Nunes, R. Sakidja, Z. Dong, J. Perepezko. "Liquidus Projection for the Mo-rich Portion of the Mo–Si–B Ternary System", Intermetallics **8** (2000) 327-337.
[40] K. Ito, K. Ihara, K. Tanaka, M. Fujikura, M. Yamaguchi. "Physical and Mechanical Properties of Single Crystals of the T2 Phase in the Mo–Si–B System", Intermetallics **9** (2001) 591-602.
[41] C. Rawn, J. Schneibel, C. Hoffmann, C. Hubbard. "The Crystal Structure and Thermal Expansion of Mo5SiB2", Intermetallics **9** (2001) 209-216.
[42] I. Rosales, J. Schneibel. "Stoichiometry and Mechanical Properties of Mo3Si", Intermetallics **8** (2000) 885-889.
[43] K. Spear, P. Liao. "The B− Mo (Boron-Molybdenum) system", Journal of Phase Equilibria **9** (1988) 457-466.
[44] J. Perepezko, R. Sakidja, S. Kim. "Phase Stability in Processing and Microstructure Control in High Temperature Mo-Si-B Alloys". MRS Proceedings, **vol. 646**: Cambridge Univ Press, 2000. p.N4. 5.1.
[45] M. Krüger, S. Franz, H. Saage, M. Heilmaier, J.H. Schneibel, P. Jéhanno, M. Böning, H. Kestler. "Mechanically Alloyed Mo–Si–B alloys with a Continuous α-Mo Matrix and Improved Mechanical Properties", Intermetallics **16** (2008) 933-941.
[46] S. Burk, B. Gorr, V. Trindade, H.-J. Christ. "Effect of Zr Addition on the High-Temperature Oxidation Behaviour of Mo–Si–B Alloys", Oxidation of metals **73** (2010) 163-181.
[47] M. Salamon, A. Strohm, T. Voss, P. Laitinen, I. Riihimäki, S. Divinski, W. Frank, J. Räisänen ¶, H. Mehrer. "Self-Diffusion of Silicon in Molybdenum Disilicide", Philosophical Magazine **84** (2006) 737-756.
[48] S. Kim, J.H. Perepezko. "Interdiffusion Kinetics in the Mo5SiB2 (T2) Phase", Journal of Phase Equilibria & Diffusion **27** (2006) 605-613.
[49] R. Sakidja, J. Myers, S. Kim, J. Perepezko. "The Effect of Refractory Metal Substitution on the Stability of Mo (ss)+ T2 Two-Phase Field in the Mo–Si–B System", International Journal of Refractory Metals and Hard Materials **18** (2000) 193-204.
[50] M. Meyer, A. Thom, M. Akinc. "Oxide Scale Formation and Isothermal Oxidation Behavior of Mo–Si–B Intermetallics at 600–1000C", Intermetallics **7** (1999) 153-162.
[51] C.W. Parmelee. "Cermaic Glazes", (1973).
[52] F.A. Rioult, S.D. Imhoff, R. Sakidja, J.H. Perepezko. "Transient Oxidation of Mo–Si–B Alloys: Effect of the Microstructure Size Scale", Acta Materialia **57** (2009) 4600-4613.
[53] R. Brückner, Y. Yue. "Non-Newtonian Flow Behaviour of Glass Melts as a Consequence of Viscoelasticity and Anisotropic Flow", Journal of Non-Crystalline Solids **175** (1994) 118-128.
[54] A. Priven. "Calculation of the Viscosity of Glass-forming Melts: V. Binary Borate Systems", Glass Physics and Chemistry **26** (2000) 541-558.

[55] N.P. Bansal, R.H. Doremus. Handbook of Glass Properties, Elsevier, 2013.
[56] D.A. Helmick. "High Temperature Oxidation Behavior of Molybdenum-Silicon-Boron Base Alloys", (2003).
[57] M. Mendiratta, T. Parthasarathy, D. Dimiduk. "Oxidation Behavior of αMo–Mo3Si–Mo5SiB2 (T2) Three Phase System", Intermetallics **10** (2002) 225-232.
[58] T. Parthasarathy, M. Mendiratta, D. Dimiduk. "Oxidation Mechanisms in Mo-Reinforced Mo5SiB2 (T2)–Mo3Si alloys", Acta Materialia **50** (2002) 1857-1868.
[59] M.R. Middlemas. Fabrication, Strength and Oxidation of Molybdenum-Silicon-Boron Alloys from Reaction Synthesis, ProQuest, 2009.
[60] T. Zhang, W.G. Fahrenholtz, S.T. Reis, R.K. Brow. "Borate volatility from SOFC sealing glasses", Journal of the American Ceramic Society **91** (2008) 2564-2569.
[61] M. Snyder, M. Mesko, J. Shelby. "Volatilization of Boron from E-glass Melts", Journal of Non-Crystalline Solids **352** (2006) 669-673.
[62] S. Burk, B. Gorr, H.-J. Christ. "High Temperature Oxidation of Mo–Si–B Alloys: Effect of Low and Very Low Oxygen Partial Pressures", Acta Materialia **58** (2010) 6154-6165.
[63] C.J. Wagner. "Active-Passive Transition in Oxidation of Silicon", J. App. Phys. **29** (1958) 1295.
[64] B. Schneider, A. Guette, R. Naslain, M. Cataldi, A. Costecalde. "A Theoretical and Experimental Approach to the Active-to-Passive Transition in the Oxidation of Silicon Carbide: Experiments at High Temperatures and Low Total Pressures", Journal of Materials Science **33** (1998) 535-547.
[65] F. Rioult, N. Sekido, R. Sakidja, J.H. Perepezko. "Aluminum Pack Cementation on Mo–Si–B Alloys", Journal of The Electrochemical Society **154** (2007) C692.
[66] R. Sakidja, F. Rioult, J. Werner, J. Perepezko. "Aluminum Pack Cementation of Mo–Si–B Alloys", Scripta Materialia **55** (2006) 903-906.
[67] H.S. R. Sakidja, and J.H. Perepezko. "The Formation of Mo Precipitates in a Supersaturated Mo5SiB2 Intermetallic Phase", Philosophical Magazine Letters **76** (1999) 351-357.
[68] J.H. Schneibel. "High Temperature Strength of Mo–Mo3Si–Mo5SiB2 Molybdenum Silicides", Intermetallics **11** (2003) 625-632.
[69] P. Jain, A.P. Alur, K.S. Kumar. "High Temperature Compressive Flow Behavior of a Mo–Si–B Solid Solution Alloy", Scripta Materialia **54** (2006) 13-17.
[70] P. Jéhanno, M. Böning, H. Kestler, M. Heilmaier, H. Saage, M. Krüger. "Molybdenum Alloys for High Temperature Applications in Air", Powder Metallurgy **51** (2008) 99-102.
[71] M.J. Murray. "Fracture of WC-Co Alloys: An Example of Spatially Constrained Crack Tip Opening Displacement", The Royal Society (1977).
[72] A.P. Alur, N. Chollacoop, K.S. Kumar. "Creep Effects on Crack Growth in a Mo–Si–B Alloy", Acta Materialia **55** (2007) 961-974.
[73] A.P. Alur, N. Chollacoop, K.S. Kumar. "High-Temperature Compression Behavior of Mo–Si–B Alloys", Acta Materialia **52** (2004) 5571-5587.
[74] A.P. Alur, K.S. Kumar. "Monotonic and Cyclic Crack Growth Response of a Mo–Si–B Alloy", Acta Materialia **54** (2006) 385-400.
[75] K.S. Kumar, A.P. Alur. "Deformation Behavior of a Two-Phase Mo–Si–B Alloy", Intermetallics **15** (2007) 687-693.

[76] S. Kumar, W.A. Curtin. "Crack Interaction with Microstructure", Materials Today **10** (2007) 34-44.
[77] R. Mitra, A.K. Srivastava, N. Eswara Prasad, S. Kumari. "Microstructure and Mechanical Behaviour of Reaction Hot Pressed Multiphase Mo–Si–B and Mo–Si–B–Al Intermetallic Alloys", Intermetallics **14** (2006) 1461-1471.
[78] D.C. H. Choe, J.H. Schneibel, and R.O. Ritchie. "Ambient to High Temperature Fracture Toughness and Fatigue-crack Propagation Behavior in a Mo-12Si-8.5 B (at.%) Intermetallic", Intermetallics **9** (2001) 319-329.
[79] J.J. Kruzic, J.H. Schneibel, R.O. Ritchie. "Fracture and Fatigue Resistance of Mo–Si–B Alloys for Ultrahigh-Temperature Structural Applications", Scripta Materialia **50** (2004) 459-464.
[80] P. Jéhanno, M. Heilmaier, H. Saage, H. Heyse, M. Böning, H. Kestler, J.H. Schneibel. "Superplasticity of a Multiphase Refractory Mo–Si–B Alloy", Scripta Materialia **55** (2006) 525-528.
[81] G.D. Quinn, R.C. Bradt. "On the Vickers Indentation Fracture Toughness Test", Journal of the American Ceramic Society **90** (2007) 673-680.
[82] T. Miyoshi. "A Study on Evaluation of KIc for Structural Ceramics", Trans. Jap. Soc. Mech. Eng. **51A** (1985) 2489-2497.
[83] JIS. "JIS R 1607: Testing Methods for Fracture Toughness of High Performance Ceramics". Tokyo, 1990.
[84] M. Kramer, S. Okumus, M. Besser, Ö. Ünal, M. Akinc. "Microstructure of a Plasma-Sprayed Mo-Si-B Alloy", Journal of Thermal Spray Technology **9** (2000) 90-94.
[85] P. Jéhanno, M. Heilmaier, H. Kestler. "Characterization of an Industrially Processed Mo-Based Silicide Alloy", Intermetallics **12** (2004) 1005-1009.
[86] C. Liu, J. Schneibel, L. Heatherly. "Processing, Microstructure, and Properties of Multiphase Mo Silicide Alloys". MRS Proceedings, **vol. 552**: Cambridge Univ Press, 1998. p.KK6. 2.1.
[87] A. Yamauchi, K. Yoshimi, K. Kurokawa, S. Hanada. "Synthesis of Mo–Si–B in situ composites by mechanical alloying", Journal of alloys and compounds **434** (2007) 420-423.
[88] M.R. Middlemas, J.K. Cochran. "Dense, Fine-Grain Mo-Si-B Alloys from Nitride-Based Reactions", JOM **60** (2008) 19-24.
[89] R. Sakidja, J.H. Perepezko. "Alloying and Microstructure Stability in the High-Temperature Mo–Si–B System", Journal of Nuclear Materials **366** (2007) 407-416.
[90] S. Ochiai. "Improvement of the Oxidation-Proof Property and the Scale Structure of Mo3Si Intermetallic Alloy through the Addition of Chromium and Aluminum Elements", Intermetallics **14** (2006) 1351-1357.
[91] M. Mendiratta, D. Dimiduk. "Effect of Alloying Additions on the Phase Equilibria and Oxidation in the Mo-Si-B System". DTIC Document, 2001.
[92] S.R. Woodard, R. Raban, J.F. Myers, D.M. Berczik. "Alloy with silicon and boron containing iron, copper, cobalt and/or nickel". Google Patents, 2003.
[93] T. Sossaman, R. Sakidja, J.H. Perepezko. "Influence of Minor Fe Addition on the Oxidation Performance of Mo–Si–B Alloys", Scripta Materialia **67** (2012) 891-894.
[94] J. Kaewkhao, W. Siriprom, S. Insiripong, T. Ratana, C. Kedkaew, P. Limsuwan. "Structural and Magnetic Properties of Glass Doped with Iron Oxide". Journal of Physics: Conference Series, **vol. 266**: IOP Publishing, 2011. p.012012.

[95] A. Milner, T. Bergstrom. "Ductility of Sintered Unworked Molybdenum-Carbon Alloys", Journal of the Less Common Metals **12** (1967) 253-257.
[96] S.J.a.W.C. JH Rendall. J. Inst. Less Common Metals **82** (1954) 345.
[97] T.B. Massalski, H. Okamoto, P. Subramanian, L. Kacprzak, W.W. Scott. Binary Alloy Phase Diagrams, American Society for Metals Metals Park, OH, 1986.
[98] R.L. Drennan, M.E. Brown. "Binary and Ternary Pyrotechnic Dystems of Mn and/or Mo and BaO_2 and/or SrO_2: Part 2. Combustion Studies", Thermochimica acta **208** (1992) 223-246.
[99] J. Bartolome, M. Díaz, J. Requena, J. Moya, A. Tomsia. "Mullite/Molybdenum Ceramic–Metal Composites", Acta materialia **47** (1999) 3891-3899.
[100] R. Sivakumar, D.D. Jayaseelan, T. Nishikawa, S. Honda, H. Awaji. "Mullite–Molybdenum Composites Fabricated by Pulse Electric Current Sintering Technique", Journal of the European Ceramic Society **22** (2002) 761-768.
[101] A.C. Akhavan. "The Silica Groups". **vol. 2013**. The Quartz Page, 2013.
[102] T. Herbell, D. Hull, G. Hallum. "Effect of High Temperature Hydrogen Exposure on the Strength and Microstructure of Mullite", Hydrogen Effects on Material Behavior (1989) 351-359.
[103] H. Scott, W. Taebel, D. Lawthers. "Consolidation of Molybdenum by Powder Metallurgy Practice". Molybdenum Conference, Detroit, September, 1956.
[104] T.O.-C. Molybdenum. "LTS Weight gain". In: Daloz W, (Ed.), 2012.
[105] T. Narushima, T. Goto, Y. Yokoyama, J. Hagiwara, Y. Iguchi, T. Hirai. "High Temperature Active Oxidation and Active to Passive Transition of Chemically Vapor Deposited Silicon Nitride in N2–O2 and Ar–O2 Atmospheres", Journal of the American Ceramic Society **77** (1994) 2369-2375.
[106] J.W. McAllister, L.-H.T. Pham, H.G. Sowman. "High Temperature Stable Reinforcement Materials". Google Patents, 1989.
[107] G. Kostorz, H. Herman, A.M. Alper. Phase Diagrams in Advanced Ceramics, Elsevier, 1995.
[108] L.U. Ogbuji, S.R. Bryan. "The SiO2-Si3N4 Interface, Part I: Nature of the Interphase", Journal of the American Ceramic Society **78** (1995) 1272-1278.
[109] M.B. Trigg, K.H. Jack. "Solubility of Aluminium in Silicon Oxynitride", Journal of Materials Science Letters **6** (1987) 407-408.
[110] K.J. Griesser, A. Beran, D. Voll, H. Schneider. "Boron Iincorporation into Mmullite", Mineralogy and Petrology **92** (2007) 309-320.
[111] B.T. Hazel, I. Spitsberg. "Thermal/Environmental Barrier Coating System for Silicon-Containing Materials". Google Patents, 2008.
[112] I.T. Spitsberg, H. Wang. "Thermal/Environmental Barrier Coating System for Silicon-Based Materials". Google Patents, 1999.
[113] K.N. Lee, D.S. Fox, N.P. Bansal. "Rare Earth Silicate Environmental Barrier Coatings for SiC/SiC Composites and Si3N4 Ceramics", Journal of the European Ceramic Society **25** (2005) 1705-1715.
[114] Smart.Conseil. "Lithium & Ceramique". Smart 2000, 2011.
[115] K. Kamata, T. Nakamura, T. Sata. "Valence Stability of Molybdenum in Alkaline Earth Mlybdates", Materials Research Bulletin **10** (1975) 373-378.
[116] N. Chouard, D. Caurant, O. Majérus, J.L. Dussossoy, A. Ledieu, S. Peuget, R. Baddour-Hadjean, J.P. Pereira-Ramos. "Effect of Neodymium Oxide on the Solubility of

MoO3 in an Aluminoborosilicate Glass", Journal of Non-Crystalline Solids **357** (2011) 2752-2762.
[117] J. Lipsch, G. Schuit. "The CoO MoO3 Al2O3 Catalyst: I. Cobalt Molybdate and the Cobalt Oxide Molybdenum Oxide System", Journal of Catalysis **15** (1969) 163-173.
[118] M.B. Volf. Chemical Approach to Glass, Elsevier, 1984.
[119] T. Murase, A.R. McBIRNEY. "Properties of Some Common Igneous Rocks and Their Melts at High Temperatures", Geological Society of America Bulletin **84** (1973) 3563-3592.
[120] D. Bahat. "Heterogeneous Nucleation of Alkaline Earth Feldspars in Glasses", Journal of Materials Science **4** (1969) 847-854.